Cover Page

Universiteit Leiden

The handle http://hdl.handle.net/1887/29081 holds various files of this Leiden University dissertation.

Author: Schinkel, Linda Danielle van
Title: MR assessment of end-organ damage in the metabolic syndrome and diabetes mellitus
Issue Date: 2014-10-07

MR assessment

of end-organ damage in the metabolic syndrome and diabetes mellitus

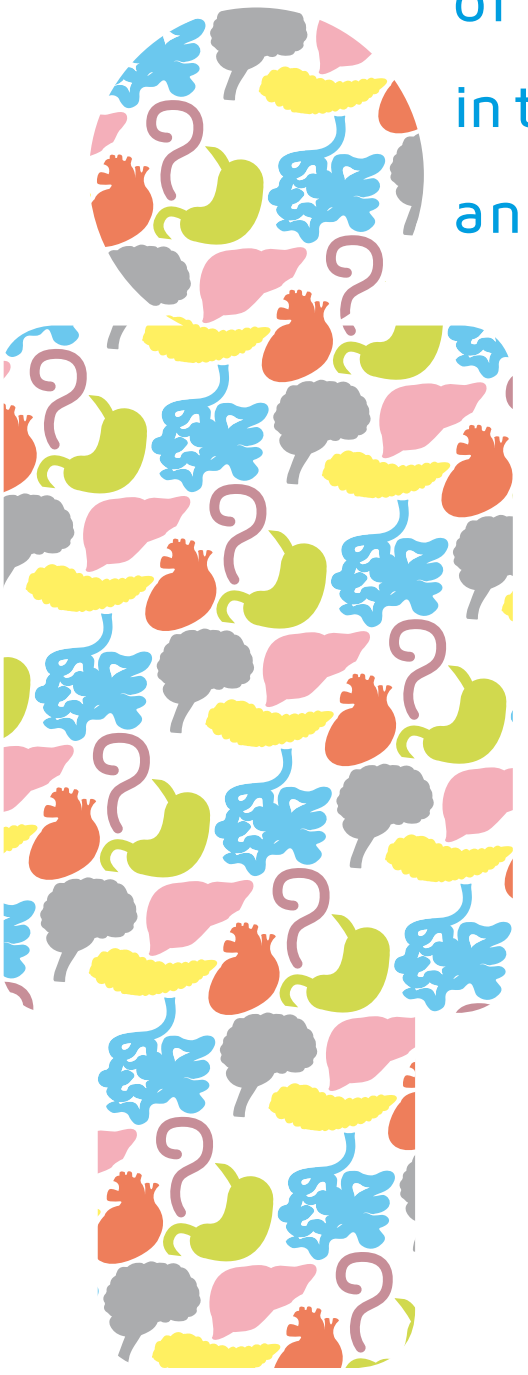

Linda D. van Schinkel

MR assessment of end-organ damage in the metabolic syndrome and diabetes mellitus

Linda Danielle van Schinkel

Cover design: Is vormgeving, Leiden, The Netherlands (www.isvormgeving.nl)
Layout and print: Optima Grafische Communicatie, Rotterdam, the Netherlands
Dit proefschrift is gedrukt op FSC-papier.

ISBN: 978-94-6169-550-0

The research described in this thesis was supported by a grant of the Dutch Heart Foundation (DHF-2009B061). Financial support by the Dutch Heart Foundation for the publication of this thesis is gratefully acknowledged. Additional financial support is provided by Novo Nordisk B.V., Boehringer Ingelheim B.V., Servier Nederland Farma B.V., Ipsen Farmaceutica B.V., Guerbet Nederland B.V. and Sanofi Nederland B.V.

© Copyright 2014, L.D. van Schinkel, The Hague, The Netherlands
The copyright of the articles that have been published or have been accepted for publication has been transferred to the respective journals. No parts of this thesis may be reproduced or transmitted in any form, by any means, without prior written permission of the author.

MR assessment of end-organ damage in the metabolic syndrome and diabetes mellitus

Proefschrift

ter verkrijging van
de graad van Doctor aan de Universiteit Leiden,
op gezag van

Rector Magnificus prof. mr. C.J.J.M. Stolker,

volgens besluit van het College voor Promoties
te verdedigen op dinsdag 7 oktober 2014
klokke 16.15 uur

door

Linda Danielle van Schinkel

geboren te 's-Gravenhage
in 1984

PROMOTIECOMMISSIE

Promotores	Prof. dr. J.W.A. Smit
	Prof. dr. A. de Roos
	Prof. dr. H.J. Lamb
Overige leden	Prof. dr. H. Pijl
	Prof. dr. P.C.N. Rensen
	Prof. dr. J.W. Jukema
	Prof. dr. C.J. Tack (UMC St. Radboud Nijmegen)
	dr. I.M. Jazet
	dr. J.J.M. Westenberg

CONTENTS

Chapter 1	General introduction and outline of the thesis	9
Chapter 2	Aortic stiffness is related to left ventricular diastolic function in patients with diabetes mellitus type 1: assessment with MRI and speckle tracking strain analysis	25
Chapter 3	Aortic stiffness is associated with white matter integrity in patients with type 1 diabetes	43
Chapter 4	Impact of type 1 diabetes mellitus on regional gray matter volume	57
Chapter 5	Caloric restriction improves cardiovascular function in advanced type 2 diabetes mellitus	69
Chapter 6	Effects of bariatric surgery on pericardial ectopic fat depositions and cardiovascular function	89
Chapter 7	Functional and metabolic imaging of the cardiovascular system in young healthy South Asians and Caucasians unveils early differences	105
Chapter 8	A 5-day high fat high calorie diet impairs insulin sensitivity in healthy, young South Asians but not in Caucasians	123
Chapter 9	Cardiovascular function in middle-aged overweight South Asians compared with Caucasians: response to short-term caloric restriction	149
Chapter 10	Chemotherapy for testicular cancer induces acute alterations in diastolic heart function	165
Chapter 11	Ultrahigh field 7T magnetic resonance carotid vessel wall imaging: initial experience in comparison with 3-T field strength.	181
Chapter 12	7 Tesla cardiovascular MR imaging: initial clinical experience	199
Chapter 13	Summary and conclusions	219
Chapter 14	Nederlandse samenvatting	233
	List of publications	247
	Curriculum Vitae	251

Chapter 1

General introduction and outline of the thesis

GENERAL INTRODUCTION

Epidemiology of obesity and type 2 diabetes mellitus

The prevalence of overweight and obesity is increasing dramatically in countries throughout the world. Since 1980, worldwide obesity has nearly doubled. The World Health Organization (WHO) defines *overweight* as a body mass index (BMI, calculated as bodyweight in kilograms divided by the square height in meters (kg/m^2)) of 25 kg/m^2 or higher; obesity is defined as a BMI of 30 kg/m^2 or more. In 2008, worldwide more than 1.4 billion adults were overweight, of whom around 500 million were obese (WHO 'Obesity and overweight' factsheet). If past trends continue, the number of overweight and obese adults is projected to reach around 2.2 billion and 1.1 billion respectively by the year 2030 (1).

Obesity is a major risk factor for developing type 2 diabetes mellitus (T2DM). It therefore comes as no surprise to find that the increasing prevalence of overweight and obesity is accompanied by an increase in prevalence of T2DM. Nowadays, diabetes is one of the most common chronic diseases in almost every country. In 2000, the global prevalence of diabetes was 2.8%. Estimations of the prevalence of diabetes in 2030 range from 4.4% to 6.4%, indicating the magnitude of this public health problem (2,3).

The prevalence of T2DM is on the rise in low-to-middle income countries, which is attributed to a shift in infrastructure, technology and food supply that promotes over-nutrition and sedentary lifestyles. Especially striking is the increasing incidence worldwide of T2DM in people of South Asian descent (4). South Asians originate from the Indian subcontinent and represent one fifth of the total world's population. Not only is the prevalence of T2DM higher in this population, South Asians are younger and tend to have a lower BMI when they develop the disease compared to Caucasians, and disease severity is higher. Although currently a topic that is attracting great interest in the literature, no explanation has yet been found for the increased incidence and severity of T2DM in the South Asian population.

Pathogenesis of T2DM and end-organ damage

Diabetes mellitus is a chronic disease characterized by disturbances in glucose homeostasis, eventually leading to hyperglycemia. Normally speaking, blood glucose concentrations are maintained within a narrow range, since both low and elevated blood glucose levels are detrimental to the body. Diabetes has negative consequences for almost all organs. Well known complications involve the cardiovascular system, (central) nervous system, kidneys and eyes. Around 50% of patients with diabetes die from cardiovascular disease (5).

The pathogenesis of T2DM and cardiovascular complications involves multiple pathways that are tightly interlinked. Although it is impossible to dissect the individual contributions of the multiple endogenous and exogenous disruptors (such as cytotoxic chemotherapy), and to establish causal relationships between the many pathological phenomena observed in T2DM, the main pathogenetic phenomena identified in T2DM are related to lipid dysfunction, inflammation and glucotoxicity.

Cardiovascular complications

The pathogenesis of cardiovascular complications in T2DM is complex, but a major role is attributed to ectopic accumulation of triglycerides (TG) in organs that normally do not store fat, such as skeletal muscles, liver and heart. Ectopic fat accumulation is closely associated with the generation of toxic intermediates of lipid oxygenation, mitochondrial dysfunction and activation of inflammatory pathways, all of which contribute to organ dysfunction (6-10). Cardiac ectopic fat includes myocardial and pericardial fat accumulation. Both are associated with impaired myocardial function (11-13) and increased cardiovascular disease (CVD) risk (14).

South Asians are at an increased risk of developing CVD compared to Caucasians (15). The mean age of first acute myocardial infarction is approximately five years earlier in South Asians than in Caucasians (16,17) and CVD in this population is more aggressive and has higher mortality rates at younger ages (15,17-19). The differences in CVD prevalence and severity between both ethnicities cannot be explained by traditional risk factors. As South Asians represent over 20% of the world's population, uncovering the underlying mechanisms involved in the higher prevalence of T2DM and CVD in this group deserves urgent attention.

Pulse wave velocity

Aortic pulse wave velocity (PWV) is a surrogate marker for arterial stiffness and a powerful independent predictor of cardiovascular events (20). Insulin resistance and T2DM are known to compromise aortic elastic function. Although the precise underlying mechanisms remain unclear, it is known that prolonged exposure to elevated insulin levels can have direct and indirect trophic effects on smooth muscle cells (21), which contribute to increased arterial wall thickness, and hence to increased arterial stiffening. Furthermore, the formation of advanced glycation end products (AGEs) on vascular walls causes collagen cross-linking, leading to the loss of collagen and a subsequent reduction in arterial compliance.

Type 1 DM (T1DM) is also associated with end-organ damage in various organs. The arterial vessel wall also exhibits structural changes in patients with T1DM, which results in stiffening of the aortic wall (22). This stiffening occurs early in the diseases

process in T1DM and is already evident at a young age (23). In patients with T1DM, PWV is an independent predictor of cardiovascular morbidity (24,25) and mortality (26). Furthermore, aortic stiffness is also reported to be associated with systolic and diastolic left ventricular (LV) dysfunction (27,28).

Brain

Although DM is not primarily a brain disease, it is associated with cerebral atrophy, white matter hyperintensities and infarctions as well as decreased cognitive functioning (29-31). Various pathophysiological mechanisms have been suggested to contribute to the brain alterations in patients with DM. Both hyperglycemia and vascular complications have been proposed as underlying mechanisms in DM associated declined cognitive functioning and volume loss, but the pathogenesis is complex and incompletely understood (32-35). Aortic stiffening may play a central role in the development of brain injury (36). Previous studies have shown that aortic stiffness is a contributing factor in the development of generalized white matter atrophy in T1DM patients (37). Aortic stiffness may contribute to microvascular brain injury by exposing the small vessels to high pressure fluctuations in the cerebral circulation (38). The brain is particularly vulnerable to high pressure fluctuations, because it is perfused at high volume flow and has very low vascular resistance. In addition to white matter injury, T1DM is also associated with gray matter density changes in general (35) and focal cortical regions, the left thalamus (39,40) and the hippocampus (41,42). However, there are no data on the volumes of subcortical structures, including the basal ganglia and amygdala, in T1DM. Recent developments in magnetic resonance imaging (MRI) techniques enable a more in-depth investigation of brain damage in T1DM patients.

Caloric restriction

Lifestyle, and in particular dietary intervention, is the most powerful intervention to prevent and treat T2DM (43). Over 80% of T2DM patients are overweight or obese, and therefore weight loss remains the hallmark of their treatment. Weight loss in overweight/obese T2DM patients has several beneficial effects, including improved insulin sensitivity (44), improved diastolic cardiac function (45) and a less stiff aorta (46). Very low calorie diets (VLCD) can be used to induce substantial weight loss. Obese subjects lose on average 20 kg in 12 to 16 weeks.

As mentioned earlier, a major role in the pathogenesis of cardiovascular complications in T2DM is attributed to ectopic accumulation of TG in organs that normally do not store fat. This ectopic fat can be modulated by dietary interventions in healthy subjects (47) as well as in obese subjects (48-51). Prolonged caloric restriction in obese patients with T2DM without established coronary atherosclerosis leads to a decrease in

ectopic fat, including hepatic, myocardial and pericardial fat and improves myocardial function (45,52). Furthermore, in these obese T2DM patients a decrease in pericardial fat was observed immediately after the diet (52). However, long-term maintenance of weight loss is extremely difficult. Short-term dietary interventions can be sufficient to induce changes in cardiac function. For example, changes in cardiac diastolic function in healthy young males (53,54) have been reported after a 3-day high fat high caloric diet (HFHC) and after 3 days of caloric restriction. Short-term caloric restriction is therefore an attractive method to study the susceptibility of patients with DM to long term dietary interventions and may also be suitable for studying underlying mechanisms of ectopic fat accumulation and cardiovascular dysfunction in patients with obesity or DM, including the differential response between ethnicities.

Bariatric surgery results in sustained weight loss (55). Furthermore, bariatric surgery leads to diabetes remission in 70-80% of T2DM patients (56) and is associated with a decreased incidence of diabetes (57) and cardiovascular events (58), as well as a long-term reduction in overall mortality (59) in obese subjects. Bariatric surgery and the subsequent weight loss may be an alternative treatment for T2DM.

As described before, exogenous disruptors, such as cytotoxic chemotherapy, are associated with adverse metabolic and cardiovascular consequences. Treatment with cisplatin-based chemotherapy in testicular cancer (TC), for example, has been found to induce metabolic perturbations, such as changes in serum lipid levels (60). Additionally, 3 years after chemotherapy, higher incidences of hypercholesterolemia, hypertension, microalbuminuria, obesity, elevated insulin-glucose ratio, and even metabolic syndrome have been reported (13,61,62). The acute effects of chemotherapy, defined as effects occurring 3 months after the start of chemotherapy, on these risk factors are largely unknown. The aforementioned indirect risk factors are all independently associated with a higher risk of cardiovascular disease and may contribute to the overall increased risk of cardiovascular complications after treatment with cisplatin-based chemotherapy. The increased risk of cardiovascular disease in cured TC patients after cisplatin-based chemotherapy is probably a combination of direct toxic effects on the cardiovascular system and indirect effects of chemotherapy (13,63).

MR assessment techniques

MRI techniques are ideally suited for assessing various aspects of cardiovascular anatomy and systolic and diastolic cardiac function. MRI provides the gold standard for cardiac chamber volume assessment. As mentioned before, PWV is a surrogate marker for aortic stiffness. PWV is defined as the velocity of the systolic pulse wave front propagating through the aorta, which reflects the elastic properties of the aortic vessel wall. MRI in

combination with velocity-encoded MRI is a non-invasive, accurate, validated technique for measuring PWV globally and regionally in the aorta.

Ectopic fat can be visualized by magnetic resonance spectroscopy (^{1}H-MRS) and MRI (10,12,64,65). ^{1}H-MRS enables an accurate assessment of myocardial and hepatic TG. We used MRI to measure the abdominal and paracardial fat compartments. The use of MRI to measure paracardial fat with MRI is relatively new, and so far, no consensus has been reached on the ideal way to study this fat compartment with MRI. However, the method developed at our department has been shown to produce interesting and reproducible results.

The introduction of relatively new methods to investigate brain structure, volume and integrity enables the effects of diabetes on the brain to be explored in more detail. Diffusion Tensor Imaging (DTI) is used for measurement of white matter microstructure (66) and voxel-based morphometry (VBM) enables the identification of subtle gray matter alterations (67).

The field of MRI is developing rapidly, as higher magnetic field strengths continue to be implemented in human imaging. The 7 Tesla (T) MRI scanners might contribute to increasing image quality and more detailed assessment of end-organ damage. In the future, this could lead to earlier recognition and maybe even earlier treatment of end-organ damage in patients with DM. For example, high field imaging of the carotid vessel wall is an area of increasing development in MRI, driven by the continued clinical interest in non-invasive imaging modalities to assess the carotid artery vessel wall (68,69).

Given the promising results when previously carotid vessel wall imaging was compared between 1.5T and 3T (70), ultrahigh field 7T might offer great potential for carotid vessel wall imaging. However, as these imaging techniques must still be optimized, imaging at a high magnetic field strength remains, at present, beset by challenges.

OUTLINE OF THE THESIS

The aim of this thesis was to assess end-organ damage in individuals with metabolic syndrome and diabetes mellitus using MRI and ^{1}H-MRS. In addition, safety, feasibility and implementation of innovative MR techniques at higher field strengths for assessment of cardiovascular disease, were evaluated.

The first part of this thesis focuses on the end-organ damage in patients with T1DM studied with relatively new imaging methods.

Since aortic stiffness is an independent predictor of cardiovascular morbidity (24,25) and mortality (26), we investigated whether an increased aortic PWV, as assessed by MRI, is associated with subclinical LV diastolic dysfunction and decreased left atrial (LA) compliance, as assessed with speckle tracking strain analysis in patients with T1DM. Speckle tracking strain analysis allows the assessment of myocardial deformation providing useful parameters describing LV diastolic function and LA function (71-74). These relatively new indices are sensitive to early detection of subtle alterations in LV diastolic function and have described LV diastolic dysfunction at early stages of the disease process (75). The results of this study are described in **Chapter 2**.

Diffusion Tensor Imaging (DTI) is a validated brain imaging technique with MRI, which, in contrast to conventional methods, enables the measurement of white matter microstructure (66). In **Chapter 3,** we assessed a possible association between aortic PWV and brain white matter integrity assessed with DTI in patients with T1DM . Voxel-based morphometry (VBM) is a relatively novel and sophisticated analysis technique, which allows regional differences in brain volume to be tested for. VBM enables subtle gray matter alterations to be identified (67). As regional specific reductions in gray matter density in areas responsible for language processing and memory have been found in T1DM (39), we performed in-depth gray matter studies in patients with T1DM, using VBM. This study is described in **Chapter 4**.

Prolonged caloric restriction in obese patients with T2DM without established coronary atherosclerosis leads to a decrease in ectopic fat, including myocardial and pericardial fat, and improves myocardial function (45,52). Because of their increased cardiovascular risk, it is important to establish whether T2DM patients with a history of cardiac disease also benefit from prolonged caloric restriction. We therefore studied the effects of 16 weeks caloric restriction on ectopic fat accumulation and cardiovascular function in overweight patients with T2DM and coronary artery disease (CAD). In **Chapter 5,** the effects of a 16-week (V)LCD on cardiovascular function and ectopic fat depositions in overweight patients with CAD and T2DM are described.

Long-term maintenance of weight loss after a low caloric diet is challenging. Although bariatric surgery certainly results in sustained weight loss, it is largely unknown whether cardiac ectopic fat depots can also be mobilized by bariatric surgery in the same way or to the same extent as a 16-week VLCD was found to achieve (76). TG can be stored in the myocardium or in pericardial fat, the adipose tissue surrounding the heart. In **Chapter 6** the effects of bariatric surgery on pericardial ectopic fat depositions and cardiovascular function are studied.

In **Chapter 7,** we used MRI and ^{1}H-MRS techniques to determine whether differences in cardiac dimensions, cardiovascular function, and myocardial TG content are present between young, healthy South Asians and matched Caucasians. A short-term high fat diet has been shown to decrease diastolic function in healthy Caucasians (53). If the higher risk of CVD in South Asians is indeed related to a higher metabolic risk, the effects of a HFHC-diet on cardiovascular function might be stronger for this ethnic group. To assess whether possible functional differences can be attributed to alterations in metabolism and fat depositions in South Asians, we subjected 12 healthy lean South Asians and 12 matched Caucasians to a 5-day HFHC-diet. **Chapter 8** describes the effects of this 5-day HFHC-diet on insulin sensitivity in the participants.

Chapter 9 focuses on cardiovascular function in middle-aged overweight South Asians compared with Caucasians, and the response to short-term caloric restriction. To assess whether cardiovascular function in middle-aged overweight South Asians is impaired compared to Caucasians and whether metabolic and functional cardiovascular flexibility in response to caloric restriction is compromised in South Asians, we subjected middle-aged, overweight South Asians and age-, sex- and BMI-matched Caucasians to an 8-day VLCD.

Treatment of TC with cisplatin-based chemotherapy is associated with subacute changes in cardiac function (77,78), and with long-term cardiovascular disease (62,79). Because of the increasing number of survivors with a long life expectancy, gaining an understanding of and the prevention of short-term and long-term cardiovascular effects of chemotoxicity are of utmost importance. Little is known about the acute effects of cisplatin-based chemotherapy on metabolic parameters and cardiac function. Therefore we performed a study, described in **Chapter 10**, in which we assessed the acute changes in cardiac function and myocardial TG, in relation to body fat distribution and metabolic parameters 3 months after start with cisplatin-based chemotherapy.

The introduction of the ultrahigh field 7T MRI scanners is an exciting and promising development. However, many challenges must be overcome before 7T MRI can be

implemented in regular clinical care. Given the promising results previously seen in comparisons between carotid vessel wall imaging at 1.5T and at 3T magnetic field strengths (70), ultrahigh field 7T might offer great potential for carotid vessel wall imaging. However, only limited data are available on the feasibility of 7T carotid MRI. We therefore objectively compared quantitative parameters related to image quality of carotid vessel wall imaging performed at 7T and 3T, which is described in **Chapter 11**.

There is only limited data available on the feasibility of cardiovascular MRI in patients with cardiovascular disease at 7T. However, before clinical cardiovascular MRI at 7T can be performed, coronary stent safety has to be determined. The static magnetic field of the MR system exerts a force during patient positioning on ferromagnetic objects, possibly causing displacement of coronary artery stents. Furthermore, medical implants can potentially interact with the rapidly changing RF field, thereby inducing unwanted currents and heating of surrounding tissue. **Chapter 12** describes the data of the tested coronary stent safety at 7T MRI. Furthermore, the initial clinical feasibility of 7T cardiovascular MRI in healthy volunteers and patients with cardiovascular disease is demonstrated.

In **Chapter 13,** the results of the studies described in this thesis are summarized and discussed.

REFERENCES

1. Kelly T, Yang W, Chen CS, Reynolds K et al.: Global burden of obesity in 2005 and projections to 2030. *Int J Obes (Lond)* 32:1431-1437, 2008
2. Shaw JE, Sicree RA, Zimmet PZ: Global estimates of the prevalence of diabetes for 2010 and 2030. *Diabetes Res Clin Pract* 87:4-14, 2010
3. Wild S, Roglic G, Green A, Sicree R et al.: Global prevalence of diabetes: estimates for the year 2000 and projections for 2030. *Diabetes Care* 27:1047-1053, 2004
4. Whiting DR, Guariguata L, Weil C, Shaw J: IDF diabetes atlas: global estimates of the prevalence of diabetes for 2011 and 2030. *Diabetes Res Clin Pract* 94:311-321, 2011
5. Morrish NJ, Wang SL, Stevens LK, Fuller JH et al.: Mortality and causes of death in the WHO Multinational Study of Vascular Disease in Diabetes. *Diabetologia* 44 Suppl 2:S14-S21, 2001
6. Gastaldelli A, Cusi K, Pettiti M, Hardies J et al.: Relationship between hepatic/visceral fat and hepatic insulin resistance in nondiabetic and type 2 diabetic subjects. *Gastroenterology* 133:496-506, 2007
7. McGavock JM, Lingvay I, Zib I, Tillery T et al.: Cardiac steatosis in diabetes mellitus: a 1H-magnetic resonance spectroscopy study. *Circulation* 116:1170-1175, 2007
8. Teupe C, Rosak C: Diabetic cardiomyopathy and diastolic heart failure -- difficulties with relaxation. *Diabetes Res Clin Pract* 97:185-194, 2012
9. van de Weijer T, Schrauwen-Hinderling VB, Schrauwen P: Lipotoxicity in type 2 diabetic cardiomyopathy. *Cardiovasc Res* 92:10-18, 2011
10. van der Meer RW, Lamb HJ, Smit JW, de Roos A: MR imaging evaluation of cardiovascular risk in metabolic syndrome. *Radiology* 264:21-37, 2012
11. Greif M, Becker A, von ZF, Lebherz C et al.: Pericardial adipose tissue determined by dual source CT is a risk factor for coronary atherosclerosis. *Arterioscler Thromb Vasc Biol* 29:781-786, 2009
12. McGavock JM, Lingvay I, Zib I, Tillery T et al.: Cardiac Steatosis in Diabetes Mellitus: A 1H-Magnetic Resonance Spectroscopy Study. *Circulation* 116:1170-1175, 2007
13. Rijzewijk LJ, van der Meer RW, Smit JW, Diamant M et al.: Myocardial steatosis is an independent predictor of diastolic dysfunction in type 2 diabetes mellitus. *J Am Coll Cardiol* 52:1793-1799, 2008
14. Thanassoulis G, Massaro JM, Hoffmann U, Mahabadi AA et al.: Prevalence, distribution, and risk factor correlates of high pericardial and intrathoracic fat depots in the Framingham heart study. *Circ Cardiovasc Imaging* 3:559-566, 2010
15. Anand SS, Yusuf S, Vuksan V, Devanesen S et al.: Differences in risk factors, atherosclerosis, and cardiovascular disease between ethnic groups in Canada: the Study of Health Assessment and Risk in Ethnic groups (SHARE). *Lancet* 356:279-284, 2000
16. Joshi P, Islam S, Pais P, Reddy S et al.: Risk factors for early myocardial infarction in South Asians compared with individuals in other countries. *JAMA* 297:286-294, 2007
17. Enas EA, Yusuf S, Mehta JL: Prevalence of coronary artery disease in Asian Indians. *Am J Cardiol* 70:945-949, 1992
18. Balarajan R: Ethnic differences in mortality from ischaemic heart disease and cerebrovascular disease in England and Wales. *BMJ* 302:560-564, 1991
19. Chaturvedi N, Fuller JH: Ethnic differences in mortality from cardiovascular disease in the UK: do they persist in people with diabetes? *J Epidemiol Community Health* 50:137-139, 1996
20. Mitchell GF, Hwang SJ, Vasan RS, Larson MG et al.: Arterial stiffness and cardiovascular events: the Framingham Heart Study. *Circulation* 121:505-511, 2010

21. Stapleton PA, James ME, Goodwill AG, Frisbee JC: Obesity and vascular dysfunction. P*athophysiology* 15:79-89, 2008
22. Oxlund H, Rasmussen LM, Andreassen TT, Heickendorff L: Increased aortic stiffness in patients with type 1 (insulin-dependent) diabetes mellitus. *Diabetologia* 32:748-752, 1989
23. Urbina EM, Wadwa RP, Davis C, Snively BM et al.: Prevalence of increased arterial stiffness in children with type 1 diabetes mellitus differs by measurement site and sex: the SEARCH for Diabetes in Youth Study. *J Pediatr* 156:731-7, 737, 2010
24. Karamitsos TD, Karvounis HI, Didangelos TP, Papadopoulos CE et al.: Aortic elastic properties are related to left ventricular diastolic function in patients with type 1 diabetes mellitus. *Cardiology* 109:99-104, 2008
25. Schram MT, Chaturvedi N, Fuller JH, Stehouwer CD: Pulse pressure is associated with age and cardiovascular disease in type 1 diabetes: the Eurodiab Prospective Complications Study. *J Hypertens* 21:2035-2044, 2003
26. Cruickshank K, Riste L, Anderson SG, Wright JS et al.: Aortic pulse-wave velocity and its relationship to mortality in diabetes and glucose intolerance: an integrated index of vascular function? *Circulation* 106:2085-2090, 2002
27. Abhayaratna WP, Srikusalanukul W, Budge MM: Aortic stiffness for the detection of preclinical left ventricular diastolic dysfunction: pulse wave velocity versus pulse pressure. *J Hypertens* 26:758-764, 2008
28. van Elderen SG, Brandts A, Westenberg JJ, van der Grond J et al.: Aortic stiffness is associated with cardiac function and cerebral small vessel disease in patients with type 1 diabetes mellitus: assessment by magnetic resonance imaging. *Eur Radiol* 20:1132-1138, 2010
29. Biessels GJ, Staekenborg S, Brunner E, Brayne C et al.: Risk of dementia in diabetes mellitus: a systematic review. *Lancet Neurol* 5:64-74, 2006
30. Gouw AA, van der Flier WM, Fazekas F, van Straaten EC et al.: Progression of white matter hyperintensities and incidence of new lacunes over a 3-year period: the Leukoaraiosis and Disability study. *Stroke* 39:1414-1420, 2008
31. Knopman DS, Mosley TH, Catellier DJ, Sharrett AR: Cardiovascular risk factors and cerebral atrophy in a middle-aged cohort. *Neurology* 65:876-881, 2005
32. Manolio TA, Kronmal RA, Burke GL, Poirier V et al.: Magnetic resonance abnormalities and cardiovascular disease in older adults. The Cardiovascular Health Study. *Stroke* 25:318-327, 1994
33. DeCarli C, Miller BL, Swan GE, Reed T et al.: Predictors of brain morphology for the men of the NHLBI twin study. *Stroke* 30:529-536, 1999
34. McCrimmon RJ, Ryan CM, Frier BM: Diabetes and cognitive dysfunction. *Lancet* 379:2291-2299, 2012
35. van Elderen SG, Brandts A, van der Grond J, Westenberg JJ et al.: Cerebral perfusion and aortic stiffness are independent predictors of white matter brain atrophy in type 1 diabetic patients assessed with magnetic resonance imaging. *Diabetes Care* 34:459-463, 2011
36. van Elderen SG, Brandts A, Westenberg JJ, van der Grond J et al.: Aortic stiffness is associated with cardiac function and cerebral small vessel disease in patients with type 1 diabetes mellitus: assessment by magnetic resonance imaging. *Eur Radiol* 20:1132-1138, 2010
37. van Elderen SG, Brandts A, van der Grond J, Westenberg JJ et al.: Cerebral perfusion and aortic stiffness are independent predictors of white matter brain atrophy in type 1 diabetic patients assessed with magnetic resonance imaging. *Diabetes Care* 34:459-463, 2011

38. O'Rourke MF, Safar ME: Relationship between aortic stiffening and microvascular disease in brain and kidney: cause and logic of therapy. *Hypertension* 46:200-204, 2005
39. Musen G, Lyoo IK, Sparks CR, Weinger K et al.: Effects of type 1 diabetes on gray matter density as measured by voxel-based morphometry. *Diabetes* 55:326-333, 2006
40. Wessels AM, Simsek S, Remijnse PL, Veltman DJ et al.: Voxel-based morphometry demonstrates reduced grey matter density on brain MRI in patients with diabetic retinopathy. *Diabetologia* 49:2474-2480, 2006
41. Hershey T, Perantie DC, Wu J, Weaver PM et al.: Hippocampal volumes in youth with type 1 diabetes. *Diabetes* 59:236-241, 2010
42. Lobnig BM, Kromeke O, Optenhostert-Porst C, Wolf OT: Hippocampal volume and cognitive performance in long-standing Type 1 diabetic patients without macrovascular complications. *Diabet Med* 23:32-39, 2006
43. The Diabetes Prevention Program (DPP): description of lifestyle intervention. *Diabetes Care* 25:2165-2171, 2002
44. Jazet IM, Schaart G, Gastaldelli A, Ferrannini E et al.: Loss of 50% of excess weight using a very low energy diet improves insulin-stimulated glucose disposal and skeletal muscle insulin signalling in obese insulin-treated type 2 diabetic patients. *Diabetologia* 51:309-319, 2008
45. Hammer S, Snel M, Lamb HJ, Jazet IM et al.: Prolonged caloric restriction in obese patients with type 2 diabetes mellitus decreases myocardial triglyceride content and improves myocardial function. *J Am Coll Cardiol* 52:1006-1012, 2008
46. Barinas-Mitchell E, Kuller LH, Sutton-Tyrrell K, Hegazi R et al.: Effect of weight loss and nutritional intervention on arterial stiffness in type 2 diabetes. *Diabetes Care* 29:2218-2222, 2006
47. Hammer S, van der Meer RW, Lamb HJ, Schar M et al.: Progressive caloric restriction induces dose-dependent changes in myocardial triglyceride content and diastolic function in healthy men. *J Clin Endocrinol Metab* 93:497-503, 2008
48. Bosy-Westphal A, Kossel E, Goele K, Blocker T et al.: Association of pericardial fat with liver fat and insulin sensitivity after diet-induced weight loss in overweight women. *Obesity (Silver Spring)* 18:2111-2117, 2010
49. Iacobellis G, Singh N, Wharton S, Sharma AM: Substantial changes in epicardial fat thickness after weight loss in severely obese subjects. *Obesity (Silver Spring)* 16:1693-1697, 2008
50. Kim MK, Tanaka K, Kim MJ, Matuso T et al.: Comparison of epicardial, abdominal and regional fat compartments in response to weight loss. *Nutr Metab Cardiovasc Dis* 19:760-766, 2009
51. Viljanen APM, Karmi A, Borra R, P+ñrkk+ñ JP et al.: Effect of Caloric Restriction on Myocardial Fatty Acid Uptake, Left Ventricular Mass, and Cardiac Work in Obese Adults. *The American Journal of Cardiology* 103:1721-1726, 2009
52. Snel M, Jonker JT, Hammer S, Kerpershoek G et al.: Long-term beneficial effect of a 16-week very low calorie diet on pericardial fat in obese type 2 diabetes mellitus patients. *Obesity (Silver Spring)* 20:1572-1576, 2012
53. van der Meer RW, Hammer S, Lamb HJ, Frolich M et al.: Effects of short-term high-fat, high-energy diet on hepatic and myocardial triglyceride content in healthy men. *J Clin Endocrinol Metab* 93:2702-2708, 2008
54. van der Meer RW, Hammer S, Smit JW, Frolich M et al.: Short-term caloric restriction induces accumulation of myocardial triglycerides and decreases left ventricular diastolic function in healthy subjects. *Diabetes* 56:2849-2853, 2007

55. Sjostrom L: Review of the key results from the Swedish Obese Subjects (SOS) trial: a prospective controlled intervention study of bariatric surgery. *J Intern Med* 2012
56. Sjostrom L, Lindroos AK, Peltonen M, Torgerson J et al.: Lifestyle, diabetes, and cardiovascular risk factors 10 years after bariatric surgery. *N Engl J Med* 351:2683-2693, 2004
57. Carlsson LM, Peltonen M, Ahlin S, Anveden A et al.: Bariatric surgery and prevention of type 2 diabetes in Swedish obese subjects. *N Engl J Med* 367:695-704, 2012
58. Romeo S, Maglio C, Burza MA, Pirazzi C et al.: Cardiovascular events after bariatric surgery in obese subjects with type 2 diabetes. *Diabetes Care* 35:2613-2617, 2012
59. Sjostrom L, Narbro K, Sjostrom CD, Karason K et al.: Effects of bariatric surgery on mortality in Swedish obese subjects. *N Engl J Med* 357:741-752, 2007
60. Raghavan D, Cox K, Childs A, Grygiel J et al.: Hypercholesterolemia after chemotherapy for testis cancer. *J Clin Oncol* 10:1386-1389, 1992
61. Katz A, Nambi SS, Mather K, Baron AD et al.: Quantitative insulin sensitivity check index: a simple, accurate method for assessing insulin sensitivity in humans. *J Clin Endocrinol Metab* 85:2402-2410, 2000
62. Nuver J, de Haas EC, Van ZM, Gietema JA et al.: Vascular damage in testicular cancer patients: a study on endothelial activation by bleomycin and cisplatin in vitro. *Oncol Re*p 23:247-253, 2010
63. Lamb HJ, Doornbos J, van der Velde EA, Kruit MC et al.: Echo planar MRI of the heart on a standard system: validation of measurements of left ventricular function and mass. *J Comput Assist Tomogr* 20:942-949, 1996
64. Nelson AJ, Worthley MI, Psaltis PJ, Carbone A et al.: Validation of cardiovascular magnetic resonance assessment of pericardial adipose tissue volume. *J Cardiovasc Magn Reson* 11:15, 2009
65. Sacks HS, Fain JN: Human epicardial adipose tissue: a review. *Am Heart J* 153:907-917, 2007
66. Kodl CT, Franc DT, Rao JP, Anderson FS et al.: Diffusion tensor imaging identifies deficits in white matter microstructure in subjects with type 1 diabetes that correlate with reduced neurocognitive function. *Diabetes* 57:3083-3089, 2008
67. Ashburner J, Friston KJ: Voxel-based morphometry--the methods. *Neuroimage* 11:805-821, 2000
68. Yuan C, Mitsumori LM, Ferguson MS, Polissar NL et al.: In vivo accuracy of multispectral magnetic resonance imaging for identifying lipid-rich necrotic cores and intraplaque hemorrhage in advanced human carotid plaques. *Circulation* 104:2051-2056, 2001
69. Yuan C, Zhang SX, Polissar NL, Echelard D et al.: Identification of fibrous cap rupture with magnetic resonance imaging is highly associated with recent transient ischemic attack or stroke. *Circulation* 105:181-185, 2002
70. Yarnykh VL, Terashima M, Hayes CE, Shimakawa A et al.: Multicontrast black-blood MRI of carotid arteries: comparison between 1.5 and 3 tesla magnetic field strengths. *J Magn Reson Imaging* 23:691-698, 2006
71. Kim DG, Lee KJ, Lee S, Jeong SY et al.: Feasibility of two-dimensional global longitudinal strain and strain rate imaging for the assessment of left atrial function: a study in subjects with a low probability of cardiovascular disease and normal exercise capacity. *Echocardiography* 26:1179-1187, 2009
72. Reisner SA, Lysyansky P, Agmon Y, Mutlak D et al.: Global longitudinal strain: a novel index of left ventricular systolic function. *J Am Soc Echocardiogr* 17:630-633, 2004

73. Saraiva RM, Demirkol S, Buakhamsri A, Greenberg N et al.: Left atrial strain measured by two-dimensional speckle tracking represents a new tool to evaluate left atrial function. *J Am Soc Echocardiogr* 23:172-180, 2010
74. Vianna-Pinton R, Moreno CA, Baxter CM, Lee KS et al.: Two-dimensional speckle-tracking echocardiography of the left atrium: feasibility and regional contraction and relaxation differences in normal subjects. *J Am Soc Echocardiogr* 22:299-305, 2009
75. Ng AC, Delgado V, Bertini M, van der Meer RW et al.: Findings from left ventricular strain and strain rate imaging in asymptomatic patients with type 2 diabetes mellitus. *Am J Cardiol* 104:1398-1401, 2009
76. Snel M, Jonker JT, Hammer S, Kerpershoek G et al.: Long-term beneficial effect of a 16-week very low calorie diet on pericardial fat in obese type 2 diabetes mellitus patients. *Obesity (Silver Spring)* 20:1572-1576, 2012
77. Altena R, de Haas EC, Nuver J, Brouwer CA et al.: Evaluation of sub-acute changes in cardiac function after cisplatin-based combination chemotherapy for testicular cancer. *Br J Cancer* 100:1861-1866, 2009
78. Stefenelli T, Kuzmits R, Ulrich W, Glogar D: Acute vascular toxicity after combination chemotherapy with cisplatin, vinblastine, and bleomycin for testicular cancer. *Eur Heart J* 9:552-556, 1988
79. Montiel M, Urso L, de la Blanca EP, Marsigliante S et al.: Cisplatin reduces endothelial cell migration via regulation of type 2-matrix metalloproteinase activity. *Cell Physiol Biochem* 23:441-448, 2009

Chapter 2

Aortic stiffness is related to left ventricular diastolic function in patients with diabetes mellitus type 1: assessment with MRI and speckle tracking strain analysis

Linda D. van Schinkel, Dominique Auger, Saskia G.C. van Elderen, Nina Ajmone Marsan, Victoria Delgado, Hildo J. Lamb, Arnold C.T. Ng, Johannes W.A. Smit, Jeroen J. Bax, Jos J.M. Westenberg, Albert de Roos

International Journal of Cardiovascular Imaging 2013; 29: 633-641

ABSTRACT

Background

Diabetes mellitus type 1 (T1DM) is associated with aortic stiffening and left ventricular (LV) diastolic dysfunction, but the relationship with LV diastolic dysfunction in T1DM patients is still largely unknown. The purpose of this study was to evaluate whether an increased aortic stiffness, expressed by increased aortic pulse wave velocity (PWV), is associated with subclinical LV diastolic dysfunction and decreased left atrial (LA) compliance as assessed with speckle tracking strain analysis in patients with T1DM.

Methods

Aortic PWV was assessed with cardiovascular magnetic resonance imaging (MRI) in 41 T1DM patients. Patients underwent echocardiography for assessment of conventional LV diastolic function indices and LV and LA longitudinal strain and strain rate were assessed with speckle tracking strain analysis. LV strain rate during the isovolumic relaxation period (SRIVR) and LA strain were recorded and the E-wave velocity to SRIVR velocity ratio (E/SRIVR) was calculated. Independent samples t-test and multivariate linear regression analyses were used for statistical analyses.

Results

Aortic PWV significantly correlated with SRIVR (β=-0.71, $p<0.001$), E/SRIVR (β=0.61, $p=0.002$) and LA strain (β=-0.47, $p=0.014$), but not with conventional echocardiographic markers of diastolic function (all $p>0.10$).

Conclusions

In T1DM patients, aortic stiffness is inversely associated with sensitive markers of LV diastolic function and decrease in LA compliance as measured with echocardiographic speckle tracking strain analysis.

INTRODUCTION

Diabetes mellitus (DM) is a chronic disease, which leads to microvascular and macrovascular complications. The arterial vessel wall reveals structural changes in patients with DM which results in stiffening of the arterial vasculature, including the aortic wall (1). This stiffening occurs early in the disease process in type 1 DM (T1DM) and is even evident at a young age (2). In patients with T1DM, the pulse wave velocity (PWV), a surrogate marker of aortic stiffness as measured by means of ultrasonography or cardiovascular magnetic resonance imaging (MRI), is an independent predictor of cardiovascular morbidity (3,4) and mortality (5). Furthermore, aortic stiffness has been described to be associated with systolic and diastolic left ventricular (LV) dysfunction (6,7).

MRI techniques are well suited for assessing various aspects of cardiovascular function. MRI provides the gold standard for cardiac chamber volume assessment. MRI in combination with velocity-encoded MRI is a non-invasive validated technique for measuring PWV globally and regionally in the aorta by using the transit-time method (8). Furthermore, recent developments in speckle tracking strain analysis have permitted the assessment of myocardial deformation providing useful parameters describing LV diastolic function and left atrial (LA) function (9-12). These new indices are sensitive to early detection of subtle alterations in LV diastolic function and have described LV diastolic dysfunction at early stages of the disease process (13).

Therefore, our hypothesis is that an increase in aortic PWV in T1DM patients is associated with early alterations in sensitive markers of LV diastolic function and with a decrease in LA compliance. To our knowledge, no previous study has evaluated the relationship between aortic PWV assessed with MRI and LV diastolic function parameters assessed with speckle tracking strain analysis. Accordingly, the purpose of this study was to evaluate whether increased aortic stiffness, expressed as an increased aortic PWV, is associated with subclinical LV diastolic dysfunction and decreased LA compliance as assessed with speckle tracking strain analysis in T1DM patients.

METHODS

Subjects

This study was approved by the local medical ethics committee and the study was conducted according to the principles in the Declaration of Helsinki. All subjects gave informed consent.

Consecutive patients with T1DM were recruited from the local outpatient clinic. All subjects were within the age range of 30-80 years and underwent MRI imaging between

February 2008 and January 2010. Forty-one patients with T1DM were included in the study (25 men and 16 women; mean age ± standard deviation 50 ± 9 years).

Exclusion criteria for the patients with T1DM were congenital aortic/heart disease, known history of cardiovascular disease, evidence of aortic valve stenosis or insufficiency and general contraindications to MRI. This patient group was partly included in a previous study describing an association between aortic stiffness and systolic LV function in patients with T1DM (7).

T1DM is defined as fasting blood glucose ≥ 7.0 mmol/l according to WHO criteria (14). The duration of DM was calculated as the time (in years) between the reported age of diagnosis and the MRI examination. Heart rate and blood pressure were measured using a semiautomated sphygmomanometer (Dinamap, Critikon, Tampa, Fla, USA). Mean arterial pressure (MAP) was calculated by adding one-third of the pulse pressure to diastolic blood pressure. Body mass index, smoking status (nonsmoker or current smoker) and glycated hemoglobin (HbA1c) were determined. All patients underwent MRI evaluation and transthoracic echocardiography including speckle tracking strain analysis. Furthermore, all patients were in sinus rhythm and had adequate echocardiographic image quality for speckle tracking analysis.

MR imaging protocol

MRI was performed on a 1.5T MRI scanner (NT 15 Gyroscan Intera; Philips Medical Systems, Best, the Netherlands). The aorta was imaged in a double-oblique parasagittal scout view. Aortic PWV was assessed using the transit-time method as previously described (8) from two consecutive one-directional through-plane velocity-encoded MRI acquisitions with high-temporal resolution performed in the ascending aorta at the level of the pulmonary trunk and 7.5 cm beneath the diaphragm in the abdominal aorta (Figure 1, left panel). Scan parameters were: TR 5.0ms, TE 2.9ms, flip angle 20°, FOV 300mm, 128×115 acquisition matrix, slice thickness 8mm, with maximal number of phases reconstructed ensuring high (6-10ms) effective temporal resolution. True temporal resolution is defined as 2 times TR = 10ms.

Flow rate-graphs were determined by automated contour segmentation on the velocity maps using the in-house developed FLOW software package (Figure 1, right panel). Pixelwise integration of the aortic velocity over the lumen area of the aorta results in the flow rate per cardiac phase. Propagation of the systolic flow wave front (which defines the PWV) was determined by the transit-time between the two measurement sites, as shown in Figure 1. This transit-time is determined by the time difference in the arrival of the systolic flow wave front at each measuring site, which is automatically assessed by the intersection of the horizontal diastolic flow and the upslope of the flow wave, modeled by linear regression of all data points between 20% and 80% of the range of flow values

along the slope. The distance between the two measurement sites was manually determined by drawing a poly-line in the center of the aorta as defined in a double-oblique parasagittal aortic scout view, using the in-house developed software package MASS. The acquisition time amounted to approximately 4 min per plane at a heart rate of 60 beats per minute. Due to the automated contour detection in the velocity maps and the automated transit-time detection from the flow graphs, image analysis per patients was under 5 minutes for an experienced user.

To determine LV volumes, function and mass, the LV was imaged in short-axis orientation in 10-12 consecutive slices, by using electrocardiographically gated breath-hold segmented cine fast gradient-echo imaging with steady-state free-precession as previously described (15). Imaging parameters were: TR 3.3ms, TE 1.7ms, flip angle 35°, FOV 400×320mm, and slice thickness 10mm. Using software package MASS, endocardial and epicardial LV contours were manually drawn in the end-systolic and end-diastolic phases of the short-axis data. Left ventricular ejection fraction (LVEF), stroke volume (SV), LV end-diastolic volume (LVEDV), LV end-systolic volume (LVESV) and LV end-diastolic mass (LVED mass) were assessed. Volumes and mass were indexed (i) for body surface area (BSA, calculated according to the Mosteller formula).

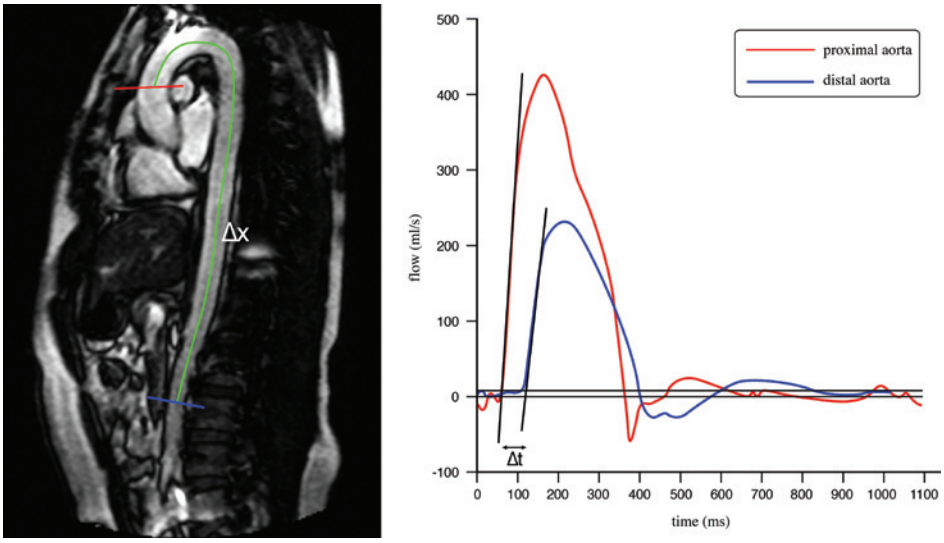

Figure 1. Aortic PWV determination with MRI**.** The left panel shows a double-oblique parasagittal image of the aorta. The red and blue lines represent the acquisition planes for velocity-encoded MRI which are positioned perpendicular to the aorta. Δx = the path length of the aorta determined along the centerline of the aorta. The right panel shows the flow rate-time curves for the proximal and distal aorta. Δt = transit-time between time-of-arrival of flow wave in the proximal and distal aorta, respectively. Aortic PWV is defined as Δx/Δt (in m/s).

Echocardiography

Transthoracic echocardiography was performed in the left lateral decubitus position using a commercially available ultrasound transducer and equipment (M4S probe, Vivid 7, GE-Vingmed, Horten, Norway). All images were analyzed off-line with Echo Pac version 110.0.0 (GE-Vingmed).

Conventional parameters of LV diastolic function

Several parameters of LV diastolic function were assessed by conventional echocardiography. Trans-mitral diastolic early wave (E) velocity, E-wave deceleration time (DT) and late diastolic wave (A) velocity were measured by applying pulsed-wave Doppler at the tip of the mitral leaflets in the apical 4-chamber view (16). Isovolumic relaxation time (IVRT) was assessed from the apical 5-chamber view, using continuous-wave Doppler with the sample volume positioned in the LV out-flow tract, at the level of the mitral valve (16). Tissue Doppler imaging (TDI) was recorded with high frame rate (≥100 frames/second) from the apical 4-chamber view to assess myocardial velocities. Peak annular early diastolic velocity (E´) was measured in 2 basal LV segments (septal and lateral) and averaged to calculate the mean early diastolic velocity (E´mean). The ratio of peak trans-mitral E-wave to E´mean (E/E´mean) was calculated, as a validated estimate of LV filling pressure (17).

In addition, maximal LA volume was calculated according to the American Society of Echocardiography guidelines, at end-systole, just before mitral valve opening, and was indexed to body surface area (18). Based on current recommendations (16), LV diastolic dysfunction was graded as follows: normal, grade I, grade II and grade III.

LV diastolic function indices by speckle tracking strain analysis

Measures of LV diastolic function were obtained with two-dimensional (2D) speckle tracking strain and strain rate (SR) analysis. Strain rate during isovolumic relaxation period (SRIVR) was measured as previously described (19). SRIVR is a load- and angle-independent parameter that is strongly related to LV relaxation (20). Briefly, the endocardial border was manually traced on LV apical 4-, 2-, and 3-chamber views and the region of interest width was adjusted to include the entire myocardium. Longitudinal SR-values over the cardiac cycle were automatically obtained for each apical view. The peak SR-value during LV isovolumic relaxation was measured and averaged from the 3 apical views (Figure 2) (19). The ratio of peak trans-mitral E-wave to SRIVR (E/SRIVR) was calculated as an index of LV filling pressures (20). LA peak strain was measured during LV systole as an index of LA compliance (9,21). For this measure, LA endocardial border was identified in the apical 4-chamber view and a region of interest was adjusted to include the entire LA wall. LA strain curves over the cardiac cycle were generated. The peak LA positive strain during ventricular systole (LAs) was subsequently measured (Figure 2) (9).

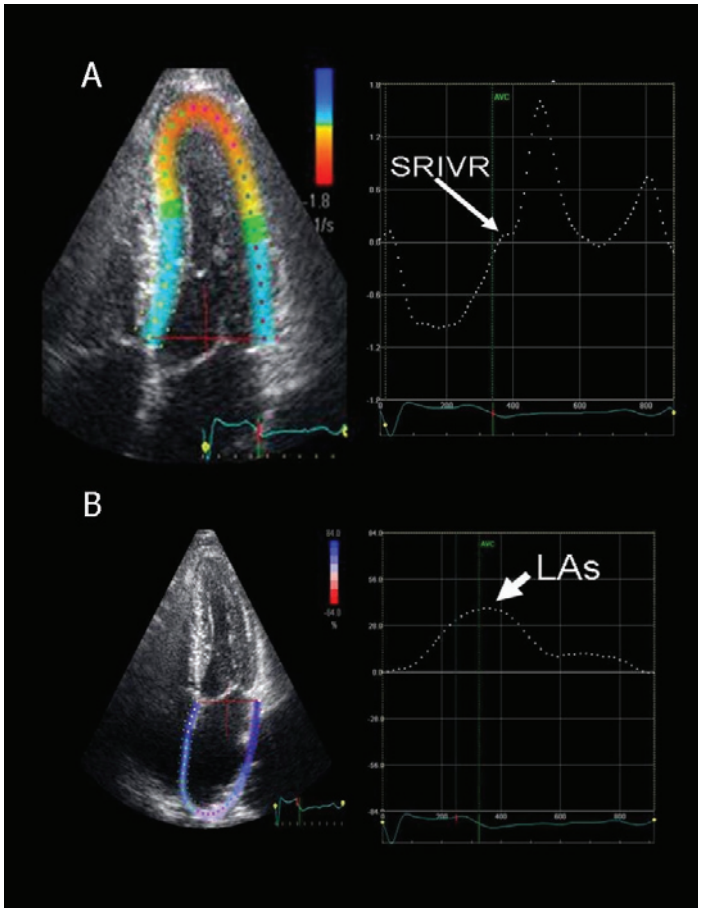

Figure 2. Parameters of LV diastolic function and LA compliance. The evaluation of peak strain rate during left ventricular isovolumic relaxation period (SRIVR) from the apical 4-chamber view is displayed in panel A. A region of interest which includes the entire left ventricular wall is first obtained. The software consequently displays the changes in longitudinal strain rate over the cardiac cycle. Left ventricular isovolumic relaxation occurs in diastole, starting immediately after the aortic valve closure and terminating with the beginning of the diastolic early (E) wave. The peak strain rate value during isovolumic relaxation period (SRIVR) is consequently measured. The assessment of left atrial peak systolic strain (LAs) is shown in panel B.

Statistical analysis

Statistical analysis was performed with SPSS (SPSS, Chicago, Illinois, USA), version 17. Data are expressed as mean ± standard deviation (sd), unless stated otherwise. Categorical variables were presented as frequencies and percentages. Multivariate linear regression analyses were performed to analyze the association between aortic PWV and the

echocardiographic parameters, adjusted for the confounding factors age, gender and MAP. The β-regression coefficients and p-values are reported. Significance was reached when $p<0.05$ (two-tailed).

Besides evaluating associations between aortic PWV and echocardiographic parameters, patients were also classified according to their age-related PWV. Normal values for age-related PWV were taken from a study by Westenberg et al. (22), in which linear regression was performed for PWV vs. age-relation, using the same imaging technique as in the current study: PWV=A×AGE+B, with A ± standard error (SE)=0.07 ± 0.01m/s/year and B ± SE=2.32 ± 0.23m/s (Pearson R=0.93 ($p<0.001$)). PWV as assessed in the patients in the current study was classified as normal if PWV≤2×SE of normal age-related PWV or increased if PWV >2×SE of normal age-related PWV. Between-group differences concerning classified aortic PWV and continuous variables were calculated using independent samples t-test. The chi-square test was used to calculate the difference in categorical variables between groups.

RESULTS

Twenty-four (59%) of the patients with T1DM were on antihypertensive treatment, consisting of ACE inhibitors, β blockers, calcium antagonists, diuretics, angiotensin II inhibitors or a combination of the aforementioned medications. Retinopathy, mostly minimal background retinopathy, was present in 32 (78%) of the patients. Only 5 (12%) patients had nephropathy. Table 1 describes the clinical characteristics of the total study population and per subgroup, classified according to normal (n=28) versus increased PWV (n=13). There were no significant differences between both groups: no differences in age, T1DM duration or blood pressure were shown.

The associations between aortic PWV and MRI and echocardiographic parameters are shown in Table 2. After adjustments for age, gender and MAP, multivariate linear regression analysis showed that aortic PWV was significantly correlated with SRIVR (β=-0.71, $p<0.001$), E/SRIVR (β=0.61, p=0.002) and LA strain (β=-0.47, p=0.014). The significant correlations are shown in Figure 3.

The mean aortic PWV in the subgroup with normal PWV was 6.0 ± 0.8m/s and in the group with increased PWV 9.9 ± 2.1m/s. Mean values of echocardiographic parameters between both subgroups are displayed in Table 3. Among the conventional echocardiographic parameters of LV function, the E/A-ratio was the only statistically different parameter between both subgroups. In contrast, all indices of LV diastolic function assessed by speckle tracking (SRIVR, E/SRIVR and LA strain) were statistically significant different between subgroups with normal versus increased PWV.

Table 1. Patient characteristics

Patient Characteristics	Total population (n=41)	Normal PWV (n=28)	Increased PWV (n=13)	p-value
Male gender, n (%)	25 (61)	17 (61)	8 (62)	0.960
Age (years)	49.9 ± 9.0	48.9 ± 8.4	52.1 ± 10.1	0.288
Diabetes duration (years)	26.2 ± 13.5	26.2 ± 13.6	26.3 ± 14.0	0.984
BMI (kg/m^2)	26.4 ± 3.2	25.9 ± 2.7	27.7 ± 3.8	0.098
Systolic blood pressure (mmHg)	138 ± 20	135 ± 19	146 ± 20	0.094
Diastolic blood pressure (mmHg)	76 ± 10	75 ± 10	77 ± 10	0.508
Mean arterial pressure (mmHg)	96 ± 11	95 ± 10	100 ± 13	0.164
Heart rate (beats/min)	67 ± 11	67 ± 11	66 ± 13	0.793
Current smokers, n (%)	8 (20)	6 (21)	2 (15)	0.650
On antihypertensive treatment	24 (59)	15 (54)	9 (69)	0.344
ACE inhibitors	11 (27)	6 (21.4)	5 (41.7)	0.189
β blockers	5 (12)	1 (3.6)	4 (30.8)	0.013*
Calcium antagonists	2 (5)	2 (7.1)	0 (0)	0.323
Diuretics	10 (24)	6 (21.4)	4 (30.8)	0.517
Angiotensin II inhibitors	11 (27)	8 (28.6)	3 (23.1)	0.712
HbA1c (%)	7.9 ± 1.1	7.8 ± 1.1	8.0 ± 1.1	0.658

Data are presented as mean ± standard deviations or n (%). BMI: body mass index, HbA1c: glycated hemoglobin.

Table 2. Association between aortic PWV and MRI and echocardiographic parameters

		PWV	
	mean ± sd	β	p-value
MRI parameters			
LVEF (%)	59.0 ± 6.1	-0.35	0.067
LVSV (i) (ml/m^2)	45.8 ± 7.9	-0.22	0.253
LVEDV (i) (ml/m^2)	77.7 ± 10.6	-0.41	0.820
LVESV (i) (ml/m^2)	31.9 ± 6.3	0.20	0.265
LVED mass (i) (g/m^2)	50.5 ± 9.4	-0.01	0.955
Conventional echocardiographic parameters			
LA volume (i) (ml/m^2)	22.2 ± 6.0	-0.02	0.942
IVRT (ms)	83.0 ± 18.3	0.33	0.101
E/A	1.13 ± 0.37	-0.21	0.275
DT (ms)	249.9 ± 73,9	-0.05	0.798
E´ (cm/s)	8.0 ± 2.2	-0.14	0.379
E/E´mean	9.53 ± 2.62	0.01	0.957
Speckle tracking parameters			
SRIVR (1/s)	0.49 ± 0.20	-0.71	<0.001*
E/SRIVR (cm)	175.6 ± 83.6	0.61	0.002*
LA strain (%)	35.9 ± 6.9	-0.47	0.014*

Data are presented as mean ± standard deviations (sd). β regression coefficients (β) and p-values are reported for the association with aortic PWV in multivariate analysis with the confounders age, gender and mean arterial pressure. PWV: pulse wave velocity, LVEF: left ventricular ejection fraction, LVSV: left ventricular stroke volume, LVEDV: left ventricular end-diastolic volume, LVESV: left ventricular end -systolic volume, LA: left atrial, IVRT: isovolumic relaxation time, E: Trans-mitral diastolic early wave, A: late diastolic wave, DT: E-wave deceleration time; E´: peak early diastolic velocity, SRIVR: strain rate during isovolumic relaxation period. i: indexed for body surface area. *p-value <0.05.

Table 3. MRI and echocardiographic parameters between PWV-groups

	Normal PWV (n=28)	Increased PWV (n=13)	p-value
MRI parameters			
LVEF (%)	60.2 ± 5.7	56.4 ± 6.5	0.068
LVSV (i) (ml/m^2)	46.9 ± 7.6	43.5 ± 8.4	0.205
LVEDV (i) (ml/m^2)	78.0 ± 11.1	76.9 ± 9.8	0.745
LVESV (i) (ml/m^2)	31.2 ± 6.6	33.3 ± 5.5	0.300
LVED mass (i) (g/m^2)	49.9 ± 8.2	51.8 ± 11.8	0.564
Conventional echocardiographic parameters			
LA volume (i) (ml/m^2)	21.6 ± 5.3	23.5 ± 7.4	0.350
IVRT (ms)	80.7 ± 14.7	87.9 ± 24.3	0.251
E/A	1.21 ± 0.38	0.95 ± 0.31	0.043*
DT (ms)	246.5 ± 67.9	257.3 ± 88.0	0.668
E´ (cm/s)	8.5 ± 1.9	7.1 ± 2.5	0.065
E/E´mean	9.21 ± 2.08	10.21 ± 3.52	0.350
Diastolic grade			
Normal, n (%)	17 (60.7)	5 (38.5)	0.165
Grade I, n (%)	9 (32.1)	8 (61.5)	
Grade II, n (%)	2 (7.1)	0 (0)	
SRIVR (1/s)	0.59 ± 0.15	0.28 ± 0.10	<0.001*
E/SRIVR (cm)	136.6 ± 44.6	256.5 ± 90.6	<0.001*
LA strain (%)	38.4 ± 6.7	30.5 ± 3.5	<0.001*

Data are presented as mean ± standard deviations. PWV: pulse wave velocity, LVEF: left ventricular ejection fraction, LVSV: left ventricular stroke volume, LVEDV: left ventricular end-diastolic volume, LVESV: left ventricular end-systolic volume; LA: left atrial; IVRT: isovolumic relaxation time; E: Trans-mitral diastolic early wave, A: late diastolic wave, DT: E-wave deceleration time, E´: peak early diastolic velocity, SRIVR: strain rate during isovolumic relaxation period. *p-value <0.05.

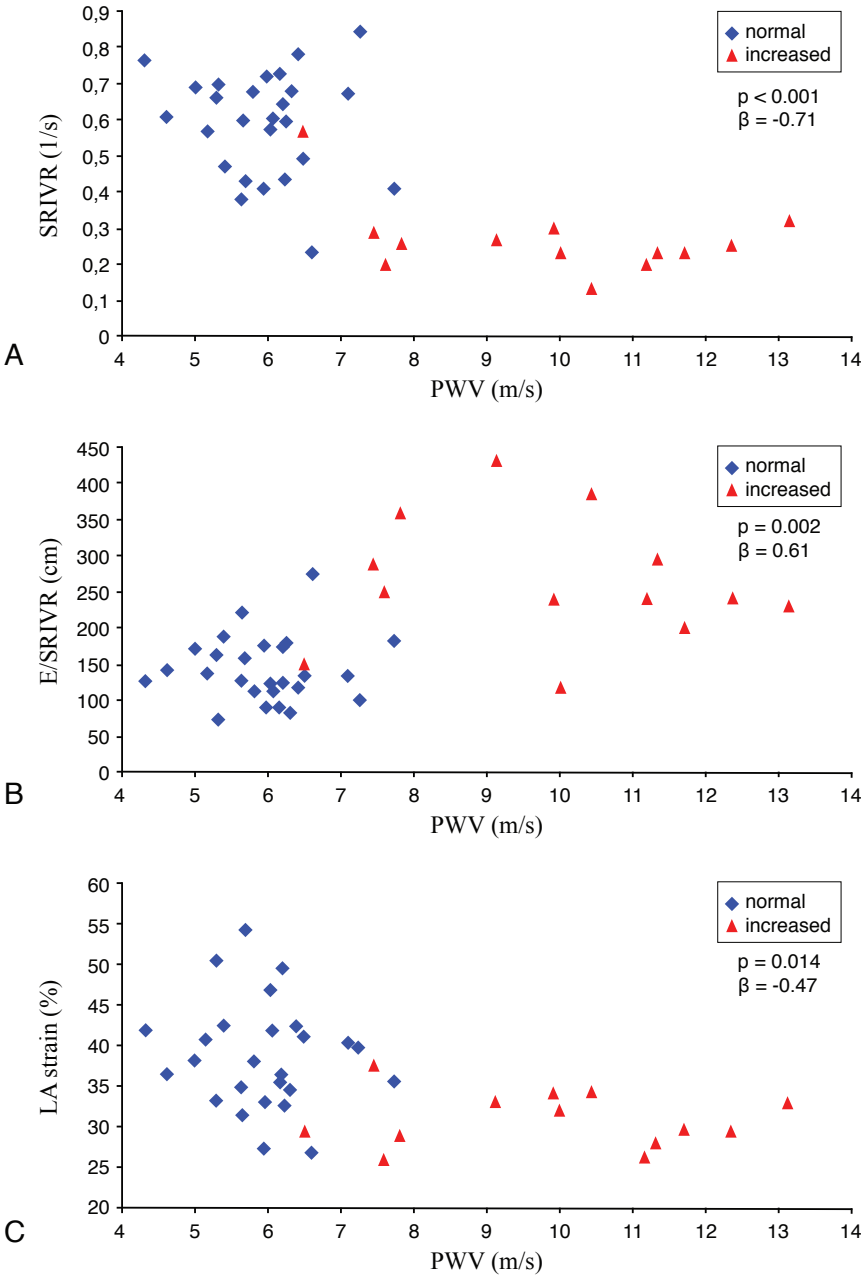

Figure 3. Correlations between pulse wave velocity (PWV) and the echocardiographic parameters. Panel A shows the correlation between PWV and strain rate during isovolumic relaxation period (SRIVR), panel B the correlation between PWV and E-wave velocity to SRIVR velocity ratio (E/SRIVR), panel C the correlation between PWV and left atrial strain (LA strain). Blue squares represent patients with normal age-related PWV and red triangles represent patients with increased age-related PWV.

DISCUSSION

The main findings of our study are: first, aortic PWV varied from normal to increased in T1DM patients with similar clinical characteristics. Secondly, a strong correlation was found between aortic PWV and LV diastolic function parameters as well as LA strain as assessed by speckle tracking strain analysis, irrespective of age.

Aortic PWV is a surrogate marker of vascular stiffness (23), which has been identified as a strong predictor of cardiovascular events and all-cause mortality (24). The definition of normal values of aortic PWV is challenging since the ageing process should be taken into consideration. Previous studies have demonstrated that patients with T1DM present with higher aortic PWV than age-matched healthy volunteers indicating that T1DM patients have increased aortic stiffness (1,2,25). Still, there is a gray zone between clearly normal and obvious abnormal PWV. Aortic PWV measurements falling in this gray zone may be considered as a starting point in the cardiovascular stiffening continuum. The present study group of T1DM patients showed a wide range of aortic PWV values. Therefore, this patient cohort may be well-suited as a model for assessment of early changes in diastolic function, not confounded by other risk factors. In our study, we used the definition of normal values for age-related PWV as described in a previous publication (22), where aortic PWV was assessed using the same technique. After classifying patients according to their age-related normal PWV-values, diastolic function indices were different between patients with normal versus increased PWV, illustrating the effect this stiffening continuum has on cardiovascular pathology.

Age and hypertension are well-known major independent risk factors for aortic stiffness in subjects with and without T1DM. Abnormal glucose metabolism may play a relative minor role in the development of increased arterial stiffness (26,27). In our study, patients with normal and increased PWV had a similar duration of T1DM and a similar cardiovascular risk profile.

Previous studies have shown that in patients with T1DM, aortic stiffness is related to cardiovascular disease (4,5). The correlation between aortic stiffness and impaired LV diastolic function can be caused by two possible separate mechanisms. First, increased aortic stiffness can directly affect LV diastolic function by higher end-diastolic pressure and increased afterload (28). Secondly, the advanced glycation products that form due to DM and cause cross linking of collagen molecules both in the myocardium and vessel walls can simultaneously affect both the myocardium and the aortic wall (29).

Such an association between aortic stiffness and impaired LV diastolic function has been reported in patients with T2DM, hypertension or both (30,31). However, only one previous study by Karamitsos et al. has investigated the relationship between aortic stiffness and LV diastolic dysfunction in patients with T1DM (3). They assessed LV func-

tion and aortic stiffness in 66 T1DM patients using conventional echocardiography and showed that LV diastolic function and aortic wall stiffness were correlated. In our study, we assessed aortic PWV using velocity-encoded MRI, which has some advantages over ultrasonography. In contrast to ultrasonography, PWV-assessment with MRI is not limited to the availability of suitable acoustic windows along the aorta. Furthermore, the true aortic path length, needed for PWV-calculations, can be accurately determined with MRI. With ultrasonography, only an estimation of the aortic path length can be obtained, usually from the sternal-notch to pubis distance measurement over the patient's body surface (32,33).

Traditionally, LV diastolic function is assessed by mitral inflow waveform analysis using echocardiographic Doppler techniques. Although these techniques are clinically useful, they have some limitations that can influence their accuracy (20). An important limitation of this technique is that the regional measurement assumes correspondence with global LV relaxation over the entire LV (20). Furthermore, the mitral inflow pattern can only be evaluated in the direction of the ultrasound beam. Speckle tracking allows for the assessment of angle independent LV myocardial deformation of the entire left ventricle, which represents the performance of all myocardial segments and therefore might provide a more sensitive evaluation of global LV diastolic function. It is especially more accurate than the conventional methods in patients with normal LV ejection fraction or regional dysfunction (20,34). Moreover, speckle tracking strain analysis is highly sensitive for early detection of alterations in LV diastolic function (10,13,20,34).

Furthermore, speckle tracking strain analysis permits a concise evaluation of LA compliance in patients with preserved LV ejection fraction (11). Generally, LA strain is dependent on LV systolic function. In our cohort, LV systolic function was preserved, so the impaired LA strain is most likely caused by LA myocardial stiffening. Interestingly, our results show a significant association between aortic stiffness and LA strain which has not been reported by previous studies. It has been reported, though, that stiffening of the aorta can result in increased afterload (28). This results in higher LV pressure, which potentially leads to LV hypertrophy, decreased LV compliance and eventually to structural changes in the LA (35). Our results are in line with the hypothesis that increased aortic stiffness can eventually lead to diminished LA compliance. This could be a risk factor for atrial fibrillation (36,37). The potential contribution of aortic stiffening in causing atrial stretch and atrial fibrillation is a hypothesis that warrants further investigation. Our study had some limitations. The design of the study is cross-sectional, therefore a causal relationship between aortic PWV and LV diastolic function cannot be determined. Longitudinal studies are required to assess the prognostic value of the correlation between aortic PWV and LV diastolic function. In this study we did not analyze aortic stiffness directly by means of aortic distensibility. For a proper calculation of the

aortic distensibility, an invasive aortic pressure assessment is required, which cannot be obtained in clinical routine. However, PWV assessed with velocity-encoded MRI has proven to be a useful surrogate marker for aortic stiffness and is pressure independent (38). Furthermore, we used normal age-related PWV values derived from the age relation described by Westenberg et al. (22), to determine whether PWV-values in our patient group were normal or increased. The age of the volunteers in the study by Westenberg et al. was slightly lower than in our patient population (18-65 years vs. 31-69 years). We have used the linear regression model from that study to extrapolate the normal values for the present evaluation. However, other studies reported approximately similar values in patient groups with broader age range (39). Therefore we considered the normal age-related PWV values we used applicable for our study.

In conclusion, aortic PWV, assessed with velocity-encoded MRI, is inversely associated with LV diastolic function indices and reduced LA compliance, assessed with speckle tracking strain analysis in patients with T1DM. These results suggest that aortic PWV can be used as an integrated marker for LV diastolic function and LA compliance in this patient group. Further study is required to assess the potential clinical and prognostic implication of our findings.

REFERENCES

1. Oxlund H, Rasmussen LM, Andreassen TT, Heickendorff L: Increased aortic stiffness in patients with type 1 (insulin-dependent) diabetes mellitus. *Diabetologia* 32:748-752, 1989
2. Urbina EM, Wadwa RP, Davis C, Snively BM et al.: Prevalence of increased arterial stiffness in children with type 1 diabetes mellitus differs by measurement site and sex: the SEARCH for Diabetes in Youth Study. *J Pediatr* 156:731-7, 737, 2010
3. Karamitsos TD, Karvounis HI, Didangelos TP, Papadopoulos CE et al.: Aortic elastic properties are related to left ventricular diastolic function in patients with type 1 diabetes mellitus. *Cardiology* 109:99-104, 2008
4. Schram MT, Chaturvedi N, Fuller JH, Stehouwer CD: Pulse pressure is associated with age and cardiovascular disease in type 1 diabetes: the Eurodiab Prospective Complications Study. *J Hypertens* 21:2035-2044, 2003
5. Cruickshank K, Riste L, Anderson SG, Wright JS et al.: Aortic pulse-wave velocity and its relationship to mortality in diabetes and glucose intolerance: an integrated index of vascular function? *Circulation* 106:2085-2090, 2002
6. Abhayaratna WP, Srikusalanukul W, Budge MM: Aortic stiffness for the detection of preclinical left ventricular diastolic dysfunction: pulse wave velocity versus pulse pressure. *J Hypertens* 26:758-764, 2008
7. van Elderen SG, Brandts A, Westenberg JJ, van der Grond J et al.: Aortic stiffness is associated with cardiac function and cerebral small vessel disease in patients with type 1 diabetes mellitus: assessment by magnetic resonance imaging. *Eur Radiol* 20:1132-1138, 2010
8. Grotenhuis HB, Westenberg JJ, Steendijk P, van der Geest RJ et al.: Validation and reproducibility of aortic pulse wave velocity as assessed with velocity-encoded MRI. *J Magn Reson Imaging* 30:521-526, 2009
9. Kim DG, Lee KJ, Lee S, Jeong SY et al.: Feasibility of two-dimensional global longitudinal strain and strain rate imaging for the assessment of left atrial function: a study in subjects with a low probability of cardiovascular disease and normal exercise capacity. *Echocardiography* 26:1179-1187, 2009
10. Reisner SA, Lysyansky P, Agmon Y, Mutlak D et al.: Global longitudinal strain: a novel index of left ventricular systolic function. *J Am Soc Echocardiogr* 17:630-633, 2004
11. Saraiva RM, Demirkol S, Buakhamsri A, Greenberg N et al.: Left atrial strain measured by two-dimensional speckle tracking represents a new tool to evaluate left atrial function. *J Am Soc Echocardiogr* 23:172-180, 2010
12. Vianna-Pinton R, Moreno CA, Baxter CM, Lee KS et al.: Two-dimensional speckle-tracking echocardiography of the left atrium: feasibility and regional contraction and relaxation differences in normal subjects. *J Am Soc Echocardiogr* 22:299-305, 2009
13. Ng AC, Delgado V, Bertini M, van der Meer RW et al.: Findings from left ventricular strain and strain rate imaging in asymptomatic patients with type 2 diabetes mellitus. *Am J Cardiol* 104:1398-1401, 2009
14. Alberti KG, Zimmet PZ: Definition, diagnosis and classification of diabetes mellitus and its complications. Part 1: diagnosis and classification of diabetes mellitus provisional report of a WHO consultation. *Diabet Med* 15:539-553, 1998

15. Lamb HJ, Doornbos J, van der Velde EA, Kruit MC et al.: Echo planar MRI of the heart on a standard system: validation of measurements of left ventricular function and mass. *J Comput Assist Tomogr* 20:942-949, 1996
16. Nagueh SF, Appleton CP, Gillebert TC, Marino PN et al.: Recommendations for the evaluation of left ventricular diastolic function by echocardiography. *Eur J Echocardiogr* 10:165-193, 2009
17. Dokainish H, Zoghbi WA, Lakkis NM, Al-Bakshy F et al.: Optimal noninvasive assessment of left ventricular filling pressures: a comparison of tissue Doppler echocardiography and B-type natriuretic peptide in patients with pulmonary artery catheters. *Circulation* 109:2432-2439, 2004
18. Lang RM, Bierig M, Devereux RB, Flachskampf FA et al.: Recommendations for chamber quantification. *Eur J Echocardiogr* 7:79-108, 2006
19. Shanks M, Ng AC, van de Veire NR, Antoni ML et al.: Incremental prognostic value of novel left ventricular diastolic indexes for prediction of clinical outcome in patients with ST-elevation myocardial infarction. *Am J Cardiol* 105:592-597, 2010
20. Wang J, Khoury DS, Thohan V, Torre-Amione G et al.: Global diastolic strain rate for the assessment of left ventricular relaxation and filling pressures. *Circulation* 115:1376-1383, 2007
21. Kurt M, Wang J, Torre-Amione G, Nagueh SF: Left atrial function in diastolic heart failure. *Circ Cardiovasc Imaging* 2:10-15, 2009
22. Westenberg JJ, Scholte AJ, Vaskova Z, van der Geest RJ et al.: Age-related and regional changes of aortic stiffness in the marfan syndrome: Assessment with velocity-encoded MRI. *J Magn Reson Imaging* 2011
23. Cavalcante JL, Lima JA, Redheuil A, Al-Mallah MH: Aortic stiffness current understanding and future directions. *J Am Coll Cardiol* 57:1511-1522, 2011
24. Vlachopoulos C, Aznaouridis K, Stefanadis C: Prediction of cardiovascular events and all-cause mortality with arterial stiffness: a systematic review and meta-analysis. *J Am Coll Cardiol* 55:1318-1327, 2010
25. van Elderen SG, Westenberg JJ, Brandts A, van der Meer RW et al.: Increased aortic stiffness measured by MRI in patients with type 1 diabetes mellitus and relationship to renal function. *AJR Am J Roentgenol* 196:697-701, 2011
26. Brandts A, van Elderen SG, Tamsma JT, Smit JW et al.: The effect of hypertension on aortic pulse wave velocity in type-1 diabetes mellitus patients: assessment with MRI. *Int J Cardiovasc Imaging* 2011
27. Cecelja M, Chowienczyk P: Dissociation of aortic pulse wave velocity with risk factors for cardiovascular disease other than hypertension: a systematic review. *Hypertension* 54:1328-1336, 2009
28. Leite-Moreira AF, Correia-Pinto J, Gillebert TC: Afterload induced changes in myocardial relaxation: a mechanism for diastolic dysfunction. *Cardiovasc Res* 43:344-353, 1999
29. Aronson D: Cross-linking of glycated collagen in the pathogenesis of arterial and myocardial stiffening of aging and diabetes. *J Hypertens* 21:3-12, 2003
30. Eren M, Gorgulu S, Uslu N, Celik S et al.: Relation between aortic stiffness and left ventricular diastolic function in patients with hypertension, diabetes, or both. *Heart* 90:37-43, 2004
31. Seyfeli E, Duru M, Saglam H, Akgul F et al.: Association of left ventricular diastolic function abnormalities with aortic elastic properties in asymptomatic patients with type 2 diabetes mellitus. A tissue doppler echocardiographic study. *Int J Clin Pract* 62:1358-1365, 2008

32. Nemeth ZK, Studinger P, Kiss I, Othmane TH et al.: The method of distance measurement and torso length influences the relationship of pulse wave velocity to cardiovascular mortality. *Am J Hypertens* 24:155-161, 2011
33. Rajzer MW, Wojciechowska W, Klocek M, Palka I et al.: Comparison of aortic pulse wave velocity measured by three techniques: Complior, SphygmoCor and Arteriograph. *J Hypertens* 26:2001-2007, 2008
34. Wang J, Nagueh SF: Current perspectives on cardiac function in patients with diastolic heart failure. *Circulation* 119:1146-1157, 2009
35. Reiffel JA: Is arterial stiffness a contributing factor to atrial fibrillation in patients with hypertension? A preliminary investigation. *Am J Hypertens* 17:213-216, 2004
36. Ravelli F, Allessie M: Effects of atrial dilatation on refractory period and vulnerability to atrial fibrillation in the isolated Langendorff-perfused rabbit heart. *Circulation* 96:1686-1695, 1997
37. Kuppahally SS, Akoum N, Burgon NS, Badger TJ et al.: Left atrial strain and strain rate in patients with paroxysmal and persistent atrial fibrillation: relationship to left atrial structural remodeling detected by delayed-enhancement MRI. *Circ Cardiovasc Imaging* 3:231-239, 2010
38. Bramwell J, Hill A: The velocity of the pulse wave in man. P*roc R Soc Lond B* 93:298-306, 1922
39. Hickson SS, Butlin M, Graves M, Taviani V et al.: The relationship of age with regional aortic stiffness and diameter. *JACC Cardiovasc Imaging* 3:1247-1255, 2010

Chapter 3

Aortic stiffness is associated with white matter integrity in patients with type 1 diabetes

Nathanja Tjeerdema, Linda D. van Schinkel, Jos J. Westenberg, Saskia G.C. van Elderen, Mark A. van Buchem, Johannes W.A. Smit, Jeroen van der Grond, Albert de Roos

Eur Radiol. 2014; in press

ABSTRACT

Background

The objective was to assess the association between aortic pulse wave velocity (PWV), as a marker of arterial stiffness and diffusion tensor imaging (DTI) of brain white matter integrity in patients with type 1 diabetes (T1DM) using advanced magnetic resonance imaging (MRI) technology.

Methods

Forty-one patients with T1DM (23 men, mean age 44 ± 12 years, mean diabetes duration 24 ± 13 years) were included. Aortic PWV was assessed using through-plane velocity-encoded MRI. Brain DTI measurements were performed on 3 Tesla MRI. Fractional anisotropy (FA) and apparent diffusion coefficient (ADC) were calculated for white and gray matter integrity. Pearson correlation and multivariable linear regression analyses including cardiovascular risk factors as covariates were assessed.

Results

Multivariable linear regression analyses revealed that aortic PWV is independently associated with white matter integrity FA (Beta= -0.777 p=0.008) in patients with T1DM. This effect was independent of age, gender, mean arterial pressure, body mass index, smoking, duration of diabetes and glycated hemoglobin levels. Aortic PWV was not significantly related to gray matter integrity.

Conclusions

Our data suggest that aortic stiffness is independently associated with reduced white matter integrity in patients with T1DM.

INTRODUCTION

Type 1 diabetes (T1DM) is a common chronic metabolic disorder, which is associated with diverse comorbidity. Although diabetes mellitus is not primarily a brain disease it may be associated with cerebral atrophy, white matter hyperintensities and infarctions as well as decreased cognitive functioning (1-3).

Besides well-recognized risk factors in patients with T1DM, like chronic hyperglycemia and alterations in insulin metabolism, vascular risk factors are thought to contribute to the occurrence of brain abnormalities. Aortic stiffening may play a central role in the development of brain injury. Of note, previous studies have shown that aortic stiffness is associated with generalized white matter atrophy and cerebral small vessel disease in T1DM (4,5). Aortic stiffness may contribute to microvascular brain injury by exposing the small vessels to the high pressure fluctuations and flow in the cerebral circulation (6). The brain is vulnerable in particular to high pressure fluctuations, because it is perfused at high volume flow and has very low vascular resistance. Pulse wave velocity (PWV) is a widely used surrogate marker for arterial stiffness. It is defined as the propagation speed of the systolic flow wave front traveling along the aorta, reflecting the elastic properties of the aortic vessel wall. PWV is estimated by dividing the distance between anatomical locations over the aorta by the time difference between the arrival of flow waves at the two locations. Higher PWV (m/s) corresponds to higher arterial stiffness (7).

Diffusion Tensor Imaging (DTI) is a validated technique of brain imaging with MRI, which, in contrast to conventional methods, enables measurement of white matter microstructure (8). DTI is based on diffusivity of water, providing two parameters of tissue integrity, namely the apparent diffusion coefficient (ADC) which reflects the magnitude of diffusion and fractional anisotropy (FA) which is a measure of the directionality of the diffusion and flow of water molecules in the brain tissue. Early detection of tissue injury reflected by an increase in ADC and reduction in FA has been observed in normal aging and cerebral small vessel disease (1). Moreover, Kodl et al. showed white matter microstructural deficits in patients with longstanding T1DM using this technique (8).

Interestingly, increased pulse pressure, an indicator of arterial stiffness, was found to be associated with lower FA in healthy volunteers (9). There are no previous publications that explored the possible relationship between aortic stiffness and diffusion tensor imaging of the brain in patients with T1DM using well-validated MRI techniques. Accordingly the purpose of this study was to assess the association between aortic pulse wave velocity, and diffusion tensor imaging of brain white matter integrity in patients with T1DM using advanced MRI technology.

METHODS

Study participants

This study was approved by the local medical ethics committee and all subjects gave written informed consent. Between February 2008 and January 2010 consecutive patients with T1DM were recruited from the local outpatient clinic. Characteristics of the study population are detailed in Table 1. Forty-one patients with T1DM (23 men and 18 women) were included with a mean age of 44 ± 12 years. Mean duration of the T1DM was 24 ± 13 years. All patients were treated with insulin. One patient was using an ACE-inhibitor in combination with an angiotensin II-antagonist for the presence of albuminuria. None of the other patients with T1DM were using blood pressure lowering medication. Statins were used by 11 (26%) patients.

Information about the characteristics of T1DM was obtained by standardized interviews and physical and laboratory examinations. Exclusion criteria for all participants were congenital aortic/heart disease, a clinical history of hypertension or cardiovascular disease, evidence of aortic valve stenosis or insufficiency, any other systemic disease than diabetes and general contraindications to MRI. At MRI examination duration of diabetes in years was estimated from self-reported year of diagnosis. Blood pressure and heart rate were measured using a semiautomated sphygmomanometer (Dinamap, Critikon, Tampa, Fla, USA) after MR imaging. Pulse pressure was defined as systolic blood pressure minus diastolic blood pressure. Mean arterial pressure (MAP) was estimated by adding up one-third of the pulse pressure to diastolic blood pressure. Body mass index and smoking status (nonsmoker or current smoker) were determined. High-density lipoprotein (HDL), total cholesterol, triglycerides, creatinine and glycated hemoglobin (HbA1c) were also determined.

This patient group was partly included in a previous study describing the predictive value of cerebral blood flow and aortic stiffness on generalized white matter brain atrophy in T1DM (4).

MRI protocol

MR imaging of the aorta and brain were performed at the same day. Aortic imaging was performed, as previously described, using a 1.5T MRI scanner (NT 15 Gyroscan Intera; Philips Medical Systems, Best, the Netherlands) (10). In short: a scout image of the aorta was acquired using a five-element phased array cardiac surface coil. Aortic PWV was assessed according to the transit-time method from two one-directional through-plane velocity-encoded MRI acquisitions with high-temporal resolution performed in the aorta at two predefined levels: at the level of the pulmonary trunk in the ascending and in the abdominal descending aorta (10). Scan parameters were: repetition time (TR) 5.0ms,

Table 1. Clinical characteristics and MR findings of patients with type 1 diabetes

	Patients with type 1 diabetes (n=41)
Clinical characteristics	
Age, years	44 ± 12
Male gender, n (%)	23 (55)
Body mass index, kg/m^2	25.3 ± 2.9
Systolic blood pressure, mmHg	128 ± 19
Diastolic blood pressure, mmHg	73 ± 10
Pulse pressure, mmHg	55 ± 14
Mean arterial pressure, mmHg	91 ± 12
Heart rate, beats/min	66 ± 10
Current smoker, n (%)	6 (15%)
Alcohol use yes, n (%)	23 (56%)
Laboratory markers	
HbA1c, %	7.6 ± 1.0
HDL-cholesterol, mmol/l	1.7 ± 0.5
Total cholesterol, mmol/l	4.8 ± 1.0
Triglycerides, mmol/l	1.2 ± 0.6
Creatinine, umol/l	75 ± 11
MRI findings	
Aortic PWV, m/s (median, IQR)	6.2 (5.2-7.6)
Stroke volume, ml/heart beat (median, IQR)	87 (81-105)
Periventricular WMHs, n (%)	7 (17)
Subcortical WMHs, n (%)	2 (5)
Gray matter brain volume, mL	574 ± 60
Gray matter FA	0.171 ± 0.008
Gray matter ADC	0.00042 ± 0.00002
White matter brain volume, mL	564 ± 69
White matter FA	0.344 ± 0.017
White matter ADC	0.00036 ± 0.00001
Total brain volume, mL	1139 ± 121
Total brain FA	0.252 ± 0.010
Total brain ADC	0.00040 ± 0.00001

Data are presented as mean ± standard deviations unless otherwise stated. BMI: body mass index, HbA1c: glycated hemoglobin, HDL: high-density lipoprotein, PWV: pulse wave velocity, IQR: inter quartile range, FA: fractional anisotropy, ADC: apparent diffusion coefficient.

echo time (TE) 2.9ms, flip angle (FA) 20°, field of view (FOV) 300mm, 128×115 acquisition matrix, slice thickness 8mm, with maximal number of phases reconstructed ensuring high (6-10ms) effective temporal resolution. Aortic velocity maps were analyzed using the in-house developed FLOW software package.

The aortic PWV is defined by the propagation of the systolic flow wave front, and was determined by the distance between the aortic measurement sites and the transit-time of the systolic flow wave front (Figure 1). This transit-time is assessed by the time difference in arrival of the systolic flow wave front at each level, automatically assessed by definition of the intersection between the horizontal diastolic flow and the upslope of the flow wave, modeled by linear regression of all data points between 20% and 80% of the range of flow values along the slope. The aortic path length between the measurements sites was measured by manually drawing a centerline in the aorta as defined in the aortic scout view, using the in-house developed software package MASS (Medis, Leiden, the Netherlands). Aortic vessel wall contour segmentation was performed by a researcher unaware of the subjects' conditions and obtained data with brain MRI. Figure 2 shows the flow chart for the processing data.

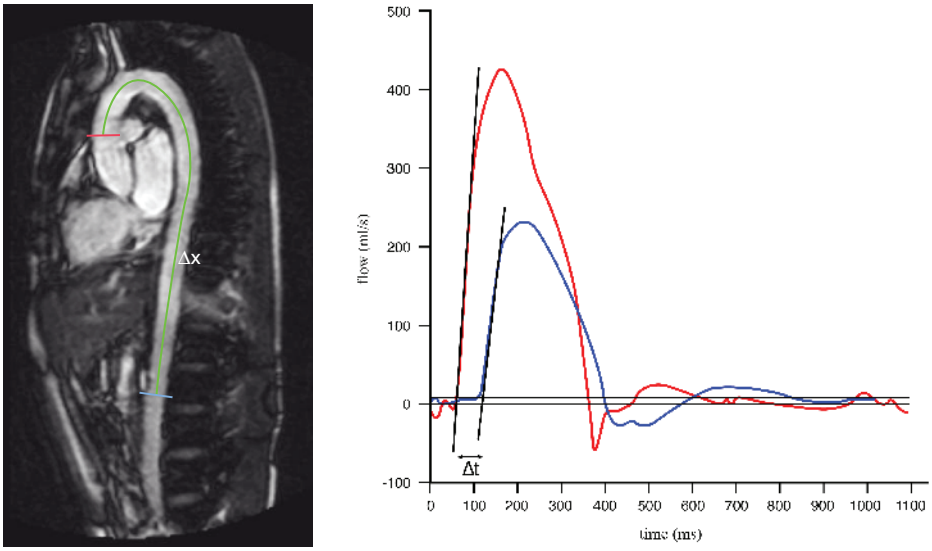

Figure 1. Aortic pulse wave velocity assessment. The left panel shows an oblique sagittal scout view of the aorta. Velocity mapping was obtained at the level of the pulmonary trunk and in the abdominal descending aorta. The aortic path length (△x) between both levels was measured, indicated by the polyline following the centerline of the aorta. The right panel illustrates the flow curves in the ascending (red line) and descending (blue line) aorta. The transit time of arrival of the pulse wave (△t) was divided by the aortic path length (△x) to calculate aortic PWV (in meters per second).

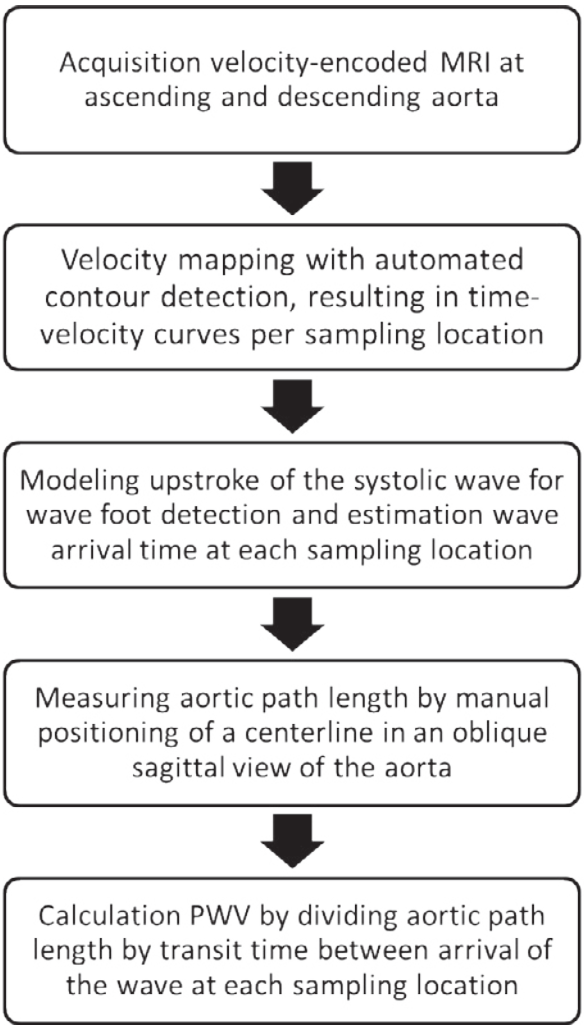

Figure 2. Flow chart of the processing of pulse wave velocity.

For the assessment of systolic LV function, the LV was imaged in short-axis orientation as previously described (11) by using a retrospectively-gated breath-hold segmented gradient-echo sequence with steady-state free-precession. Ten to twelve consecutive slices of 10mm thickness and without gap were obtained with one signal average and 40 reconstructed phases. Scan parameters: echo time TE 1.7 ms, repetition time TR 3.3 ms, flip angle 50°, acquisition matrix 256×194, acquisition voxel size 1.7×1.7×10mm3. Using the software package MASS, end-systolic and end-diastolic LV volumes were obtained using manual contour definition of the endocardial borders in these multi-slice

and multi-phase datasets. Left ventricular end-systolic and -diastolic volume, cardiac output and stroke volume were assessed (12).

All brain MRIs were performed on a 3.0 Tesla (Achieva; Philips Medical Systems, Best, The Netherlands). Brain MRI consisted of a 3 dimensional T1 (3D T1) sequence for brain volume assessment. Diffusion tensor imaging was performed to assess FA and ADC. 3D T1 acquisition parameters were: TR 9.8ms, TE 4.6 ms, FA 8º, FOV 224mm, 192×152 acquisition matrix, 256×256 reconstruction matrix, slice thickness 1.2mm, 120 slices, no slice gap). For DTI, a single-shot echo-planar sequence was applied with 32 measurement directions having the following scan parameters: TR 10,004ms, TE 56ms, FOV 220×220×128 with an acquisition matrix of 112×110, 2.00mm slice thickness, transversal slice orientation, slice gap = 0, FA 90°, single reconstruction voxel dimensions were 1.96×1.96×2.00mm, number of slices = 64, B factor = 1,000, halfscan factor = 0.61. Parallel imaging (SENSE) was used with a reduction factor of 2, NSA = 1 and fat suppression was applied. DTI acquisition time was 6.55min.

MRI post processing

Evaluation of cerebral small vessel disease was evaluated on a spin-echo T2-weighted and fluid-attenuated inversion recovery (FLAIR) sequences. White matter hyperintensities (WMHs) were defined as areas of brain parenchyma with increased signal on T2-weighted and FLAIR images without mass effect. Lacunes defined as areas of more or less complete focal tissue destruction are not included in the rating of WMHs. WMHs were classified according to Fazekas et al (13,14) and subdivided into either periventricular or subcortical. Periventricular lesions were defined as starting directly at the ventricular border. When these abnormalities extend > 1cm into the adjacent white matter, this by convention indicates damage to both the periventricular and deep white matter. Deep WMH are characterized by a rim of normal appearing tissue which separates them from the periventricular region. Subjects were divided into those with normal [0] vs abnormal [1] amounts of WMHs. Fazekas scores of 0 and 1 were considered normal, a score of 2 was considered abnormal below the age of 75 years, and a score of 3 was considered abnormal in any age group.

All T1-weighted scans were analyzed using software provided by FMRIB's Software Library (FSL) (15). Total brain tissue volume was estimated with SIENAX (16,17). This program extracts brain and skull images from the single whole-head input data (18). The brain images were then affine-registered to MNI152 space, using the skull images to determine the registration scaling with 7 degrees of freedom (FSL-FLIRT). FSL's FAST was used to create GM and WM tissue segmentations. A visual inspection of all registrations was performed and of the final segmentations 20 % were selected at random and visually inspected for accuracy. ADC and FA reconstructions were performed direct after

data acquisition using software provide by the manufacturer (Philips Medical Systems, Best, The Netherlands). To correct for possible partial volume effects in ADC and FA data, especially from CSF, an eroded mask of GM and WM segmentations was created by removing one voxel in plane for all above named VOIs. FA and ADC reconstructions were then registered to the eroded whole brain, WM and GM volumes, using the same transformation matrix obtained from the original linear registration of the T1-w volume to MNI space. Finally, mean ADC and FA values were calculated for (eroded) whole brain, (eroded) WM and (eroded) GM. The researcher who obtained the FA and ADC data was unaware of the subjects' conditions and pulse wave velocity data.

Statistical analysis

Statistical analysis was performed with SPSS (SPSS, Chicago, Illinois, USA), version 17. Continuous variables are expressed as mean ± standard deviation (sd) unless otherwise stated. Categorical variables were presented as frequencies and percentages. Aortic PWV and stroke data were non-normally distributed and therefore were log-transformed for further analyses. Regression analysis, corrected for age and gender was used to test whether subjects with white matter hyperintensities have a different PWV than subjects without. The correlation between aortic PWV and between stroke volume with brain integrity was tested by Pearson correlation analysis. Multivariate linear regression analyses were performed to adjust for confounding factors, defined as age, gender, mean arterial pressure, body mass index, smoking, duration of diabetes and HbA1c. These covariates were entered simultaneously into a multivariable linear regression model. The β-regression coefficients and p-values are reported. Significance was reached when $p<0.05$ (two-tailed).

RESULTS

PWV did not differ between patients with or without periventricular WMHs ($p=0.250$) but was higher in subjects with subcortical WMHs (Beta=0.235, $p=0.008$). There were significant correlations between the aortic PWV and white matter integrity FA ($r=-0.529$, $p<0.001$) and ADC ($r=0.406$, $p=0.009$). The correlation between PWV and white matter FA is shown in Figure 3. For gray matter integrity a significant correlation was found for ADC ($r=0.518$, $p=0.001$) but not for FA ($r=0.016$, $p=0.923$). Stroke volume correlated with gray matter integrity FA ($r=0.342$, $p=0.029$) and ADC ($r=-0.368$, $p=0.018$) and with white matter FA ($r=0.326$, $p=0.038$). Multivariable linear regression analyses showed that aortic PWV is independently associated with WM integrity expressed as FA (Beta=-0.777, $p=0.008$) in patients with T1DM (Table 2). This effect was independent of age, gender, MAP, BMI, smoking, duration of diabetes and HbA1c levels. In a similar multivariable linear regression

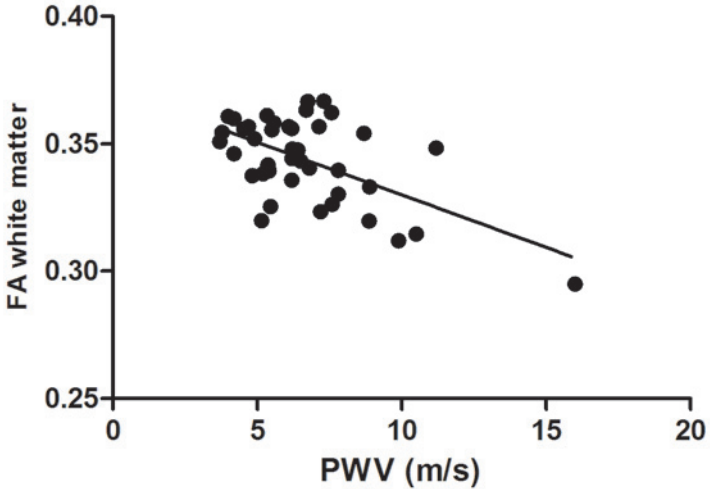

Figure 3. Correlation between pulse wave velocity (PWV) and fractional anisotropy (FA), a DTI parameter of the white matter.

Table 2. Results of multivariable linear regression analyses performed in patients with type 1 diabetes (n=41) to assess independent predictors of WM and GM integrity

	White matter integrity				Gray matter integrity			
	ADC		FA		ADC		FA	
	Beta	p-value	Beta	p-value	Beta	p-value	Beta	p-value
Age, years	-0.068	0.859	0.111	0.731	0.252	0.444	-0.157	0.700
Female gender (n=19)	-0.166	0.418	0.123	0.474	-0.230	0.192	0.091	0.676
Mean arterial pressure, mmHg	-0.048	0.830	0.064	0.731	-0.245	0.202	0.044	0.850
Body mass index, kg/m2	0.079	0.666	-0.057	0.712	0.039	0.804	-0.100	0.607
Current smoker	-0.037	0.831	0.149	0.319	-0.015	0.922	0.253	0.182
Duration of diabetes, years	-0.078	0.753	-0.058	0.781	0.313	0.146	-0.052	0.844
HbA1c, %	-0.112	0.600	-0.011	0.949	-0.166	0.363	-0.203	0.357
Aortic PWV, m/s	0.532	0.111	-0.777	0.008*	0.270	0.338	-0.098	0.778

ADC: apparent diffusion coefficient, FA: fractional anisotropy, HbA1c: glycated hemoglobin, PWV: pulse wave velocity. *p-value <0.05.

model for the prediction of gray matter (GM) integrity no significant effect of aortic PWV was observed. Lipid lowering drugs (used by 26% of the patients) may reduce arterial stiffness. Therefore further adjustment for the use of statins was performed but this did not yield different results for the association between PWV and WM integrity (FA Beta=-0.798, p=0.006, ADC Beta=0.555, p=0.203). No significant association between stroke volume and integrity was found in multivariable linear regression analyses.

DISCUSSION

The main finding of our study is the observation, that aortic stiffness is associated with white matter integrity independently of other potential confounders in patients with T1DM.

So far few studies have reported on white matter integrity in T1DM. White matter microstructural deficits have been observed in patients with type 2 diabetes (19,20) independent of age and blood pressure levels. Kodl et al. showed white matter microstructural deficits expressed as reduced FA in 25 patients with longstanding T1DM, as compared to 25 age- and gender-matched healthy volunteers (8). The patients in our study have a similar age and a somewhat shorter duration of diabetes (24 ± 13 years vs. 30 ± 11 years).

As hypothesized we found that arterial stiffness was associated with white matter microstructure expressed as reduced FA in patients with T1DM. The association with PWV was not found for ADC. Possibly this may be due to the fact that ADC reflects general diffusional properties, therefore being a more heterogeneous white matter measure than FA, which reflects organizational aspects. Crucial in this analysis was to incorporate age as a covariate as it is known that measures of diffusion such as FA and ADC, as well as arterial stiffness are dependent on age (19,21). Aortic PWV is a surrogate marker for arterial stiffness and has been shown to be an independent predictor for stroke, cerebral small vessel disease (5,6,20,21) and might be a predictor for cognitive decline (22). Furthermore in T1DM aortic PWV measured with MRI has been demonstrated a predictor of white but not gray matter atrophy (4). In line with this study we could not show an independent association for aortic PWV with gray matter integrity.

It is known that the blood flow in the white matter is substantially lower compared to the blood flow in gray matter. White matter may be more susceptible to subtle pressure fluctuations than gray matter, because of the vulnerable end-arterioles penetrating the white matter (23). It has been hypothesized that in particular "watershed" areas of the brain may be sensitive to arterial stiffness (24). In line, PWV has been associated with processing speed and memory, cognitive functions represented in these watershed locations (25). To the best of our knowledge we are the first to show an association between PWV and white matter integrity in patients with T1DM as evaluated by MRI techniques. In agreement with our study, a relation between pulse pressure, another marker of arterial stiffness, and white matter deficits has been observed (9). However that relationship was studied in healthy normotensive subjects. Furthermore aortic PWV is considered to be a more accurate method for assessing arterial stiffness than the measurement of pulse pressure made in the peripheral vessels which does not always accurately reflect the actual central pulse pressure and which may be unreliable in older subjects.

In diabetes mellitus both glucose toxicity and abnormal insulin metabolism have been suggested to contribute to brain pathology (26,27). Up to now few studies

investigated the relationship between clinical parameters of disease severity and microstructural white matter changes in diabetes. In patients with type 2 diabetes disease duration rather than HbA1C was related to DTI assessed white matter changes when investigated simultaneously (19). Interestingly we did not observe associations between white matter microstructure and clinical parameters such as disease duration or HbA1c. This is in contrast to an earlier study that identified a significant relationship between FA and HbA1c and between FA and disease duration in T1DM. However in that study no adjustments for age were performed. Furthermore those authors did not report on blood pressure while we investigated patients with T1DM without a history of hypertension. Since high blood pressure was shown to be associated with a decrease in FA (28) and is frequently occurring in diabetes it is not clear to which degree this may have influenced these previous results.

MR-DTI is a technique that allows early detection of white matter damage even in regions that appear normal on conventional anatomical images.

Despite a limited understanding the exact pathophysiology, DTI changes could be of clinical relevance. In children DTI assessed structural integrity is associated with higher IQ and loss of integrity in normal aging is associated with cognitive decline (29,30). In addition in patients with T1DM white matter deficits were associated with performance on neurocognitive tests (8). In order to develop targeted treatments to prevent brain damage it is important to understand the underlying mechanisms that cause subtle brain alterations. Our findings support the role of vascular mechanisms leading to a decline in white matter microstructure in T1DM, which adds to current knowledge.

Smoking is known to increase arterial stiffness (31-33) consequently we adjusted for smoking in the linear regression analyses. Alcohol consumption may have a divergent effect on arterial stiffness and may also directly affect the brain, however as the number of alcohol units were not registered we were not able to explore the effect of alcohol. Furthermore this was an explorative study and associations already detected in this small patient group need to be confirmed in a larger population. Given the cross-sectional design of this study no insight into the changes over time or a causal relationship between aortic PWV and white matter damage can be determined. Another limitation of our study is that we did not include cognitive testing in the current study. Longitudinal studies are needed to assess the impact of our findings on cognitive decline and to assess the prognostic and therapeutic implications.

In conclusion we found that aortic stiffness is independently associated with reduced white matter integrity in patients with T1DM, which suggests a vascular contribution to early subtle microstructural deficits. Future prospective studies are needed to improve knowledge of the prognostic and therapeutic implications of these microstructural changes.

REFERENCES

1. Biessels GJ, Staekenborg S, Brunner E, Brayne C et al.: Risk of dementia in diabetes mellitus: a systematic review. *Lancet Neurol* 5:64-74, 2006
2. Gouw AA, van der Flier WM, Fazekas F, van Straaten EC et al.: Progression of white matter hyperintensities and incidence of new lacunes over a 3-year period: the Leukoaraiosis and Disability study. *Stroke* 39:1414-1420, 2008
3. Knopman DS, Mosley TH, Catellier DJ, Sharrett AR: Cardiovascular risk factors and cerebral atrophy in a middle-aged cohort. *Neurology* 65:876-881, 2005
4. van Elderen SG, Brandts A, van der Grond J, Westenberg JJ et al.: Cerebral perfusion and aortic stiffness are independent predictors of white matter brain atrophy in type 1 diabetic patients assessed with magnetic resonance imaging. *Diabetes Care* 34:459-463, 2011
5. van Elderen SG, Brandts A, Westenberg JJ, van der Grond J et al.: Aortic stiffness is associated with cardiac function and cerebral small vessel disease in patients with type 1 diabetes mellitus: assessment by magnetic resonance imaging. *Eur Radiol* 20:1132-1138, 2010
6. O'Rourke MF, Safar ME: Relationship between aortic stiffening and microvascular disease in brain and kidney: cause and logic of therapy. *Hypertension* 46:200-204, 2005
7. Laurent S, Cockcroft J, Van BL, Boutouyrie P et al.: Expert consensus document on arterial stiffness: methodological issues and clinical applications. *Eur Heart J* 27:2588-2605, 2006
8. Kodl CT, Franc DT, Rao JP, Anderson FS et al.: Diffusion tensor imaging identifies deficits in white matter microstructure in subjects with type 1 diabetes that correlate with reduced neurocognitive function. *Diabetes* 57:3083-3089, 2008
9. Kennedy KM, Raz N: Pattern of normal age-related regional differences in white matter microstructure is modified by vascular risk. *Brain Res* 1297:41-56, 2009
10. Grotenhuis HB, Westenberg JJ, Steendijk P, van der Geest RJ et al.: Validation and reproducibility of aortic pulse wave velocity as assessed with velocity-encoded MRI. *J Magn Reson Imaging* 30:521-526, 2009
11. Brandts A, van Elderen SG, Westenberg JJ, van der Grond J et al.: Association of aortic arch pulse wave velocity with left ventricular mass and lacunar brain infarcts in hypertensive patients: assessment with MR imaging. *Radiology* 253:681-688, 2009
12. van der Geest RJ, Reiber JH: Quantification in cardiac MRI. *J Magn Reson Imaging* 10:602-608, 1999
13. Fazekas F, Schmidt R, Scheltens P: Pathophysiologic mechanisms in the development of age-related white matter changes of the brain. *Dement Geriatr Cogn Disord* 9 Suppl 1:2-5, 1998
14. Fazekas F, Barkhof F, Wahlund LO, Pantoni L et al.: CT and MRI rating of white matter lesions. *Cerebrovasc Dis* 13 Suppl 2:31-36, 2002
15. Smith SM, Jenkinson M, Woolrich MW, Beckmann CF et al.: Advances in functional and structural MR image analysis and implementation as FSL. *Neuroimage* 23 Suppl 1:S208-S219, 2004
16. Smith SM, De SN, Jenkinson M, Matthews PM: Normalized accurate measurement of longitudinal brain change. *J Comput Assist Tomogr* 25:466-475, 2001
17. Smith SM, Zhang Y, Jenkinson M, Chen J et al.: Accurate, robust, and automated longitudinal and cross-sectional brain change analysis. *Neuroimage* 17:479-489, 2002
18. Smith SM: Fast robust automated brain extraction. *Hum Brain Ma*pp 17:143-155, 2002
19. Hsu JL, Van HW, Bai CH, Lee CH et al.: Microstructural white matter changes in normal aging: a diffusion tensor imaging study with higher-order polynomial regression models. *Neuroimage* 49:32-43, 2010

20. Yau PL, Javier D, Tsui W, Sweat V et al.: Emotional and neutral declarative memory impairments and associated white matter microstructural abnormalities in adults with type 2 diabetes. P*sychiatry Res* 174:223-230, 2009
21. Salat DH, Tuch DS, Greve DN, van der Kouwe AJ et al.: Age-related alterations in white matter microstructure measured by diffusion tensor imaging. *Neurobiol Aging* 26:1215-1227, 2005
22. Hanon O, Haulon S, Lenoir H, Seux ML et al.: Relationship between arterial stiffness and cognitive function in elderly subjects with complaints of memory loss. *Stroke* 36:2193-2197, 2005
23. Catafau AM, Lomena FJ, Pavia J, Parellada E et al.: Regional cerebral blood flow pattern in normal young and aged volunteers: a 99mTc-HMPAO SPET study. *Eur J Nucl Med* 23:1329-1337, 1996
24. Mitchell GF: Effects of central arterial aging on the structure and function of the peripheral vasculature: implications for end-organ damage. *J Appl Physiol (1985)* 105:1652-1660, 2008
25. Watson NL, Sutton-Tyrrell K, Rosano C, Boudreau RM et al.: Arterial stiffness and cognitive decline in well-functioning older adults. *J Gerontol A Biol Sci Med Sci* 66:1336-1342, 2011
26. Brands AM, Kessels RP, de Haan EH, Kappelle LJ et al.: Cerebral dysfunction in type 1 diabetes: effects of insulin, vascular risk factors and blood-glucose levels. *Eur J Pharmacol* 490:159-168, 2004
27. Wessels AM, Scheltens P, Barkhof F, Heine RJ: Hyperglycaemia as a determinant of cognitive decline in patients with type 1 diabetes. *Eur J Pharmacol* 585:88-96, 2008
28. Burgmans S, van Boxtel MP, Gronenschild EH, Vuurman EF et al.: Multiple indicators of age-related differences in cerebral white matter and the modifying effects of hypertension. *Neuroimage* 49:2083-2093, 2010
29. Schmithorst VJ, Wilke M, Dardzinski BJ, Holland SK: Cognitive functions correlate with white matter architecture in a normal pediatric population: a diffusion tensor MRI study. *Hum Brain Map* 26:139-147, 2005
30. Charlton RA, Barrick TR, McIntyre DJ, Shen Y et al.: White matter damage on diffusion tensor imaging correlates with age-related cognitive decline. *Neurology* 66:217-222, 2006
31. Jatoi NA, Jerrard-Dunne P, Feely J, Mahmud A: Impact of smoking and smoking cessation on arterial stiffness and aortic wave reflection in hypertension. *Hypertension* 49:981-985, 2007
32. Liang YL, Shiel LM, Teede H, Kotsopoulos D et al.: Effects of Blood Pressure, Smoking, and Their Interaction on Carotid Artery Structure and Function. *Hypertension* 37:6-11, 2001
33. Mahmud A, Feely J: Effect of smoking on arterial stiffness and pulse pressure amplification. *Hypertension* 41:183-187, 2003

Chapter 4

Impact of type 1 diabetes mellitus on regional gray matter volume

Linda D. van Schinkel, Nathanja Tjeerdema, Saskia G.C. van Elderen, Jeroen van der Grond, Johannes W.A. Smit, Albert de Roos

Submitted

ABSTRACT

Background

Type 1 diabetes mellitus (T1DM) is associated with brain damage, such as white matter hyperintensities and early development of cerebral atrophy, and impaired cognitive functioning. Metabolic factors, like hyperglycemia, and vascular complications have been proposed to affect the brain in T1DM. Cortical gray matter and the thalamus and hippocampus, two subcortical structures, are affected in patients with T1DM. No studies have yet investigated the effects on other subcortical gray matter structures. Our objective was to assess, with the advanced magnetic resonance imaging (MRI) technique voxel-based morphometry (VBM), whether volumes of the basal ganglia differ between patients with longstanding T1DM and healthy controls.

Methods

62 patients with T1DM and 62 age- and gender-matched healthy controls underwent MRI of the brain. Volumes of the basal ganglia, amygdala, hippocampus and thalamus were assessed with VBM.

Results

T1DM patients showed volume loss of all of these gray matter areas, except for the amygdala. Furthermore, after correcting for potential confounding factors, the thalamus, hippocampus and putamen were still significantly smaller.

Conclusions

Using MRI VBM technique, volume loss of the basal ganglia, hippocampus and thalamus is observed in patients with T1DM compared to controls.

INTRODUCTION

Type 1 diabetes mellitus (T1DM) is associated with micro- and macrovascular complications (1,2). It has become increasingly clear that T1DM also affects the brain (3,4). Several structural brain abnormalities such as white matter hyperintensities, brain infarctions and the early development of cerebral atrophy (5-7) have been observed with magnetic resonance imaging (MRI). Cross sectional studies have demonstrated that generalized white and gray matter volume loss in patients with T1DM is associated with cognitive functioning and even dementia (8). Both hyperglycemia and vascular complications have been proposed as underlying mechanisms in T1DM associated declined cognitive functioning and volume loss, but the pathogenesis is complex and incompletely understood (7,9-11). Although previous studies have shown that T1DM is associated with gray matter density changes in general (7) and focal cortical regions and the left thalamus (12,13) and hippocampus (14,15), there are no data on the volumes of subcortical structures including the basal ganglia and amygdala in T1DM. Since the thalamus and the hippocampus are subcortical structures, we hypothesized that other subcortical structures, like the basal ganglia and the amygdala could also be affected in patients with T1DM.

Voxel-based morphometry (VBM) is a relatively novel and sophisticated analysis technique which enables to test for regional differences in brain volume. VBM enables to identify subtle gray matter alterations (16). As regional specific reductions in gray matter density in areas responsible for language processing and memory have been found in T1DM (12) we set out to perform in-depth gray matter studies in T1DM, using VBM. We hypothesized that subcortical structures differ between patients with longstanding T1DM and healthy controls.

METHODS

Study participants

Patients with T1DM were recruited from the local outpatient clinic between February 2008 and January 2010. For inclusion, patients had to be older than 18 years and diagnosed with T1DM. A total of 62 patients (34 men, 28 women; mean age 51.6 ± 12.4 years) gave written informed consent to participate in the study. Healthy volunteers were recruited by advertisement in local newspaper. Sixty-two age- and gender-matched controls were enrolled in the study. Exclusion criteria for all participants were congenital aortic/heart disease, evidence of aortic valve stenosis or insufficiency, a history of stroke and general contraindications to MRI, like claustrophobia or a pacemaker. T1DM was defined according to WHO criteria (17).

Medical data were obtained in all participants by standardized interviews and physical and laboratory examinations. Duration of T1DM in years was estimated as the time passed between the reported age of diagnosis and the MRI examination. Blood pressure and heart rate were measured using a semiautomated sphygmomanometer (Dinamap, Critikon, Tampa, Fla, USA).

Hypertension was defined as: systolic blood pressure > 140 mmHg and/or diastolic blood pressure > 90 mmHg, on repeated physical examination before antihypertensive therapy was instituted and according to the criteria of the European Society of Hypertension (18), or a blood pressure > 140/90 mmHg at time of MR imaging. Furthermore, smoking status (i.e. nonsmoker or current smoker), body mass index (BMI) and high-density lipoprotein (HDL), total cholesterol, triglycerides, creatinine, glycated hemoglobin (HbA1c) in T1DM and fasting glucose in controls were determined. Renal function defined as estimated glomerular filtration rate (GFR) was calculated with the Modification of Diet in Renal Disease (MDRD) equation: $186 * (\text{serum creatinine } \mu mol/L / 88.4)^{-1.154} \times (age)^{-0.203}$ (x 0,742 if female)). Retinopathy was diagnosed based on fundoscopy.

This study was approved by the local medical ethics committee and was conducted according to the principles in the Declaration of Helsinki.

MRI protocol

All brain MRIs were performed on a 3.0 Tesla (Achieva; Philips Medical Systems, Best, The Netherlands). Brain MRI consisted of a 3 dimensional T1 (3D T1) sequence for brain volume assessment. 3D T1 acquisition parameters were: repetition time (TR) 9.8 ms, echo time (TE) 4.6 ms, flip angle (FA) 8º, field of view (FOV) 224 mm, 192x152 acquisition matrix, 256x256 reconstruction matrix, slice thickness 1.2 mm, 120 slices, no slice gap).

MRI post processing

All MRI scans were analyzed using different tools of FSL (FMRIB Software Library) (19). Whole brain volume, gray and white matter volumes were calculated using the FSL-tool SIENAX (Structural Image Evaluation, using Normalization, of Atrophy) (20,21). SIENAX starts by extracting brain and skull images from the single whole-head input data (22). The brain image is then affine-registered to MNI152 space (19), using the skull image to determine the registration scaling. This is primarily done in order to obtain the volumetric scaling factor, to be used as a normalization for head size. Next, tissue-type segmentation with partial volume estimation is performed to calculate total volume of brain tissue, including separate estimates of volumes of gray matter and white matter (23). To determine the volume of the subcortical twin structures nucleus accumbens, amygdala, caudate nucleus, hippocampus, pallidum, putamen and thalamus FMRIB's Integrated Registration and Segmentation Tool (FIRST) was used. FIRST starts by registering all im-

ages to MNI152 templates. Secondly it fits models for all different structures (meshes) to the images and finally applies boundary correction for the volumetric output.

A visual inspection of all registrations was performed and all final segmentations were visually inspected for accuracy.

Statistical analysis

Statistical analysis was performed by using SPSS (SPSS, Chicago, Illinois, USA), version 20. To compare clinical characteristics between T1DM and age- and gender-matched controls paired samples t-test for continuous variables with a normal distribution and nonparametric tests for non-normally distributed variables were used. Furthermore the McNemar test for dichotomous variables was used. Continuous variables are expressed as mean ± standard deviation (sd) or if non-normally distributed as median (interquartile range) and categorical variables were presented as frequencies and percentages.

The left and right volumes of the subcortical structures including the basal ganglia, the hippocampus and thalamus were added up and divided by 2 in order to obtain mean volumes.

Multivariate linear regression analyses were performed to assess the independent contribution of T1DM to the volumes of subcortical structures, by controlling for the following confounders: age, gender, GFR, smoking, BMI, hypertension, HDL-cholesterol and triglycerides. The β-regression coefficients and p-values are reported. Significance was reached when $p<0.05$ (two-tailed).

RESULTS

Three-dimensional T1-weighted MRI of the brain was performed in 62 patients with T1DM and 62 age- and gender-matched volunteers (52 ± 12 years, 55% male). Mean T1DM duration was 27.4 ± 12.7 years, all patients used insulin and diabetic retinopathy was present in 47 (76%) diabetic patients. The clinical characteristics of the study population are shown in Table 1. There were no differences between groups with respect to smoking, BMI and triglycerides. Cholesterol was lower and HDL higher in patients with T1DM compared to controls ($p= 0.011$ respectively 0.006). Twenty eight (45%) T1DM patients and 1 control subject used lipid lowering medication. Patients with T1DM were more often diagnosed with hypertension (37% vs 5%, $p<0.001$) and used more often blood pressure lowering drugs (34 % vs 2 %, $p<0.001$). Renal function estimated by GFR was higher in T1DM (92.3 ± 19.4 ml/min/1.73^2) compared to healthy volunteers (82.4 ± 12.4 ml/min/1.73^2, $p<0.001$)

Table 1. Clinical characteristics

	Type 1 diabetes mellitus (n=62)	Healthy controls (n=62)	p-value
Male sex, n (%)	34 (54.8)	34 (54.8)	1.000
Age, years	52 ± 12	52 ±13	0.381
Type 1 diabetes duration, years	27.4 ± 12.7	-	
Hypertension, n (%)	23 (37.1)	3 (4.8)	<0.001*
Current smoker, n (%)	8 (12.9)	8 (12.9)	1.000
Body mass index, kg/m2	25.3 ± 3.3	25.4 ±3.4	0.791
ACE inhibitors, n (%)	10 (16.1)	0 (0)	0.004*
AT2 antagonist, n (%)	11 (17.7)	0 (0)	0.125
Ca antagonist, n (%)	5 (8.1)	0 (0)	0.125
Diuretics, n (%)	7 (11.5)	0 (0)	0.016*
B blocker, n (%)	6 (9.7)	1 (1.6)	0.125
Use of statin, n (%)	28 (45.2)	1 (1.6)	<0.001*
Retinopathy, n (%)	47 (77)	-	
HbA1c, %	7.7 ± 1.1	-	-
HbA1c, mmol/mol	60.9 ± 11.7		
Fasting plasma glucose, mmol/l	-	5.22 ±0.86	-
Creatinine, mmol/l	74.8 ± 12.4	81.6 ±11.8	0.001*
Estimated GFR (MDRD), ml/min	92.3 ± 19.4	82.4 ±12.4	<0.001*
Total cholesterol, mmol/l	4.85 ± 0.95	5.33 ±1.30	0.011*
HDL cholesterol, mmol/l	4.80 (4.29-5.40)	5.32 (4.56-6.36)	0.013*
Triglycerides, mmol/l (median)	1.16 (0.79-1.39)	1.12 (0.82-1.55)	0.504

Data are means ± sd, number (%) or median (interquartile range). HbA1c: glycated hemoglobin, GFR: glomerular filtration rate, HDL: high density lipoprotein. Data were compared by paired samples t-test. *p<0.05.

Magnetic resonance imaging of the brain

Brain gray and white matter volumes were smaller in T1DM (Table 2). Both the thalamus (p<0.001) and the hippocampus (p=0.003) were significantly smaller in T1DM. Of the basal ganglia, volumes of the nucleus accumbens (p=0.044), the globus pallidus (=0.013), the putamen (p<0.001) and the nucleus caudate (p=0.044) were smaller in patients with T1DM compared to healthy volunteers. The amygdala was the only one

Table 2. Magnetic resonance imaging characteristics of patients with type 1 diabetes mellitus and healthy controls

	Diabetes mellitus (n=62)	Healthy controls (n=62)	p-value
	Volume, cm^3	Volume, cm^3	
Nucleus accumbens	0.46 ± 0.13	0.50 ± 0.10	0.043*
Globus pallidus	1.92 ± 0.25	2.02 ± 0.20	0.013*
Amygdala	1.38 ± 0.23	1.38 ± 0.21	0.984
Putamen	4.77 ± 0.47	5.17 ± 0.57	<0.001*
Nucleus caudate	3.57 ± 0.41	3.70 ± 0.44	0.044*
Thalamus	7.53 ± 0.87	7.98 ± 0.77	<0.001*
Hippocampus	3.96 ± 0.40	4.17 ± 0.41	0.003*
Whole brain			
Gray matter	7.09 ± 0.45×10^2	7.34 ± 0.43×10^2	<0.001*
White matter	7.04 ± 0.47×10^2	7.24 ± 0.46×10^2	0.014*
Gray + white matter	14.14 ± 0.72×10^2	14.57 ± 0.74×10^2	<0.001*

Values are means ± sd unless otherwise indicated. Volumes are corrected for head size. Gray matter: volume of normalized gray matter, White matter: volume of normalized white matter, Gray + white matter: volume of white and gray matter. Data were compared by paired samples t-test. *p<0.05.

structure of the gray matter areas explored in this study which did not differ in size between groups (p=0.984).

After correcting for the potential confounding factors age, gender, GFR, smoking, BMI, hypertension, HDL-cholesterol and triglycerides, the volumes of the thalamus (p=0.034), hippocampus (p=0.010) and putamen (p=0.002) remained significantly smaller in T1DM (Table 3). HbA1c was not associated with volumes of any of the gray matter areas.

DISCUSSION

The main purpose of the current study was to investigate with VBM technique whether the volumes of the hippocampus, thalamus, amygdala and basal ganglia, differed between patients with longstanding T1DM and healthy controls. The main finding of this study is that T1DM patients showed volume loss of all of these gray matter areas, except for the amygdala. Secondly our results show that after correcting for potential confounding factors, the thalamus, hippocampus and putamen were still significantly smaller in patients with T1DM.

Previous studies on hippocampal and thalamic volumes in T1DM have been performed (12,14,15,24). However, to our knowledge this is the first study to investigate in-depth volume loss in gray matter areas other than the hippocampus and thalamus, in T1DM with VBM. Earlier studies on gray matter in T1DM showed equivocal results with respect to the hippocampus and thalamus (12,14,15,24). However, three of these studies were performed on MR scanners with lower field strengths 1.0T (15) and 1.5T (12,14), as compared to our 3.0T MR scanner. In addition two of these studies did not use VBM to calculate the hippocampal volumes (14,15).

In our study the amygdala was the only structure with preserved volume in T1DM patients which is in contrast to a study performed in patients with type 2 diabetes mellitus (25). The amygdala has an important role in the reaction to hypoglycemia (26). Although the mechanism behind the differential volume remains unclear, the preservation of the volume of the amygdala could be related to its important function in the hypoglycemia awareness.

The underlying mechanisms for gray matter changes in T1DM are incompletely understood. There are several hypotheses on the pathological mechanisms causing these brain alterations. Both hyper- and hypoglycemia have been proposed to be involved. Hypoglycemic events are associated with less gray matter density (4,12,27). Furthermore hyperglycemia, expressed as a higher HbA1c, was suggested to contribute to lower gray-matter density in the left hippocampus (12), which was not confirmed in our study. In addition, accelerated formation and accumulation of advanced glycation end products have also been suggested to contribute to brain alterations and brain damage in T1DM (13,28,29). It has also been proposed that diabetes mellitus contributes to accelerated aging of the brain, which can lead to microvascular abnormalities (5,13). Furthermore, prior studies suggest that higher blood pressure or hypertension also negatively affect gray matter (30-33). However, in our study, effects of T1DM on specific gray matter structures remained significant after correction for hypertension. The intriguing finding that T1DM differentially affects specific gray matter areas is challenging but difficult to

explain. Potential differences in the susceptibility of the thalamus, hippocampus and putamen and other gray matter structures to T1DM related factors may be involved.

In conclusion using VBM technique, we found differential volume loss of the hippocampus, thalamus and basal ganglia in patients with T1DM, which was independent of potential confounding factors. The clinical significance and underlying mechanisms remain to be elucidated.

REFERENCES

1. Charles M, Soedamah-Muthu SS, Tesfaye S, Fuller JH et al.: Low peripheral nerve conduction velocities and amplitudes are strongly related to diabetic microvascular complications in type 1 diabetes: the EURODIAB Prospective Complications Study. *Diabetes Care* 33:2648-2653, 2010
2. Cho YH, Craig ME, Hing S, Gallego PH et al.: Microvascular complications assessment in adolescents with 2- to 5-yr duration of type 1 diabetes from 1990 to 2006. P*ediatr Diabetes* 12:682-689, 2011
3. Kodl CT, Franc DT, Rao JP, Anderson FS et al.: Diffusion tensor imaging identifies deficits in white matter microstructure in subjects with type 1 diabetes that correlate with reduced neurocognitive function. *Diabetes* 57:3083-3089, 2008
4. Perros P, Deary IJ, Sellar RJ, Best JJ et al.: Brain abnormalities demonstrated by magnetic resonance imaging in adult IDDM patients with and without a history of recurrent severe hypoglycemia. *Diabetes Care* 20:1013-1018, 1997
5. Biessels GJ, Staekenborg S, Brunner E, Brayne C et al.: Risk of dementia in diabetes mellitus: a systematic review. *Lancet Neurol* 5:64-74, 2006
6. Gouw AA, van der Flier WM, Fazekas F, van Straaten EC et al.: Progression of white matter hyperintensities and incidence of new lacunes over a 3-year period: the Leukoaraiosis and Disability study. *Stroke* 39:1414-1420, 2008
7. van Elderen SG, Brandts A, van der Grond J, Westenberg JJ et al.: Cerebral perfusion and aortic stiffness are independent predictors of white matter brain atrophy in type 1 diabetic patients assessed with magnetic resonance imaging. *Diabetes Care* 34:459-463, 2011
8. Ott A, Stolk RP, van HF, Pols HA et al.: Diabetes mellitus and the risk of dementia: The Rotterdam Study. *Neurology* 53:1937-1942, 1999
9. Manolio TA, Kronmal RA, Burke GL, Poirier V et al.: Magnetic resonance abnormalities and cardiovascular disease in older adults. The Cardiovascular Health Study. *Stroke* 25:318-327, 1994
10. DeCarli C, Miller BL, Swan GE, Reed T et al.: Predictors of brain morphology for the men of the NHLBI twin study. *Stroke* 30:529-536, 1999
11. McCrimmon RJ, Ryan CM, Frier BM: Diabetes and cognitive dysfunction. *Lancet* 379:2291-2299, 2012
12. Musen G, Lyoo IK, Sparks CR, Weinger K et al.: Effects of type 1 diabetes on gray matter density as measured by voxel-based morphometry. *Diabetes* 55:326-333, 2006
13. Wessels AM, Simsek S, Remijnse PL, Veltman DJ et al.: Voxel-based morphometry demonstrates reduced grey matter density on brain MRI in patients with diabetic retinopathy. *Diabetologia* 49:2474-2480, 2006
14. Hershey T, Perantie DC, Wu J, Weaver PM et al.: Hippocampal volumes in youth with type 1 diabetes. *Diabetes* 59:236-241, 2010
15. Lobnig BM, Kromeke O, Optenhostert-Porst C, Wolf OT: Hippocampal volume and cognitive performance in long-standing Type 1 diabetic patients without macrovascular complications. *Diabet Med* 23:32-39, 2006
16. Ashburner J, Friston KJ: Voxel-based morphometry--the methods. *Neuroimage* 11:805-821, 2000
17. Alberti KG, Zimmet PZ: Definition, diagnosis and classification of diabetes mellitus and its complications. Part 1: diagnosis and classification of diabetes mellitus provisional report of a WHO consultation. *Diabet Med* 15:539-553, 1998

18. Mancia G, De BG, Dominiczak A, Cifkova R et al.: 2007 Guidelines for the Management of Arterial Hypertension: The Task Force for the Management of Arterial Hypertension of the European Society of Hypertension (ESH) and of the European Society of Cardiology (ESC). *J Hypertens* 25:1105-1187, 2007
19. Smith SM, Jenkinson M, Woolrich MW, Beckmann CF et al.: Advances in functional and structural MR image analysis and implementation as FSL. *Neuroimage* 23 Suppl 1:S208-S219, 2004
20. Smith SM, De SN, Jenkinson M, Matthews PM: Normalized accurate measurement of longitudinal brain change. *J Comput Assist Tomogr* 25:466-475, 2001
21. Smith SM, Zhang Y, Jenkinson M, Chen J et al.: Accurate, robust, and automated longitudinal and cross-sectional brain change analysis. *Neuroimage* 17:479-489, 2002
22. Smith SM: Fast robust automated brain extraction. *Hum Brain Ma*pp 17:143-155, 2002
23. Zhang Y, Brady M, Smith S: Segmentation of brain MR images through a hidden Markov random field model and the expectation-maximization algorithm. *IEEE Trans Med Imaging* 20:45-57, 2001
24. Northam EA, Rankins D, Lin A, Wellard RM et al.: Central nervous system function in youth with type 1 diabetes 12 years after disease onset. *Diabetes Care* 32:445-450, 2009
25. den HT, Vermeer SE, van Dijk EJ, Prins ND et al.: Type 2 diabetes and atrophy of medial temporal lobe structures on brain MRI. *Diabetologia* 46:1604-1610, 2003
26. Dunn JT, Cranston I, Marsden PK, Amiel SA et al.: Attenuation of amydgala and frontal cortical responses to low blood glucose concentration in asymptomatic hypoglycemia in type 1 diabetes: a new player in hypoglycemia unawareness? *Diabetes* 56:2766-2773, 2007
27. Perantie DC, Wu J, Koller JM, Lim A et al.: Regional brain volume differences associated with hyperglycemia and severe hypoglycemia in youth with type 1 diabetes. *Diabetes Care* 30:2331-2337, 2007
28. Wrighten SA, Piroli GG, Grillo CA, Reagan LP: A look inside the diabetic brain: Contributors to diabetes-induced brain aging. *Biochim Biophys Acta* 1792:444-453, 2009
29. McIntyre RS, Kenna HA, Nguyen HT, Law CW et al.: Brain volume abnormalities and neurocognitive deficits in diabetes mellitus: points of pathophysiological commonality with mood disorders? *Adv Ther* 27:63-80, 2010
30. Chen X, Wen W, Anstey KJ, Sachdev PS: Effects of cerebrovascular risk factors on gray matter volume in adults aged 60-64 years: a voxel-based morphometric study. P*sychiatry Res* 147:105-114, 2006
31. Korf ES, White LR, Scheltens P, Launer LJ: Brain aging in very old men with type 2 diabetes: the Honolulu-Asia Aging Study. *Diabetes Care* 29:2268-2274, 2006
32. Salerno JA, Murphy DG, Horwitz B, DeCarli C et al.: Brain atrophy in hypertension. A volumetric magnetic resonance imaging study. *Hypertension* 20:340-348, 1992
33. Taki Y, Goto R, Evans A, Zijdenbos A et al.: Voxel-based morphometry of human brain with age and cerebrovascular risk factors. *Neurobiol Aging* 25:455-463, 2004

Chapter 5

Caloric restriction improves cardiovascular function in advanced type 2 diabetes mellitus

Linda D. van Schinkel, Hildo J. Lamb, Jos J.M. Westenberg, Charlotte E.A. Dronkers, J. Wouter Jukema, Albert de Roos, Johannes W.A. Smit

Submitted

ABSTRACT

Background

It is currently unknown whether prolonged caloric restriction improves cardiovascular function and reverses myocardial triglyceride (TG) accumulation in obese patients with type 2 diabetes mellitus (T2DM) and coronary artery disease (CAD). Our objective was to study whether caloric restriction improves cardiovascular function and decreases myocardial TG accumulation in patients with T2DM and coronary atherosclerosis.

Methods

Twenty-seven overweight or obese T2DM patients with documented CAD, i.e. myocardial infarction or percutaneous coronary intervention and/or coronary artery occlusion of >50%, were included. Patients followed a 16-week (very) low calorie diet (V)LCD (450-1000 kcal/day). A subgroup was observed for 16 weeks without intervention. Cardiovascular function, cardiac ectopic fat accumulation and aortic pulse wave velocity (PWV), a marker for vascular stiffness, were assessed with magnetic resonance spectroscopy and imaging.

Results

After intervention BMI decreased from 32.2 ± 4.7 (mean ± sd) to 26.8 ± 4.1kg/m^2, $p<0.001$ and HbA1c from 6.9 ± 0.9 to 5.8 ± 0.5%, $p<0.001$. Left ventricular ejection fraction increased from 54.8 ± 8.7 to 56.2 ± 7.9%, $p=0.016$. Myocardial TG decreased from 1.23 ± 0.60 to 0.82 ± 0.37%, $p=0.001$. Epicardial and paracardial fat volumes decreased from 5.5 ± 1.7 to 4.7 ± 1.7 ml and from 7.8 ± 3.8 to 5.6 ± 3.2 ml respectively, $p<0.001$. PWV decreased from 7.9 ± 1.9 to 7.2 ± 1.1 m/s, $p=0.016$, reflecting a less stiff aorta.

Conclusion

Prolonged caloric restriction in overweight T2DM patients with CAD improves cardiovascular function which is paralleled by decreased ectopic fat accumulation. The results of this study are clinically relevant and prove that dietary interventions, superposed on optimal pharmacological therapy, are worthwhile strategies, even in advanced T2DM.

INTRODUCTION

Cardiovascular disease (CVD) is the main cause of death in type 2 diabetes (T2DM) (1,2). Patients with T2DM who survived myocardial infarction (MI) are at an even higher risk of cardiovascular mortality, despite treatment with antidiabetic, antihypertensive drugs and statins (3). The pathogenesis of cardiovascular complications in T2DM is complex but a major role is attributed to ectopic accumulation of triglycerides (TG) in organs that normally do not store fat, such as the liver and heart. Ectopic fat accumulation is closely associated with the generation of toxic intermediates of lipid oxygenation, mitochondrial dysfunction and activation of inflammatory pathways which all contribute to organ dysfunction (4-8). Cardiac ectopic fat includes myocardial and pericardial fat accumulation. Both are associated with impaired myocardial function (5,9,10) and increased CVD risk (11). Ectopic fat can be visualized by magnetic resonance (MR) spectroscopy and -imaging (MRI) (5,8,12,13) and can be modulated by dietary interventions in healthy subjects (14) as well as in obese subjects (15-18). Prolonged caloric restriction in obese patients with T2DM without established coronary atherosclerosis leads to a decrease in ectopic fat, including myocardial and pericardial fat and improves myocardial function (19,20). Because of their increased cardiovascular risk, it is important to establish whether T2DM patients with coronary artery disease (CAD) also benefit from prolonged caloric restriction. We therefore studied the effects of 16 weeks caloric restriction cardiovascular function and ectopic fat accumulation in overweight patients with T2DM and established CAD. Additionally, to study the effect of the dietary intervention on vascular function, we also assessed aortic pulse wave velocity (PWV), which is an important cardiovascular risk indicator (21).

METHODS

Subjects

Twenty-seven T2DM patients were included. Patients were recruited from the outpatient clinic of the Leiden University Medical Center and via advertisement. Inclusion criteria were T2DM, BMI>25 kg/m^2 and documented CAD. Established atherosclerosis or CAD were defined as a history of myocardial infarction and/or percutaneous coronary intervention (PCI) and/or a >50% stenosis in a coronary artery as documented by CT angiography. Exclusion criteria were: hepatic disease, glomerular filtration rate <60ml/min, congenital heart disease and general contraindications to MR scanning. Subjects underwent a medical screening including physical examination and blood chemistry tests. The study was approved by the local ethics committee and performed in accor-

dance with the revised Declaration of Helsinki. Written informed consent was obtained from all subjects. The study was registered in the Dutch Trial Register (NTR 2897).

Study design

Patients were studied on two days, separated by a 16-week dietary intervention period, during which a (very) low calorie diet ((V)LCD) was prescribed. In order to assess the variability in study parameters without dietary intervention, 13 of the 27 patients were also studied during 16 weeks prior to start of the (V)LCD (baseline observation period). Patients were instructed not to alter life style during the study.

The (V)LCD consisted of Prodimed products (Prodimed®, Prodimed Benelux BV, Valkenswaard, The Netherlands) which are low in calories, with a relatively high protein content (www.prodimed.nl/producten). All patients started with total meal replacement: 4-6 sachets a day (400-600 kcal/day) including a warm meal of Prodimed for three weeks, supplemented with a limited choice of vegetables. After these 3 weeks caloric intake was increased, by replacing a Prodimed at dinnertime by meat or fish. Afterwards, when an additional 3% weight loss was achieved, the caloric intake was further expanded with one Prodimed being replaced with a normal meal. One week before the last study day, the diet was expanded, with a normal breakfast to achieve a caloric intake of 1000 kcal/day. During the intervention period, weekly visits were performed and blood pressure and weight were measured. Blood was drawn monthly to assess safety parameters (liver and kidney function).

Use of sulphonyl urea derivatives was discontinued the day the (V)LCD started and insulin therapy was adjusted according to glucose levels. Patients on insulin treatment were asked to measure their blood glucose levels 4 times a day throughout the study.

Anthropometric measurements, blood sampling and MR imaging and spectroscopy were performed after ≥5 hours of fasting at each study day. Blood was centrifuged immediately at 4°C and serum was stored at -80°C until analyses.

Magnetic Resonance spectroscopy and Imaging

MR measurements were performed at a 1.5-Tesla MR scanner (Gyroscan ACS-NT15; Philips Medical Systems, The Netherlands).

MR spectroscopy

MR spectroscopy (^{1}H-MRS) was performed to quantify myocardial and hepatic TG content. Details on ^{1}H-MRS acquisition and post processing were published before (22,23). Shortly, for the heart an 8-ml voxel was positioned in the interventricular septum on four-chamber and short-axis images in end-systole. Electrocardiographically (ECG) triggering (for myocardial spectra) and respiratory pencil beam navigator were used

during acquisition (22). For the liver, voxel sites were matched at all study occasions Acquisitions were performed with and without water suppression. jMRUI v2.2 (Leuven, Belgium) was used for fitting the spectra. Myocardial and hepatic TG were calculated as a percentage of the unsuppressed water signal.

Delayed enhancement

Delayed enhancement (DCE) MRI for detection of myocardial scar was performed 15 minutes after injection of gadetorate meglumine, 0.3ml/kg (DOTAREM, Guerbet, USA), as described before (24). The optimal inversion time was determined using the Look-Locker sequence.

Left ventricular dimensions and function

The heart was imaged in short-axis orientation, as previously described (25), using an ECG gated breath-hold cine steady-state free-procession sequences to assess systolic function. Left ventricular (LV) end-diastolic and end-systolic contours were drawn, using in-house developed validated MASS® software (Leiden University Medical Center, Leiden, The Netherlands). LV end-diastolic volume (EDV), end-systolic volume (ESV), ejection fraction (EF), mass, cardiac output (CO) and stroke volume (SV) were calculated. Several function parameters were indexed to body surface area (BSA) (26). We divided LV mass by LVEDV to obtain the LV mass/LVEDV ratio (also known as concentricity).

LV diastolic function was studied from transmitral flow rate graphs, assessed from 3D three-directional velocity-encoded (VE) MRI with retrospective valve tracking as previously described (27). From the transmitral flow rate graphs, the following LV diastolic function parameters were determined using MASS® software (Leiden University Medical Center, Leiden, The Netherlands): maximal flow velocities and peak filling rate in early diastole (E) and at atrial contraction (A) and the ratio between peak filling at E and A were calculated (E/A ratio). In addition, the downslope after early peak filling rate (E deceleration) and the ratio between maximal flow velocity during E and the through-plane velocity assessed in the myocardial wall Ea (E/Ea), the LV filling pressure, were assessed (26,28).

Pericardial fat

Pericardial fat volume, consisting of epicardial and paracardial fat, was derived from fat-selective imaging using SPIR, as described before (29). The heart was imaged using a multi shot turbo spin echo sequence in a four-chamber view orientation. Contours were drawn around both pericardial fat layers surrounding the ventricles and atria us-

ing MASS® (Figure 1). The number of pixels were converted to square centimeters and multiplied by the slice thickness to obtain volume.

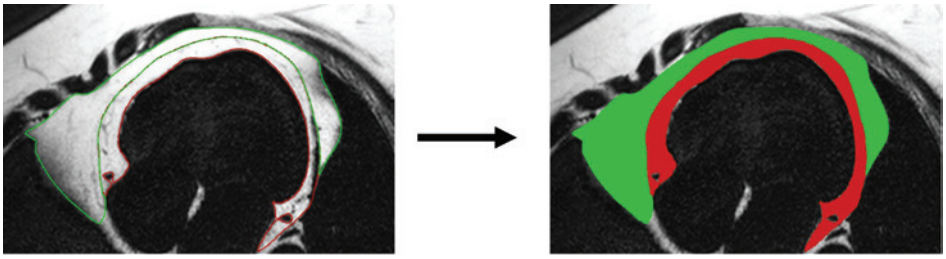

Figure 1. This figure shows the quantification of the pericardial fat layer, which can be divided in an epicardial (red) and paracardial (green) fat layer.

Visceral and subcutaneous fat

Abdominal visceral and subcutaneous fat volumes were quantified at the level of the fifth lumbar vertebra, using a turbo spin echo imaging sequence (10). During one breath-hold, three consecutive transversal slices of 10mm thickness were scanned. Visceral and subcutaneous fat areas of each slice were multiplied by the slice thickness to acquire a volume and the volumes of all three slices were summed. Volumes of visceral and subcutaneous fat accumulation were quantified using MASS®.

Pulse Wave Velocity

To evaluate the aortic stiffness, aortic PWV was determined, using a previously described protocol (21). A scout view of the aorta was obtained. Subsequently, two time-resolved velocity-encoded acquisitions perpendicular to the ascending aorta at the level of the pulmonary trunk and at the level of the aortic bifurcation were assessed, resulting in through-plane flow measurements. PWV was calculated with the formula: $\Delta x/\Delta t$. Δx is the length of the aorta between two measurement sites and Δt is the time delay between the arrivals of the foot of the pulse wave at the respective measurements site. The distance between the measurement sites was determined manually with MASS®. MASS® and FLOW® were used for analyzing the data.

Biochemical Assays

Serum concentrations of glucose, total cholesterol, HDL and TG were measured on a Modular P800 analyzer (Roche, The Netherlands) and insulin on an Immulite 2500 analyzer (Siemens, The Netherlands). HbA1c was measured on a HPLC system (Kordia, The Netherlands). FFA concentrations were measured in duplicate by a commercial kit, an in vitro enzymatic colorimetric method assay for the quantitative determination of

FFAs in serum (Wako Chemicals, Neuss, Germany). hsCRP levels and plasma levels of the various cytokines were assessed using precoated 96-well multispot plates from Meso Scale Discovery (MSD; Gaithersburg, Maryland, USA), an enzyme linked immunosorbent assay (ELISA) based electrochemiluminiscence assay. Plasma CETP was quantified using a quantitative assay CETP ELISA kit (ALPCO Diagnostics, Salem, New Hampshire, USA).

Statistical analysis

Statistical analyses were performed with SPSS, version 20.0 (SPSS Inc., Chicago, U.S.A.). Within group changes were assessed using paired sample t-test for variables with normal distribution. Data are presented as mean ± standard deviation (sd). $p<0.05$ was considered to be statistically significant.

Based on the previous 16-week VLCD study in obese patients with T2DM *without* cardiovascular complications (19), we performed a sample size calculation. In order to detect an improvement of the E/A ratio of 16% with a power of 0.90 and alpha of 0.05 it was calculated that 9 patients are needed. In addition, to detect a decrease of myocardial TG content with 27%, power of 0.90 and alpha of 0.05, 8 patients are needed. To anticipate on patients leaving the study prematurely because of dietary incompliance and insufficient MR spectra, we aimed to include 30 patients.

The Dutch Heart Foundation funded this study, but was not involved in study design or execution.

RESULTS

Most patients underwent the dietary intervention without problems. Thirty-two patients started the (V)LCD, however 3 patients left the study (2 due to intolerance of the diet and one because of worsening of Ménière's disease). Two patients were excluded because they did not adhere to the diet.

Characteristics of the study population are shown in Table 1. Mean age of the participants was 62.2 ± 6.0 years. Sixteen patients had previously experienced a MI, 24 underwent PCI and 3 patients had a coronary artery bypass grafting (CABG). One patient had >50% occlusion of the coronary arteries on CT without a subsequent intervention (i.e. PCI or CABG). There were no differences in age, duration of T2DM or anthropometric measurements between patients with and without a MI in medical history. At the start of the (V)LCD 12 patients used insulin and all patients were on oral anti-diabetic drugs. All patients were on anti-hypertensive treatment, consisting of β-blockers, α-blockers, ACE inhibitors, AT II antagonists, nitrates, calcium antagonists, diuretics or a combination of the aforementioned medications. During the (V)LCD, 3 patients discontinued insulin

treatment and 3 patients discontinued all anti-diabetic drugs. Average weight loss was 16.5 ± 5.5 kg and BMI reduced from 32.2 ± 4.7 to 26.8 ± 4.1 kg/m^2, p<0.001 (Table 1). Glycemic control was significantly improved after 16 weeks of (V)LCD, reflected by decreased fasting glucose levels, from 7.4 ± 1.7 to 6.3 ± 1.2 mmol/L, p=0.002 and decreased HbA1c levels from 6.9 ± 0.9% to 5.8 ± 0.5%, p<0.001. Total cholesterol, HDL-cholesterol and plasma TG decreased after the (V)LCD. Plasma free fatty acids (FFA) did not change after the (V)LCD nor did interleukin (IL) 6, IL 10 and high sensitive c-reactive protein (hsCRP).

Table 1. Clinical and metabolic characteristics

	Before (V)LCD	After (V)LCD	p-value
Clinical characteristics			
Age (years)	62.2 ± 6.0		
Male sex, n (%)	22 (82)		
DM type 2 duration (years)	11.0 ± 8.5		
BMI (kg/m^2)	32.2 ± 4.7	26.8 ± 4.1	<0.001
Patients on insulin, n (%)	12 (44.4)	9 (33.3)	
Insulin dose (units/day)	79 ± 36	16 ± 12	
Metabolic characteristics			
Glucose (mmol/L)	7.4 ± 1.7	6.3 ± 1.2	0.002
HbA1c (%)	6.9 ± 0.9	5.8 ± 0.5	<0.001
TG (mmol/L)	1.80 ± 0.89	1.17 ± 0.43	<0.001
Total cholesterol (mmol/L)	4.18 ± 0.86	3.82 ± 0.67	0.018
HDL-cholesterol (mmol/L)	1.18 ± 0.28	1.32 ± 0.34	0.001
Interleukin 6 (pg/mL)	1.30 ± 1.82	0.81 ± 0.50	0.168
Interleukin 10 (pg/mL)	0.52 ± 0.26	0.51 ± 0.24	0.813
hsCRP (mg/L)	3.82 ± 4.34	2.17 ± 3.03	0.078
Free fatty acids (mmol/L)	0.61 ± 0.25	0.59 ± 0.29	0.836

Data are mean ± sd. HbA1c: glycated hemoglobin, TG: triglycerides, HDL: high density lipoprotein, hsCRP: high sensitive c-reactive protein.

Fat distribution

Delayed enhancement MRI revealed a septal MI in 5 patients, which prohibited myocardial TG measurements in these patients. Therefore we excluded these 5 patients for analyses of myocardial TG. Myocardial TG in the other patients decreased from 1.23 ± 0.60% at baseline to 0.82 ± 0.37% after (V)LCD, p=0.001 (-28%) (Figure 2, upper panel).

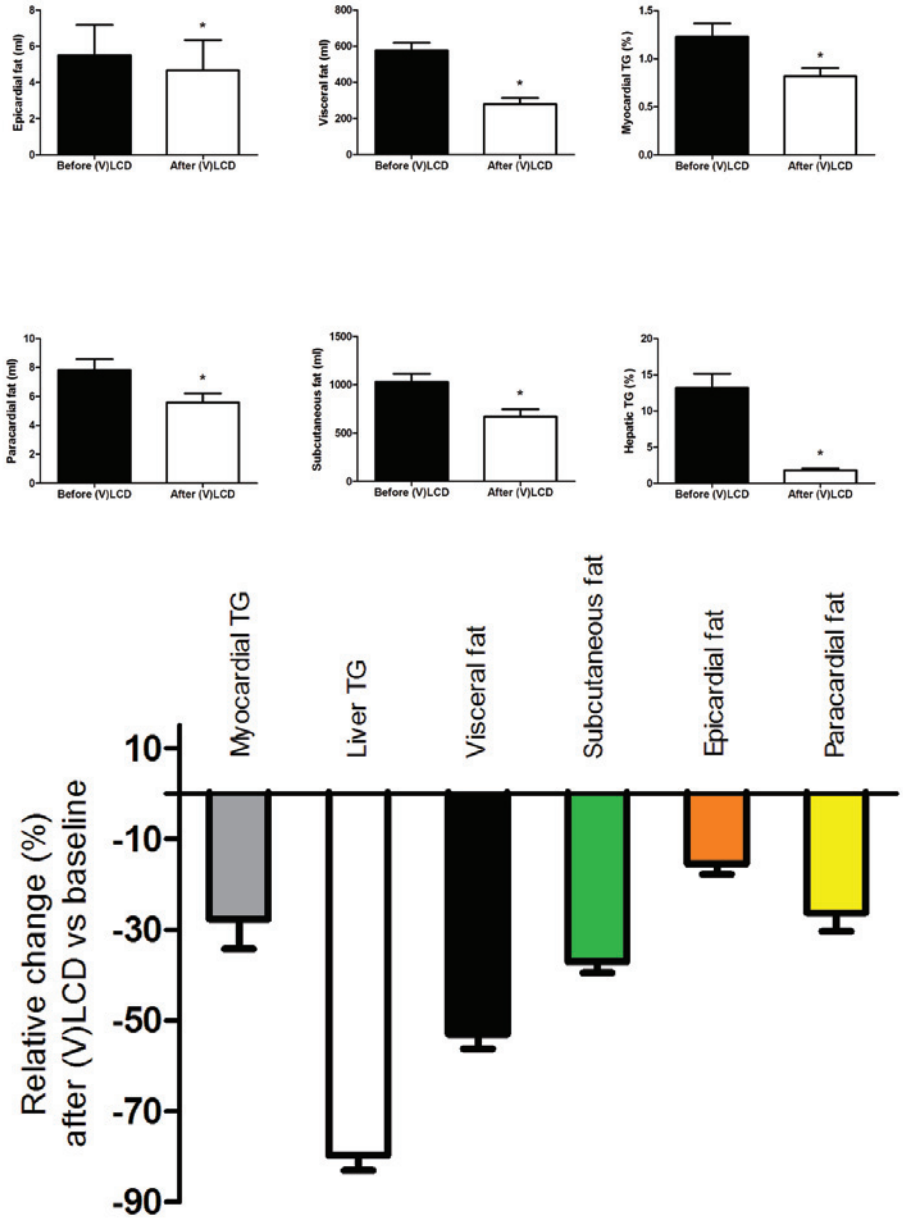

Figure 2. The upper panel shows changes in the various fat compartments before and after a 16-week (very) low calorie diet ((V)LCD). The lower panel shows relative changes in the fat compartments after (V)LCD as compared to baseline. TG: triglycerides, *p<0.001.

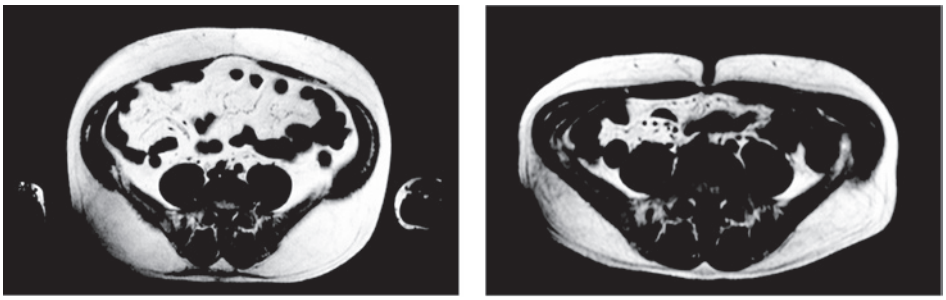

Figure 3. Example of a waistfat measurement at the level of the fifth lumbar vertebrae, showing visceral and subcutaneous fat accumulation. The left panel shows the effect of the 16-week (V)LCD in one patient on these fat accumulations before (left) and after (right) the (V)LCD.

There were no differences in myocardial TG in patients with or without MI. Hepatic TG content at baseline was 13.2 ± 10.4% and decreased dramatically after (V)LCD to 1.8 ± 1.3%, p<0.001(-80%) (Figure 2, upper panel). Epicardial and paracardial fat volumes reduced from 5.5 ± 1.7 to 4.7 ± 1.7 ml, p<0.001 (-15%) and from 7.8 ± 3.8 to 5.6 ± 3.2 ml, p<0.001 (-26%) respectively (Figure 2, upper panel). Furthermore, visceral fat volume and subcutaneous fat volumes decreased significantly after (V)LCD, respectively from 577 ± 216 to 279 ± 177 ml and from 1029 ± 447 to 671 ± 390 ml, p<0.001 (-53% and -37% respectively) (Figure 2, upper panel, and 3). The relative changes in the above mentioned fat compartments are given in Figure 2, lower panel.

Cardiac dimensions and function

Table 2 shows the changes in cardiac dimensions and function before and after 16 weeks caloric restriction. Systolic and diastolic blood pressures and heart rate decreased after weight loss (Table 2). LV mass decreased significantly, from 114 ± 27 to 104 ± 27 g, p<0.001 after the (V)LCD and systolic cardiac function improved. Cardiac output (CO) decreased significantly. LVEDV and LVSV increased after 16 weeks and LVEF increased.

The E/A ratio increased, however it did not reach statistical significance. E deceleration, another parameter of diastolic function, did not change. The estimated filling pressures remained unchanged after weight loss.

Pulse wave velocity

The aortic PWV decreased significantly from 7.9 ± 1.9 m/s at baseline to 7.2 ± 1.1 m/s, p=0.016, after the (V)LCD.

Baseline observation period

All clinical, biochemical and MR parameters of the subgroup of 13 patients that was studied during 16 weeks prior to the start of the (V)LCD, did not change during this period (see Supplemental Tables 1 and 2).

Table 2. Effects of 16 weeks caloric restriction on systolic and diastolic cardiac function

	Before (V)LCD	After (V)LCD	p-value
Systolic blood pressure (mm Hg)	146 ± 14	129 ± 12	<0.001
Diastolic blood pressure (mm Hg)	83 ± 10	75 ± 9	0.002
Heart rate (beats/min)	68 ± 12	60 ± 8	0.002
Cardiac dimensions and function			
LV mass (g)	114 ± 27	104 ± 27	<0.001
LV mass index (g/m^2)	53.4 ± 11.1	52.8 ± 12.3	0.418
EDV (ml)	175 ± 7.3	183 ± 7.6	0.033
EDVI (ml/m^2)	81.9 ± 15.1	92.6 ± 16.7	<0.001
ESV (ml)	81 ± 29	82 ± 31	0.481
ESVI (ml/m^2)	37.9 ± 13.0	41.4 ± 14.7	<0.001
LV mass/EDV	0.66 ± 0.11	0.57 ± 0.09	<0.001
SV (ml)	94 ± 18	101 ± 17	0.007
SVI (ml/m^2)	44.1 ± 7.1	51.1 ± 6.4	<0.001
CO (L/min)	6225 ± 982	5619 ± 1410	0.029
CI (L/min/m^2)	2921 ± 390	2846 ± 643	0.571
EF (%)	54.8 ± 8.7	56.2 ± 7.9	0.016
E/A-peak ratio	0.95 ± 0.28	1.08 ± 0.27	0.063
E deceleration (ml/s^{2}x10^{-3})	-2.20 ± 0.96	-1.87 ± 0.53	0.108
E/Ea	8.9 ± 5.0	6.6 ± 4.4	0.076

Data are mean ± sd. LV: left ventricular, EDV: end-diastolic volume, I: indexed for body surface area, ESV: end-systolic volume, SV: stroke volume, CO: cardiac output, CI: cardiac index, EF: ejection fraction, E: early diastolic filling phase, A: diastolic atrial contraction, E/Ea: estimate of LV filling pressure.

DISCUSSION

The present study was performed to evaluate the effects of 16 weeks caloric restriction in overweight patients with T2DM and established coronary atherosclerosis on cardiovascular function and ectopic fat accumulation. We found substantial beneficial changes in glucoregulation and cardiovascular function. These improvements were paralleled by reductions in all fat compartments as well as ectopic fat accumulation in the liver and heart. These data show that cardiovascular function and ectopic fat accumulation are susceptible to dietary intervention in complicated T2DM, which has important clinical implications.

Fat accumulation

Myocardial TG accumulation is the net result of excessive FFA uptake in relation to FFA oxidation. Patients with T2DM have increased myocardial TG content (5), which is associated with impaired myocardial function (10). Reducing myocardial TG leads to improved cardiac function in uncomplicated T2DM patients (19) and according to our study also in patients with T2DM and CAD. Although the association between cardiac fat accumulation and cardiac function does not prove a causal relationship, in a previous study we demonstrated that inhibiting lipolysis leads to decrease in myocardial TG accumulation and improved cardiac function (19). In addition, multiple direct and indirect beneficial effects of caloric restriction and weight loss may have added to the results observed, such as decreased blood pressure, improved glycemic control, decreased hepatic fat accumulation (30) and improved PWV.

In addition to myocardial TG, we found a decrease in pericardial fat. Pericardial fat consists of two layers, epicardial fat (located between the myocardium and visceral pericardium) and paracardial fat (located outside the parietal pericardium) which are both associated with insulin resistance, T2DM and cardiovascular disease (9,31-33). Therefore, the effects as observed in our study in pericardial fat are considered beneficial.

As expected, hepatic TG content and visceral fat decreased dramatically. This is in accordance with previous diet intervention studies in patients with T2DM (19,34).

Cardiac dimensions and function

LV mass and heart rate decreased, which is beneficial, since both are important predictors for cardiovascular disease (35,36). Furthermore, parameters of LV function improved even after correction for BSA (19,37,38) which was also observed in uncomplicated T2DM (19). The E/Ea ratio, an estimate of LV filling pressure, did not change after the diet. The increased LV EDV at similar estimates of LV filling pressure is compatible with an improved LV compliance (39).

An interesting finding of the current study is that LVEF increased after the (V)LCD (19). In some studies no effect on systolic function was observed (19,40,41). Others observed an improved LV systolic function, though based on other parameters than an improved LVEF (42-44). However, these studies differed considerably from ours, as not all patients had T2DM and/or coronary artery disease (40). In addition, interventions were heterogeneous, including exercise (44), other dietary products (19) or bariatric surgery (40-43). The follow-up period varied widely, from 3 months up to 3.6 years and except for one study (19), all studies used cardiac ultrasound which is considered less accurate than MRI (45). The improvement of LVEF in the current study is clinically relevant, since LVEF is one of the most important predictors of survival (46).

Diastolic function did not significantly change after the 16-week (V)LCD in contrast to previous studies in uncomplicated T2DM that found significant improvements in E/A ratio after prolonged caloric restriction (19,38).

Pulse wave velocity

PWV is a surrogate marker for arterial stiffness and a powerful independent predictor of cardiovascular events (47). Our study revealed a decrease in PWV of 0.7 m/s, indicating a less stiff aorta. Given the fact that PWV increases with 0.7m/s per 10 years of aging (48) this is a significant improvement. No prior studies have been published on the effects of dietary intervention on PWV in complicated T2DM (49-51). As most factors that contribute to arterial stiffness improved in our study, including blood pressure (52), obesity, insulin resistance and diabetes mellitus (53-55), no single causal mechanism can be identified from our data.

Laboratory markers

FFA did not change after the (V)LCD. Serum FFA concentrations are a reflection of dietary lipids and lipolysis on the one hand and FFA clearance on the other hand. During caloric restriction, both lipolysis and FFA oxygenation increase which can account for a net unchanged serum FFA concentration. In addition, the inflammation markers, IL 6, IL 10 and hsCRP, which were already low at baseline, did not change. Obesity and T2DM associated inflammation is concentrated in organs and tissues, like adipose tissue and the liver, and may not be reflected in serum concentrations of cytokines. These results are in line with a previous study showing no changes in FFA and inflammation markers after a 16-week VLCD (56).

The strength of this study is that it is the first to document the effects of prolonged caloric restriction on cardiovascular function and ectopic fat distribution in overweight T2DM patients *with* established CAD. A possible limitation to this study is the relatively small sample size. However, power calculation revealed that our study had sufficient

power to detect changes in outcome measures. Furthermore in a subgroup, it was established that study parameters did not change over time without dietary intervention.

Since T2DM is associated with increased cardiovascular risk (57) and CVD is the main cause of death in patients T2DM (1,2), the results of this study are clinically relevant and prove that dietary interventions, superposed on optimal pharmacological therapy, are worthwhile strategies, even in advanced complicated T2DM.

REFERENCES

1. Centers for Disease Control and Prevention: 2011 National Diabetes Fact Sheet. *www cdc gov/diabetes/pubs/factsheet11 htm* 2011
2. Stamler J, Vaccaro O, Neaton JD, Wentworth D: Diabetes, other risk factors, and 12-yr cardiovascular mortality for men screened in the Multiple Risk Factor Intervention Trial. *Diabetes Care* 16:434-444, 1993
3. Murcia AM, Hennekens CH, Lamas GA, Jimenez-Navarro M et al.: Impact of diabetes on mortality in patients with myocardial infarction and left ventricular dysfunction. *Arch Intern Med* 164:2273-2279, 2004
4. Gastaldelli A, Cusi K, Pettiti M, Hardies J et al.: Relationship between hepatic/visceral fat and hepatic insulin resistance in nondiabetic and type 2 diabetic subjects. *Gastroenterology* 133:496-506, 2007
5. McGavock JM, Lingvay I, Zib I, Tillery T et al.: Cardiac steatosis in diabetes mellitus: a 1H-magnetic resonance spectroscopy study. *Circulation* 116:1170-1175, 2007
6. Teupe C, Rosak C: Diabetic cardiomyopathy and diastolic heart failure -- difficulties with relaxation. *Diabetes Res Clin Pract* 97:185-194, 2012
7. van de Weijer T, Schrauwen-Hinderling VB, Schrauwen P: Lipotoxicity in type 2 diabetic cardiomyopathy. *Cardiovasc Res* 92:10-18, 2011
8. van der Meer RW, Lamb HJ, Smit JW, de Roos A: MR imaging evaluation of cardiovascular risk in metabolic syndrome. *Radiology* 264:21-37, 2012
9. Greif M, Becker A, von ZF, Lebherz C et al.: Pericardial adipose tissue determined by dual source CT is a risk factor for coronary atherosclerosis. *Arterioscler Thromb Vasc Biol* 29:781-786, 2009
10. Rijzewijk LJ, van der Meer RW, Smit JW, Diamant M et al.: Myocardial steatosis is an independent predictor of diastolic dysfunction in type 2 diabetes mellitus. *J Am Coll Cardiol* 52:1793-1799, 2008
11. Thanassoulis G, Massaro JM, Hoffmann U, Mahabadi AA et al.: Prevalence, distribution, and risk factor correlates of high pericardial and intrathoracic fat depots in the Framingham heart study. *Circ Cardiovasc Imaging* 3:559-566, 2010
12. Nelson AJ, Worthley MI, Psaltis PJ, Carbone A et al.: Validation of cardiovascular magnetic resonance assessment of pericardial adipose tissue volume. *J Cardiovasc Magn Reson* 11:15, 2009
13. Sacks HS, Fain JN: Human epicardial adipose tissue: a review. *Am Heart J* 153:907-917, 2007
14. Hammer S, van der Meer RW, Lamb HJ, Schar M et al.: Progressive caloric restriction induces dose-dependent changes in myocardial triglyceride content and diastolic function in healthy men. *J Clin Endocrinol Metab* 93:497-503, 2008
15. Bosy-Westphal A, Kossel E, Goele K, Blocker T et al.: Association of pericardial fat with liver fat and insulin sensitivity after diet-induced weight loss in overweight women. *Obesity (Silver Spring)* 18:2111-2117, 2010
16. Iacobellis G, Singh N, Wharton S, Sharma AM: Substantial changes in epicardial fat thickness after weight loss in severely obese subjects. *Obesity (Silver Spring)* 16:1693-1697, 2008
17. Kim MK, Tanaka K, Kim MJ, Matuso T et al.: Comparison of epicardial, abdominal and regional fat compartments in response to weight loss. *Nutr Metab Cardiovasc Dis* 19:760-766, 2009
18. Viljanen APM, Karmi A, Borra R, P+ñrkk+ñ JP et al.: Effect of Caloric Restriction on Myocardial Fatty Acid Uptake, Left Ventricular Mass, and Cardiac Work in Obese Adults. *The American Journal of Cardiology* 103:1721-1726, 2009

19. Hammer S, Snel M, Lamb HJ, Jazet IM et al.: Prolonged caloric restriction in obese patients with type 2 diabetes mellitus decreases myocardial triglyceride content and improves myocardial function. *J Am Coll Cardiol* 52:1006-1012, 2008
20. Snel M, Jonker JT, Hammer S, Kerpershoek G et al.: Long-term beneficial effect of a 16-week very low calorie diet on pericardial fat in obese type 2 diabetes mellitus patients. *Obesity (Silver Spring)* 20:1572-1576, 2012
21. Grotenhuis HB, Westenberg JJ, Steendijk P, van Der Geest RJ et al.: Validation and reproducibility of aortic pulse wave velocity as assessed with velocity-encoded MRI. *J Magn Reson Imaging* 30:521-526, 2009
22. van der Meer RW, Doornbos J, Kozerke S, Schar M et al.: Metabolic imaging of myocardial triglyceride content: reproducibility of 1H MR spectroscopy with respiratory navigator gating in volunteers. *Radiology* 245:251-257, 2007
23. Vanhamme L, van den Boogaart A, Van HS: Improved method for accurate and efficient quantification of MRS data with use of prior knowledge. *J Magn Reson* 129:35-43, 1997
24. Ng AC, Auger D, Delgado V, van Elderen SG et al.: Association between diffuse myocardial fibrosis by cardiac magnetic resonance contrast-enhanced T(1) mapping and subclinical myocardial dysfunction in diabetic patients: a pilot study. *Circ Cardiovasc Imaging* 5:51-59, 2012
25. Lamb HJ, Doornbos J, van der Velde EA, Kruit MC et al.: Echo planar MRI of the heart on a standard system: validation of measurements of left ventricular function and mass. *J Comput Assist Tomogr* 20:942-949, 1996
26. Pattynama PM, Lamb HJ, van der Velde EA, van der Wall EE et al.: Left ventricular measurements with cine and spin-echo MR imaging: a study of reproducibility with variance component analysis. *Radiology* 187:261-268, 1993
27. Brandts A, Bertini M, van Dijk EJ, Delgado V et al.: Left ventricular diastolic function assessment from three-dimensional three-directional velocity-encoded MRI with retrospective valve tracking. *J Magn Reson Imaging* 33:312-319, 2011
28. Paelinck BP, de Roos A, Bax JJ, Bosmans JM et al.: Feasibility of tissue magnetic resonance imaging: a pilot study in comparison with tissue Doppler imaging and invasive measurement. *J Am Coll Cardiol* 45:1109-1116, 2005
29. Jonker JT, de MP, de Vries ST, Widya RL et al.: Exercise and Type 2 Diabetes Mellitus: Changes in Tissue-Specific Fat Distribution and Cardiac Function. *Radiology* 2013
30. Rijzewijk LJ, Jonker JT, van der Meer RW, Lubberink M et al.: Effects of hepatic triglyceride content on myocardial metabolism in type 2 diabetes. *J Am Coll Cardiol* 56:225-233, 2010
31. Iacobellis G, Leonetti F: Epicardial adipose tissue and insulin resistance in obese subjects. *J Clin Endocrinol Metab* 90:6300-6302, 2005
32. Rosito GA, Massaro JM, Hoffmann U, Ruberg FL et al.: Pericardial fat, visceral abdominal fat, cardiovascular disease risk factors, and vascular calcification in a community-based sample: the Framingham Heart Study. *Circulation* 117:605-613, 2008
33. Wang CP, Hsu HL, Hung WC, Yu TH et al.: Increased epicardial adipose tissue (EAT) volume in type 2 diabetes mellitus and association with metabolic syndrome and severity of coronary atherosclerosis. *Clin Endocrinol (Oxf)* 70:876-882, 2009
34. Hammer S, van der Meer RW, Lamb HJ, de Boer HH et al.: Short-term flexibility of myocardial triglycerides and diastolic function in patients with type 2 diabetes mellitus. *Am J Physiol Endocrinol Metab* 295:E714-E718, 2008

35. Kannel WB, Kannel C, Paffenbarger RS, Jr., Cupples LA: Heart rate and cardiovascular mortality: the Framingham Study. *Am Heart J* 113:1489-1494, 1987
36. Levy D, Garrison RJ, Savage DD, Kannel WB et al.: Prognostic implications of echocardiographically determined left ventricular mass in the Framingham Heart Study. *N Engl J Med* 322:1561-1566, 1990
37. Poirier P, Giles TD, Bray GA, Hong Y et al.: Obesity and cardiovascular disease: pathophysiology, evaluation, and effect of weight loss: an update of the 1997 American Heart Association Scientific Statement on Obesity and Heart Disease from the Obesity Committee of the Council on Nutrition, Physical Activity, and Metabolism. *Circulation* 113:898-918, 2006
38. Gaborit B, Jacquier A, Kober F, Abdesselam I et al.: Effects of bariatric surgery on cardiac ectopic fat: lesser decrease in epicardial fat compared to visceral fat loss and no change in myocardial triglyceride content. *J Am Coll Cardiol* 60:1381-1389, 2012
39. van der Meer RW, Rijzewijk LJ, de Jong HW, Lamb HJ et al.: Pioglitazone improves cardiac function and alters myocardial substrate metabolism without affecting cardiac triglyceride accumulation and high-energy phosphate metabolism in patients with well-controlled type 2 diabetes mellitus. *Circulation* 119:2069-2077, 2009
40. Garza CA, Pellikka PA, Somers VK, Sarr MG et al.: Structural and functional changes in left and right ventricles after major weight loss following bariatric surgery for morbid obesity. *Am J Cardiol* 105:550-556, 2010
41. Leichman JG, Aguilar D, King TM, Mehta S et al.: Improvements in systemic metabolism, anthropometrics, and left ventricular geometry 3 months after bariatric surgery. *Surg Obes Relat Dis* 2:592-599, 2006
42. Alpert MA, Terry BE, Mulekar M, Cohen MV et al.: Cardiac morphology and left ventricular function in normotensive morbidly obese patients with and without congestive heart failure, and effect of weight loss. *Am J Cardiol* 80:736-740, 1997
43. Alpert MA, Terry BE, Kelly DL: Effect of weight loss on cardiac chamber size, wall thickness and left ventricular function in morbid obesity. *Am J Cardiol* 55:783-786, 1985
44. Kosmala W, O'Moore-Sullivan T, Plaksej R, Przewlocka-Kosmala M et al.: Improvement of left ventricular function by lifestyle intervention in obesity: contributions of weight loss and reduced insulin resistance. *Diabetologia* 52:2306-2316, 2009
45. Chandra S, Skali H, Blankstein R: Novel techniques for assessment of left ventricular systolic function. *Heart Fail Rev* 16:327-337, 2011
46. Chareonthaitawee P, Sorajja P, Rajagopalan N, Miller TD et al.: Prevalence and prognosis of left ventricular systolic dysfunction in asymptomatic diabetic patients without known coronary artery disease referred for stress single-photon emission computed tomography and assessment of left ventricular function. *Am Heart J* 154:567-574, 2007
47. Mitchell GF, Hwang SJ, Vasan RS, Larson MG et al.: Arterial stiffness and cardiovascular events: the Framingham Heart Study. *Circulation* 121:505-511, 2010
48. Westenberg JJ, Scholte AJ, Vaskova Z, van der Geest RJ et al.: Age-related and regional changes of aortic stiffness in the marfan syndrome: Assessment with velocity-encoded MRI. *J Magn Reson Imaging* 2011
49. Barinas-Mitchell E, Kuller LH, Sutton-Tyrrell K, Hegazi R et al.: Effect of weight loss and nutritional intervention on arterial stiffness in type 2 diabetes. *Diabetes Care* 29:2218-2222, 2006

50. Dengo AL, Dennis EA, Orr JS, Marinik EL et al.: Arterial destiffening with weight loss in overweight and obese middle-aged and older adults. *Hypertension* 55:855-861, 2010
51. Goldberg Y, Boaz M, Matas Z, Goldberg I et al.: Weight loss induced by nutritional and exercise intervention decreases arterial stiffness in obese subjects. *Clin Nutr* 28:21-25, 2009
52. Cecelja M, Chowienczyk P: Dissociation of aortic pulse wave velocity with risk factors for cardiovascular disease other than hypertension: a systematic review. *Hypertension* 54:1328-1336, 2009
53. Salomaa V, Riley W, Kark JD, Nardo C et al.: Non-insulin-dependent diabetes mellitus and fasting glucose and insulin concentrations are associated with arterial stiffness indexes. The ARIC Study. Atherosclerosis Risk in Communities Study. *Circulation* 91:1432-1443, 1995
54. Schram MT, Henry RM, van Dijk RA, Kostense PJ et al.: Increased central artery stiffness in impaired glucose metabolism and type 2 diabetes: the Hoorn Study. *Hypertension* 43:176-181, 2004
55. Sutton-Tyrrell K, Newman A, Simonsick EM, Havlik R et al.: Aortic stiffness is associated with visceral adiposity in older adults enrolled in the study of health, aging, and body composition. *Hypertension* 38:429-433, 2001
56. Snel M, van Diepen JA, Stijnen T, Pijl H et al.: Immediate and long-term effects of addition of exercise to a 16-week very low calorie diet on low-grade inflammation in obese, insulin-dependent type 2 diabetic patients. *Food Chem Toxicol* 49:3104-3111, 2011
57. Wang CC, Reusch JE: Diabetes and cardiovascular disease: changing the focus from glycemic control to improving long-term survival. *Am J Cardiol* 110:58B-68B, 2012

Supplemental Table 1. Clinical and metabolic characteristics

	4 months before (V)LCD	before (V)LCD	p-value
Clinical characteristics			
Male sex, n (%)	12 (92)		
DM type 2 duration (years)	7.8 ± 4.1		
BMI (kg/m^2)	31.7 ± 3.9	31.9 ± 4.1	0.328
Patients on insulin, n (%)	3 (23)	4 (31)	
Insulin dose (units/day)	68 ± 14	70 ± 11	
Metabolic characteristics			
Glucose (mmol/L)	6.8 ± 1.4	7.4 ± 1.8	0.203
HbA1c (%)	7.2 ± 1.5	6.8 ± 1.1	0.422
TG (mmol/L)	2.01 ± 1.02	2.14 ± 1.00	0.600
Total cholesterol (mmol/L)	4.26 ± 0.76	4.42 ± 0.80	0.404
HDL-cholesterol (mmol/L)	1.15 ± 0.31	1.17 ± 0.30	0.604
Interleukin 6 (pg/mL)	1.19 ± 0.62	0.88 ± 0.48	0.100
Interleukin 10 (pg/mL)	0.46 ± 0.16	0.50 ± 0.21	0.448
hsCRP (mg/L)	3.62 ± 4.03	3.99 ± 4.81	0.807
Free fatty acids (mmol/L)	0.50 ± 0.20	0.54 ± 0.19	0.473

Data are mean ± sd. HbA1c: glycated hemoglobin, TG: triglycerides, HDL: high density lipoprotein, hsCRP: high sensitive c-reactive protein.

Supplemental Table 2. Systolic and diastolic cardiac function

	4 months before (V)LCD	Before (V)LCD	p-value
Systolic blood pressure (mm Hg)	149 ± 14	143 ± 12	0.212
Diastolic blood pressure (mm Hg)	87 ± 9	84 ± 11	0.129
Heart rate (beats/min)	67 ± 15	63 ± 13	0.276
Cardiac dimensions and function			
LV mass (g)	118 ± 27	116 ± 23	0.470
LV mass index (g/m^2)	57 ± 12	56 ± 11	0.452
EDV (ml)	178 ± 40	178 ± 40	0.897
EDVI (ml/m^2)	85 ± 15	85 ± 17	0.867
ESV (ml)	86 ± 31	86 ± 33	0.919
ESVI (ml/m^2)	41 ± 13	41 ± 15	0.994
LV mass/EDV	0.68 ± 0.17	0.67 ± 0.13	0.571
SV (ml)	92 ± 20	93 ± 20	0.695
SVI (ml/m^2)	44 ± 8	44 ± 8	0.739
CO (L/min)	5844 ± 834	5762 ± 956	0.701
CI (L/min/m^2)	2793 ± 281	2746 ± 355	0.645
EF (%)	52.4 ± 9.2	53.0 ± 10.0	0.443
E/A-peak ratio	0.86 ± 0.27	0.93 ± 0.26	0.304
E deceleration (ml/s^{2}x10^{-3})	-2.10 ± 1.02	-1.92 ± 0.94	0.653
E/Ea	7.2 ± 4.9	6.8 ± 4.4	0.769

Data are mean ± sd. LV: left ventricular, EDV: end-diastolic volume, I: indexed for body surface area, ESV: end-systolic volume, SV: stroke volume, CO: cardiac output, CI: cardiac index, EF: ejection fraction, E: early diastolic filling phase, A: diastolic atrial contraction, E/Ea: estimate of LV filling pressure.

Chapter 6

Effects of bariatric surgery on pericardial ectopic fat depositions and cardiovascular function

Linda D. van Schinkel*, Maria A. Sleddering*, Mirjam A. Lips, Jacqueline T. Jonker, Albert de Roos, Hildo J. Lamb, Ingrid M. Jazet, Hanno Pijl, Johannes W.A. Smit

** both authors contributed equally*

Clinical Endocrinology 2014; in press

ABSTRACT

Background

Cardiac ectopic fat depositions are thought to play a role in the pathogenesis of cardiovascular disease (CVD), the main cause of death in type 2 diabetes (T2DM) patients. Diet-induced weight loss results in a decrease in cardiac ectopic fat stores, however if this is the same for surgically-induced weight loss is less clear. Therefore, we assessed myocardial triglyceride (TG) content, pericardial fat and cardiac function in obese, insulin-dependent T2DM patients before and 16 weeks after Roux-en-Y gastric bypass (RYGB) surgery.

Methods

Ten obese, insulin-dependent T2DM patients (40% male, age 53.7 ± 8.9 years (mean ± sd)) scheduled to undergo RYGB surgery were included. Ectopic fat accumulation and cardiovascular function and were assessed with magnetic resonance (MR) imaging and myocardial TG content with MR spectroscopy before and 16 weeks after RYGB surgery.

Results

BMI decreased from 41.3 ± 4.3 at baseline to 34.1 ± 2.8 kg/m^2 ($p<0.001$) after 16 weeks. Glycemic control improved as well (HbA1c: 7.8 ± 1.1 to 6.8 ± 1.3% (62 ± 12 to 51 ± 14 mmol/l) ($p<0.05$)). We did not observe an effect of the RYGB surgery on myocardial TG content, cardiac function or pulse wave velocity. There was a greater relative decrease in visceral (-35.5 ± 9.6%) as compared to subcutaneous fat volume (-25.0 ± 6.3%) and in paracardial (-17.3 ± 17.2%) as compared to epicardial fat volume (-6.4 ± 6.0%).

Conclusions

This study shows that surgical-induced weight loss leads to a larger decrease in paracardial than epicardial fat. Myocardial TG and cardiovascular function did not change.

INTRODUCTION

Cardiovascular disease (CVD) is the main cause of death in type 2 diabetes (T2DM) patients (1). Apart from an increased risk of ischemic heart disease, T2DM is associated with non-ischemic heart disease, also referred to as diabetic cardiomyopathy. In the early stages this is mainly characterized by diastolic dysfunction (2,3). Several mechanisms have been proposed to explain the pathogenesis of diabetic cardiomyopathy, such as hyperinsulinemia, insulin resistance, inflammation, deposition of collagen and advanced glycation end products, altered calcium handling and lipotoxicity (2,3).

Lipotoxicity is caused by accumulation of triglycerides (TG) in tissues other than adipose tissue, also called ectopic fat deposition. Obesity as well as T2DM are associated with ectopic fat depositions in liver, skeletal muscle and heart (4). Concerning the heart, TG can be stored in the myocardium or in pericardial fat, the adipose tissue surrounding the heart. These ectopic fat depots can be visualized non-invasively by magnetic resonance imaging (MRI) and magnetic resonance (MR) spectroscopy (3,5-7). Pericardial fat consists of two distinctive fat depots, epicardial fat and paracardial fat (5). An increased pericardial fat volume is associated with insulin resistance and an increased cardiovascular risk (8-10). Furthermore, myocardial TG content is increased in subjects with impaired glucose tolerance and is associated with diastolic dysfunction in T2DM patients (6,11). A previous study showed that a 16-week very low calorie diet (VLCD) results in a decrease in myocardial TG content and an improvement in diastolic function in obese insulin-dependent T2DM patients (12). Furthermore, in these patients a decrease in pericardial fat was seen directly after the diet, but also after 14 months follow-up, despite considerable weight regain (13). These data suggest that cardiac ectopic fat stores are flexible and can be modulated by weight loss. Indeed, others also showed a decrease in cardiac ectopic fat in response to diet-induced weight loss (14,15).

Over 80% of T2DM patients are overweight or obese, and weight loss remains the hallmark of their treatment. However, long-term maintenance of weight loss is extremely difficult. Bariatric surgery results in sustained weight loss (16). Furthermore, bariatric surgery leads to diabetes remission in 70-80% of T2DM patients (17) and is associated with a decreased incidence of diabetes (18) and cardiovascular events (19) as well as a long-term reduction in overall mortality (20) in obese subjects. It is largely unknown whether cardiac ectopic fat depots can also be mobilized by bariatric surgery. In one study in obese subjects using MRI a decrease in epicardial fat content was seen 6 months after bariatric surgery. However, there was no decrease in myocardial TG content and paracardial fat was not assessed (21). In addition, since only 26% of the subjects in this study had T2DM, the effects of bariatric surgery on cardiac fat depots in T2DM patients, who are at particularly high risk of developing myocardial dysfunction, are currently

unknown. We hypothesize that surgically-induced weight loss can lead to mobilization of cardiac ectopic fat accumulation in T2DM patients, with a focus on pericardial fat, and thereby improve cardiovascular function. Therefore, we assessed pericardial fat, myocardial TG content and cardiac function in obese, insulin-dependent T2DM patients before and 4 months after a Roux-en-Y gastric bypass (RYGB) using MRI and MR spectroscopy. Furthermore, we studied aortic pulse wave velocity (PWV), which is surrogate marker for arterial stiffness and a cardiovascular risk indicator, using MRI.

METHODS

Patients

Ten morbidly obese subjects with T2DM scheduled to undergo RYGB surgery were included in this study. Subjects eligible for surgical treatment were recruited from the waiting lists of several Dutch bariatric surgery centers, after referral for a weight loss program by their GP or internist. They had been screened previously by a multidisciplinary team of the Nederlandse Obesitaskliniek (Dutch Obesity Clinic) to establish if they fulfilled the international criteria for bariatric surgery as described by Fried et. al. (22): BMI > 35 kg/m^2 with co-morbidity (i.e. T2DM), which is expected to improve after surgically-induced weight loss, a history of longstanding obesity (>5 years), proven failed attempts to lose weight in a conventional way, or initially successful weight loss with eventual weight regain. Other inclusion criteria were age between 18-60 years and the use of insulin to control T2DM. Exclusion criteria were any significant chronic disease except for T2DM, known cardiovascular disease, weight > 150 kg (because of the weight restrictions of a standard MRI table) and general contraindications for MRI (for example claustrophobia or a pacemaker).

The study was approved by the local ethics committee and performed in accordance with the principles of the revised Declaration of Helsinki. Written informed consent was obtained from all subjects.

Study design

Patients were studied on 2 occasions. MR studies were performed shortly before and 16 weeks after the RYGB. The first MRI was planned as close as possible to the planned RYGB surgery, however due to scheduling difficulties of the surgery, two patients had a longer time interval. An incidental finding at the first MRI, which eventually was proven to be a benign cyst in the kidney, prolonged the time interval in a third patient. The median time interval between the first MRI and the RYGB was 16 days (interquartile range (IQR) 62 days). Anthropometric measurements and blood samples were obtained on both

study days after ≥ 5 hours of fasting. Fat mass was assessed by bioelectrical impedance analysis (BIA; Bodystat® 1500, Bodystat Ltd., Douglas, UK).

MR protocol

All measurements were performed using a 1.5-Tesla whole-body MR scanner (Gyroscan ACS-NT15; Philips Medical Systems, Netherlands) in postprandial state (≥ 5 hours after the last meal).

Myocardial and liver triglyceride content

MR spectroscopy (^{1}H-MRS) data were obtained as described before and were used to quantify myocardial TG content (23). Briefly, a 8-ml voxel was positioned in the myocardial interventricular septum in end-systole, avoiding contamination from epicardial fat. Electrocardiographically (ECG) triggering and respiratory pencil beam navigation were used during acquisition. For the liver, at both study occasions, voxel sites were matched, avoiding blood vessels and bile ducts. Spectra with water suppression were acquired with TE=26ms and TR≥3,000ms. 1,024 data points were collected using a 1,000-Hz spectral width and averaged over 128 acquisitions. Spectra without water suppression with TR=10s and four averages were obtained without changing other parameters. Spectroscopic data were fitted using validated software (jMRUI version 2.2, Leuven, Belgium). The TG content was calculated as (amplitude of TG signal/amplitude water signal) x 100%.

Epicardial and paracardial fat quantification

To quantify the pericardial fat volume, the heart was imaged in a four chamber view orientation using ECG gated breath-holds with a multi shot turbo spin echo sequence, as described before (24). Water was suppressed using Spectral Inversion Recovery (SPIR). Imaging parameters were: slice thickness 4mm, scan matrix: 251x256 pixels, FA=90°, TE=8.6 ms and TR≥1000 ms. Adipose tissue around the heart was easily identified because of the water suppression, and contours were drawn around the epicardial and paracardial fat surrounding the ventricles and atria using MASS® software (Medis, Leiden, the Netherlands). The number of pixels were converted to square centimeters and multiplied by the slice thickness to obtain volume.

Visceral and subcutaneous fat

Abdominal visceral and subcutaneous fat volumes were imaged using a turbo spin echo imaging sequence (11). During one breath-hold, three consecutive transversal slices of 10mm thickness were scanned at the fifth lumbar vertebrae. Imaging parameters were TR=168ms, TE=11ms, FA=90º. Contours were drawn around visceral and subcutaneous

abdominal fat depots using Mass®. Visceral and subcutaneous fat areas of each individual slice were multiplied by the slice thickness to acquire a volume and the volumes of all three slices were summed.

Left ventricular dimensions and function

The entire heart was imaged in short-axis orientation, using ECG gated breath-hold cine steady-state free-precession sequences, as previously described(25). Imaging parameters were: repetition time (TR) 3.4ms, echo time (TE) 1.7ms, flip angle (FA) 35º, field of view (FOV) 400×320mm, and slice thickness 10mm, no slice gap was used. To assess left ventricular (LV) systolic function, epicardial and endocardial contours were manually drawn in the end-systolic and end-diastolic phases of the short-axis images, using validated MASS® software (Medis, Leiden, Netherlands). LV end-diastolic volume (EDV), end-systolic volume (ESV), ejection fraction (EF), stroke volume (SV) and end-diastolic mass (EDM) were calculated. Volumes and mass were indexed (I) for body surface area (BSA).

Furthermore, to assess LV diastolic function, flow across the mitral valve was measured using an ECG gated gradient-echo sequence with velocity encoding. Scan parameters were: TR=9.1ms, TE=1.0ms, FA=20º, slice thickness=8mm, FOV 350x350mm, matrix 256x256 pixels, velocity encoding = 100 cm/sec. Analysis was performed using FLOW® software (Medis, Leiden, Netherlands). Flow velocities in early diastole (E) and at atrial contraction (A) were measured and the peak flow ratio was calculated (E/A ratio). In addition the peak deceleration gradient of E and LV filling pressures E/Ea were assessed (26,27).

Pulse Wave Velocity

Aortic PWV was determined to assess aortic stiffness, using a previously described protocol (28). In short, the aorta was imaged in a double-oblique parasagittal scout view. Subsequently, a velocity-encoded image perpendicular to the ascending aorta at the level of the pulmonary trunk and at the abdominal descending aorta was assessed. This resulted in through-plane flow measurements of the ascending and descending aorta. Scan parameters were: TR=5.0ms, TE 3.0ms, flip angle=20º, FOV=300mm, 128×128 acquisition matrix, slice thickness=8mm, with maximal number of phases reconstructed ensuring high (6-10ms) effective temporal resolution. True temporal resolution is defined as 2 times TR=10ms. PWV was calculated using the formula: $\Delta x/\Delta t$, where Δx is the aortic path length between two measurement sites and Δt is the time delay between the arrivals of the foot of the pulse wave at the respective measurements site. The distance between the two measurement sites was manually determined by drawing a poly-line in the center of the aorta as defined in a double-oblique parasagittal aortic scout view,

using the software package MASS®. Data were analyzed using MASS® and FLOW® (Medis, Leiden, Netherlands).

Surgical Intervention

During RYGB, a 25 ml gastric pouch was created and connected to a 100 cm Roux-en-Y limb. The Roux limb was connected end-to-side to the jejunum 100 cm distal of the ligament of Treitz.

Assays

Serum concentrations of glucose, total cholesterol, HDL and triglycerides were measured on a Modular P800 analyzer (Roche, Netherlands), and serum insulin levels on an Immulite 2500 (Siemens, Netherlands). HbA1c was measured on an HPLC system (Kordia, Netherlands).

Statistical analysis

Data are presented as mean ± sd. We used two-tailed paired t-tests to compare the two study time points. Nonparametric tests (Wilcoxon signed-rank test for paired samples) were performed as appropriate. A p-value of <0.05 was considered statistically significant. Statistical analyses were performed using SPSS for Windows version 20.0 (IBM, USA).

RESULTS

Clinical and metabolic characteristics

The mean age of the patients was 53.7 ± 8.9 years and mean duration of T2DM was 13.9 ± 8.2 years. Clinical and metabolic parameters before and after bariatric surgery are shown in Table 1. BMI decreased from 41.3 ± 4.3 at baseline to 34.1 ± 2.8 kg/m^2 ($p<0.001$) 16 weeks after bariatric surgery. After the RYGB, glycemic control was significantly improved, as shown by a decrease in HbA1c from 7.8 ± 1.1 to 6.8 ± 1.3 % (62 ± 12 to 51 ± 14 mmol/l) ($p<0.05$). According to the inclusion criteria, all patients used insulin at baseline. After 16 weeks the average total daily dose of insulin decreased from 134 ± 66 units at baseline to 26 ± 25 units. Two patients were able to discontinue insulin treatment completely.

Table 1. Clinical and metabolic characteristics

	Before RYGB	After RYGB	p-value
Clinical characteristics (n= 10)			
age (years)	53.7 ± 8.9		
male sex, n (%)	4 (40)		
height (m)	1.72 ± 0.08		
weight (kg)	122.4 ± 11.3	101.0 ± 7.7	<0.001
BMI (kg/m^2)	41.3 ± 4.3	34.1 ± 2.8	<0.001
systolic BP (mmHg)	143 ± 24	132 ± 12	0.154
diastolic BP (mmHg)	77 ± 11	76 ± 8	0.959
heart rate (bpm) (n= 7)	75 ± 11	63 ± 15	0.031
fat percentage (%)	48.3 ± 6.6	41.3 ± 7.1	<0.001
Metabolic characteristics (n= 9)			
HbA1c (%)	7.8 ± 1.1	6.8 ± 1.3	0.028
glucose (mmol/L)	9.8 ± 3.9	7.4 ± 3.0	0.037
triglycerides (mmol/L)	2.5 ± 1.1	1.9 ± 0.7	0.037
total cholesterol (mmol/L)	4.3 ± 0.7	3.6 ± 0.7	0.070
HDL-cholesterol (mmol/L)	0.98 ± 0.36	1.01 ± 0.25	0.594
LDL-cholesterol (mmol/L) (n= 8)	2.1 ± 0.5	1.7 ± 0.7	0.215
CRP (mg/L) (n= 8)	8.24 ± 6.4	6.13 ± 4.6	0.038

Data are presented as mean ± sd. DM: diabetes mellitus, BMI: body mass index, BP: blood pressure.

MRI and MRS studies

Results from the MR studies are shown in Table 2 and Table 3. Due to technical difficulties MRI data are not available for all patients (see tables for details on specific scans).

Fat compartments

Pericardial fat volume decreased 16 weeks after the RYGB. When the two pericardial fat compartments (epicardial and paracardial fat) were assessed separately, a significant reduction in both fat depots was shown (Table 2). A difference in proportional decreases was seen, with a higher relative proportional decrease in paracardial (-17.3 ± 17.2 %) as compared to epicardial (-6.4 ± 6.0%) fat volume (Figure 1). Myocardial TG content decreased as well, however this did not reach statistical significance.

Table 2. Ectopic fat distribution and myocardial and hepatic triglyceride content assessed with MRS and MRI before and after RYGB.

	Before RYGB	After RYGB	p-value
Visceral fat (ml)	891 ± 210	576 ± 168	<0.001
Subcutaneous fat (ml) (n= 9)	1652 ± 189	1234 ± 141	<0.001
Visceral / subcutaneous ratio (n= 9)	0.54 ± 0.19	0.46 ± 0.17	0.040
Myocardial TG content (%) (n= 9)	1.18 ± 0.44	0.91 ± 0.56	0.192
Hepatic TG content (%) (n= 9)	20.2 ± 12.4	6.6 ± 5.3	0.002
Paracardial fat (ml) (n= 7)	7.5 ± 3.3	6.3 ± 3.4	0.028
Epicardial fat (ml) (n= 7)	6.7 ± 2.3	6.2 ± 2.0	0.047
Pericardial fat (ml) (n= 7)	14.1 ± 4.7	12.5 ± 4.6	0.008

Data are mean ± sd. TG: triglyceride.

Table 3. Cardiac dimensions and parameters of cardiovascular function assessed with MRI before and after RYGB.

	Before RYGB	After RYGB	p-value
Cardiac dimensions and basic function (n= 9)			
LVEDMI (g/m^2)	50.2 ± 8.9	47.7 ± 8.4	0.339
EDVI (ml/m^2)	86.2 ± 18.4	93.2 ± 19.4	0.096
ESVI (ml/m^2)	35.3 ± 8.8	37.6 ± 11.2	0.186
SVI (ml/m^2)	55.6 ± 9.1	50.9 ± 10.4	0.112
CI ($ml/min/m^2$)	3276 ± 498	3030 ± 388	0.085
EF (%)	59.2 ± 3.4	60.2 ± 5.0	0.374
Diastolic cardiac function (n= 9)			
E peak filling rate (ml/s)	510 ± 161	492 ± 135	0.110
E acceleration peak (ml/s^2x10^{-3})	7.3 ± 1.9	7.0 ± 2.4	0.542
E deceleration peak (ml/s^2x10^{-3})	-4.3 ± 2.0	-4.0 ± 1.5	0.272
A peak filling rate (ml/s)	414 ± 118	410 ± 116	0.848
A acceleration peak (ml/s^2x10^{-3})	7.1 ± 2.4	7.1 ± 1.8	0.984
A deceleration peak (ml/s^2x10^{-3})	-8.0 ± 3.1	-8.2 ± 3.4	0.671
E/A-peak ratio	1.26 ± 0.36	1.28 ± 0.51	0.885
E/Ea	8.4 ± 3.2	8.8 ± 2.6	0.801
Pulse wave velocity (n= 7)			
PWV total aorta (m/s)	7.5 ± 1.5	6.2 ± 0.8	0.055

Data are mean ± sd. LV: left ventricular, EDM: end-diastolic mass, EDV: end-diastolic volume, ESV: end-systolic volume, SV: stroke volume, CI: cardiac index, EF: ejection fraction, ESWS: end-systolic wall stress. I: indexed for body surface area, E: early diastolic wave, A: atrial diastolic wave, E/Ea: estimated left ventricular filling pressure, PWV: pulse wave velocity.

After the RYGB the visceral and subcutaneous fat volumes were significantly reduced. There was a higher relative decrease in visceral as compared to subcutaneous fat volume, as reflected by a decrease in the visceral/subcutaneous fat ratio (Table 2 and Figure 1).

Cardiovascular function

Parameters for cardiac dimensions and systolic and diastolic function are shown in Table 3. Sixteen weeks after RYGB the parameters of systolic and diastolic cardiac function had not changed significantly. However, a trend was seen for a decrease in PVW (baseline: 7.5 ± 1.5; 16 weeks: 6.2 ± 0.8 m/s; p=0.055).

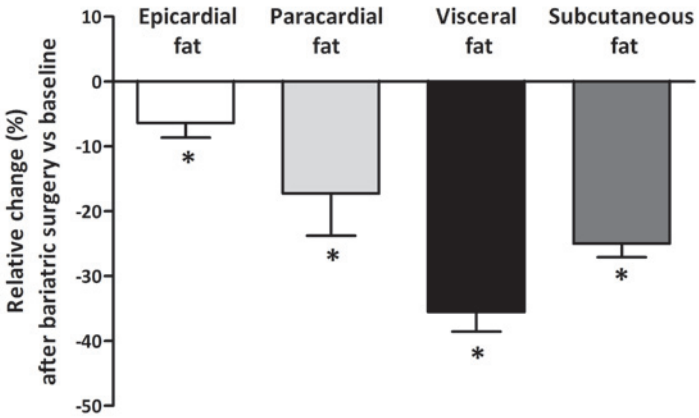

Figure 1. This figure shows the relative changes in epicardial, paracardial, visceral and subcutaneous abdominal fat volume. *p<0.05 significant change in fat volume compared to baseline.

DISCUSSION

This study was performed to assess the effects of bariatric surgery on cardiac ectopic fat accumulation in T2DM patients, with a focus on pericardial fat, which has not been studied in detail before. We found a substantial reduction in ectopic cardiac fat, after 16 weeks follow-up. Interestingly, we observed a differential response of the pericardial fat layers after RYGB surgery, which has not been shown before. Pericardial fat consists of two layers, epicardial fat (located between the myocardium and visceral pericardium) and paracardial fat (located outside the parietal pericardium). Epicardial fat is a visceral fat depot, originating from mesothelial cells, and it is supplied by branches of the coronary arteries (5). Epicardial fat is thought to have several beneficial functions, for instance serving as a buffer to protect the myocardium from a toxic overload of free fatty acids (FFAs) and, on the other hand, supplying FFAs as an immediate energy source for the cardiac muscle in times of need. Furthermore, it might protect the coronary arteries from torsion (5,29,30). However, increased epicardial fat volume has been associated with insulin resistance, T2DM and cardiovascular disease (8-10,31). Studies that assessed epicardial fat volume with MRI showed that epicardial fat volume is related to visceral fat volume at baseline (32) and decreases after diet-induced weight loss and exercise in obese subjects (4). Previous studies with echocardiography revealed that epicardial fat thickness decreases after diet-induced weight loss (33). Bariatric surgery also leads to a decrease in epicardial fat in obese subjects as measured by echocardiography (14,34) and MRI (21). In our study there was a decrease in epicardial fat volume as well; however the relative decrease in paracardial fat volume was much higher. The role of paracardial fat is currently less clear. Some studies have shown that paracardial fat is a better predictor of cardiovascular risk than epicardial fat (35). Furthermore, a 6-month exercise intervention in T2DM patients led to a decrease in visceral and paracardial, but not epicardial fat (24). This study and our findings might suggest that exercise and weight loss in T2DM patients have differential effects on paracardial adipose tissue as opposed to epicardial adipose tissue. In contrast, a very recent study showed no differences in epicardial nor in paracardial fat after bariatric surgery. However, the follow-up duration in that study was shorter (mean 80 ± 24 days), as compared to our follow-up, which might explain the different results (36). Long-term follow-up of our patient group would be interesting to determine whether epicardial fat response is delayed compared with visceral and subcutaneous fat.

We also observed that the abdominal fat compartments did not respond equally to the surgically-induced weight loss. The observed preferential loss of visceral fat as compared to subcutaneous fat confirms findings of earlier studies in obese subjects after bariatric surgery (21) and in T2DM patients after a VLCD (13).

We did not observe a decrease in myocardial TG after RYBG surgery. Gaborit et al. also did not show a decrease in myocardial TG content 6 months after bariatric surgery (21). It is an interesting finding that previous studies with dietary-induced weight loss interventions did find decreased myocardial TG in obese subjects with and without T2DM (12,15), whereas this is not found in studies on weight loss induced by bariatric surgery. It could be suggested that the surgical-induced weight loss has a differential effect on myocardial TG as compared to diet induced weight loss. It is, however, unclear what the cause of this difference might be. It could be that a major surgery results in a higher inflammatory stress response as compared to dietary intervention. However, the CRP levels of our patients significantly decreased 4 months after surgery. A rapid decrease in markers of a chronic low grade inflammatory state after bariatric surgery has been found by others as well (37). In contrast to dietary interventions, bariatric surgery also directly induces significant changes in gastro-intestinal hormone secretion (38), which might contribute to the differences. The exact mechanism explaining the differences between dietary- and surgical-induced weight loss on myocardial TG content therefore warrants further investigation.

The high myocardial TG content at baseline in our study is striking. Other studies report myocardial TG contents of around 1.0% (12,21), whereas we found a value of 1.18 ± 0.44%. This high baseline value might indicate more severe cardiac lipotoxicity in our patient group and concomitant less flexibility of the myocardial TG content.

After the RYGB, we found a (non-significant) decrease in pulse wave velocity, suggesting an improvement of central arterial stiffness. We did not observe an effect of RYGB surgery on cardiac function. The most important parameter for diastolic function, the E/A ratio, however, was already within the normal range (> 1.0) at baseline, with a mean value of 1.26 ± 0.36. Therefore an improvement in diastolic function might not be expected. In a previous study that did find improved diastolic function after weight loss using a VLCD, the E/A ratio at baseline was lower as compared to our study (12). In contrast, diastolic cardiac function did improve in the study by Gaborit et al. (21) 6 months after bariatric surgery, even though a high E/A ratio was present at baseline as well. The difference might be explained by the fact that only 26% of the patients in that study had T2DM, whereas all of our patients were insulin-dependent T2DM patients. Furthermore, in our study only 2 of the 10 patients were able to stop insulin treatment 4 months after the bypass surgery. It can therefore not be excluded that continued hyperinsulinemia may have influenced cardiac function.

A limitation of our study is the small sample size. Because of the narrow interior of the MRI scanner and the maximum allowable weight of the MRI table many candidates for bariatric surgery are not eligible for MR studies. However, our study was successful in showing substantial changes of bariatric surgery on ectopic fat accumulation and

in particular provided new data on fat distribution in epi- and paracardial fat. Another limitation is the relatively short follow-up period, which could be an explanation for the fact that we did not find statistically significant differences in cardiovascular function parameters between the two time points.

In conclusion, this study shows that weight loss induced by bariatric surgery leads to a decrease in abdominal and pericardial fat depots, with a higher relative decrease of visceral and paracardial fat volumes. These findings contribute to the existing evidence suggesting tissue-specific changes in body fat distribution after weight loss and exercise interventions. However, the decrease in pericardial fat did not lead to improved cardiovascular function after the RYGB.

REFERENCES

1. Centers for Disease Control and Prevention: 2011 National Diabetes Fact Sheet. *www cdc gov/diabetes/pubs/factsheet11 htm* 2011
2. van de Weijer T, Schrauwen-Hinderling VB, Schrauwen P: Lipotoxicity in type 2 diabetic cardiomyopathy. *Cardiovascular Research* 92:10-18, 2011
3. van der Meer RW, Lamb HJ, Smit JW, de Roos A: MR imaging evaluation of cardiovascular risk in metabolic syndrome. *Radiology* 264:21-37, 2012
4. Snel M, Jonker JT, Schoones J, Lamb H et al.: Ectopic fat and insulin resistance: pathophysiology and effect of diet and lifestyle interventions. *Int J Endocrinol* 2012:983814, 2012
5. Sacks HS, Fain JN: Human epicardial adipose tissue: a review. *Am Heart J* 153:907-917, 2007
6. McGavock JM, Lingvay I, Zib I, Tillery T et al.: Cardiac Steatosis in Diabetes Mellitus: A 1H-Magnetic Resonance Spectroscopy Study. *Circulation* 116:1170-1175, 2007
7. Nelson AJ, Worthley MI, Psaltis PJ, Carbone A et al.: Validation of cardiovascular magnetic resonance assessment of pericardial adipose tissue volume. *J Cardiovasc Magn Reson* 11:15, 2009
8. Greif M, Becker A, von ZF, Lebherz C et al.: Pericardial adipose tissue determined by dual source CT is a risk factor for coronary atherosclerosis. *Arterioscler Thromb Vasc Biol* 29:781-786, 2009
9. Rosito GA, Massaro JM, Hoffmann U, Ruberg FL et al.: Pericardial fat, visceral abdominal fat, cardiovascular disease risk factors, and vascular calcification in a community-based sample: the Framingham Heart Study. *Circulation* 117:605-613, 2008
10. Wang CP, Hsu HL, Hung WC, Yu TH et al.: Increased epicardial adipose tissue (EAT) volume in type 2 diabetes mellitus and association with metabolic syndrome and severity of coronary atherosclerosis. *Clin Endocrinol (Oxf)* 70:876-882, 2009
11. Rijzewijk LJ, van der Meer RW, Smit JW, Diamant M et al.: Myocardial steatosis is an independent predictor of diastolic dysfunction in type 2 diabetes mellitus. *J Am Coll Cardiol* 52:1793-1799, 2008
12. Hammer S, Snel M, Lamb HJ, Jazet IM et al.: Prolonged caloric restriction in obese patients with type 2 diabetes mellitus decreases myocardial triglyceride content and improves myocardial function. *J Am Coll Cardiol* 52:1006-1012, 2008
13. Snel M, Jonker JT, Hammer S, Kerpershoek G et al.: Long-term beneficial effect of a 16-week very low calorie diet on pericardial fat in obese type 2 diabetes mellitus patients. *Obesity (Silver Spring)* 20:1572-1576, 2012
14. Iacobellis G, Singh N, Wharton S, Sharma AM: Substantial changes in epicardial fat thickness after weight loss in severely obese subjects. *Obesity (Silver Spring)* 16:1693-1697, 2008
15. Viljanen APM, Karmi A, Borra R, P+ñrkk+ñ JP et al.: Effect of Caloric Restriction on Myocardial Fatty Acid Uptake, Left Ventricular Mass, and Cardiac Work in Obese Adults. *The American Journal of Cardiology* 103:1721-1726, 2009
16. Sjostrom L: Review of the key results from the Swedish Obese Subjects (SOS) trial: a prospective controlled intervention study of bariatric surgery. *J Intern Med* 2012
17. Sjostrom L, Lindroos AK, Peltonen M, Torgerson J et al.: Lifestyle, diabetes, and cardiovascular risk factors 10 years after bariatric surgery. *N Engl J Med* 351:2683-2693, 2004
18. Carlsson LM, Peltonen M, Ahlin S, Anveden A et al.: Bariatric surgery and prevention of type 2 diabetes in Swedish obese subjects. *N Engl J Med* 367:695-704, 2012
19. Romeo S, Maglio C, Burza MA, Pirazzi C et al.: Cardiovascular events after bariatric surgery in obese subjects with type 2 diabetes. *Diabetes Care* 35:2613-2617, 2012

20. Sjostrom L, Narbro K, Sjostrom CD, Karason K et al.: Effects of bariatric surgery on mortality in Swedish obese subjects. *N Engl J Med* 357:741-752, 2007
21. Gaborit B, Jacquier A, Kober F, Abdesselam I et al.: Effects of bariatric surgery on cardiac ectopic fat: lesser decrease in epicardial fat compared to visceral fat loss and no change in myocardial triglyceride content. *J Am Coll Cardiol* 60:1381-1389, 2012
22. Fried M, Hainer V, Basdevant A, Buchwald H et al.: Inter-disciplinary European guidelines on surgery of severe obesity. *Int J Obes (Lond)* 31:569-577, 2007
23. van der Meer RW, Doornbos J, Kozerke S, Schar M et al.: Metabolic imaging of myocardial triglyceride content: reproducibility of 1H MR spectroscopy with respiratory navigator gating in volunteers. *Radiology* 245:251-257, 2007
24. Jonker JT, de MP, de Vries ST, Widya RL et al.: Exercise and Type 2 Diabetes Mellitus: Changes in Tissue-Specific Fat Distribution and Cardiac Function. *Radiology* 2013
25. Lamb HJ, Doornbos J, van der Velde EA, Kruit MC et al.: Echo planar MRI of the heart on a standard system: validation of measurements of left ventricular function and mass. *J Comput Assist Tomogr* 20:942-949, 1996
26. Pattynama PM, Lamb HJ, van der Velde EA, van der Wall EE et al.: Left ventricular measurements with cine and spin-echo MR imaging: a study of reproducibility with variance component analysis. *Radiology* 187:261-268, 1993
27. Paelinck BP, de Roos A, Bax JJ, Bosmans JM et al.: Feasibility of tissue magnetic resonance imaging: a pilot study in comparison with tissue Doppler imaging and invasive measurement. *J Am Coll Cardiol* 45:1109-1116, 2005
28. Grotenhuis HB, Westenberg JJ, Steendijk P, van Der Geest RJ et al.: Validation and reproducibility of aortic pulse wave velocity as assessed with velocity-encoded MRI. *J Magn Reson Imaging* 30:521-526, 2009
29. Marchington JM, Pond CM: Site-specific properties of pericardial and epicardial adipose tissue: the effects of insulin and high-fat feeding on lipogenesis and the incorporation of fatty acids in vitro. *Int J Obes* 14:1013-1022, 1990
30. Rabkin SW: Epicardial fat: properties, function and relationship to obesity. *Obes Rev* 8:253-261, 2007
31. Iacobellis G, Leonetti F: Epicardial adipose tissue and insulin resistance in obese subjects. *J Clin Endocrinol Metab* 90:6300-6302, 2005
32. Gaborit B, Kober F, Jacquier A, Moro PJ et al.: Assessment of epicardial fat volume and myocardial triglyceride content in severely obese subjects: relationship to metabolic profile, cardiac function and visceral fat. *Int J Obes (Lond)* 36:422-430, 2012
33. Kim MK, Tanaka K, Kim MJ, Matuso T et al.: Comparison of epicardial, abdominal and regional fat compartments in response to weight loss. *Nutr Metab Cardiovasc Dis* 19:760-766, 2009
34. Willens HJ, Byers P, Chirinos JA, Labrador E et al.: Effects of Weight Loss After Bariatric Surgery on Epicardial Fat Measured Using Echocardiography. *The American Journal of Cardiology* 99:1242-1245, 2007
35. Sicari R, Sironi AM, Petz R, Frassi F et al.: Pericardial rather than epicardial fat is a cardiometabolic risk marker: an MRI vs echo study. *J Am Soc Echocardiogr* 24:1156-1162, 2011
36. Foppa M, Pond KK, Jones DB, Schneider B et al.: Subcutaneous fat thickness, but not epicardial fat thickness, parallels weight reduction three months after bariatric surgery: A cardiac magnetic resonance study. *Int J Cardiol* 168:4532-4533, 2013

37. Rao SR: Inflammatory markers and bariatric surgery: a meta-analysis. *Inflamm Res* 61:789-807, 2012
38. Ionut V, Burch M, Youdim A, Bergman RN: Gastrointestinal hormones and bariatric surgery induced weight loss. *Obesity (Silver Spring)* 2013

Chapter 7

Functional and metabolic imaging of the cardiovascular system in young healthy South Asians and Caucasians unveils early differences

Linda D. van Schinkel*, Leontine E.H. Bakker*, Jacqueline T. Jonker, Albert de Roos, Hanno Pijl, A. Edo Meinders, Ingrid M. Jazet, Johannes W.A. Smit, Hildo J. Lamb

**Both authors contributed equally*

Diabetes Care 2013; 36: 178-179 (Published as Letter to the Editor)

ABSTRACT

Background

South Asians have a higher risk of developing cardiovascular disease (CVD) than Caucasians. Whether there are already differences in cardiac dimensions and cardiovascular function at a young age between South Asians and Caucasians is unknown. The increased CVD risk might relate to alterations in metabolism or ectopic fat deposition. Our objective was to assess whether cardiac dimensions and cardiovascular function differ between young South Asians and Caucasians and whether there is a differential response to a high fat diet.

Methods

Cardiac dimensions and cardiovascular function were assessed using a 1.5T MR scanner in 12 young, healthy male South Asians and 12 matched Caucasians. To elucidate if differences in cardiovascular function are related to metabolism, participants were subjected to a 5-day high fat high caloric (HFHC) diet.

Results

At baseline South Asians had lower left ventricular mass ($p<0.001$) and end-diastolic volume ($p<0.001$), indexed for body surface area, than Caucasians. Furthermore, differences in cardiac function profile were observed. E acceleration peak ($p=0.010$) and E deceleration peak ($p=0.005$) were lower in South Asians. Additionally, South Asians had lower acceleration ($p=0.001$) and deceleration peak flows ($p<0.001$) over the aorta. A 5-day HFHC-diet did not increase these differences. Finally, pulse wave velocity at baseline was higher in South Asians ($p=0.022$), which normalized after the diet.

Conclusions

Young, healthy South Asians have smaller cardiac dimensions and a different cardiovascular function profile than Caucasians. A 5-day HFHC-diet did not increase these differences, suggesting these findings cannot be explained by a different metabolic response to dietary fat.

INTRODUCTION

People of South Asian descent, originating from the Indian subcontinent, represent one fifth of the world's population. South Asians are at an increased risk of developing cardiovascular disease (CVD) compared to Caucasians (1). The age-standardized mortality rate from CVD is around 50% higher for South Asians than for Caucasians (2-5). Furthermore, the mean age of first acute myocardial infarction is approximately five years earlier in South Asians than in Caucasians (6,7). Moreover, CVD in this population is more aggressive and has higher mortality rates at younger ages (1-3,7).

The differences in CVD prevalence and severity between both ethnicities cannot be explained by traditional risk factors (4). Since insulin resistance (IR) and type 2 diabetes mellitus (T2DM) are highly prevalent in South Asians (8,9) and the mortality risk of CVD associated with T2DM is higher in this ethnicity compared to Caucasians (4,10), the increased CVD risk might be related to altered or earlier detrimental metabolic changes as reflected by ectopic fat deposition in organs such as the heart, liver and skeletal muscle (11).

Little is known about differences in cardiovascular function between South Asians and Caucasians at a relatively young age. In a previous study, in which cardiac function was assessed with echocardiography, middle-aged South Asians had attenuated longitudinal left ventricular (LV) function, higher LV filling pressure and a greater degree of concentric remodeling compared to Caucasians (12). Whether these findings are related to the increased CVD risk, however, remains to be determined.

The aim of the present study was to assess whether differences in cardiac dimensions, cardiovascular function, and myocardial triglyceride (TG) content are present between young, healthy South Asians and matched Caucasians using Magnetic Resonance (MR) Imaging (MRI) and Spectroscopic (MRS) techniques. In addition, we measured abdominal fat distribution and hepatic TG content. We hypothesize that possible differences in cardiovascular function between South Asians and Caucasians can be attributed to alterations in energy metabolism, including differential fat distribution in South Asians. In a previous study, short-term high fat feeding decreased diastolic function (13). If the differences in cardiovascular function and dimensions in South Asians can indeed be attributed to a higher metabolic risk, a high fat high caloric (HFHC) diet may have more profound effects on cardiovascular function in this ethnicity then in Caucasians. Therefore, we subjected the participants to a 5-day HFHC-diet.

METHODS

Subjects

Twelve Dutch South Asian and twelve Dutch Caucasian healthy males matched for age (19-25 years) and BMI (<25 kg/m^2), with a positive family history for T2DM were enrolled. Exclusion criteria were: any significant chronic disease (including T2DM), use of medication known to influence glucose and/or lipid metabolism, smoking, recent weight change and general contraindications to MR scanning. Subjects were recruited via advertisements in newspapers. The study was approved by the local ethics committee and written informed consent was obtained from all subjects.

Study design

The study consisted of 2 occasions separated by a 5-day HFHC-diet. The HFHC-diet consisted of the subject's regular diet, supplemented with 375 ml of cream per day (=1275 kcal/day, 94% fat), yielding to around 3775 kcal/day and 54% of fat. Subjects underwent MRI/MRS shortly before the start of the HFHC-diet and at the end of the 5th day of the diet. Participants were instructed not to alter lifestyle habits. Anthropometric measurements and blood samples were obtained on both occasions after a 10-hour overnight fast.

MR protocol

All measurements were performed on a 1.5 Tesla MR scanner (Gyroscan ACS-NT15; Philips Medical Systems, Netherlands) in supine position, and were made in postprandial state (four hours after the last meal).

Left ventricular dimensions and function

Data were analyzed blinded for ethnicity and study occasion.

The heart was imaged in short-axis orientation, using electrocardiographically gated breath-hold cine steady-state free-precession sequences as previously described (14). Imaging parameters were: repetition time (TR) 3.4ms, echo time (TE) 1.7ms, flip angle (FA) 35º, field of view (FOV) 400×320mm, and slice thickness 10mm, no slice gap was used. Epicardial and endocardial LV contours were manually drawn in the end-systolic and end-diastolic phases of the short-axis data, using validated MASS® software (Medis, Leiden, Netherlands). LV end-diastolic volume (EDV), end-systolic volume (ESV), ejection fraction (EF), stroke volume (SV) and end-diastolic mass (EDM) were assessed. We divided LVEDM by LVEDV to obtain the LVEDM/LVEDV ratio (also known as concentricity). Volumes and mass were indexed (I) for body surface area (BSA).

We calculated LV end-systolic wall stress (LVESWS) with the formula 0.133*systolic blood pressure*((3xESV/wall volume)+1) (15).

For assessment of LV diastolic function, transmitral flow was measured, using electrocardiographically gated gradient echo sequence with a velocity sensitivity of 100 cm/sec (TR 9.1ms, TE 1.0ms, FA 20°, slice thickness 8mm, FOV 350mm^2, matrix 256x256 pixels). Flow velocities in early diastole (E) and at atrial contraction (A) were measured and their peak flow ratio was calculated (E/A ratio) using FLOW® software (Medis, Leiden, Netherlands). Furthermore, the peak deceleration gradient of E, the E/A peak ratio and LV filling pressures E/Ea were determined (15,16). Heart rate was monitored and stored during the transmitral flow measurements.

As a measurement of more subtle changes in systolic function of the heart, aortic flow curves were acquired, using electrocardiographically gated gradient echo sequence with a velocity sensitivity of 150 cm/sec (TR 5.0ms, TE 1.0ms, FA 20°, slice thickness 8mm, FOV 300mm^2, matrix 128x128 pixels). Flow velocities in the ascending aorta at the level of the pulmonary trunk were measured and calculated using FLOW® software (Medis, Leiden, Netherlands). The peak slope of the acceleration (aortic (AO) acceleration peak) and deceleration (AO deceleration peak) of the aortic flow curve were calculated. Furthermore, AO duration, AO peak filling rate and AO deceleration duration were determined (Figure 1).

Pulse Wave Velocity

Aortic pulse wave velocity (PWV) was determined for the evaluation of aortic stiffness, using a previously described protocol (17). In short, a scout view of the aorta was performed. Next, a velocity-encoded image perpendicular to the ascending aorta at the level of the pulmonary trunk, and at the level of the aortic bifurcation was assessed. This resulted in through-plane flow measurements of the ascending and descending aorta. Scan parameters were: TR 5.0ms, TE 1.0ms, FA 20°, FOV 300mm, 128×128 acquisition matrix, slice thickness 8mm, with maximal number of phases reconstructed ensuring high (6-10ms) effective temporal resolution. True temporal resolution is defined as 2 times TR = 10ms. PWV was calculated using the formula: $\Delta x/\Delta t$, where Δx describes the aortic path length between two measurement sites and Δt describes the transit time between the arrival of the PWV at three respective sites. The distance between the measurement sites was manually determined by drawing a poly-line in the center of the aorta as defined in a double-oblique parasagittal aortic scout view, using the software package MASS®. Data were analyzed using MASS® and FLOW® (Medis, Leiden, Netherlands).

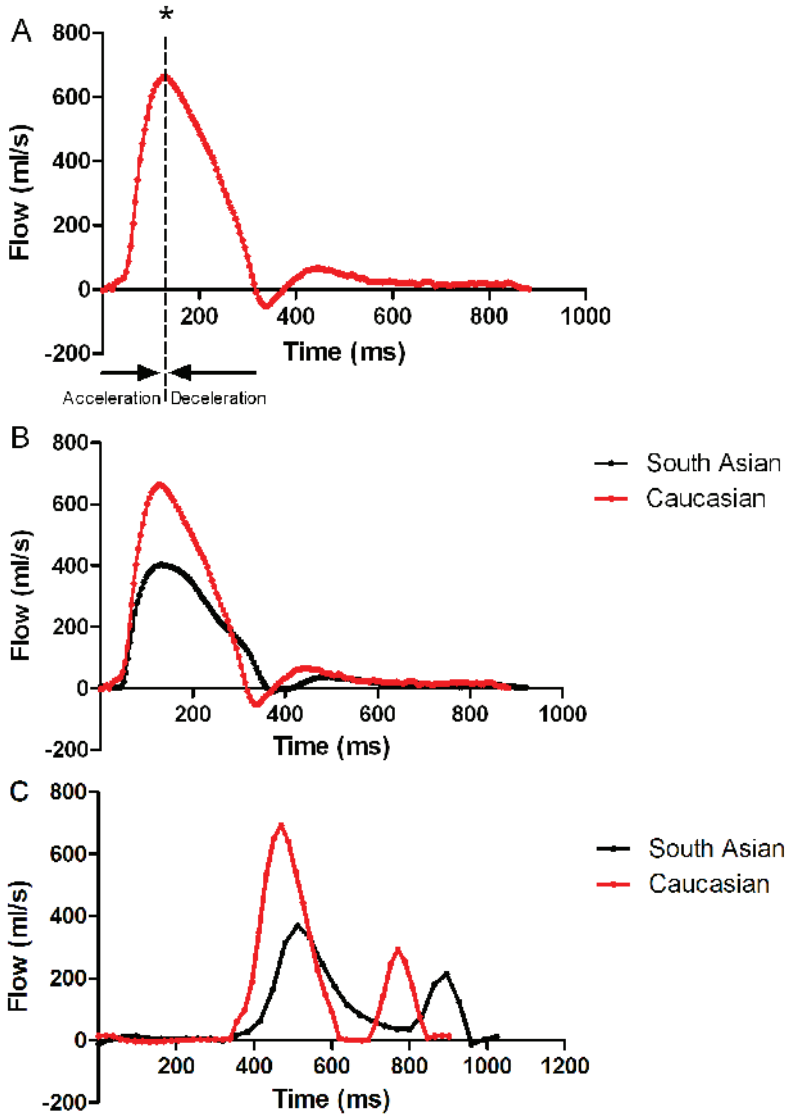

Figure 1. Panel A and B: Aortic flow curve. Panel C: Mitral valve flow curve.
Panel A shows how aortic flow parameters are assessed. * is the AO peak flow rate. Acceleration duration is the time between the beginning of the flow curve and the peak flow rate. The deceleration duration is the time between the peak flow rate and the end of the deceleration period. The acceleration peak is the peak slope (dy/dx) of the acceleration phase, the deceleration peak the peak slope (dy/dx) of the deceleration phase. **Panel B** shows an example of flow velocity curve through the ascending aorta. The black line represents a typical curve of a South Asian subject, the red line of a Caucasian subject: the cardiac contraction is somewhat prolonged in South Asians. **Panel C** shows an example of the flow through the mitral valve, representing diastolic cardiac function. The black line represents a South Asian subject, the red line a Caucasian subject. These curves suggest that cardiac relaxation is prolonged in South Asians.

Myocardial and liver triglyceride content

MR spectroscopy (^{1}H-MRS) was used to quantify myocardial and hepatic TG content. Details on ^{1}H-MRS acquisition and post processing were published before (18,19). In short, myocardial and hepatic ^{1}H-MR single voxel MR spectroscopic data were acquired using a point resolved spectroscopy sequence. For the heart an 8-ml voxel was positioned in the interventricular septum on four-chamber and short-axis images in end-systole, avoiding contamination from epicardial fat. Electrocardiographically triggering (only for myocardial spectra) and respiratory pencil beam navigator were used during acquisition (18). For the liver, voxel sites were matched at both study occasions, avoiding blood vessels and bile ducts. Main acquisition parameters for water suppressed spectra were: TE 26ms, TR 3000ms, 1,024 data points, spectral bandwidth 1,000-Hz, 128 averages. Acquisitions were performed with and without (TE 10000ms, 4 averages) water suppression, with myocardial TG expressed as percentage of the unsuppressed water signal. Hepatic ^{1}H-MRS was performed using the same acquisition parameters, except for 64 averages for the suppressed spectrum. Java-based MR user interface software (jMRUI v2.2, Leuven, Belgium) was used for fitting of the spectra (19). The TG content was calculated as the amplitude of the (TG signal/amplitude of water signal)*100.

Visceral and subcutaneous fat

Abdominal visceral and subcutaneous fat volumes were imaged using a turbo spin echo imaging sequence (20). During one breath-hold, three consecutive transversal slices of 10mm thickness were scanned at level of L5 (TR 168ms, TE 11ms, FA 90^{o}). Volumes of visceral and subcutaneous fat depots were quantified using MASS® software (Medis, Leiden, Netherlands). Visceral and subcutaneous fat areas of each individual slice were multiplied by the slice thickness to acquire a volume and the volumes of all three slices were summed.

Assays

Serum concentrations of glucose, total cholesterol, HDL and triglycerides were measured on a Modular P800 analyzer (Roche, Netherlands), and serum insulin levels on an Immulite 2500 (Siemens, Netherlands). HbA1c was measured on an HPLC system (Kordia, Netherlands). Plasma free fatty acids (FFAs) concentrations were measured by a commercial kit (Wako Chemicals, Germany).

Statistical analysis

Data are presented as mean ± SEM or median (interquartile range (IQR)). A mixed model was applied to assess mean differences before and after the intervention within and between groups, and to assess differences in diet effect. Nonparametric tests (Wilcoxon

signed-rank test within group, Mann-Whitney between groups) were performed when appropriate. Significance level was set at $p<0.05$. Statistical analyses were performed using SPSS for Windows version 20.0 (IBM, USA).

RESULTS

Clinical and metabolic characteristics

Mean age was 22.1 ± 0.4 years. BSA was lower in South Asians. As expected, BMI did not differ between groups (South Asians: 20.9 ± 0.6 kg/m^2 vs. Caucasians: 22.2 ± 0.6 kg/m^2 ($p=0.11$)), but South Asians were shorter and weighed less. After the HFHC-diet a very small increase in BMI and weight to a similar extent in both groups was observed. Waist circumference did not differ between groups. Blood pressure and heart rate were comparable between groups and did not change after the HFHC-diet (Table 1).

HbA1c was higher in South Asians. Fasting glucose, insulin levels and HOMA-B, a measure for pancreas function, were similar at baseline, but were significantly higher in South Asians after the diet. FFAs were comparable between groups and no diet effect was found. LDL-cholesterol was slightly higher in South Asians, whereas other lipid levels did not differ significantly (Table 1).

Left ventricular dimensions and function

At baseline all cardiac left ventricular dimensions indexed for BSA, i.e. EDVI, ESVI, SVI, CI and EDMI, were lower in South Asians than in Caucasians (Table 2). EF did not differ between groups at baseline. In addition, LVESWS and LVEDM/LVEDV were comparable (Table 2).

Flow velocities through the ascending aorta were measured. Typical aortic flow curves of a South Asian versus a Caucasian subject are depicted in Figure 1B. The acceleration peak and duration were significantly lower in South Asians. Furthermore, the aortic peak flow rate, deceleration peak and duration were significantly lower in South Asians. After the HFHC-diet the acceleration peak and deceleration duration over the aorta significantly changed in South Asians, but not in Caucasians (Table 2).

Several parameters of diastolic cardiac function differed at baseline between both groups: E peak filling rate, E acceleration peak and E deceleration peak were significantly lower in South Asians as compared with Caucasians. In addition, the A peak filling rate, the A acceleration peak and A deceleration peak were significantly lower in South Asians (Table 2). E/A ratio and the estimated filling pressure E/Ea were the same in both groups and did not change after the HFHC-diet. Examples of mitral valve flow curves of a South Asian versus a Caucasian subject are depicted in Figure 1C.

Table 1. Clinical and metabolic characteristics

	Caucasians		South Asians	
	before	**after**	**before**	**after**
Clinical characteristics				
age (years)	22.1 ± 0.6		22.2 ± 0.7	
height (m)	1.84 ± 0.01		1.74 ± 0.02**	
weight (kg)	75.1 ± 1.8	75.6 ± 1.8	63.2 ± 2.3**	63.7 ± 2.3† **
BSA (m^2)	1.97 ± 0.02	1.98 ± 0.02	1.76 ± 0.04**	1.76 ± 0.04† **
BMI (kg/m^2)	22.2 ± 0.6	22.4 ± 0.6	20.9 ± 0.6	21.0 ± 0.6†
waist (cm)	81 ± 2	82 ± 2	79 ± 2	80 ± 3
systolic BP (mmHg)	135 ± 3	133 ± 3	129 ± 3	129 ± 3
diastolic BP (mmHg)	79 ± 3	80 ± 2	76.8 ± 2.3	76 ± 2
heart rate (bpm)	65 ± 2	64 ± 2	61 ± 2	66 ± 3
Metabolic characteristics				
HbA1c (%)	5.02 ± 0.06		5.24 ± 0.05*	
HbA1c (mmol/mol)	31.2 ± 0.5		33.8 ± 0.6*	
glucose (mmol/L)	5.09 ± 0.09	5.22 ± 0.07	5.26 ± 0.09	5.53 ± 0.08†† *
insulin (pmol/L)	16 (24)	30 (37)	30 (26)	52 (31)†† ** §§
HOMA-B%	52 ± 11	55 ± 10	65 ± 14	90 ± 11†† * §
free fatty acids (mmol/L)	0.46 ± 0.05	0.43 ± 0.04	0.51 ± 0.04	0.54 ± 0.05
triglycerides (mmol/L)	0.79 (0.26)	0.75 (0.67)	1.01 (0.65)	1.12 (0.77)
total cholesterol (mmol/L)	3.10 (1.80)		4.34 (2.21)	
HDL-cholesterol (mmol/L)	1.05 (0.35)		1.02 (0.38)	
LDL-cholesterol (mmol/L)	1.84 (0.91)		2.77 (1.69)*	
total cholesterol/HDL ratio	3.00 (0.80)		4.05 (2.48)	

Data are presented as mean ± SEM or median (IQR). BSA: body surface area, BMI: body mass index, BP: blood pressure. † $p<0.05$, †† $p<0.05$ within groups. * $p<0.05$, ** $p<0.005$ between groups. § $p<0.05$, §§ $p<0.005$ diet effect between groups.

Pulse Wave Velocity

The aortic PWV was significantly higher in South Asians than in Caucasians at baseline, 4.7 ± 0.1 m/s vs. 4.3 ± 0.1 m/s, p=0.022. After the HFHC-diet, PWV decreased significantly only in South Asians, and was no longer different from Caucasians.

Fat distribution

Although South Asians tended to have more visceral and subcutaneous adipose tissue, differences were not significant between groups (Table 3). Also, the visceral/subcutaneous fat ratio did not differ between groups. Furthermore, no diet effect was observed. Additionally, there was no significant difference between groups in hepatic and myocar-

Table 2. Cardiac dimensions and parameters of cardiovascular function assessed with MRI

	Caucasians		South Asians	
	before	**after**	**before**	**after**
Cardiac dimensions and basic function				
LVEDMI (g/m^2)	62.2 ± 1.2	62.0 ± 1.5	50.7 ± 1.4**	50.0 ± 1.3**
EDVI (ml/m^2)	102.2 ± 3.0	102.7 ± 2.8	83.3 ± 3.4**	81.5 ± 2.9**
ESVI (ml/m^2)	42.8 ± 2.1	42.3 ± 2.4	33.9 ± 2.0*	33.1 ± 1.7**
SVI (ml/m^2)	59.4 ± 2.2	60.4 ± 1.3	49.3 ± 2.1**	48.3 ± 1.7**
CI (ml/min/m^2)	3845 ± 256	3834 ± 159	2994 ± 96**	3161 ± 159*
EF (%)	58.2 ± 1.5	5901 ± 1.4	59.4 ± 1.4	59.4 ± 1.1
LVESWS (kN/m^2)	56.3 ± 1.4	55.4 ± 2.1	53.0 ± 1.8	52.4 ± 1.2
LVEDM/EDV (g/ml)	0.61 ± 0.02	0.61 ± 0.02	0.62 ± 0.02	0.62 ± 0.02
Systolic cardiac function				
AO peak filling rate (ml/s)	538 ± 17	549 ± 18	404 ± 17**	429 ± 14**
AO acceleration peak (ml/s^{2}x10^{-3})	13.1 ± 0.5	13.6 ± 0.7	10.6 ± 0.4**	12.6 ± 0.5†
AO acceleration duration (ms)	101 ± 3	99 ± 4	91 ± 2*	88 ± 3*
AO deceleration peak (ml/s^{2}x10^{-3})	-5.9 ± 0.3	-5.9 ± 0.4	-3.7 ± 0.2**	-3.9 ± 0.2**
AO deceleration duration (ms)	227 ± 6	231 ± 4	252 ± 4**	240 ± 5† §
AO duration (ms)	328 ± 6	330 ± 5	343 ± 5	328 ± 6†
Diastolic cardiac function				
E peak filling rate (ml/s)	570 ± 20	571 ± 13	431 ± 18**	447 ± 14**
E acceleration peak (ml/s^{2}x10^{-3})	7.5 ± 0.5	7.3 ± 0.4	5.9 ± 0.3**	6.4 ± 0.3
E deceleration peak (ml/s^{2}x10^{-3})	-5.0 ± 0.3	-4.9 ± 0.4	-3.8 ± 0.2*	-4.1 ± 0.2
A peak filling rate (ml/s)	262 ± 10	266 ± 13	201 ± 9**	205 ± 10**
A acceleration peak (ml/s^{2}x10^{-3})	4.4 ± 0.3	4.8 ± 0.4	3.3 ± 0.2*	3.7 ± 0.3*
A deceleration peak (ml/s^{2}x10^{-3})	-4.6 ± 0.3	-4.7 ± 0.3	-3.7 ± 0.3*	-4.2 ± 0.5
E/A-peak ratio	2.2 ± 0.1	2.2 ± 0.1	2.2 ± 0.1	2.2 ± 0.1
E/Ea	8.8 ± 1.0	8.6 ± 0.6	11.0 ± 1.3	10.4 ± 1.1
Pulse wave velocity				
PWV total aorta (m/s)	4.3 ± 0.1	4.4 ± 0.1	4.7 ± 0.1*	4.4 ± 0.1†

Data are mean ± SEM. LV: left ventricular, EDM: end-diastolic mass, EDV: end-diastolic volume, ESV: end-systolic volume, SV: stroke volume, CI: cardiac index, EF: ejection fraction, ESWS: end-systolic wall stress. I, indexed for body surface area, AO: Aortic, E: early diastolic wave, A: atrial diastolic wave, E/Ea: estimated left ventricular filling pressure, PWV: pulse wave velocity. † $p<0.05$ within groups. * $p<0.05$, ** $p<0.005$ between groups. § $p<0.05$ diet effect between groups.

dial TG content at baseline (Table 3). After the HFHC-diet hepatic TG content increased in both groups, whereas myocardial TG content did not change.

Table 3. Waist fat distribution and myocardial and hepatic triglyceride content

	Caucasians		South Asians	
	before	**after**	**before**	**after**
Visceral fat (ml)	104 ± 14	111 ± 12	120 ± 19	125 ± 18
Subcutaneous fat (ml)	348 ± 54	363 ± 59	442 ± 61	432 ± 54
Visceral / subcutaneous ratio	0.33 ± 0.04	0.36 ± 0.05	0.28 ± 0.03	0.29 ± 0.03
Total fat (ml)	453 ± 65	474 ± 70	563 ± 76	558 ± 71
Myocardial TG content (%)	0.34 ± 0.06	0.32 ± 0.03	0.33 ± 0.04	0.34 ± 0.08
Hepatic TG content (%)	1.7 ± 0.4	4.5 ± 0.8††	1.3 ± 0.4	3.0 ± 0.5††

Data are mean ± SEM. TG: triglyceride. †† $p<0.005$ within groups.

DISCUSSION

South Asians have a higher risk of developing CVD than Caucasians (1). The cause of these differences between both ethnicities is still unknown. This study showed that young, healthy South Asians have smaller cardiac dimensions compared to age- and BMI-matched Caucasians, even after correction for BSA. Furthermore, diastolic cardiac function in South Asians is different. In addition, although the EF, a gross parameter of systolic function, was similar between both groups, more subtle parameters of systolic function were different. A 5-day HFHC-diet did not increase these differences. Finally, South Asians had a higher aortic PWV on baseline.

Cardiac dimensions

Little is known about differences in cardiac dimensions and cardiovascular function at a young age between South Asians and Caucasians. Previous studies showed smaller left heart volumes, i.e. LVEDV, LVESV, and LV mass in South Asians, which is in line with our results (12,21). However, these studies were performed in older subjects (mean age ~50yr) using echocardiography, while in the current study young adults (mean age ~22yr) were included and MRI was used. One might suggest that the smaller cardiac dimensions observed in South Asians are a consequence of their overall smaller body size. However, adjustment for different parameters of body size such as BMI, BSA and lean body mass did not attenuate the observed differences in the present and other studies.

Left ventricular function

Besides smaller cardiac dimensions, we found a different diastolic and systolic functional profile between both ethnicities. Although the traditional parameters of diastolic function (E/A) and systolic function (EF) did not differ between both groups, more sensitive parameters were significantly different. E and A peak filling rate, and E and A acceleration peak were lower and E and A deceleration peak were higher in South Asians, suggesting that cardiac relaxation is prolonged in South Asians compared to Caucasians. The E/Ea ratio, an estimation of LV filling pressure, was the same for both ethnicities, which is expected in two groups with comparable blood pressures. In concordance with the present study, Chahal et al. also found that E/A ratio did not differ between South Asians and Caucasians (12). However, in contrast to the present study, they did find a higher E/Ea ratio in South Asians. This discrepancy could be due to differences in age of subjects and/or to different methods of cardiac assessment between the studies. In this study we assessed flow through the aorta ascendens at the level of the pulmonary trunk. This showed a flow profile difference between groups (Figure 1B). The difference is similar to

what we observed in the diastolic flow profile as described above: the cardiac contraction is somewhat prolonged in South Asians (Figure 1C).

LVESWS, which is considered to be an important determinant of cardiac function and myocardial oxygen demand, did not differ between South Asians and Caucasians. This finding indicates that no pressure overload was present in either of the groups, which is compatible with the normal LV mass in both groups. Additionally, LVEDM/EDV, a measure for concentricity, was the same between both groups, suggesting there was no difference in LV concentric remodeling either.

HFHC-diet

With respect to the increased risk of CVD, an important notion is that IR and T2DM are also highly prevalent in South Asians (8,9). Moreover, South Asians develop T2DM at a younger age and lower BMI compared to Caucasians (22,23), suggesting South Asians are metabolically at a higher risk. The increased risk of CVD might be related to the metabolic changes that occur with IR. Therefore, we hypothesized that metabolic differences and altered fat depositions between South Asians and Caucasians might be responsible for the higher risk of CVD in South Asians. In this study, South Asians were already more insulin resistant at baseline compared to Caucasians, as reflected by a similar glucose but higher insulin curve and area under the curve measured by an OGTT (data not shown). Since people with IR are known to have abnormal cardiac relaxation (24), the prolonged cardiac relaxation observed in South Asians in this study might be due to their underlying IR.

To test whether possible differences in cardiovascular function between South Asians and Caucasians can be attributed to alterations in energy metabolism the effect of a 5-day HFHC-diet, inducing fat overload, on cardiovascular function was assessed. Previous studies showed that short-term dietary interventions can induce changes in cardiac function (13,25). A short-term HFHC-diet, consisting of 800 ml cream per day, in 15 Caucasian healthy males (age 25.0 ± 6.6yr), already decreased diastolic function after 3 days (13). Therefore, we expected that if metabolic variations were the cause of differences in cardiovascular function, these differences would become more pronounced after a HFHC-diet.

However, although both insulin levels and HOMA-B% increased significantly only in South Asians, indicating they were even more insulin resistant, cardiovascular function did not deteriorate after the diet. Therefore, we did not find support for our hypothesis. It might be that the observed differences in cardiovascular function are innate and that these findings are simply representative of differing normal reference values in these two ethnic groups. Whether these findings are related to increased CVD risk in South Asians is unclear.

After the HFHC-diet hepatic TG content significantly increased in both groups, indicating good dietary compliance of the volunteers. In contrast to accumulation of

hepatic TG content, myocardial TGs did not increase after the diet in both groups. A possible explanation is that the liver acts as a buffer for excessive postprandial flux of FFAs and TGs resulting in no net change in myocardial TG content. This is in line with results of the above mentioned study in Caucasian males who received a 3-day HFHC-diet (13). However, in contrast to other studies, which observed higher hepatic TG in (young) healthy South Asians compared to Caucasians (26,27), in the present study no differences were found between groups before and after the diet. Surprisingly, we did not find a significant difference in abdominal fat distribution between groups either, although South Asians tended to have more visceral and subcutaneous fat mass. Other studies did find significantly more abdominal fat mass in South Asians compared to Caucasians (27-29), though not all studies reached significance (30). These differences in (ectopic) fat distribution might be attributed to the relatively young age and low BMI of subjects in the present study compared to other studies. Possibly, the differences in body fat distribution become stronger with increasing age. Other explanations might be that we included only males, or that the group sizes were too small to reach significance.

Vascular function

PWV is a surrogate marker for arterial stiffness and is a powerful independent predictor of cardiovascular events (31). The aortic PWV in this study was significantly higher in South Asians at baseline, indicating a stiffer aorta. Previous studies in older subjects also reported a higher PWV in South Asians than in Caucasians (32,33). After the HFHC-diet the PWV decreased significantly in South Asians, but not in Caucasians. This difference in diet effect might be explained by the significant increase in insulin levels after the diet occurring only in South Asians. Insulin is known to acutely act as a vasodilator via stimulation of the vasculature to produce endothelial-derived vasodilator nitric oxide (34,35). In contrast, long-term increased insulin levels, as present in IR and T2DM, can contribute to increased arterial wall thickness by direct and indirect trophic effects on smooth muscle cells (36).

In conclusion, already at a young age, South Asians have smaller cardiac dimensions and different diastolic and systolic cardiac function profiles as compared to Caucasians. To our knowledge, these differences in cardiac dimensions and function between healthy, lean South Asians and Caucasians of young age have not been described before. Additionally, South Asians have higher aortic PWV, indicating increased arterial stiffness. Whether these differences contribute to the higher incidence of CVD in South Asians, however, remains to be determined. A 5-day HFHC-diet did not increase the observed functional cardiovascular differences between both groups, suggesting that these findings cannot be explained by a different metabolic response to dietary fat consumption between both ethnicities at young age.

REFERENCES

1. Anand SS, Yusuf S, Vuksan V, Devanesen S et al.: Differences in risk factors, atherosclerosis, and cardiovascular disease between ethnic groups in Canada: the Study of Health Assessment and Risk in Ethnic groups (SHARE). *Lancet* 356:279-284, 2000
2. Balarajan R: Ethnic differences in mortality from ischaemic heart disease and cerebrovascular disease in England and Wales. *BMJ* 302:560-564, 1991
3. Chaturvedi N, Fuller JH: Ethnic differences in mortality from cardiovascular disease in the UK: do they persist in people with diabetes? *J Epidemiol Community Health* 50:137-139, 1996
4. Forouhi NG, Sattar N, Tillin T, McKeigue PM et al.: Do known risk factors explain the higher coronary heart disease mortality in South Asian compared with European men? Prospective follow-up of the Southall and Brent studies, UK. *Diabetologia* 49:2580-2588, 2006
5. Wild SH, Fischbacher C, Brock A, Griffiths C et al.: Mortality from all causes and circulatory disease by country of birth in England and Wales 2001-2003. *J Public Health (Oxf)* 29:191-198, 2007
6. Joshi P, Islam S, Pais P, Reddy S et al.: Risk factors for early myocardial infarction in South Asians compared with individuals in other countries. *JAMA* 297:286-294, 2007
7. Enas EA, Yusuf S, Mehta JL: Prevalence of coronary artery disease in Asian Indians. *Am J Cardiol* 70:945-949, 1992
8. Anjana RM, Pradeepa R, Deepa M, Datta M et al.: Prevalence of diabetes and prediabetes (impaired fasting glucose and/or impaired glucose tolerance) in urban and rural India: phase I results of the Indian Council of Medical Research-INdia DIABetes (ICMR-INDIAB) study. *Diabetologia* 54:3022-3027, 2011
9. Becker E, Boreham R, Chaudhury M, Craig R, Deverill C, Doyle M, Erens B, Falaschetti E, Fuller E, Hills A, Hirani V, Jotangia D, Mindell J, Natarajan L, Stamatakis E, Wardle H, Zaninotto P: *Health Survey for England 2004 Volume 1 The health of minority ethnic groups*. The Information Centre, 2006
10. Wilkinson P, Sayer J, Laji K, Grundy C et al.: Comparison of case fatality in south Asian and white patients after acute myocardial infarction: observational study. *BMJ* 312:1330-1333, 1996
11. Snel M, Jonker JT, Schoones J, Lamb H et al.: Ectopic fat and insulin resistance: pathophysiology and effect of diet and lifestyle interventions. *Int J Endocrinol* 2012:983814, 2012
12. Chahal NS, Lim TK, Jain P, Chambers JC et al.: Ethnicity-related differences in left ventricular function, structure and geometry: a population study of UK Indian Asian and European white subjects. *Heart* 96:466-471, 2010
13. van der Meer RW, Hammer S, Lamb HJ, Frolich M et al.: Effects of short-term high-fat, high-energy diet on hepatic and myocardial triglyceride content in healthy men. *J Clin Endocrinol Metab* 93:2702-2708, 2008
14. Lamb HJ, Doornbos J, van der Velde EA, Kruit MC et al.: Echo planar MRI of the heart on a standard system: validation of measurements of left ventricular function and mass. *J Comput Assist Tomogr* 20:942-949, 1996
15. Pattynama PM, Lamb HJ, van der Velde EA, van der Wall EE et al.: Left ventricular measurements with cine and spin-echo MR imaging: a study of reproducibility with variance component analysis. *Radiology* 187:261-268, 1993
16. Paelinck BP, de Roos A, Bax JJ, Bosmans JM et al.: Feasibility of tissue magnetic resonance imaging: a pilot study in comparison with tissue Doppler imaging and invasive measurement. *J Am Coll Cardiol* 45:1109-1116, 2005

17. Grotenhuis HB, Westenberg JJ, Steendijk P, van Der Geest RJ et al.: Validation and reproducibility of aortic pulse wave velocity as assessed with velocity-encoded MRI. *J Magn Reson Imaging* 30:521-526, 2009
18. van der Meer RW, Doornbos J, Kozerke S, Schar M et al.: Metabolic imaging of myocardial triglyceride content: reproducibility of 1H MR spectroscopy with respiratory navigator gating in volunteers. *Radiology* 245:251-257, 2007
19. Vanhamme L, van den Boogaart A, Van HS: Improved method for accurate and efficient quantification of MRS data with use of prior knowledge. *J Magn Reson* 129:35-43, 1997
20. Rijzewijk LJ, van der Meer RW, Smit JW, Diamant M et al.: Myocardial steatosis is an independent predictor of diastolic dysfunction in type 2 diabetes mellitus. *J Am Coll Cardiol* 52:1793-1799, 2008
21. Kumaran K, Fall CH, Martyn CN, Vijayakumar M et al.: Left ventricular mass and arterial compliance: relation to coronary heart disease and its risk factors in South Indian adults. *Int J Cardiol* 83:1-9, 2002
22. Gray LJ, Yates T, Davies MJ, Brady E et al.: Defining obesity cut-off points for migrant South Asians. P*LoS One* 6:e26464, 2011
23. Gholap N, Davies M, Patel K, Sattar N et al.: Type 2 diabetes and cardiovascular disease in South Asians. P*rim Care Diabetes* 5:45-56, 2011
24. Celentano A, Vaccaro O, Tammaro P, Galderisi M et al.: Early abnormalities of cardiac function in non-insulin-dependent diabetes mellitus and impaired glucose tolerance. *Am J Cardiol* 76:1173-1176, 1995
25. van der Meer RW, Hammer S, Smit JW, Frolich M et al.: Short-term caloric restriction induces accumulation of myocardial triglycerides and decreases left ventricular diastolic function in healthy subjects. *Diabetes* 56:2849-2853, 2007
26. Petersen KF, Dufour S, Feng J, Befroy D et al.: Increased prevalence of insulin resistance and nonalcoholic fatty liver disease in Asian-Indian men. P*roc Natl Acad Sci U S A* 103:18273-18277, 2006
27. Anand SS, Tarnopolsky MA, Rashid S, Schulze KM et al.: Adipocyte hypertrophy, fatty liver and metabolic risk factors in South Asians: the Molecular Study of Health and Risk in Ethnic Groups (mol-SHARE). P*LoS One* 6:e22112, 2011
28. Raji A, Seely EW, Arky RA, Simonson DC: Body fat distribution and insulin resistance in healthy Asian Indians and Caucasians. *J Clin Endocrinol Metab* 86:5366-5371, 2001
29. Lear SA, Humphries KH, Kohli S, Chockalingam A et al.: Visceral adipose tissue accumulation differs according to ethnic background: results of the Multicultural Community Health Assessment Trial (M-CHAT). *Am J Clin Nutr* 86:353-359, 2007
30. Raji A, Gerhard-Herman MD, Warren M, Silverman SG et al.: Insulin resistance and vascular dysfunction in nondiabetic Asian Indians. *J Clin Endocrinol Metab* 89:3965-3972, 2004
31. Mitchell GF, Hwang SJ, Vasan RS, Larson MG et al.: Arterial stiffness and cardiovascular events: the Framingham Heart Study. *Circulation* 121:505-511, 2010
32. Rezai MR, Wallace AM, Sattar N, Finn JD et al.: Ethnic differences in aortic pulse wave velocity occur in the descending aorta and may be related to vitamin D. *Hypertension* 58:247-253, 2011
33. Webb DR, Khunti K, Lacy P, Gray LJ et al.: Conduit vessel stiffness in British south Asians of Indian descent relates to 25-hydroxyvitamin D status. *J Hypertens* 30:1588-1596, 2012
34. Schnyder B, Pittet M, Durand J, Schnyder-Candrian S: Rapid effects of glucose on the insulin signaling of endothelial NO generation and epithelial Na transport. *Am J Physiol Endocrinol Metab* 282:E87-E94, 2002

35. Westerbacka J, Wilkinson I, Cockcroft J, Utriainen T et al.: Diminished wave reflection in the aorta. A novel physiological action of insulin on large blood vessels. *Hypertension* 33:1118-1122, 1999
36. Stapleton PA, James ME, Goodwill AG, Frisbee JC: Obesity and vascular dysfunction. P*athophysiol-ogy* 15:79-89, 2008

Chapter 8

A 5-day high fat high calorie diet impairs insulin sensitivity in healthy, young South Asian men but not in Caucasian men

Leontine E.H. Bakker, Linda D. van Schinkel, Bruno Guigas, Trea C.M. Streefland, Jacqueline T. Jonker, Jan B. van Klinken, Gerard C.M. van der Zon, Hildo J. Lamb, Johannes W.A. Smit, Hanno Pijl, A. Edo Meinders, Ingrid M. Jazet

Diabetes 2014; 63: 248-258

ABSTRACT

South Asians develop type 2 diabetes (T2DM) at a younger age and lower BMI compared to Caucasians. The underlying cause is still poorly understood but might result from an innate inability to adapt to the Westernized diet. This study aimed to compare the metabolic adaptation to a high-fat-high-calorie (HFHC) diet between both ethnicities. Twelve healthy young lean male South Asians and 12 matched Caucasians underwent a 2-step hyperinsulinemic-euglycemic clamp with skeletal muscle biopsies and indirect calorimetry before and after a 5-day HFHC-diet. Hepatic triglyceride content (HTG) and abdominal fat distribution were assessed using MRI/S. At baseline, South Asians had higher insulin clamp levels than Caucasians, indicating reduced insulin clearance rate. Despite the higher insulin levels, endogenous glucose production was comparable between groups, suggesting lower hepatic insulin sensitivity in South Asians. Furthermore, a 5-day HFHC-diet decreased insulin-stimulated (non-oxidative) glucose disposal rate only in South Asians. In skeletal muscle no significant differences were found between groups in insulin/mTOR-signaling, metabolic gene expression and mitochondrial respiratory-chain content. Furthermore, no differences in (mobilization of) HTG and abdominal fat were detected. We conclude that HFHC-feeding rapidly induces insulin resistance only in South Asians. Thus, distinct adaptation to "Western" food may partly explain their propensity to develop T2DM.

INTRODUCTION

The incidence of type 2 diabetes (T2DM) is increasing rapidly worldwide, especially in people of South Asian descent (1). South Asians originate from the Indian subcontinent and represent one fifth of the world's population. Both native and migrant South Asians are at high risk of developing T2DM compared to Caucasians (2-4). Not only is the prevalence of T2DM four to six times higher, it also occurs at a younger age and lower BMI (4-6). Moreover, the risk of cardiovascular and renal complications is higher (7-10). The underlying cause of this excess risk is still incompletely understood, and only few in-depth studies have been conducted to investigate the pathogenesis of T2DM in South Asians (11,12).

The observation that South Asians have high hepatic and intramyocellular lipid content compared to people of Caucasian descent (13,14) might suggest that South Asians have an impaired mitochondrial fatty acid beta-oxidation in either skeletal muscle and/or adipose tissue, resulting in ectopic fat deposition in peripheral tissues, eventually leading to insulin resistance (IR) and other metabolic dysfunctions (15). South Asians may therefore be less capable to handle the Western-type high fat (HF)-diet as compared to Caucasians.

Interesting in this context are recent findings on the nutrient and energy-sensing mammalian target of rapamycin (mTOR)-pathway. The mTOR-pathway regulates cell growth according to cellular energy status and nutrient availability (16). Activated mTOR complex 1 (mTORC1) controls key cellular processes, e.g. it inhibits insulin signaling (17) and plays a crucial role in the regulation of oxidative metabolism and mitochondrial biogenesis (18-21). Importantly, mTORC1 also appears to promote lipid synthesis and storage, while inhibiting processes leading to lipid consumption (22). Indeed, there is growing evidence that mTORC1 suppresses fatty acid beta-oxidation (21,23,24). Therefore, we hypothesize that differences in mTOR activity between the two ethnicities may underlie or contribute to the increased risk of T2DM in South Asians.

The aim of this study was to investigate whether the metabolic adaptation to a 5-day high fat high calorie (HFHC) diet is different between young healthy lean South Asian males and matched Caucasians. In particular, we were interested whether differences in the activity of mTOR in skeletal muscle exist between the two ethnicities, both at baseline and in response to the HFHC-diet. Furthermore, hepatic and peripheral insulin sensitivity, substrate oxidation, abdominal fat distribution and skeletal muscle insulin signaling and mitochondrial respiratory-chain content were assessed.

METHODS

Subjects

Twelve Dutch South Asian and twelve Dutch Caucasian, lean (BMI < 25 kg/m^2) and healthy males, aged 19-25 years with a positive family history of T2DM were enrolled via local advertisements. Subjects underwent a medical screening including their medical history, a physical examination, blood chemistry tests and an oral glucose tolerance test to exclude individuals with T2DM according to the American Diabetes Association 2010 criteria. Other exclusion criteria were rigorous exercise, smoking and recent body weight change. The study was approved by the Medical Ethical Committee of the Leiden University Medical Center and performed in accordance with the principles of the revised Declaration of Helsinki. All volunteers gave written informed consent before participation.

Study design

Subjects were studied before and after a 5-day HFHC-diet, consisting of the subject's regular diet supplemented with 375 ml of cream per day (=1275 kcal/day, 94% fat). At the end of the first study day, subjects received 15 125ml cups of cream. They were instructed to continue their regular diet and, on top of that, to consume three cups of cream per day, directly following a meal in order to make sure they could adhere to their regular dietary habits. In addition, they kept a food diary before and during the HFHC-diet to estimate normal dietary intake, to maximize compliance with the diet, and to check for compliance and compensation behavior. Diaries were entered and analyzed using a specialized internet application (http://www.dieetinzicht.nl, Dutch). Compliance was measured by asking to bring leftover cups, asking, analyzing the food diaries and laboratory parameters. Subjects were instructed not to alter life style habits, and not to perform physical activity in the last 48 hours before the study days. Magnetic resonance (MR) studies were performed shortly before and on the fifth day of the HFHC-diet. Metabolic studies were performed one day before and one day after the diet.

MR studies

Abdominal fat depots were quantified with turbo spin echo MR-imaging using a 1.5 Tesla whole body MR scanner (Gyroscan ACS-NT15; Philips, The Netherlands) four hours after the last meal (25). During one breath hold, three transverse images were obtained at the level of L5. Volumes of visceral and subcutaneous fat depots were quantified using MASS analytical software (Medis, The Netherlands). The number of pixels were converted to cm^2 and multiplied by the slice thickness (10mm). Hepatic triglyceride content (HTG) was assessed by proton MR-spectroscopy (^{1}H-MRS) (26). A spectrum without water suppression, four averages, as internal standard was obtained, and 64 averages were collected with

water suppression. The spectra were fitted using Java-base MR user interface software (jMRUI version 2.2) (26). The percentage of hepatic triglyceride signals was calculated as: (signal amplitude hepatic triglycerides / signal amplitude water) x 100.

Metabolic studies

Anthropometric measurements, a 2-step hyperinsulinemic-euglycemic clamp with stable isotopes and indirect calorimetry were performed after an overnight fast. In addition, skeletal muscle biopsies were obtained. Fat and lean body mass (LBM) were assessed by bioelectrical impedance analysis (BIA; Bodystat® 1500, Bodystat Ltd., Douglas, UK).

Hyperinsulinemic-euglycemic clamp

A 6-h 2-step hyperinsulinemic-euglycemic clamp was performed as described previously (27). In short, a primed constant infusion of glucose tracer ([6,6-$^2H_2$]-glucose; 0.22 µmol/kg/min) was used to determine rates of glucose appearance (R_a) and disposal (R_d). At t=120 min (step 1) and t=240 min (step 2), a primed constant infusion of insulin (step 1: 10 mU/m^2/min, step 2: 40 mU/m^2/min) was started and glucose-20% enriched with 3% [6,6-$^2H_2$]-glucose was infused at a variable rate to maintain glucose level at 5.0 mmol/L. In basal state (t=0 min), at the end of the non-insulin stimulated period (t=95-115 min) and at the end of each step (t=210-240 min and t=330-360 min), blood samples were taken for determination of glucose, insulin, C-peptide, free fatty acids (FFAs), and [6,6-$^2H_2$]-glucose specific activity.

Indirect calorimetry

Indirect calorimetry was performed with a ventilated hood (Oxycon Pro™, CareFusion, Germany) in basal condition and during both steps of the clamp.

Skeletal muscle biopsies

Muscle biopsies from the *m. vastus lateralis* (~75-100 mg) were collected in basal and hyperinsulinemic condition (at 30 minutes of step 2) under localized anesthesia, using a modified Bergström needle (28). Muscle samples were divided into two parts, snap-frozen in liquid nitrogen and stored at -80°C until further analysis.

Calculations

Glucose R_a and R_d were calculated as the tracer infusion rate divided by the tracer-to-tracee ratio (29). Endogenous glucose production (EGP) was calculated as the difference between the rates of R_a and glucose infusion. R_d and EGP were adjusted for kilograms LBM. The metabolic clearance rate of insulin (MCR_i) was computed according to Elahi et al. (30). Resting energy expenditure (REE), respiratory quotient (RQ) and substrate oxida-

tion rates were determined as described by Simonson and DeFronzo (31). Non-oxidative glucose disposal (NOGD) was calculated by subtracting the glucose oxidation rate from R_d. The hepatic insulin resistance index (HIR) was calculated as the product of non-insulin stimulated EGP and fasting serum insulin concentration (32). Glucose metabolic clearance rate (MCR_g) was calculated as the rate of disappearance of glucose (R_d) divided by the serum glucose concentration (average of steady-state measurements) (33).

Laboratory analysis

Fasting serum glucose and triglycerides were measured on a Modular P800 analyzer (Roche, The Netherlands), serum insulin and C-peptide levels on an Immulite 2500 (Siemens, The Netherlands), HbA1c on an HPLC machine Primus Ultra 2 (Kordia, The Netherlands), and plasma FFAs were determined by a colorimetric method (Wako Chemicals, Germany). Arterialized whole blood glucose levels during the clamp were measured by glucose dehydrogenase-NAD technique (Precision Xtra Blood Glucose Monitoring System, Abbott USA). [6,6-$^2H_2$]-glucose enrichment was measured in a single analytical run using gas chromatography-mass spectrometry as described previously (34).

DNA/RNA isolation and real-time RT-PCR

Total RNA was isolated from skeletal muscle biopsies (~25-30 mg) using the phenol-chloroform extraction method (Tripure RNA Isolation reagent, Roche, Germany), treated with a DNAse kit according to the manufacturer instruction (TURBO DNAse, Life Technologies, The Netherlands), and quantified by NanoDrop. First-strand cDNA were synthesized from 1 µg total RNA using a Superscript first strand synthesis kit (Invitrogen, The Netherlands). Real-time PCR assays were performed using specific primers sets (sequences provided on request) and SYBR Green on a StepOne Plus Real-time PCR system (Applied Biosystems, USA). mRNA expression was normalized to ribosomal protein S18 (Rps18) and expressed as arbitrary units. Genomic DNA was extracted using the Qiagen Tissue and Blood Kit (Qiagen, Germany) and concentrations were measured spectrophotometrically (GeneQuant, GE Healthcare, Germany). Mitochondrial (mtDNA) and nuclear (nDNA) DNA copy numbers were quantified as described before (35) and the mtDNA-to-nDNA-ratio was used as an index of mitochondrial density. A complete overview of all analyzed genes can be found in Supplemental Table 1.

Western Blot

Skeletal muscle biopsies (~30-45mg) were homogenized by Ultra-Turrax (22.000 rpm; 2x5sec) in a 6:1 (v/w) ratio of ice-cold buffer containing: 50mM HEPES (pH 7.6), 50mM NaF, 50mM KCl, 5mM NaPPi, 1mM EDTA, 1mM EGTA, 5mM β-GP, 1mM Na3VO4, 1mM DTT, 1% NP40 and protease inhibitors cocktail (Complete, Roche, The Netherlands). Western blots

were performed using phospho-specific (Ser473-PKB, phospho-Akt substrate, Ser2448-mTOR, and Thr389-S6K from Cell Signaling; Thr246-PRAS40 from Biosource) or total primary antibodies (Tubulin, Akt1+2, Akt substrate of 160kDa, mTOR and S6K from Cell Signaling; PRAS40 from Biosource; MitoProfile OXPHOS from AbCam; IRβ from Santa Cruz) (36). Blots were quantified by densitometric analysis using Image J software (NIH USA).

Table 1. Clinical characteristics, body composition, and fasting plasma and serum levels before and after a 5-day HFHC-diet in healthy, young South Asian males and matched Caucasians.

	Caucasians		South Asians	
	before	**after**	**before**	**after**
Clinical characteristics				
age (years)	22.1 ± 0.6		22.2 ± 0.7	
length (m)	1.84 ± 0.01		1.74 ± 0.02**	
weight (kg)	75.1 ± 1.8	75.6 ± 1.8	63.2 ± 2.3**	63.7 ± 2.3† **
BMI (kg/m^2)	22.2 ± 0.6	22.4 ± 0.6	20.9 ± 0.6	21.0 ± 0.6†
waist (cm)	81.3 ± 2.2	82.0 ± 2.3	78.9 ± 2.2	79.5 ± 2.6
Body composition				
fat mass (%)	11.3 ± 0.9	11.3 ± 0.8	15.1 ± 0.9*	14.7 ± 0.8*
visceral fat (ml)	104 ± 14	111 ± 12	120 ± 19	125 ± 18
subcutaneous fat (ml)	348 ± 54	363 ± 59	442 ± 61	432 ± 54
hepatic TG content (%)	1.7 ± 0.4	4.5 ± 0.8††	1.3 ± 0.4	3.0 ± 0.5††
Fasting plasma and serum levels				
HbA1c (%)	5.0 ± 0.1		5.2 ± 0.1*	
HbA1c (mmol/mol)	31.2 ± 0.5		33.8 ± 0.6*	
glucose (mmol/L)	5.1 ± 0.1	5.2 ± 0.1	5.3 ± 0.1	5.5 ± 0.1†† *
insulin (pmol/L)	34 (32)	49 (46)	49 (29)	73 (34)†† ** ‡‡
C-peptide (nmol/L)	0.47 (0.15)	0.57 (0.28)†	0.48 (0.11)	0.61 (0.18)††
FFA (g/L)	0.131 ± 0.01	0.121 ± 0.01	0.144 ± 0.01	0.151 ± 0.01
TG (mmol/L)	0.79 (0.26)	0.75 (0.67)	1.01 (0.65)	1.12 (0.77)

Data are presented as mean ± SEM or median (IQR). BMI: body mass index, TG: triglyceride, FFA: free fatty acid. † $p<0.05$, †† $p<0.005$ within group vs. before diet. * $p<0.05$, ** $p<0.005$ vs. Caucasians. ‡ $p<0.05$, ‡‡ $p<0.005$ diet effect vs. Caucasians.

Statistical analysis

Data are presented as mean ± SEM when normally distributed or as median (IQR) when not normally distributed. A mixed effects model was applied to assess mean differences before and after the intervention within and between groups, and to determine differences in diet effect. Groups and intervention were modeled as fixed effects and the subject specific deviances from the group mean were modeled as random effects.

Nonparametric tests (Wilcoxon signed-rank test within group, Mann-Whitney between groups) were performed when appropriate. Significance level was set at $p<0.05$. Statistical analyses were performed using SPSS for Windows version 20.0 (IBM, USA).

RESULTS

Clinical characteristics

BMI did not differ between groups (South Asians: 20.9 ± 0.6 *vs.* Caucasians (C): 22.2 ± 0.6 kg/m^2, p=0.11), but South Asian subjects were significantly shorter and lighter (Table 1). The percentage of fat mass was significantly higher in South Asians on both study days, and, consequently, the percentage of LBM was lower. Waist circumference did not differ between groups. Fasting glucose and insulin levels were similar at baseline, but were significantly higher in South Asians after the HFHC-diet. Fasting C-peptide levels increased significantly to a similar degree in both groups. HbA1c was higher in South Asians, as was LDL-cholesterol (2.77 (1.69) *vs.* 1.84 (0.91) mmol/L, p=0.03).

Diet and exercise

The physical activity level was comparable between both ethnicities (Supplemental Table 2). The South Asian diet consisted of fewer calories per day (South Asians: 2170 ± 102 *vs.* Caucasians: 2593 ± 100 kcal, p=0.008), but corrected for bodyweight the amount of calories was similar (South Asians: 34 ± 2 *vs.* Caucasians: 35 ± 1 kcal/day/kg, p=0.91). Both ethnicities ate the same percentage of fat (~30%), carbohydrates (~50%) and proteins (~16%). Both groups complied well with the diet. Mean daily calorie intake was ~55% higher compared to their normal diet, and ~54% of energy was derived from fat (Supplemental Table 2).

Fat distribution

No differences were found between groups for visceral and subcutaneous fat volumes both at baseline and after the HFHC-diet. Furthermore, no diet effect was observed. HTG increased significantly after the diet in both groups, but no differences between groups were observed (Table 1).

Endogenous glucose production and rate of glucose disposal

During the hyperinsulinemic-euglycemic clamp glucose concentrations were similar within and between groups for both steps (Table 2). Clamp insulin levels were significantly higher in South Asians compared to Caucasians before and after the HFHC-diet; no diet effect was observed. The MCR_i was significantly lower in South Asians on both

Table 2. Metabolic parameters of a 2-step hyperinsulinemic-euglycemic clamp with stable isotopes before and after a 5-day HFHC-diet in healthy, young South Asian males and matched Caucasians.

	Caucasians		South Asians	
	before	**after**	**before**	**after**
Basal steady state				
average glucose (mmol/L)	5.1 ± 0.1	5.1 ± 0.1	5.2 ± 0.1	5.4 ± 0.1†
average insulin (pmol/L)	41 (26)	41 (27)	49 (36)	68 (45)† *
EGP = Rd (µmol/kgLBM/min)	16.3 ± 0.4	17.0 ± 0.3	17.5 ± 0.5	17.5 ± 0.4
HIR (µmol*pmol/kgLBM/min/L)	562 (600)	760 (778)	763 (512)	1269 (520)†† ** ‡
MCRg (ml/kgLBM/min)	3.2 ± 0.1	3.3 ± 0.1	3.4 ± 0.1	3.3 ± 0.1
Step 1				
average glucose (mmol/L)	5.1 ± 0.1	5.2 ± 0.1	5.0 ± 0.1	5.2 ± 0.1
average insulin (pmol/L)	83 ± 12	89 ± 11	116 ± 6**	126 ± 11**
average C-peptide (nmol/L)	0.26 (0.13)	0.27 (0.13)	0.22 (0.14)	0.29 (0.15)†
EGP (µmol/kgLBM/min)	12.6 ± 0.5	13.4 ± 0.4	12.8 ± 0.4	12.8 ± 0.4
suppression EGP (%)	-22.6 ± 1.8	-21.6 ± 1.6	-26.8 ± 1.3	-27.2 ± 1.0
Rd (µmol/kgLBM/min)	15.3 ± 0.8	17.4 ± 1.2	16.2 ± 0.9	15.3 ± 1.1
MCRg (ml/kgLBM/min)	3.0 ± 0.2	3.4 ± 0.2	3.2 ± 0.2	3.0 ± 0.2
Step 2				
average glucose (mmol/L)	4.8 ± 0.1	4.8 ± 0.1	4.6 ± 0.1	4.6 ± 0.1
average insulin (pmol/L)	276 ± 19	285 ± 19	396 ± 15**	386 ± 21**
average C-peptide (nmol/L)	0.07 (0.12)	0.07 (0.09)	0.06 (0.12)	0.08 (0.08)†
EGP (µmol/kgLBM/min)	10.0 ± 0.7	1.2 ± 0.5	9.7 ± 0.7	9.6 ± 0.5
suppression EGP (%)	-38.9 ± 3.5	-39.8 ± 2.7	-43.9 ± 3.0	-45.7 ± 2.3
Rd (µmol/kgLBM/min)	41.7 ± 2.9	41.0 ± 2.8	48.7 ± 2.9**	39.0 ± 2.1†† ‡‡
Rd / insulin (µmol*L/kgLBM/min/mU)	1.14 ± 0.13	1.07 ± 0.12	0.87 ± 0.07	0.72 ± 0.05† *
MCRi (ml/m^2/min)	1076 (397)	1054 (270)	735 (70)**	771 (164)† ** ‡
MCRg (ml/kgLBM/min)	8.8 ± 0.7	8.7 ± 0.6	10.7 ± 0.8**	8.6 ± 0.5†† ‡‡

Data are presented as mean ± SEM or median (IQR). Due to hypoglycemia in the last part of step 2 of the clamp, two South Asian subjects on occasion 1 and one Caucasian subject on occasion 2 were excluded in the analysis of step 2. EGP: endogenous glucose production, Rd: rate of glucose disposal, HIR: hepatic insulin resistance, MCRg: metabolic clearance rate of glucose, MCRi: metabolic clearance rate of insulin. † $p<0.05$, †† $p < 0.005$ within group vs. before diet. * $p<0.05$, ** $p<0.005$ vs. Caucasians. ‡ $p<0.05$, ‡‡ $p<0.005$ diet effect vs. Caucasians.

study days. EGP in basal and insulin-stimulated conditions was similar for both groups, despite higher insulin levels in insulin-stimulated conditions in South Asians. Further-

more, no diet effect was observed. However, the calculated HIR index was higher in South Asians compared to Caucasians (p=0.065 before diet, p=0.002 after diet), and showed a significant increase after the diet only in South Asians (p diet effect = 0.008). Suppression of EGP by insulin was comparable between groups and was around 24% in step 1 and 42% in step 2. Insulin-stimulated R_d in step 1 was similar for both groups on both occasions. In step 2 R_d was higher in South Asians compared to Caucasians before the diet (South Asians: 48.7 ± 2.9 *vs.* Caucasians: 41.7 ± 2.9 μmol/kg_{LBM}/min; p=0.003). However, when corrected for insulin level, this difference disappeared and was almost reversed (p=0.052). After the diet R_d decreased significantly in South Asians despite similar insulin levels, whereas no diet effect was found in Caucasians (South Asians: 39.0 ± 2.1 μmol/kg_{LBM}/min (p<0.001) *vs.* Caucasians: 41.0 ± 2.8 μmol/kg_{LBM}/min (p=0.78); p diet effect = 0.002).

Glucose and lipid oxidation rates

REE, corrected for LBM, RQ, substrate oxidation rates and NOGD in basal condition and step 1 of the clamp were comparable for both groups before and after the HFHC-diet (Table 3). In step 2, however, glucose oxidation increased significantly in South Asians, whereas no diet effect was observed in Caucasians. Interestingly, NOGD in step 2 was significantly higher in South Asians compared to Caucasians at baseline (p<0.001), but decreased significantly after the HFHC-diet only in South Asians (South Asians: 34.4 ± 4.0 *vs.* 19.3 ± 2.0 μmol/kg_{LBM}/min (p<0.001), Caucasians: 24.1 ± 2.1 *vs.* 23.8 ± 1.6 μmol/kg_{LBM}/min (p=0.87); p diet effect < 0.001).

Skeletal muscle signaling

The protein expression and phosphorylation state of key molecules involved in the insulin and mTOR signaling pathways were determined in basal condition and during the hyperinsulinemic-euglycemic clamp in skeletal muscle (Figure 1). A trend for a reduced IRβ expression was observed in South Asians. During hyperinsulinemia, the phosphorylation state of key proteins involved in the insulin/mTOR pathway (PKB, AS160, PRAS40, mTOR and S6K1) was significantly increased when compared to basal, as expected (Figure 1). No obvious differences were observed between groups whatever the conditions.

Skeletal muscle metabolic gene expression

The skeletal muscle expression of key metabolic genes involved in the regulation of glucose and fatty acid metabolism was determined (Supplemental Table 1).

At baseline, no significant differences between groups were observed in the transcript levels of all analyzed genes. The HFHC-diet induced significant downregulation of

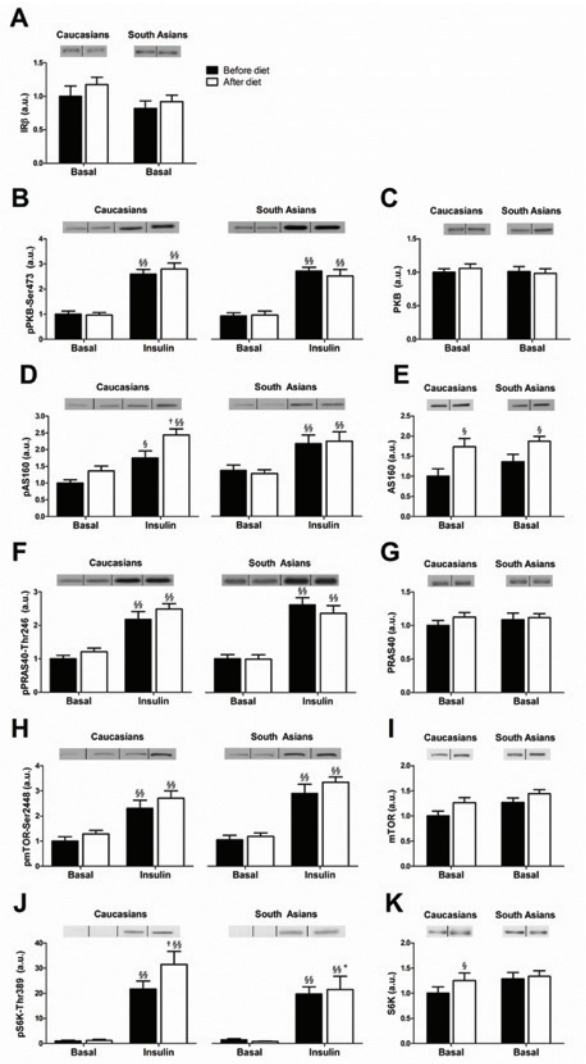

Figure 1. Insulin and mTOR signaling in skeletal muscle from healthy, young South Asian males and matched Caucasians before (black bars) and after (white bars) a 5-day HFHC-diet. The protein expression of A. IRβ, B. Ser473-PKB, C. PKB, D. phospho-AS160, E. AS160, F. Thr246-PRAS40, G. PRAS40, H. Ser2448-mTOR, I. mTOR, J. Thr389-S6K, and K. S6K, were assessed by Western Blot. The phosphorylation state in basal and hyperinsulinemic (step 2) conditions (B, D, F, H, J), or the protein expression in basal conditions (A, C, E, G, I, K) are shown. Representative blots for one subject per group are shown. Results are normalized to Caucasian subjects (before diet, basal condition) and expressed as mean ± SEM. Due to a small amount of tissue two Caucasian subjects were excluded for Western Blot analysis. † $p<0.05$ within group *vs.* before diet. § $p<0.05$, §§ $p<0.005$ within groups *vs.* basal condition. * $p<0.05$ *vs.* Caucasians. IRβ, insulin receptor isoform β. PKB, protein kinase B. AS160, Akt substrate of 160 kDa. PRAS40, Proline rich Akt substrate of 40 kDa. mTOR, mammalian target of rapamycin. S6K1, ribosomal protein S6 kinase β1.

SLC2A4, GSK3A, GYS1, AGL, PPP1R3A, PDK2, ACACA, PPARA and PPARD mRNA expression in Caucasian subjects, with a comparable response in South Asians. Only PKM2 was differentially affected in South Asians in response to the HFHC-diet.

Skeletal muscle mitochondrial respiratory-chain content

The protein expression of several mitochondrial respiratory chain complex subunits was determined (Figure 2A). Although at baseline no differences were observed between groups, the expression of respiratory chain complex 1 and 2 was significantly increased after the HFHC-diet only in Caucasians (Figure 2B). However, the complex 2-on-complex 1 ratio, as a measure of change in fat *vs.* glucose oxidation, was not significantly different between both ethnicities (Figure 2C). The mtDNA-on-nDNA-ratio was significantly lower in South Asians compared to Caucasians, but was not affected in response to the diet (Figure 2D). Of note, the mRNA expression of key genes involved in mitochondrial biogenesis and tricarboxylic acid cycle was not different between groups, whatever the conditions (Supplemental Table 1).

Table 3. Parameters for indirect calorimetry before and after a 5-day HFHC-diet in healthy, young South Asian males and matched Caucasians.

	Caucasians		South Asians	
	before	after	before	after
Basal				
REE (kcal/day)	1469 ± 50	1523 ± 38	1220 ± 31**	1224 ± 22**
REE (kcal/day/kgLBM)	22.4 ± 0.7	22.7 ± 0.5	23.0 ± 0.9	22.8 ± 0.9
RQ	0.88 ± 0.01	0.87 ± 0.01	0.87 ± 0.02	0.89 ± 0.02
glucose oxidation	14.3 ± 1.0	13.6 ± 1.1	13.9 ± 1.3	14.7 ± 1.5
lipid oxidation	2.4 ± 0.3	2.7 ± 0.3	2.7 ± 0.4	2.4 ± 0.5
NOGD	2.3 ± 0.7	3.7 ± 0.8	4.2 ± 1.2	3.5 ± 1.4
Step 1				
RQ	0.90 ± 0.02	0.91 ± 0.02	0.88 ± 0.02	0.90 ± 0.03
glucose oxidation	16.2 ± 1.6	16.4 ± 1.6	14.3 ± 1.7	14.8 ± 1.5
lipid oxidation	2.2 ± 0.5	1.9 ± 0.4	2.6 ± 0.5	2.3 ± 0.5
NOGD	1.8 ± 0.9	2.8 ± 0.9	3.1 ± 1.2	2.5 ± 1.2
Step 2				
RQ	0.92 ± 0.02	0.93 ± 0.02	0.88 ± 0.02	0.95 ± 0.02†
glucose oxidation	17.7 ± 1.5	18.2 ± 1.8	14.4 ± 1.2	19.2 ± 1.5†
lipid oxidation	1.8 ± 0.4	1.6 ± 0.4	2.5 ± 0.4	1.4 ± 0.4
NOGD	24.1 ± 2.1	23.8 ± 1.6	34.4 ± 4.0**	19.3 ± 2.0†† ‡‡

Data are presented as mean ± SEM. Units are in µmol/kgLBM/min. REE: resting energy expenditure, RQ: respiratory quotient, NOGD: non-oxidative glucose disposal rate. † $p<0.05$, †† $p<0.005$ within group vs. before diet. **$p<0.005$ vs. Caucasians. ‡‡ $p<0.005$ diet effect vs. Caucasians.

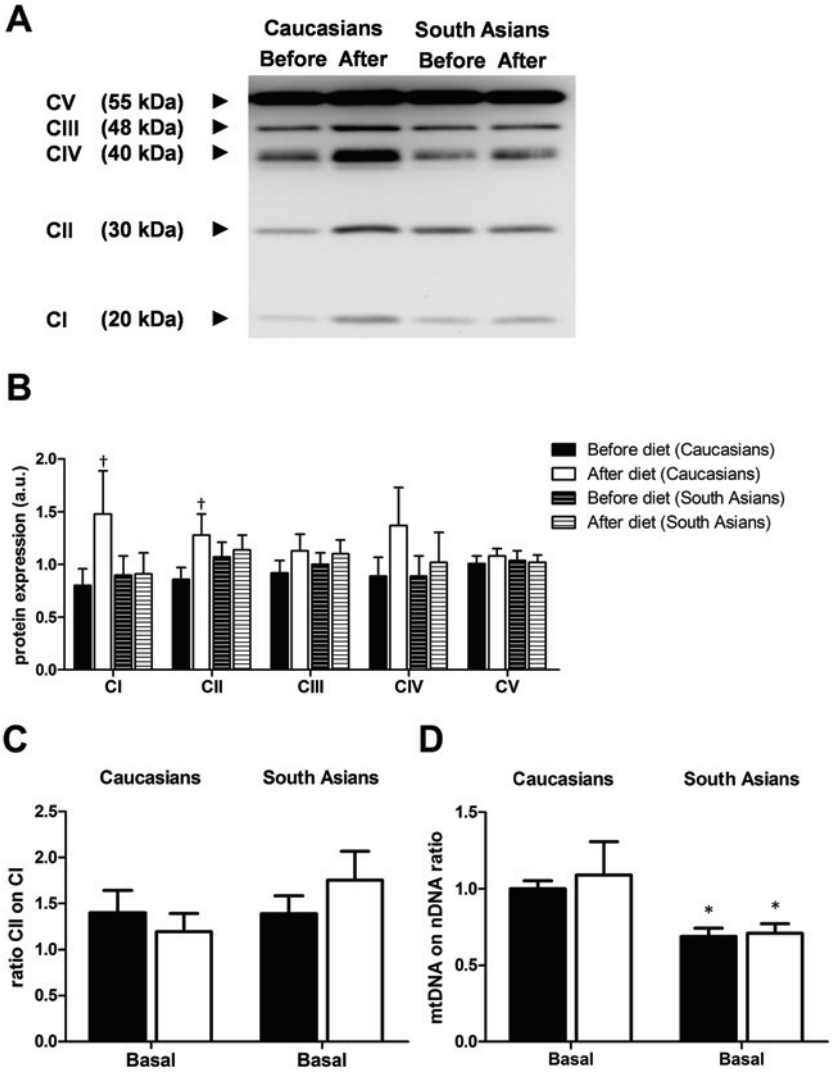

Figure 2. Protein expression of mitochondrial respiratory-chain subunits in skeletal muscle from healthy, young South Asian (striped bars) males and matched Caucasians (closed bars) before (black bars) and after (white bars) a 5-day HFHC-diet. A. Representative blots for one subject per group. B. The expression of various mitochondrial-respiratory chain subunits (CI: NDUFB8, CII: SDHB, CIII: UQCRC2, CIV: MTCO1, CV: ATP5A) were assessed by Western Blot in basal condition. C. The respiratory-chain complex 2-on-complex 1 ratios were calculated. D. The mtDNA on nDNA ratio as assessed by qPCR in basal condition (n=7/12 (Caucasian/South Asian)). Results are normalized to Caucasian subjects (before diet) and expressed as mean ± SEM. Due to a small amount of tissue two Caucasian subjects were excluded for Western Blot analysis. † $p<0.05$ within group *vs.* before diet. *$p<0.05$ *vs.* Caucasians. CI–V: mitochondrial respiratory chain subunits I–V.

DISCUSSION

This is the first study in South Asians in which a 2-step hyperinsulinemic-euglycemic clamp with stable isotopes was performed to measure peripheral and hepatic insulin sensitivity, and the first one in this ethnicity which assessed the effect of HF-feeding on both insulin sensitivity and skeletal muscle insulin and mTOR signaling. Strikingly, a 5-day HFHC-diet was already sufficient to impair insulin-stimulated (non-oxidative) glucose disposal in South Asians, while such an effect was not observed in Caucasians.

Baseline comparisons

In contrast to other studies, waist fat distribution and HTG did not significantly differ between both ethnicities (13,14,37,38). In addition, we did not find higher fasting serum insulin levels (14,37-41), nor lower peripheral insulin sensitivity in South Asians compared to Caucasians at baseline in both basal and insulin-stimulated conditions (12,38,40-42). Instead, South Asians seemed to have even higher insulin-stimulated peripheral insulin sensitivity. However, insulin levels during the clamp were higher in South Asians on both study days, which is in line with other studies (40-42). After correction for insulin levels, the difference in R_d between groups disappeared and was almost reversed. The higher insulin levels were presumably due to a lower MCR_i in South Asians, which has been shown before (40). The lower MCR_i together with the higher HIR index in South Asians indicates lower hepatic insulin sensitivity both at baseline and after the diet.

The difference in above-mentioned findings compared to literature might be explained by the relatively young age, low BMI and sex (no females were included) of our subjects, geographical differences as reflected by dietary and/or other acculturation changes, and/or the small sample size (despite power calculation beforehand).

Response to a 5-day HFHC-diet

The mean daily calorie intake during the HFHC-diet was ~55% higher compared to their normal diet, and both groups reached ~54% of energy derived from fat compared to ~30% of their normal daily energy intake. HTG increased significantly after the diet in both groups, indicating good compliance to the diet, and consistent with a previous study in which young, healthy Caucasian males were subjected to a 3-day HF-diet (26). In contrast, fasting glucose and insulin levels increased significantly only in South Asians. No effect of the diet on basal EGP or on the capacity of insulin to suppress EGP was observed in either group, although the HIR index, which corrects EGP for insulin level (32), was significantly increased in South Asians only. Strikingly, insulin-stimulated R_d was significantly impaired after the diet in South Asians, whereas no diet effect was observed in Caucasians.

The response to a HF-diet on (skeletal muscle) insulin sensitivity in people of Caucasian descent is variable in the literature, depending on the percentage of fat and carbohydrates, duration of the diet, amount of calories (eucaloric or hypercaloric), effect on bodyweight, and method used to assess insulin sensitivity. In general, HF-diets of several hours up to 3 days induce whole-body IR (43,44), whereas after HF-diets of several days up to 3 weeks usually no effect is seen on insulin sensitivity (45-48). This difference in effect on insulin sensitivity might be attributed to a greater intramuscular lipid storage and/or use after several days, compensating for the increase in FFA availability induced by the HF-diet (47).

The impairment in insulin-stimulated R_d after the diet in South Asians appears to be due to a decrease in NOGD, suggesting a defect in glycogen storage. Impaired non-oxidative glucose disposal is the main defect observed in patients with T2DM (49). Interestingly, at baseline insulin-stimulated NOGD was significantly higher in South Asians compared to Caucasians, but this was possibly due to the higher insulin levels in South Asians. Because of the impairment in NOGD in South Asians after the diet, we also analyzed proteins (Supplemental Figure 1) and genes involved in glycolysis and glycogen synthesis. However, no obvious differences were found between groups. The mRNA expression of GYS was significantly reduced in both groups after the diet (Supplemental Table 1). Of note, in contrast to what was observed in South Asians in the present study, in several short-term HF-diet studies in Caucasians an increase in NOGD and a decrease in glucose oxidation was observed (45,47,48,50), accompanied by an increase in skeletal muscle mRNA level of pyruvate dehydrogenase kinase 4 (PDK4) and a corresponding decrease in pyruvate dehydrogenase enzyme complex (PDH) in basal and insulin-stimulated conditions (44,47,48). In the present study, PDK4 was not affected by the diet, and PDH was reduced only in South Asians (Supplemental Table 1). Therefore, it would have been interesting to determine skeletal muscle glycogen content. Further research is required to clarify the pathophysiological relevance of these apparent paradoxical findings in glycogen metabolism in South Asians.

The nutrient-sensing mTOR-pathway is mostly known for its regulating role in cellular proliferation and growth but it was also recently shown to be involved in key metabolic processes (16). Therefore, it constitutes an interesting and relevant pathway to be investigated in the context of increased IR together with increased ectopic fat deposition in South Asians *vs.* Caucasians. Interestingly, mTORC1 appears to have negative effects on insulin signaling (17). There are various mechanisms through which this negative feedback loop of mTORC1 on insulin signaling is initiated. When activated by mTORC1, downstream target S6K1 can suppress IRS-1 via direct phosphorylation of IRS1 on multiple serine residues, and via transcription repression of IRS1 gene expression.

Additionally, mTORC1 directly interacts with IRS1 via raptor and phosphorylates IRS1 at Ser636/639. Furthermore, several biochemical and genetic studies have shown that mTORC1 plays a crucial role in the regulation of oxidative metabolism and mitochondrial biogenesis (18-21) as well as in lipid metabolism (22). In particular, mTORC1 seems to suppress FA beta-oxidation (21,23,24). Therefore, we hypothesized that differences in mTOR activity between the two ethnicities might underlie or contribute to the increased risk of IR and T2DM in South Asians. However, we did not find obvious differences in the mTOR-pathway between or within groups, neither at baseline nor after a 5-day HFHC-diet. Additionally, apart from a small difference in diet effect on respiratory chain complex subunits 1 and 2, we did not observe relevant differences in diet effect on skeletal muscle insulin signaling, mitochondrial density and expression of genes involved in oxidative phosphorylation and mitochondrial biogenesis that could explain the diet-induced impairment in insulin-stimulated R_d in South Asians, which is in line with a previous study in which young, healthy Caucasian males were subjected to a 5-day HFHC-diet (46). The fact that we did not find obvious differences between groups might be explained by the relatively good health of our subjects and/or the small sample size. Of note, to confirm our findings on mitochondrial function other mitochondrial markers, such as *ex vivo* determination of activities of mitochondrial respiratory-chain complexes and citrate synthase activity should be measured in future studies.

Only two other studies have been performed before in South Asians in which skeletal muscle biopsies were obtained to assess insulin signaling and/or mitochondrial function, and none assessed the mTOR-pathway. Nair *et al* found no impairment in mitochondrial function in healthy, middle-aged South Asians, even despite the finding that they were more insulin resistant than matched Caucasians (12). Correspondingly, Hall and colleagues reported that healthy, young, lean South Asian males did not exhibit lower expression of skeletal muscle oxidative and lipid metabolism genes compared to matched white Caucasians, and that mtDNA-to-nDNA-ratio, an index of mitochondrial content, did not significantly differ between groups, although a trend for a lower ratio in South Asians was observed (11). Thus, both studies concluded that mitochondrial dysfunction did not account for the observed IR in South Asians, which is in line with our present findings concerning the effect of a HFHC-diet. Additionally, Hall's study showed that South Asians had reduced skeletal muscle protein expression of key insulin signaling proteins in the fasted state (11). In that study, insulin sensitivity, as measured from the Matsuda insulin sensitivity index, was however significantly lower in South Asians. Thus, these subjects might have been more insulin resistant, explaining the reduced expression of insulin signaling proteins as compared to our study. Other possibilities for the different findings on insulin signaling are the larger group size in the study of

Hall, and/or geographical differences as reflected by dietary and/or other acculturation changes.

Finally, we cannot exclude the possibility that white adipose tissue (WAT) might have contributed to the diet-induced impairment in insulin-stimulated R_d in South Asians. Indeed, about 10-20% of whole-body glucose uptake occurs in WAT, which corresponds to the observed reduction in R_d in South Asians (mean percentage decrease: 20 ± 5%).

In conclusion, we showed that a 5-day HFHC-diet is already sufficient to affect insulin-stimulated (non-oxidative) glucose disposal in healthy, young, lean South Asian males, whereas no diet effect was found in age- and BMI-matched Caucasians, suggesting that the propensity of South Asians to develop T2DM may be partly explained by the way they adapt to HF western food. The mTOR-pathway does not seem to be involved, at least in skeletal muscle. These findings might provide new leads for further investigation aimed to elucidate the pathogenesis of IR and T2DM in South Asians.

REFERENCES

1. Whiting DR, Guariguata L, Weil C, Shaw J: IDF diabetes atlas: global estimates of the prevalence of diabetes for 2011 and 2030. *Diabetes Res Clin Pract* 94:311-321, 2011
2. Anjana RM, Pradeepa R, Deepa M, Datta M et al.: Prevalence of diabetes and prediabetes (impaired fasting glucose and/or impaired glucose tolerance) in urban and rural India: phase I results of the Indian Council of Medical Research-INdia DIABetes (ICMR-INDIAB) study. *Diabetologia* 54:3022-3027, 2011
3. Becker E, Boreham R, Chaudhury M, Craig R, Deverill C, Doyle M, Erens B, Falaschetti E, Fuller E, Hills A, Hirani V, Jotangia D, Mindell J, Natarajan L, Stamatakis E, Wardle H, Zaninotto P: Health Survey for England 2004 Volume 1 The *health of minority ethnic groups*. The Information Centre, 2006
4. Bindraban NR, van Valkengoed IG, Mairuhu G, Holleman F et al.: Prevalence of diabetes mellitus and the performance of a risk score among Hindustani Surinamese, African Surinamese and ethnic Dutch: a cross-sectional population-based study. *BMC Public Health* 8:271, 2008
5. Chiu M, Austin PC, Manuel DG, Shah BR et al.: Deriving ethnic-specific BMI cutoff points for assessing diabetes risk. *Diabetes Care* 34:1741-1748, 2011
6. Simmons D, Williams DR, Powell MJ: Prevalence of diabetes in a predominantly Asian community: preliminary findings of the Coventry diabetes study. *BMJ* 298: 1989
7. Chandie Shaw PK, Baboe F, van Es LA, van der Vijver JC et al.: South-Asian type 2 diabetic patients have higher incidence and faster progression of renal disease compared with Dutch-European diabetic patients. *Diabetes Care* 29:1383-1385, 2006
8. Chaturvedi N, Fuller JH: Ethnic differences in mortality from cardiovascular disease in the UK: do they persist in people with diabetes? *J Epidemiol Community Health* 50:137-139, 1996
9. McKeigue PM, Ferrie JE, Pierpoint T, Marmot MG: Association of early-onset coronary heart disease in South Asian men with glucose intolerance and hyperinsulinemia. *Circulation* 87:152-161, 1993
10. Wilkinson P, Sayer J, Laji K, Grundy C et al.: Comparison of case fatality in south Asian and white patients after acute myocardial infarction: observational study. *BMJ* 312:1330-1333, 1996
11. Hall LM, Moran CN, Milne GR, Wilson J et al.: Fat oxidation, fitness and skeletal muscle expression of oxidative/lipid metabolism genes in South Asians: implications for insulin resistance? P*LoS One* 5:e14197, 2010
12. Nair KS, Bigelow ML, Asmann YW, Chow LS et al.: Asian Indians have enhanced skeletal muscle mitochondrial capacity to produce ATP in association with severe insulin resistance. *Diabetes* 57:1166-1175, 2008
13. Anand SS, Tarnopolsky MA, Rashid S, Schulze KM et al.: Adipocyte hypertrophy, fatty liver and metabolic risk factors in South Asians: the Molecular Study of Health and Risk in Ethnic Groups (mol-SHARE). P*LoS One* 6:e22112, 2011
14. Petersen KF, Dufour S, Feng J, Befroy D et al.: Increased prevalence of insulin resistance and nonalcoholic fatty liver disease in Asian-Indian men. P*roc Natl Acad Sci U S A* 103:18273-18277, 2006
15. Snel M, Jonker JT, Schoones J, Lamb H et al.: Ectopic fat and insulin resistance: pathophysiology and effect of diet and lifestyle interventions. *Int J Endocrinol* 2012:983814, 2012
16. Laplante M, Sabatini DM: mTOR signaling in growth control and disease. *Cell* 149:274-293, 2012
17. Copps KD, White MF: Regulation of insulin sensitivity by serine/threonine phosphorylation of insulin receptor substrate proteins IRS1 and IRS2. *Diabetologia* 55:2565-2582, 2012

18. Cunningham JT, Rodgers JT, Arlow DH, Vazquez F et al.: mTOR controls mitochondrial oxidative function through a YY1-PGC-1alpha transcriptional complex. *Nature* 450:736-740, 2007
19. Le BO, Petroulakis E, Paglialunga S, Poulin F et al.: Elevated sensitivity to diet-induced obesity and insulin resistance in mice lacking 4E-BP1 and 4E-BP2. *J Clin Invest* 117:387-396, 2007
20. Schieke SM, Phillips D, McCoy JP, Jr., Aponte AM et al.: The mammalian target of rapamycin (mTOR) pathway regulates mitochondrial oxygen consumption and oxidative capacity. *J Biol Chem* 281:27643-27652, 2006
21. Um SH, Frigerio F, Watanabe M, Picard F et al.: Absence of S6K1 protects against age- and diet-induced obesity while enhancing insulin sensitivity. *Nature* 431:200-205, 2004
22. Ricoult SJ, Manning BD: The multifaceted role of mTORC1 in the control of lipid metabolism. *EMBO Re*p 14:242-251, 2013
23. Peng T, Golub TR, Sabatini DM: The immunosuppressant rapamycin mimics a starvation-like signal distinct from amino acid and glucose deprivation. *Mol Cell Biol* 22:5575-5584, 2002
24. Sipula IJ, Brown NF, Perdomo G: Rapamycin-mediated inhibition of mammalian target of rapamycin in skeletal muscle cells reduces glucose utilization and increases fatty acid oxidation. *Metabolism* 55:1637-1644, 2006
25. Hammer S, van der Meer RW, Lamb HJ, de Boer HH et al.: Short-term flexibility of myocardial triglycerides and diastolic function in patients with type 2 diabetes mellitus. *Am J Physiol Endocrinol Metab* 295:E714-E718, 2008
26. van der Meer RW, Hammer S, Lamb HJ, Frolich M et al.: Effects of short-term high-fat, high-energy diet on hepatic and myocardial triglyceride content in healthy men. *J Clin Endocrinol Metab* 93:2702-2708, 2008
27. Sleddering MA, Snel M, Streefland TC, Pijl H et al.: Short-term topiramate treatment does not improve insulin sensitivity or secretion in obese insulin-resistant women. *Eur J Endocrinol* 167:839-845, 2012
28. Bergstrom J: Percutaneous needle biopsy of skeletal muscle in physiological and clinical research. *Scand J Clin Lab Invest* 35:609-616, 1975
29. STEELE R: Influences of glucose loading and of injected insulin on hepatic glucose output. *Ann N Y Acad Sci* 82:420-430, 1959
30. Elahi D, Nagulesparan M, Hershcopf RJ, Muller DC et al.: Feedback inhibition of insulin secretion by insulin: relation to the hyperinsulinemia of obesity. *N Engl J Med* 306:1196-1202, 1982
31. Simonson DC, DeFronzo RA: Indirect calorimetry: methodological and interpretative problems. *Am J Physiol* 258:E399-E412, 1990
32. Gastaldelli A, Natali A, Vettor R, Corradini SG: Insulin resistance, adipose depots and gut: interactions and pathological implications. *Dig Liver Dis* 42:310-319, 2010
33. Ferrannini E, Mari A: How to measure insulin sensitivity. *J Hypertens* 16:895-906, 1998
34. Gastaldelli A, Coggan AR, Wolfe RR: Assessment of methods for improving tracer estimation of non-steady-state rate of appearance. *J Appl Physiol* 87:1813-1822, 1999
35. Szuhai K, Ouweland J, Dirks R, Lemaitre M et al.: Simultaneous A8344G heteroplasmy and mitochondrial DNA copy number quantification in myoclonus epilepsy and ragged-red fibers (MERRF) syndrome by a multiplex molecular beacon based real-time fluorescence PCR. *Nucleic Acids Res* 29:E13, 2001

36. Wijngaarden MA, van der Zon GC, Willems van Dijk KW, Pijl H et al.: Effects of prolonged fasting on AMPK signaling, gene expression and mitochondrial respiratory-chain content in skeletal muscle from lean and obese individuals. *Am J Physiol Endocrinol Metab* 2013
37. Lear SA, Humphries KH, Kohli S, Chockalingam A et al.: Visceral adipose tissue accumulation differs according to ethnic background: results of the Multicultural Community Health Assessment Trial (M-CHAT). *Am J Clin Nutr* 86:353-359, 2007
38. Raji A, Seely EW, Arky RA, Simonson DC: Body fat distribution and insulin resistance in healthy Asian Indians and Caucasians. *J Clin Endocrinol Metab* 86:5366-5371, 2001
39. Boon MR, Karamali NS, de Groot CJ, van SL et al.: E-Selectin is Elevated in Cord Blood of South Asian Neonates Compared with Caucasian Neonates. *J Pediatr* 2011
40. Liew CF, Seah ES, Yeo KP, Lee KO et al.: Lean, nondiabetic Asian Indians have decreased insulin sensitivity and insulin clearance, and raised leptin compared to Caucasians and Chinese subjects. *Int J Obes Relat Metab Disord* 27:784-789, 2003
41. Raji A, Gerhard-Herman MD, Warren M, Silverman SG et al.: Insulin resistance and vascular dysfunction in nondiabetic Asian Indians. *J Clin Endocrinol Metab* 89:3965-3972, 2004
42. Chandalia M, Abate N, Garg A, Stray-Gundersen J et al.: Relationship between generalized and upper body obesity to insulin resistance in Asian Indian men. *J Clin Endocrinol Metab* 84:2329-2335, 1999
43. Bachmann OP, Dahl DB, Brechtel K, Machann J et al.: Effects of intravenous and dietary lipid challenge on intramyocellular lipid content and the relation with insulin sensitivity in humans. *Diabetes* 50:2579-2584, 2001
44. Pehleman TL, Peters SJ, Heigenhauser GJ, Spriet LL: Enzymatic regulation of glucose disposal in human skeletal muscle after a high-fat, low-carbohydrate diet. *J Appl Physiol* 98:100-107, 2005
45. Bisschop PH, de MJ, Ackermans MT, Endert E et al.: Dietary fat content alters insulin-mediated glucose metabolism in healthy men. *Am J Clin Nutr* 73:554-559, 2001
46. Brons C, Jensen CB, Storgaard H, Hiscock NJ et al.: Impact of short-term high-fat feeding on glucose and insulin metabolism in young healthy men. *J Physiol* 587:2387-2397, 2009
47. Chokkalingam K, Jewell K, Norton L, Littlewood J et al.: High-fat/low-carbohydrate diet reduces insulin-stimulated carbohydrate oxidation but stimulates nonoxidative glucose disposal in humans: An important role for skeletal muscle pyruvate dehydrogenase kinase 4. *J Clin Endocrinol Metab* 92:284-292, 2007
48. Cutler DL, Gray CG, Park SW, Hickman MG et al.: Low-carbohydrate diet alters intracellular glucose metabolism but not overall glucose disposal in exercise-trained subjects. *Metabolism* 44:1264-1270, 1995
49. Shulman GI, Rothman DL, Jue T, Stein P et al.: Quantitation of muscle glycogen synthesis in normal subjects and subjects with non-insulin-dependent diabetes by 13C nuclear magnetic resonance spectroscopy. *N Engl J Med* 322:223-228, 1990
50. Bisschop PH, Ackermans MT, Endert E, Ruiter AF et al.: The effect of carbohydrate and fat variation in euenergetic diets on postabsorptive free fatty acid release. *Br J Nutr* 87:555-559, 2002

Supplemental Table 1. Overview of metabolic gene expression analysis in skeletal muscle from young, healthy South Asian males and matched Caucasians before and after a 5-day HFHC-diet.

Gene name	Gene symbol	Entrez gene	Caucasians		South Asians		Interaction p-value
			before	after	before	after	
Glucose Metabolism							
Glucose transport & phosphorylation							
Insulin receptor	INSR	3643	1.00 ± 0.13	0.89 ± 0.11	0.86 ± 0.16	0.77 ± 0.14	0.99
Akt substrate of 160 kDa (AS160)	TBC1D4	9882	1.00 (0.88)	0.67 (0.64)	1.05 (0.64)	0.80 (1.07)	0.44
TBC1D1	TBC1D1	23216	1.00 ± 0.15	0.88 ± 0.11	1.05 ± 0.13	0.68 ± 0.11†	0.27
Solute carrier family 2, member 1 (GLUT-1)	SLC2A1	6513	1.00 (1.68)	1.63 (2.79)	1.01 (0.46)	1.33 (1.17)	0.20
Solute carrier family 2, member 4 (GLUT-4)	SLC2A4	6517	1.00 ± 0.26	0.61 ± 0.12†	0.70 ± 0.14	0.48 ± 0.09	0.44
Hexokinase 1	HK1	3098	1.00 (0.87)	1.01 (0.89)	1.28 (1.16)	1.12 (0.71)	0.61
Hexokinase 2	HK2	3099	1.00 ± 0.22	1.30 ± 0.36	0.40 ± 0.07	0.83 ± 0.21	0.90
Glycolysis							
Phosphofructokinase	PFKM	5213	1.00 (0.44)	1.00 (0.78)	1.10 (0.58)	0.67 (0.48)†	0.10
Glyceraldehyde-3-phosphate dehydrogenase	GAPDH	2597	1.00 (0.21)	0.81 (0.13)	0.86 (0.12)	0.76 (0.14)†	0.75
Pyruvate kinase	PKM2	5315	1.00 ± 0.07	0.89 ± 0.06	1.18 ± 0.13	0.73 ± 0.09†‡	0.04
Glycogen metabolism							
Glycogen synthase kinase 3α	GSK3A	2931	1.00 ± 0.23	0.71 ± 0.11†	0.82 ± 0.14	0.66 ± 0.09	0.46
Glycogen synthase kinase 3β	GSK3B	2932	1.00 (0.74)	1.17 (1.05)	1.26 (0.67)	1.87 (1.82)	0.28
Glycogen synthase 1	GYS1	2997	1.00 ± 0.16	0.73 ± 0.11†	0.98 ± 0.14	0.60 ± 0.09†	0.65
Glycogen phosphorylase	PYGM	5837	1.00 ± 0.11	0.70 ± 0.07	0.95 ± 0.15	0.55 ± 0.07†	0.42
UDP-glucose pyrophosphorylase 2	UGP2	7360	1.00 (0.87)	0.84 (0.51)	0.69 (0.80)	0.40 (0.44)	0.80
Glycogen debranching enzyme	AGL	178	1.00 (0.41)	0.61 (0.37)†	1.30 (1.13)	0.78 (0.54)	0.61
Glycogen-branching enzyme	GBE1	2632	1.00 (0.16)	0.88 (0.36)	0.99 (0.15)	0.98 (0.44)	0.95
Phosphorylase kinase α1	PHKA1	5255	1.00 (0.88)	1.05 (0.66)	1.13 (0.80)	0.94 (1.09)	0.65
Phosphorylase kinase γ1	PHKG1	5260	1.00 (0.91)	0.82 (0.24)	1.03 (0.80)	0.71 (0.47)	0.81
Protein phosphatase 1, regulatory subunit 3A	PPP1R3A	5506	1.00 (0.47)	0.69 (0.54)†	1.17 (0.69)	0.68 (0.62)	0.56

Gene name	Gene symbol	Entrez gene	Caucasians		South Asians		Interaction p-value
			before	after	before	after	
Fatty acid metabolism							
Transcription factors							
PPARα	PPARA	5465	1.00 (0.49)	0.70 (0.22)†	0.80 (0.49)	0.93 (0.64)	0.15
PPARδ	PPARD	5467	1.00 ± 0.21	0.69 ± 0.10†	0.83 ± 0.15	0.68 ± 0.09	0.51
PPARγ	PPARG	5468	1.00 (0.36)	1.21 (0.40)	0.83 (0.43)	0.89 (0.31)	0.48
Fatty acid transport, synthesis & oxidation							
Lipoprotein lipase	LPL	4023	1.00 (1.47)	0.63 (0.78)	0.58 (1.28)	0.36 (0.43)	0.91
Fatty acid translocase/CD36	CD36	948	1.00 ± 0.06	1.05 ± 0.07	0.89 ± 0.07	0.89 ± 0.16	0.83
Acetyl-CoA carboxylase α	ACACA	31	1.00 (1.02)	0.82 (0.40)†	1.09 (0.39)	0.97 (0.32)	0.17
Acetyl-CoA carboxylase β	ACACB	32	1.00 ± 0.21	0.95 ± 0.16	0.86 ± 0.11	1.00 ± 0.13	0.43
Mitochondrial fatty acid transport							
CPT 1A	CPT1A	1374	1.00 (0.92)	0.71 (0.85)	0.76 (0.25)	0.89 (0.70)	0.19
CPT 1B	CPT1B	1375	1.00 ± 0.10	1.11 ± 0.09	1.01 ± 0.10	0.90 ± 0.11	0.14
CPT 2	CPT2	1376	1.00 ± 0.13	0.91 ± 0.10	1.04 ± 0.11	1.17 ± 0.19	0.28
AMP-activated protein kinase subunits							
AMPK α1	PRKAA1	5562	1.00 ± 0.15	0.70 ± 0.09	0.85 ± 0.11	0.73 ± 0.12	0.35
AMPK α2	PRKAA2	5563	1.00 (0.42)	0.72 (0.63)	1.05 (0.84)	0.74 (0.58)	1.00
AMPK β1	PRKAB1	5564	1.00 ± 0.14	0.79 ± 0.06	0.77 ± 0.11	0.88 ± 0.15	0.12
AMPK β2	PRKAB2	5565	1.00 ± 0.21	0.61 ± 0.12	0.89 ± 0.19	0.93 ± 0.19	0.28
AMPK γ1	PRKAG1	5571	1.00 ± 0.19	0.94 ± 0.19	1.22 ± 0.21	0.65 ± 0.09†‡	0.05
AMPK γ2	PRKAG2	51422	1.00 (0.33)	0.65 (0.59)	0.66 (0.21)	0.49 (0.24)*	0.56
AMPK γ3	PRKAG3	53632	1.00 ± 0.35	0.96 ± 0.32	1.00 ± 0.23	1.18 ± 0.26	0.75
Mitochondrial metabolism							
Mitochondrial biogenesis							
PPARα, coactivator 1α (PGC-1α)	PPARGC1A	10891	1.00 ± 0.16	0.52 ± 0.09†	0.73 ± 0.11	0.44 ± 0.09	0.35

Gene name	Gene symbol	Entrez gene	Caucasians		South Asians		Interaction p-value
			before	after	before	after	
PPARβ, coactivator 1b (PGC-1β)	PPARGC1B	133522	1.00 ± 0.16	0.92 ± 0.13	0.87 ± 0.16	0.62 ± 0.13	0.71
Transcription factor A	TFAM	7019	1.00 ± 0.09	0.80 ± 0.10	0.98 ± 0.14	0.66 ± 0.12†	0.48
Nuclear respiratory factor 1	NRF1	4899	1.00 ± 0.16	0.83 ± 0.12	0.98 ± 0.16	0.71 ± 0.10†	0.64
Nuclear factor (erythroid-derived 2)-like 2	NFE2L2	4780	1.00 (0.46)	0.83 (0.23)	0.80 (0.37)	0.78 (0.47)	0.85
Tricarboxylic acid cycle & electron transport chain							
Pyruvate dehydrogenase kinase 2	PDK2	5164	1.00 ± 0.12	0.68 ± 0.13†	0.87 ± 0.11	0.72 ± 0.06	0.23
Pyruvate dehydrogenase kinase 4	PDK4	5166	1.00 (1.14)	0.63 (0.94)	0.83 (1.65)	0.86 (0.52)	0.61
Pyruvate dehydrogenase α1	PDHA1	5160	1.00 ± 0.06	0.93 ± 0.06	1.04 ± 0.09	0.75 ± 0.13†	0.31
Pyruvate carboxylase	PC	5091	1.00 (0.38)	1.32 (0.39)	0.91 (0.37)	1.13 (0.48)	0.61
Citrate synthase	CS	1431	1.00 (0.52)	0.70 (0.13)†	0.94 (0.63)	0.59 (0.42)	0.52
ATPase, Ca++ transporting, cardiac muscle, fast twitch 1	ATP2A1	487	1.00 ± 0.06	0.79 ± 0.09	1.10 ± 0.12	0.83 ± 0.05†	0.25
Uncoupling protein 3	UCP3	7352	1.00 ± 0.10	0.94 ± 0.12	1.01 ± 0.16	0.88 ± 0.13	0.28
NADH dehydrogenase (ubiquinone) 1 β subcomplex, 8	NDUFB8	4714	1.00 (0.22)	0.94 (0.14)	0.94 (0.23)	0.94 (0.32)	0.25
Succinate dehydrogenase complex, subunit A	SDHA	6389	1.00 ± 0.06	1.02 ± 0.06	1.17 ± 0.06	1.00 ± 0.07†	0.06
Succinate dehydrogenase complex, subunit B	SDHB	6390	1.00 ± 0.04	0.80 ± 0.06†	0.92 ± 0.07	0.72 ± 0.06†	0.82
Ubiquinol-cytochrome c reductase core protein II	UQCRC2	7385	1.00 ± 0.09	0.88 ± 0.07	0.98 ± 0 0.11	0.64 ± 0.11	0.51
ATP synthase, H+ transporting, mitochondrial F1 complex, α subunit 1	ATP5A1	498	1.00 (0.30)	0.83 (0.27)	0.92 (0.13)	0.82 (0.28)	0.48

Data are presented as mean ± SEM or median (IQR). Due to a small amount of tissue one Caucasian and one South Asian subject were excluded for qPCR analysis. PPAR: Peroxisome proliferator-activated receptor, AMPK: AMP-activated protein kinase, CPT: Carnitine palmitoyltransferase. † $p<0.05$, †† $p<0.005$ within group vs. before diet. * $p<0.05$ between groups vs. Caucasians. ‡ $p<0.05$ diet effect vs. Caucasians (interaction p-value).

Supplemental Table 2. Activity level, normal dietary intake and intake during a 5-day HFHC-diet of healthy, young South Asian males and matched Caucasians.

	Caucasians	South Asians
Activity level		
exercise (min/week)	150 (203)	125 (210)
exercise (category)	2.5 (4)	2.5 (4)
activity factor	1.375 (0.22)	1.375 (0.26)
Normal diet		
total kcal per day	2593 ± 100	2170 ± 102 *
kcal per day per kg	34.6 ± 1.2	34.3 ± 2.0
fat (kcal/day)	835 ± 63	674 ± 60
carbohydrates (kcal/day)	1217 ± 47	1079 ± 48
protein (kcal/day)	404 ± 19	363 ± 35
fat (%)	31.6 ± 1.6	29.8 ± 1.9
carbohydrates (%)	47.6 ± 1.6	51.6 ± 2.1
protein (%)	15.8 ± 0.7	16.5 ± 1.0
Intake during a 5-day HFHC-diet		
total kcal per day	3824 ± 177	3453 ± 149
kcal per day per kg	51.1 ± 2.5	54.5 ± 2.9
fat (kcal/day)	2041 ± 92	1839 ± 62
carbohydrates (kcal/day)	1220 ± 81	1128 ± 65
protein (kcal/day)	439 ± 27	434 ± 31
fat (%)	54.0 ± 1.2	53.9 ± 1.2
carbohydrates (%)	31.6 ± 1.3	32.4 ± 0.9
protein (%)	11.4 ± 0.3	12.4 ± 0.6

Data are presented as mean ± SEM or median (IQR), n=12-11. Exercise categories: 0 = 0 minutes, 1 = 1-60 minutes, 2 = 61-120 minutes, 3 = 121-180 minutes, 4 = 181-240 minutes, 5 = 241-300 minutes. Activity factor according to the Harris-Benedict principle.

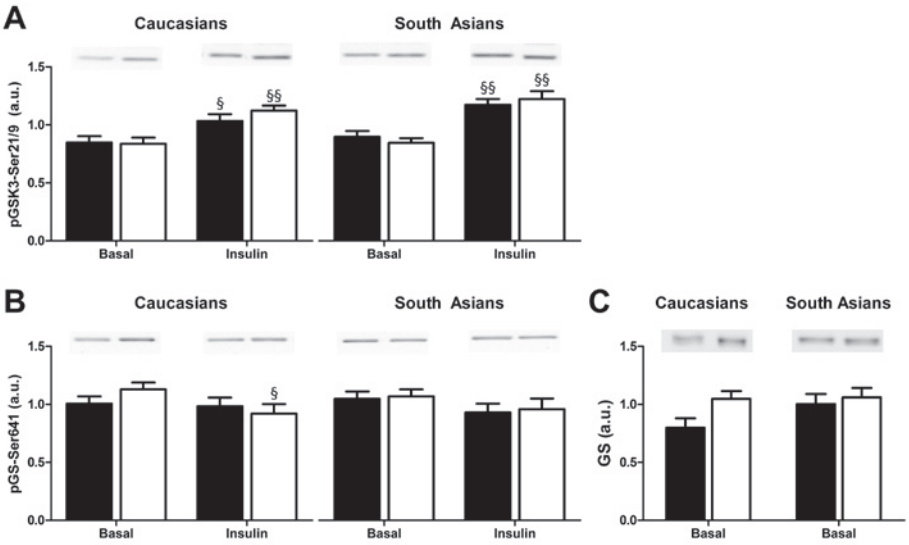

Supplemental Figure 1. Phosphorylation state of glycogen synthase kinase 3 and protein expression and phosphorylation state of glycogen synthase in skeletal muscle from healthy, young South Asian males and matched Caucasians before (black bars) and after (white bars) a 5-day HFHC-diet. The protein expression of A. Ser21/9-GSK3, B. Ser641-GS, and C. GS were assessed by Western Blot. The phosphorylation state in basal and hyperinsulinemic (step 2) conditions (A, B), or the protein expression in basal conditions (C) are shown. Results are normalized to Caucasian subjects (before diet, basal condition) and expressed as mean ± SEM. Due to a small amount of tissue two Caucasian subjects were excluded for Western Blot analysis. § $p<0.05$, §§ $p<0.005$ within groups *vs.* basal condition. GS: glycogen synthase. GSK3: glycogen synthase kinase 3.

Chapter 9

Cardiovascular function in middle-aged overweight South Asians compared with Caucasians: response to short-term caloric restriction

Linda D. van Schinkel*, Leontine E.H. Bakker*, Jacqueline T. Jonker, Albert de Roos, Hanno Pijl, A. Edo Meinders, Ingrid M. Jazet, Hildo J. Lamb, Johannes W.A. Smit

** both authors contributed equally*

Submitted

ABSTRACT

Background

South Asians have a higher risk of developing cardiovascular disease than Caucasians. The underlying cause is unknown, but might be related to higher cardiac susceptibility to metabolic disorders. Short-term caloric restriction (CR) can be used as a metabolic stress test to study cardiac flexibility. The objective was to assess whether metabolic and functional cardiovascular flexibility to CR differs between South Asians and Caucasians.

Methods

Cardiovascular function and myocardial triglycerides (TG) were assessed using a 1.5T MRI/S-scanner in 12 middle-aged overweight male South Asians and 12 matched Caucasians before and after an 8-day very low calorie diet (VLCD).

Results

At baseline South Asians were more insulin resistant than Caucasians. Cardiac dimensions were smaller, despite correction for body surface area, and PWV in the distal aorta was higher in South Asians. Systolic and diastolic function, myocardial TG and pericardial fat did not differ between groups. After the VLCD body weight reduced on average with 4.0 ± 0.2 kg. Myocardial TG increased in both ethnicities with 69 ± 18%, and diastolic function decreased. Pericardial fat and PWV in the proximal and total aorta were reduced in Caucasians only.

Conclusion

At baseline middle-aged overweight South Asians were more insulin resistant than Caucasians. Cardiac dimensions were smaller and PWV was higher in South Asians. After an 8-day VLCD, myocardial TG increased and diastolic function decreased to a similar extent in both groups, indicating comparable myocardial metabolic and functional flexibility in response to short-term CR. However, paracardial fat and PWV showed a differential effect in response to the VLCD, with a more favorable response in Caucasians.

INTRODUCTION

People of South Asian descent are at an increased risk of developing cardiovascular disease (CVD) compared to Caucasians. The age-standardized mortality rate from CVD is approximately 50% higher for South Asians (1-4). Furthermore, CVD in South Asians is more aggressive and has higher mortality rates at younger ages (1,2,5,6). The mean age of first acute myocardial infarction is around five years earlier than in Caucasians (6,7).

Traditional risk factors, such as smoking, hypertension and cholesterol levels, do not seem to account for the excess risk for CVD in South Asians (3,8). Major contributing factors to the high prevalence of CVD in South Asians are insulin resistance (IR) and type 2 diabetes mellitus (T2DM), which are also highly prevalent in this ethnicity. Mortality risk of CVD associated with T2DM is higher in South Asians compared to Caucasians (3,9), which might suggest that South Asians have a higher cardiac susceptibility to metabolic disorders. Since South Asians represent one fifth of the world's population, the increased risk for CVD and T2DM in this ethnicity poses a major burden on the health care system. Therefore, gaining more insight in the interrelationship between metabolic disorders and cardiac function in people of South Asians descent is of great importance.

We have shown previously that short-term caloric restriction (CR) can be used as a metabolic stress test to induce a short-term physiological increase of plasma free fatty acid (FFA) levels, which enables us to study the flexibility of myocardial triglyceride (TG) content and cardiac function, as assessed by magnetic resonance (MR) techniques (10-13). Surprisingly, so far no studies have been published on the effect of CR on cardiovascular function in South Asians.

Given the high risk of CVD in South Asians, we hypothesize that cardiovascular function in middle-aged overweight South Asians is impaired compared to Caucasians. Furthermore, we hypothesize that the metabolic and functional cardiovascular flexibility in response to CR is compromised in people of South Asians descent. Therefore, we subjected middle-aged, overweight South Asians and age-, sex- and BMI-matched Caucasians to an 8-day very low calorie diet (VLCD) and studied cardiac function and myocardial TG content using MR techniques. In addition, we studied aortic pulse wave velocity (PWV), which is a cardiovascular risk indicator.

METHODS

Subjects

Twelve Dutch South Asians and twelve Dutch Caucasian males, aged 40-50 year, with a positive family history for T2DM were enrolled. Subjects were overweight (BMI 25-30 kg/m^2) and had a waist circumference of >90 cm (South Asians) or >94 cm (Caucasians). Subjects were recruited via local advertisements, and underwent a medical screening including a physical examination, blood chemistry tests and an oral glucose tolerance test (OGTT) to exclude T2DM. Other exclusion criteria were: CVD, any significant chronic disease, use of medication known to influence glucose and/or lipid metabolism, smoking, recent weight change, and general contraindications to MR scanning. The study was approved by the local ethics committee and performed in accordance with the principles of the revised Declaration of Helsinki. Subjects gave written informed consent prior to participation.

Study design

Participants were studied on 2 study days separated by an 8-day VLCD. The VLCD consisted of three sachets of Modifast® (Nutrition & Santé Benelux, Breda, The Netherlands**)** per day (~450 kcal/day; ~50 g protein, 50-60 g carbohydrates, ~7 g lipids and ~15 g dietary fibers). MR studies were performed shortly before the start and at the end of the 8th day of the diet. Subjects were instructed not to alter life style habits. Anthropometric measurements and blood samples were obtained on both study days after a 10-hour overnight fast.

MR protocol

All measurements were performed using a 1.5-Tesla whole-body MR scanner (Gyroscan ACS-NT15; Philips Medical Systems, The Netherlands) in postprandial state (four hours after the last meal).

Myocardial triglyceride content

MR spectroscopy (^{1}H-MRS) was used to quantify myocardial TG content. Details on ^{1}H-MRS acquisition and post processing were published before (14,15). In summary, a 8-ml voxel was placed in the interventricular septum on four-chamber and short-axis images at end-systole. Electrocardiographic (ECG) triggering (for myocardial spectra) and respiratory pencil beam navigator were used during acquisition (14). Acquisitions were performed with and without water suppression, with myocardial TG expressed as percentage of the unsuppressed water signal.

Pericardial fat quantification

As described before (16), to quantify the pericardial fat volume, the heart was imaged using electrocardiographically gated breath-holds with a multi shot turbo spin echo sequence in a four-chamber view orientation. Water was suppressed using Spectral Inversion Recovery (SPIR). Contours were drawn around both pericardial fat layers surrounding the ventricles and atria using MASS® software (Medis, Leiden, The Netherlands) (Figure 1). The number of pixels were converted to square centimeters and multiplied by the slice thickness to obtain volume.

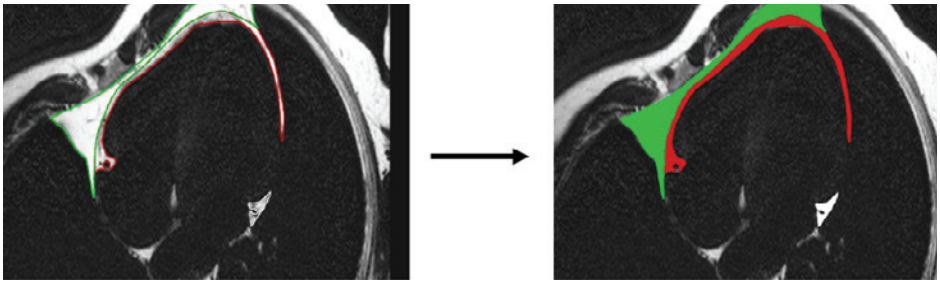

Figure 1. Quantification of the pericardial fat layer. This figure shows the quantification of the pericardial fat layer, which can be divided in an epicardial (red) and paracardial (green) fat layer.

Left ventricular dimensions and function

Data were analyzed blinded for ethnicity and study occasion. As previously described, the entire heart was imaged in short-axis orientation, using ECG gated breath-hold cine steady-state free-precession sequences (17). Left ventricular (LV) epicardial and endocardial contours were manually drawn in the end-systolic and end-diastolic phases of the short-axis images, using validated MASS® software. LV end-diastolic volume (EDV), end-systolic volume (ESV), ejection fraction (EF), stroke volume (SV) and end-diastolic mass (EDM) were calculated.

Furthermore, an ECG gated gradient-echo sequence with velocity encoding (100 cm/sec) was performed to measure transmitral blood, for the determination of LV diastolic function. Analysis was performed by using FLOW® software (Medis, Leiden, The Netherlands). The early filling phase (E) and the atrial contraction (A) were analyzed and their peak flow ratio was calculated (E/A ratio). Additionally, the peak deceleration gradient of E and LV filling pressures (E/Ea) were assessed (18,19). Heart rate was monitored and stored during the transmitral flow measurements.

Pulse Wave Velocity

To evaluate the aortic stiffness, aortic PWV was determined, using a previously described protocol (20). Shortly, a scout view of the aorta was performed. Subsequently, a velocity-encoded image perpendicular to the ascending aorta at the level of the pulmonary trunk, at the level of the aorta crossing the diaphragm and at the level of the aortic bifurcation was assessed (Figure 2). This resulted in through-plane flow measurements of the ascending and descending aorta. PWV was calculated using the formula: $\Delta x/\Delta t$, where Δx is the aortic path length between two measurement sites and Δt is the time delay between the arrivals of the foot of the pulse wave at the respective measurements site. The distance between the measurement sites was determined manually using MASS®. Data were analyzed using MASS® and FLOW®.

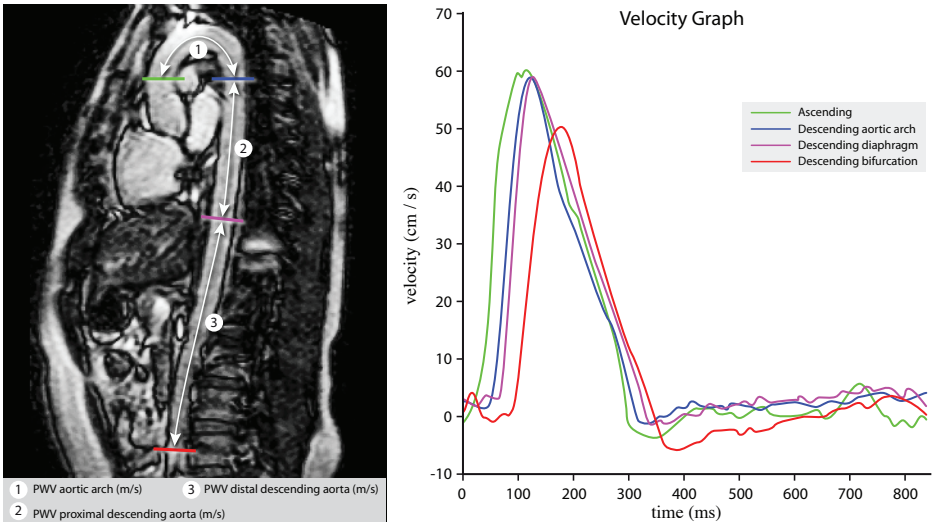

Figure 2. Aortic PWV determination with MRI. The left panel shows a double-oblique parasagittal image of the aorta. The colored lines represent the acquisition planes for velocity-encoded MRI which are positioned perpendicular to the aorta. 1 is the path length of the aortic arch, 2 of the proximal descending aorta and 3 of the distal descending aorta, determined along the centerline of the aorta. The right panel shows the velocity-time curves for the four different measurement sites in the aorta.

Assays

Serum concentrations of glucose, total cholesterol, HDL and TG were measured on a Modular P800 analyzer (Roche, The Netherlands), and serum insulin levels on an Immulite 2500 (Siemens, The Netherlands). HbA1c was measured on an HPLC system (Kordia, The Netherlands). Plasma FFAs were measured by a commercial kit (Wako Chemicals, Germany).

Statistical analysis

Data are presented as mean ± SEM or median (interquartile range (IQR)). A mixed effects model was applied to assess mean differences within and between groups, and to determine differences in diet effect. Groups and intervention were modeled as fixed effects and the subject specific deviances from the group mean were modeled as random effects. Nonparametric tests were performed when appropriate. Significance level was set at $p<0.05$ (two-sided). Statistical analyses were performed using SPSS for Windows version 20.0 (IBM, USA).

RESULTS

Clinical and metabolic characteristics

Baseline

Mean age was 44.6 ± 0.8 year. Body surface area (BSA) was significantly lower in South Asians compared to Caucasians. However, BMI (28.3 ± 0.3 kg/m^2), waist and hip circumference and percentage of fat mass were comparable between groups. The same was true for blood pressure and heart rate. Both ethnicities had similar fasting glucose levels, but HbA1c and insulin levels (both fasting and during OGTT) were higher in South Asians. Fasting FFAs, TGs and cholesterol levels did not significantly differ between groups, except LDL-cholesterol, which was higher in South Asians (Table 1).

Effect of VLCD

Anthropometric measurements were significantly reduced after the diet in both groups. The mean reduction in body weight for both groups was 4.0 ± 0.2 kg, of which approximately 50% was fat mass. BMI decreased on average with 1.28 ± 0.07 kg/m^2. Systolic and diastolic blood pressure were reduced in both ethnicities. The heart rate was not affected. In both groups, fasting glucose, insulin and TG levels decreased significantly, while FFAs increased in response to the VLCD (Table 1).

Myocardial TG content

Baseline

No differences in myocardial TG content were found between both groups at baseline (Table 2).

Effect of VLCD

Myocardial TG content increased in both ethnicities, although in Caucasians this did not reach significance (p=0.067). The percentage of myocardial TG increase, however, was comparable between groups (69 ± 18%, p=0.868) (Table 2 and Figure 3).

Pericardial fat distribution

Baseline

There were no differences in pericardial, epicardial or paracardial fat volumes between groups at baseline (Table 2).

Effect of VLCD

The pericardial and paracardial fat volumes decreased significantly in Caucasians in response to the VLCD (p=0.003 and p=0.050, respectively), whereas no significant changes occurred in South Asians (Table 2).

Left ventricular dimensions and function

Baseline

Despite correction for BSA EDV, ESV and SV were significantly lower in South Asians. EF was on average 61 ± 4%, and was comparable between ethnicities (p=0.808). There were no significant differences in diastolic cardiac function, as reflected in the E/A ratio (p=0.168) and the E/Ea ratio (p=0.088) (Table 3).

Effect of VLCD

LV mass, indexed for BSA, decreased slightly in both groups after the diet. EDV reduced in Caucasians, however no significant change occurred in South Asians. The cardiac index reduced equally in both ethnicities. The E/A ratio reduced significantly in Caucasians, whereas no significant diet effect was observed in South Asians. In contrast, the VLCD did not induce significant changes in the E/Ea ratio in Caucasians, while in South Asians E/Ea decreased significantly. The early peak filling rate (EPFR) and early deceleration mean showed a significant decrease in both groups in response to the VLCD (Table 3).

Pulse wave velocity

Baseline

PWV in the distal segment of the aorta was significantly higher in South Asians compared to Caucasians. Furthermore, PWV in the total aorta tended to be higher in South Asians, however this did not reach statistical significance (p=0.068) (Table 3).

Table 1. Clinical and metabolic characteristics

	Caucasians		South Asians	
	Baseline	**VLCD**	**Baseline**	**VLCD**
Clinical characteristics				
age (years)	44.3 ± 1.1		44.9 ± 0.9	
height (m)	1.81 ± 0.02		1.75 ± 0.01**	
weight (kg)	92.6 ± 2.5	88.2 ± 2.5††	86.7 ± 1.4	83.2 ± 1.6†† ‡
BSA (m^2)	2.14 ± 0.04	2.09 ± 0.04††	2.02 ± 0.02*	1.99 ± 0.02††*‡
BMI (kg/m^2)	28.1 ± 0.5	26.8 ± 0.5††	28.4 ± 0.4	27.3 ± 0.4††
waist (cm)	103 ± 2	100 ± 2††	99 ± 2	97 ± 1††
hip (cm)	102 ± 1	100 ± 1	99 ± 2	97 ± 1†
WHR	1.01 ± 0.01	0.99 ± 0.01†	1.02 ± 0.01	1.01 ± 0.01
fat mass (%)	23.1 ± 0.6	21.8 ± 0.6††	23.8 ± 0.6	23.0 ± 0.6††
systolic BP (mmHg)	130 ± 3	118 ± 2††	136 ± 3	124 ± 3††
diastolic BP (mmHg)	85 ± 3	77 ± 3††	90 ± 4	85 ± 3††
heart rate (bpm)	64 ± 3	61 ± 2	70 ± 3	65 ± 3
Metabolic characteristics				
free fatty acids (mmol/L)	0.53 ± 0.03	1.36 ± 0.13††	0.58 ± 0.04	0.85 ± 0.06†**‡‡
triglycerides (mmol/L)	1.29 (2.48)	0.89 (0.18) ††	1.78 (2.91)	0.91 (0.25)††
total cholesterol (mmol/L)	4.93 ± 0.16		5.05 ± 0.27	
HDL-cholesterol (mmol/L)	0.92 ± 0.05		0.84 ± 0.07	
LDL-cholesterol (mmol/L)	3.11 ± 0.16		3.13 ± 0.23	
total cholesterol/HDL ratio	5.53 ± 0.33		6.61 ± 0.78	
HbA1c (mmol/mol)	33.0 (6)		36.5 (1)*	
glucose (mmol/L)	5.33 ± 0.20	4.45 ± 0.22††	5.30 ± 0.11	4.51 ± 0.14††
insulin (mU/L)	6.0 (3.0)	1.7 (3.7)††	8.5 (2.5)**	2.3 (4.7)††
Oral glucose tolerance test				
2 hour insulin (mU/L)	31 (29)		77 (76)*	
glucose AUC (mmol/L)	959 ± 32		1027 ± 58	
insulin AUC (mU/L)	4477 ± 586		8790 ± 711**	

Data are presented as mean ± SEM or median (IQR). VLCD: very low calorie diet, BSA: body surface area, BMI: body mass index, WHR: waist hip ratio, BP: blood pressure, AUC: area under the curve.
† p<0.05, †† p<0.005 within group vs. before diet. * p<0.05, ** p<0.005 vs. Caucasians. ‡ p<0.05, ‡‡ p<0.005 diet effect vs. Caucasians.

Table 2. Pericardial fat distribution and myocardial triglyceride content assessed with MRI and MRS before and after an 8-day VLCD

	Caucasians		South Asians	
	Baseline	**VLCD**	**Baseline**	**VLCD**
Epicardial fat (ml)	3.1 (1.8)	3.6 (1.4)	3.3 (1.4)	3.0 (1.0)
Paracardial fat (ml)	4.8 (3.7)	3.7 (3.0)††	3.5 (2.1)	2.7 (2.6)‡
Pericardial fat (ml)	7.6 (4.0)	6.6 (3.5)†	6.7 (3.0)	6.0 (4.0)
Myocardial TG content (%)	0.56 ± 0.08	0.74 ± 0.08	0.59 ± 0.08	0.98 ± 0.13††

Data are mean ± SEM or median (IQR). VLCD: very low calorie diet, TG: triglyceride. † p<0.05, †† p<0.005 within group vs. before diet. * p<0.05, ** p<0.005 vs. Caucasians. ‡ p<0.05, ‡‡ p<0.005 diet effect vs. Caucasians.

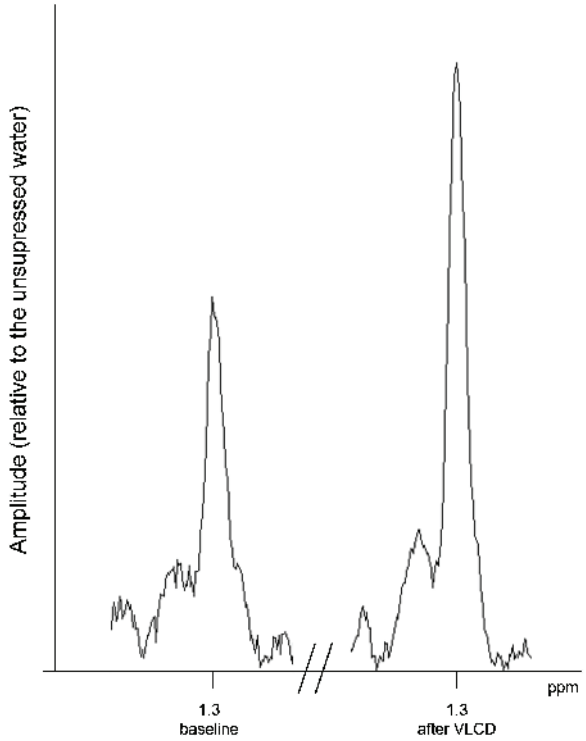

Figure 3: Myocardial spectra. Example of typical myocardial spectra of one subject before and after an 8-day VLCD.

Effect of VLCD

After the VLCD, PWV in the proximal descending part of the aorta and PWV of the total aorta were significantly reduced in Caucasians. In contrast, no diet effect on PWV in any of the segments of the aorta was observed in South Asians (Table 3).

Table 3. Cardiac dimensions and parameters of cardiovascular function assessed with MRI before and after an 8-day VLCD

	Caucasians		South Asians	
	Baseline	**VLCD**	**Baseline**	**VLCD**
Cardiac dimensions and basic function				
LVEDMI (g/m^2)	51 ± 2	48 ± 2††	52 ± 1	50 ± 1†
EDVI (ml/m^2)	87 ± 3	83 ± 2†	74 ± 3**	72 ± 3*
ESVI (ml/m^2)	34 ± 1	32 ± 1	29 ± 1*	27 ± 1*
SVI (ml/m^2)	5 ± 2	51 ± 2	46 ± 2*	45 ± 2*
CI ($ml/min/m^2$)	3366 ± 104	3074 ± 84†	3204 ± 175*	2916 ± 74†*
EF (%)	61 ± 2	62 ± 1	62 ± 1	63 ± 1
Diastolic cardiac function				
E peak filling rate (ml/s)	549 ± 28	477 ± 26††	493 ± 26	445 ± 22†
E acceleration peak (ml/s^2x10^{-3})	8.4 ± 0.6	7.0 ± 0.5††	7.5 ± 0.5	6.4 ± 0.3
E deceleration peak (ml/s^2x10^{-3})	-4.7 ± 0.3	-3.7 ± 0.2††	-4.9 ± 0.3	-4.1 ± 0.3†
E deceleration mean (ml/s^2x10^{-3})	-3.2 ± 0.2	-2.5 ± 0.2††	-3.4 ± 0.3	-2.8 ± 0.3†
A peak filling rate (ml/s)	392 ± 18	364 ± 20	365 ± 17	360 ± 10
E/A-peak ratio	1.43 ± 0.10	1.34 ± 0.09†	1.37 ± 0.08	1.24 ± 0.07
E/Ea	9.4 ± 0.7	8.3 ± 1.0	9.8 ± 0.8	7.2 ± 0.8†
Pulse wave velocity				
PWV aortic arch (m/s)	5.6 (0.9)	5.3 (1.1)	5.7 (1.3)	5.7 (0.9)
PWV proximal aorta (m/s)	6.7 (2.4)	5.2 (1.4)†	7.2 (3.7)	7.1 (2.6)**
PWV distal aorta (m/s)	5.0 (0.5)	4.9 (1.7)	5.5 (1.2)*	5.2 (1.0)
PWV total aorta (m/s)	5.5 (1.0)	5.2 (0.4)†	6.1 (0.9)	5.8 (0.9)*

Data are mean ± SEM or median (IQR). VLCD: very low calorie diet, LV: left ventricular, EDM: end- diastolic mass, EDV: end-diastolic volume, ESV: end-systolic volume, SV: stroke volume, CI: cardiac index, EF: ejection fraction, ESWS: end-systolic wall stress, I: indexed for body surface area, E: early diastolic wave, A: atrial diastolic wave, E/Ea: estimated left ventricular filling pressure, PWV: pulse wave velocity. † $p<0.05$, †† $p<0.005$ within group vs. before diet. * $p<0.05$, ** $p<0.005$ vs. Caucasians. ‡ $p<0.05$, ‡‡ $p<0.005$ diet effect vs. Caucasians.

DISCUSSION

South Asians have a higher risk of developing CVD than Caucasians. Additionally, the risk of cardiac complications in subjects with IR and T2DM is higher in this population, indicating they are metabolically more at risk. Previous studies in healthy subjects and obese patients with T2DM with and without CVD of Caucasian descent demonstrated metabolic and functional flexibility of the heart in response to both short- and long-term CR. To date, however, it was unknown if CR in South Asians has comparable effects. This study showed that an 8-day VLCD increased myocardial TG content and decreased diastolic function to a similar degree in middle-age overweight South Asians as compared to age-, sex- and BMI-matched but less insulin resistant Caucasians, indicating comparable flexibility of the heart. Paracardial fat volume and PWV, however, showed a differential effect in response to CR in favor of Caucasians.

Myocardial TG content

At baseline, South Asians were more insulin resistant, indicated by higher insulin levels (both in fasted condition and during OGTT) (Table 1). Studies in animals and humans have demonstrated that increased myocardial TG content in IR is associated with impaired myocardial function (21-23). Paradoxically, however, the increase in myocardial TG observed after a short-term VLCD is a sign of preserved metabolic flexibility of the heart. Given the high risk on CVD and T2DM in South Asians, we hypothesized, therefore, that the flexibility of the heart to adjust myocardial TG content in response to CR was diminished in South Asians compared to Caucasians. Surprisingly, however, an 8-day VLCD increased myocardial TG similarly in both groups. Thus, South Asians showed a similar physiological flexibility of myocardial lipid metabolism as Caucasians.

Previous short-term VLCD studies have shown that the increase in myocardial TG is the net result of increased uptake of FFAs in cardiomyocytes in relation to oxidative FFA requirements. This increased uptake is due to an increased release of FFAs from the adipose tissue into the circulation, which is caused by increased lipolysis of TG in adipose tissue in response to CR (11,13). Indeed, in the present study FFAs were significantly increased after the diet in both ethnicities, and waist fat was significantly reduced (data not shown), indicating increased lipolysis in the adipose tissue.

Pericardial fat

Pericardial fat, the layer of fat surrounding the heart, can be divided in an epicardial and paracardial layer. Both fat layers are metabolically different. Whereas epicardial fat has been shown to be a source of several inflammatory mediators, paracardial fat seems to have a greater importance in mechanical restriction, which exerts an unfavorable effect

on the coronary vasculature (24). In the present study, pericardial fat distribution was similar between groups at baseline. However, pericardial fat decreased significantly in Caucasians in response to the dietary intervention, mainly due to a reduction in the paracardial fat layer, whereas in South Asians no significant diet effect was observed. Since the paracardial fat layer has been found to be a predictor of CVD, the decrease in this specific fat compartment in Caucasians probably conveys reduced cardiovascular risk (25).

Cardiac dimensions and function

Cardiac dimensions were smaller in South Asians compared to Caucasians, despite correction for BSA. This is in line with other studies, which showed smaller left heart volumes in middle-aged South Asians (26,27), using echocardiography. In a recent study in healthy young adults, we showed that these smaller cardiac dimensions are already present at a young age (28). No major effects of the diet on cardiac dimensions were observed.

Cardiac systolic function, reflected as the LV ejection fraction, was normal (~62%) and comparable in both groups. Systolic function was not affected by the diet, which is in line with previous VLCD studies (11,13,29).

Diastolic cardiac function, reflected as the E/A ratio, decreased after the diet as expected from previous studies (11,13,30). The reduction, however, was only significant in Caucasians. This difference in diet effect might be attributed to a decrease in filling pressure (E/Ea ratio) in South Asians. In addition, other parameters for diastolic function did decrease in both groups. The decrease in diastolic function can probably be explained by changes in elastic properties of the LV. In animal models, TG accumulation in cardiomyocytes is directly related to impaired cardiac function via complex mechanisms involving fatty acid derivatives (21). An alternative explanation may be that changes in plasma FFAs, induced by CR, change the calcium homeostasis in the myocardium, thereby influencing LV diastolic function (31).

Pulse wave velocity

The PWV is a powerful independent predictor of cardiovascular events (32). In the present study, PWV in the distal aorta was significantly higher in South Asians compared to Caucasians at baseline, indicating a stiffer aorta. This is in line with other studies that showed a higher PWV in middle-aged South Asians compared to Caucasians (33,34). In addition, we have shown recently that PWV is already higher in healthy young South Asians (28). It is known that IR and T2DM compromise aortic elastic function. Although the precise underlying mechanisms remain unclear, it is known that long-term increased insulin levels can contribute to increased arterial wall thickness, and thereby to increased

arterial stiffening, by direct and indirect trophic effects on smooth muscle cells (35). In the present study, South Asians were more insulin resistant than Caucasian subjects – as reflected in higher insulin levels (both fasting and during OGTT) – which might explain the higher PWV observed in South Asians.

The PWV responded differentially to an 8-day VLCD, consisting of a reduction in proximal and total PWV in Caucasians, whereas no diet effect was observed in South Asians, suggesting that large arteries are less flexible in South Asians in response to CR. This might be due to the, probably long-term existing, higher IR observed in South Asians which may have induced irreversible changes in the arterial wall according to the aforementioned mechanism.

A strength of this study is that for the first time the response to a VLCD on cardiovascular function was assessed in South Asians. Furthermore, this is, to our knowledge, the first study measuring myocardial and pericardial TG content in people of South Asians descent, which is in our opinion very relevant given their high risk on CVD. A possible limitation is the relatively small sample size, which might limit generalization potential. However, subjects were their own controls, which increases power to detect relevant differences.

In conclusion, this study proves that myocardial TG stores in middle-aged overweight and insulin resistant South Asians are as flexible and amenable to therapeutic intervention by CR as age-, sex- and BMI-matched but less insulin resistant Caucasians. However, paracardial fat volume and PWV showed a differential effect in response to an 8-day VLCD in favor of Caucasians.

REFERENCES

1. Balarajan R: Ethnic differences in mortality from ischaemic heart disease and cerebrovascular disease in England and Wales. *BMJ* 302:560-564, 1991
2. Chaturvedi N, Fuller JH: Ethnic differences in mortality from cardiovascular disease in the UK: do they persist in people with diabetes? *J Epidemiol Community Health* 50:137-139, 1996
3. Forouhi NG, Sattar N, Tillin T, McKeigue PM et al.: Do known risk factors explain the higher coronary heart disease mortality in South Asian compared with European men? Prospective follow-up of the Southall and Brent studies, UK. *Diabetologia* 49:2580-2588, 2006
4. Wild SH, Fischbacher C, Brock A, Griffiths C et al.: Mortality from all causes and circulatory disease by country of birth in England and Wales 2001-2003. *J Public Health (Oxf)* 29:191-198, 2007
5. Anand SS, Yusuf S, Vuksan V, Devanesen S et al.: Differences in risk factors, atherosclerosis, and cardiovascular disease between ethnic groups in Canada: the Study of Health Assessment and Risk in Ethnic groups (SHARE). *Lancet* 356:279-284, 2000
6. Enas EA, Yusuf S, Mehta JL: Prevalence of coronary artery disease in Asian Indians. *Am J Cardiol* 70:945-949, 1992
7. Joshi P, Islam S, Pais P, Reddy S et al.: Risk factors for early myocardial infarction in South Asians compared with individuals in other countries. *JAMA* 297:286-294, 2007
8. McKeigue PM, Ferrie JE, Pierpoint T, Marmot MG: Association of early-onset coronary heart disease in South Asian men with glucose intolerance and hyperinsulinemia. *Circulation* 87:152-161, 1993
9. Wilkinson P, Sayer J, Laji K, Grundy C et al.: Comparison of case fatality in south Asian and white patients after acute myocardial infarction: observational study. *BMJ* 312:1330-1333, 1996
10. Hammer S, van der Meer RW, Lamb HJ, Schar M et al.: Progressive caloric restriction induces dose-dependent changes in myocardial triglyceride content and diastolic function in healthy men. *J Clin Endocrinol Metab* 93:497-503, 2008
11. van der Meer RW, Hammer S, Smit JW, Frolich M et al.: Short-term caloric restriction induces accumulation of myocardial triglycerides and decreases left ventricular diastolic function in healthy subjects. *Diabetes* 56:2849-2853, 2007
12. Hammer S, Snel M, Lamb HJ, Jazet IM et al.: Prolonged caloric restriction in obese patients with type 2 diabetes mellitus decreases myocardial triglyceride content and improves myocardial function. *J Am Coll Cardiol* 52:1006-1012, 2008
13. Hammer S, van der Meer RW, Lamb HJ, de Boer HH et al.: Short-term flexibility of myocardial triglycerides and diastolic function in patients with type 2 diabetes mellitus. *Am J Physiol Endocrinol Metab* 295:E714-E718, 2008
14. van der Meer RW, Doornbos J, Kozerke S, Schar M et al.: Metabolic imaging of myocardial triglyceride content: reproducibility of 1H MR spectroscopy with respiratory navigator gating in volunteers. *Radiology* 245:251-257, 2007
15. Vanhamme L, van den Boogaart A, Van HS: Improved method for accurate and efficient quantification of MRS data with use of prior knowledge. *J Magn Reson* 129:35-43, 1997
16. Jonker JT, de Mol P, de Vries S, Widya R et al.: Does Exercise in Type 2 Diabetes Induce Changes in Tissue-Specific Fat Distribution and Cardiac Function? *Radiology* 2013
17. Lamb HJ, Doornbos J, van der Velde EA, Kruit MC et al.: Echo planar MRI of the heart on a standard system: validation of measurements of left ventricular function and mass. *J Comput Assist Tomogr* 20:942-949, 1996

18. Pattynama PM, Lamb HJ, van der Velde EA, van der Wall EE et al.: Left ventricular measurements with cine and spin-echo MR imaging: a study of reproducibility with variance component analysis. *Radiology* 187:261-268, 1993
19. Paelinck BP, de Roos A, Bax JJ, Bosmans JM et al.: Feasibility of tissue magnetic resonance imaging: a pilot study in comparison with tissue Doppler imaging and invasive measurement. *J Am Coll Cardiol* 45:1109-1116, 2005
20. Grotenhuis HB, Westenberg JJ, Steendijk P, van Der Geest RJ et al.: Validation and reproducibility of aortic pulse wave velocity as assessed with velocity-encoded MRI. *J Magn Reson Imaging* 30:521-526, 2009
21. Christoffersen C, Bollano E, Lindegaard ML, Bartels ED et al.: Cardiac lipid accumulation associated with diastolic dysfunction in obese mice. *Endocrinology* 144:3483-3490, 2003
22. McGavock JM, Lingvay I, Zib I, Tillery T et al.: Cardiac steatosis in diabetes mellitus: a 1H-magnetic resonance spectroscopy study. *Circulation* 116:1170-1175, 2007
23. Szczepaniak LS, Dobbins RL, Metzger GJ, Sartoni-D'Ambrosia G et al.: Myocardial triglycerides and systolic function in humans: in vivo evaluation by localized proton spectroscopy and cardiac imaging. *Magn Reson Med* 49:417-423, 2003
24. van der Meer RW, Lamb HJ, Smit JW, de Roos A: MR imaging evaluation of cardiovascular risk in metabolic syndrome. *Radiology* 264:21-37, 2012
25. Sicari R, Sironi AM, Petz R, Frassi F et al.: Pericardial rather than epicardial fat is a cardiometabolic risk marker: an MRI vs echo study. *J Am Soc Echocardiogr* 24:1156-1162, 2011
26. Chahal NS, Lim TK, Jain P, Chambers JC et al.: Ethnicity-related differences in left ventricular function, structure and geometry: a population study of UK Indian Asian and European white subjects. *Heart* 96:466-471, 2010
27. Kumaran K, Fall CH, Martyn CN, Vijayakumar M et al.: Left ventricular mass and arterial compliance: relation to coronary heart disease and its risk factors in South Indian adults. *Int J Cardiol* 83:1-9, 2002
28. Schinkel LD, Bakker LEH, Jonker JT, de Roos A et al.: Functional and Metabolic Imaging of the Cardiovascular system in Young Healthy South Asians and Caucasians unveils early differences. *Diabetes Care* 2013
29. Hammer S, Snel M, Lamb HJ, Jazet IM et al.: Prolonged caloric restriction in obese patients with type 2 diabetes mellitus decreases myocardial triglyceride content and improves myocardial function. *J Am Coll Cardiol* 52:1006-1012, 2008
30. Hammer S, van der Meer RW, Lamb HJ, Schar M et al.: Progressive caloric restriction induces dose-dependent changes in myocardial triglyceride content and diastolic function in healthy men. *J Clin Endocrinol Metab* 93:497-503, 2008
31. Huang JM, Xian H, Bacaner M: Long-chain fatty acids activate calcium channels in ventricular myocytes. P*roc Natl Acad Sci U S A* 89:6452-6456, 1992
32. Mitchell GF, Hwang SJ, Vasan RS, Larson MG et al.: Arterial stiffness and cardiovascular events: the Framingham Heart Study. *Circulation* 121:505-511, 2010
33. Rezai MR, Wallace AM, Sattar N, Finn JD et al.: Ethnic differences in aortic pulse wave velocity occur in the descending aorta and may be related to vitamin D. *Hypertension* 58:247-253, 2011
34. Webb DR, Khunti K, Lacy P, Gray LJ et al.: Conduit vessel stiffness in British south Asians of Indian descent relates to 25-hydroxyvitamin D status. *J Hypertens* 30:1588-1596, 2012
35. Stapleton PA, James ME, Goodwill AG, Frisbee JC: Obesity and vascular dysfunction. P*athophysiology* 15:79-89, 2008

Chapter 10

Chemotherapy for testicular cancer induces acute alterations in diastolic heart function

Linda D. van Schinkel, Peter-Paul M. Willemse, Rutger W. van der Meer, Jacobus Burggraaf, Saskia G.C. van Elderen, Johannes W.A. Smit, Albert de Roos, Susanne Osanto, Hildo J. Lamb

British Journal of Cancer 2013; 109: 891-896

ABSTRACT

Background

After treatment with cisplatin-based chemotherapy for testicular cancer (TC), patients have higher prevalence of cardiovascular complications after long-term follow up. Little is known about acute cardiovascular effects of cisplatin-based chemotherapy. The aim of this study was to explore acute effects of chemotherapy on cardiac function in patients treated for TC.

Methods

Fourteen TC patients (age 34.6 ± 12.3 years) were studied before and 3 months after start with cisplatin-based chemotherapy. Cardiac function was assessed with magnetic resonance imaging. Fasting glucose and insulin levels were measured and insulin sensitivity, reflected by the Quicki index, was calculated.

Results

Left ventricular (LV) end-diastolic volume and LV stroke volume significantly decreased from 192 ± 27 ml to 175 ± 26 ml ($p<0.05$) and 109 ± 18 ml to 95 ± 16 ml ($p<0.05$) respectively. The ratio of early and atrial filling velocities across the mitral valve, a parameter of diastolic heart function, decreased after chemotherapy from 1.87 ± 0.43 to 1.64 ± 0.45 ($p<0.01$). Metabolic parameters were unfavorably changed, reflected by a decreased Quicki index, which reduced from 0.39 ± 0.05 to 0.36 ± 0.05 ($p<0.05$).

Conclusion

Chemotherapy for TC induces acute alterations in diastolic heart function, paralleled by unfavorable metabolic changes. Therefore, early after chemotherapy, metabolic treatment may be indicated to possibly reduce long-term cardiovascular complications.

INTRODUCTION

Testicular cancer (TC) is the most frequent form of cancer in young men. The prognosis of TC is good, with high cure rates since the introduction of treatment with cisplatin-based chemotherapy (1,2). Because of the increasing number of survivors with a long life expectancy, understanding and prevention of short-term and long-term cardiovascular effects of chemotoxicity is very important.

Treatment of TC with cisplatin, bleomycin and etoposide (BEP) combination chemotherapy is associated with acute vascular toxicity and subacute changes in cardiac function (3,4), as well as with long-term cardiovascular disease (5,6). Previous studies showed that cisplatin and bleomycin induce alterations in endothelial function and endothelial damage in vitro (7,8). These findings suggest direct toxic effects of chemotherapy on the cardiovascular system. Little is known about acute effects of cisplatin-based chemotherapy on cardiac function. More insight in the pathophysiology of the direct toxic effect of cisplatin-based chemotherapy on cardiac function and vessel wall is relevant to possibly prevent long-term cardiovascular disease. One previous study reported subacute deterioration of diastolic function, assessed with echocardiography 10 months after cisplatin-based chemotherapy (3).

Indirect effects of chemotherapy also seem to play a role in the increased risk of cardiovascular complications. For example, early after treatment with cisplatin-based chemotherapy changes in serum lipids have been described (9). Additionally, higher incidences of hypercholesterolemia, hypertension, microalbuminuria, obesity, elevated insulin-glucose ratio, and thereby metabolic syndrome have been reported at least 3 years after chemotherapy (6,10,11). The acute effects of chemotherapy, defined as effects occurring 3 months after start of chemotherapy, on these risk factors are largely unknown. The aforementioned indirect risk factors are all independently associated with a higher risk of cardiovascular disease and may contribute to the overall increased risk of cardiovascular complications after treatment with cisplatin-based chemotherapy. The increased risk of cardiovascular disease in cured TC patients after cisplatin-based chemotherapy is probably a combination of direct and indirect effects of chemotherapy (10,12). Early changes in cardiac function and risk factors may have prognostic value for long-term development of cardiovascular complications (13). Magnetic resonance (MR) imaging is a highly reproducible imaging modality to assess cardiac function. Furthermore, myocardial triglyceride (TG) content can be measured with proton (^{1}H)MR spectroscopy (14). Additionally, abdominal visceral and subcutaneous fat volume can be accurately assessed with MRI (15). Therefore, the purpose of this study was to investigate acute changes in cardiac function and myocardial TG, in relation to body fat distribution

and metabolic parameters 3 months after start with chemotherapy for TC, assessed with MR techniques.

METHODS

This study was approved by the local medical ethics committee and all subjects gave written informed consent. Metastatic TC patients, scheduled for first-line curative cisplatin-based combination chemotherapy in the Leiden University Medical Center were included between 2007-2009. Exclusion criteria were co-morbidities, including cardiovascular disease and diabetes mellitus.

Patients received three or four cycles of standard BEP-chemotherapy repeated every 3 weeks. Each cycle consisted of intravenously administered etoposide (100mg/m^2 over 1 hr, days 1-5), cisplatin (20mg/m^2 over 4 hr, days 1-5), and bleomycin (30 IUSP over 30min) at days 2, 8, and 15. According to Dutch oncological guidelines, TC patients with good prognosis were treated with three cycles of BEP and patients with intermediate prognosis were treated with four cycles BEP. One patient, in addition received paclitaxel (175mg/m^2) on day 1 of each of his 4 chemotherapy cycles as part of a randomized phase III study comparing paclitaxel-BEP and standard BEP in patients with intermediate prognosis TC. All patients were orchidectomized before adjuvant chemotherapeutic treatment.

BMI was determined at baseline and after chemotherapy. Fasting serum glucose, insulin, total cholesterol, high-density lipoprotein (HDL), low-density lipoprotein (LDL) and triglycerides were determined. Insulin resistance was assessed with the quantitative insulin sensitivity index (Quicki index), which is calculated using the formula: 1 / (log(fasting insulin μU/mL) + log(fasting glucose mg/dL)) (16). Renal function defined as estimated glomerular filtration rate was calculated with the Modification of Diet in Renal Disease (MDRD) equation: 186 * (serum creatinine μmol/L / 88,4)$^{-1.154}$ x (age)$^{-0.203}$.

Patients underwent MRI before start and shortly after the last chemotherapy cycle, which was approximately three months after start of chemotherapy.

Blood pressure and heart rate were measured during MRI using a semiautomated sphygmomanometer (Dinamap, Critikon, Tampa, Fla, USA).

We have included part of a studygroup from a previous study, describing metabolic changes and MRI assessment of hepatic triglyceride content, aortic pulse wave velocity and abdominal fat mass in TC patients undergoing curative chemotherapy at 3 and 9 months after start of chemotherapy (submitted).

MRI protocol

Left and right ventricular function

Cardiac imaging was performed using a 1.5 Tesla whole-body MRI scanner (Gyroscan ACS-NT15; Philips Medical Systems, Best, The Netherlands) after a night fast. The heart was imaged in short-axis orientation, using electrocardiographically gated breath-hold cine steady-state free-precession sequences as previously described (17). Imaging parameters were: repetition time (TR) 3.4ms, echo time (TE) 1.7ms, flip angle (FA) 35º, field of view (FOV) 400×320mm, slice thickness 10mm, no slice gap was used. To assess LV and RV systolic function, endocardial contours were manually drawn, using MASS® software (Medis, Leiden, the Netherlands). LV and RV ejection fraction (EF), stroke volume (SV), end-diastolic volume (EDV) and end-systolic volume (ESV) were assessed. Epicardial contours of the LV were drawn to calculate LV end-diastolic mass (LVED mass).

To assess LV and RV diastolic function, flow across mitral and tricuspid valve was measured using an electrocardiographically gated gradient echo sequence with velocity-encoding. Scan parameters: TR=9.1ms, TE=1.0ms, FA=20º, slice thickness=8mm, FOV=350mm^2 and matrix=256x256 pixels. Flow velocities in early diastole (E) and at atrial contraction (A) were measured and peak flow ratio was calculated (E/A ratio) using FLOW® software (Medis, Leiden, the Netherlands). The downslope of the early filling phase (E deceleration peak) and LV filling pressures (E/Ea) were calculated (18,19)

Myocardial triglyceride content

Myocardial ^{1}H-MR spectra were obtained as described before (14). A voxel was positioned in the myocardial interventricular septum in end-systole. ECG triggering and respiratory pencil beam navigator were used during acquisition. Spectra with water suppression were acquired with TE=26ms and TR≥3,000ms. 1,024 data points were collected using a 1,000-Hz spectral width and averaged over 128 acquisitions. Spectra without water suppression with TR=10s and four averages were obtained without changing other parameters. Spectroscopic data were fitted using validated software (jMRUI version 2.2, Leuven, Belgium) (20). Myocardial TG content was calculated as (amplitude of TG signal/amplitude water signal) x 100%.

Pericardial fat

Pericardial fat was quantified as described previously using electrocardiographically gated breath-holds with balanced turbo-field echo MR sequence (21). Imaging parameters: TR=3.2ms, TE=1.60ms, FA=50°, slice thickness=10mm, FOV=400mm^2. The four-chamber view was analyzed, with the plane of respiratory mitral and tricuspid valves as margins. To quantify periventricular fat volume, contours around pericardial fat were

drawn manually at end-systole and multiplied by the thickness of the slice. We used MASS® for postprocessing.

Visceral and subcutaneous fat

Visceral and subcutaneous fat volumes were imaged using a turbo spin echo imaging sequence (15). During one breath-hold, three consecutive transversal slices of 10mm thickness were scanned at the fifth lumbar vertebrae. Imaging parameters: TR=168ms, TE=11ms and FA=90º. Contours were drawn around visceral and subcutaneous abdominal fat depots using MASS®. Visceral and subcutaneous fat areas of each slice were multiplied by the slice thickness to acquire a volume, the volumes of all three slices were summed.

Statistical Analysis

Statistical analyses were performed using SPSS 17.0 (SPSS Inc.Chicago, Illinois, USA). We used two-tailed paired t-tests to compare the two study timepoints, since all data were normally distributed. To determine which significantly changed parameters influenced the differences of the other cardiac parameters, univariate regression analyses were performed. In these regression analyses the delta of the significantly changed parameter (the difference of the parameter before and after chemotherapy) was the independent variable and the delta of the cardiac parameter of interest was the dependent variable. In case of a significant influence the corrected difference between baseline and follow-up was extracted from the regression analysis. A p-value of <0.05 was considered statistically significant. Data are expressed as mean ± standard deviation (sd).

RESULTS

Forty consecutive patients were asked to participate. Twenty-one patients could not participate, based on logistic reasons (n=5), refusal or non-eligibility (n=16). These patients had unwillingness to undergo frequent blood drawings during chemotherapy or MRI. Nineteen patients underwent baseline MRI. Five patients missed the follow-up MRI due to treatment-related sickness (n=2), study withdrawal (n=2) and treatment-related death (n=1). Accordingly, 14 patients were included in data analysis of the present study. Three HDL-concentration and 1 insulin-concentration were missing.

Table 1 shows the tumor characteristics and staging. Table 2 shows the patient characteristics at baseline and after chemotherapy. Average age was 35 ± 12 years. Average time between the two MRI scans was 2.6 ± 0.5 months. Time between the last day of chemotherapy and the MRI after chemotherapy was 18 ± 18 days. Weight, BMI and blood pressure did not change during follow-up. Heart rate increased significantly

from 64 ± 9 beats/minute to 76 ± 15 bpats/minute (p=0.007). Laboratory parameters at baseline and at follow-up are described in Table 2. The Quicki index decreased, from 0.39 ± 0.05 to 0.36 ± 0.05 (p=0.018), reflecting greater insulin resistance.

Table 1. Tumor and staging characteristics of the patients

Histology; n (%)	
Seminoma	4 (28.6)
Non-seminoma	2 (14.3)
Combined tumor	8 (57.1)
TNM Tumor Staging; n (%)	
Stage II (para-aortic lymph node metastasis)	7 (50)
Stage III (distant metastasis)	7 (50)

Table 2. Patient characteristics at baseline and after chemotherapy

	Baseline	After chemotherapy
Systolic blood pressure (mmHg)	123 ± 17	118 ± 11
Diastolic blood pressure (mmHg)	73 ± 11	70 ± 12
Heart rate (beats per minute)	64 ± 9	76 ± 15†
Weight (kg)	83.3 ± 15.5	84.5 ± 18.5
Body Mass Index (kg/m^2)	24.4 ± 4.0	24.7 ± 4.6
Cholesterol (mmol/l)	4.7 ± 1.3	5.5 ± 1.5†
Estimated GFR (MDRD), ml/min	102 ± 16	113 ± 18†
HDL (mmol/l)	1.30 ± 0.31	1.36 ± 0.25
LDL (mmol/l)	3.12 ± 1.15	3.74 ± 1.41*
Triglycerides (mmol/l)	1.16 ± 0.60	1.64 ± 1.11
Fasting glucose (mmol/l)	5.1 ± 0.5	5.2 ± 0.6
Insulin (mU/l)	6.2 ± 5.0	9.8 ± 6.8
Quicki index	0.39 ± 0.05	0.36 ± 0.05*

*p<0.05, †p<0.01. Data are mean ± standard deviation.

Left and right ventricular function

Due to technical difficulties two diastolic LV and RV scans and one systolic RV were missing.

LV EDV and SV significantly decreased, respectively from 192 ± 27 ml to 175 ± 26 ml (p=0.012) and from 109 ± 18 ml to 95 ± 16 ml (p=0.025) (Table 3). Although LV EDV and SV were significantly influenced by the increased heart rate, the difference between

Table 3. Parameters of myocardial function, assessed with MRI at baseline and after chemotherapy

	Baseline	After chemotherapy
Left ventricle		
Systolic function		
EDV (ml)	192 ± 27	175 ± 126*
ESV (ml)	84 ± 16	80 ± 14
SV (ml)	109 ± 18	95 ± 16*
CO (ml/min)	6816 ± 1112	7050 ± 1160
EF (%)	56.6 ± 5.3	54.3 ± 5.1
Diastolic function		
E peak filling rate (ml/s)	657 ± 119	662 ± 122
E deceleration (ml/s^{2}x10^{-3})	6.3 ± 2.2	6.0 ± 1.7
A peak filling rate (ml/s)	362 ± 78	425 ± 111*
E/A-peak ratio	1.87 ± 0.43	1.64 ± 0.45†
E/Ea	6.8 ± 2.0	6.8 ± 2.0
Right ventricle		
Systolic function		
EDV (ml)	210 ± 32	196 ± 38*
ESV (ml)	105 ± 29	103 ± 25
SV (ml)	105 ± 14	93 ± 16*
CO (ml/min)	6595 ± 927	6976 ± 851
EF (%)	49.9 ± 6.7	47.9 ± 4.6
Diastolic function		
E peak filling rate (ml/s)	415 ± 55	406 ± 60
E deceleration (ml/s^{2}x10^{-3})	3.7 ± 1.9	3.0 ± 1.2
A peak filling rate (ml/s)	311 ± 57	325 ± 100
E/A-peak ratio	1.37 ± 0.25	1.32 ± 0.31

SV: stroke volume, ED: end-diastolic, ES: end-systolic, CO: cardiac output, EF: ejection fraction, E: early diastolic wave, A: atrial diastolic wave, E/Ea: estimated left ventricular filling pressure. *p<0.05, †p<0.01. Data are mean ± standard deviation.

baseline and follow-up remained significant after correction for heart rate. The other systolic LV parameters did not change after chemotherapy (Table 3).

LV E/A ratio decreased significantly after chemotherapy from 1.87 ± 0.43 to 1.64 ± 0.45 (p=0.009). In addition, the atrial peak filling rate increased significantly after chemotherapy. The LV E/A ratio and the atrial peak filling rate were not significantly influenced by the increased heart rate, thus correction for heart rate was not required. Other LV diastolic function parameters did not change after chemotherapy.

Right ventricular EDV and SV decreased significantly, from 210 ± 32 ml to 196 ± 32 ml and from 105 ± 14 (p=0.011) to 93 ± 16 ml (p=0.038) respectively. Both parameters were influenced by the increased heart rate. After correction for heart rate the difference between baseline and follow-up remained statistically significant. All other RV parameters, systolic or diastolic, remained unchanged after chemotherapy (Table 3).

Fat distribution

Myocardial triglyceride content

Baseline and follow-up data from eight myocardial ^{1}H-MR spectra were present. Myocardial triglyceride content did not significantly change after chemotherapy. At baseline TG content was 0.69 ± 0.41%, after chemotherapy 0.74 ± 0.35% (p=0.742).

Pericardial fat

Pericardial fat volume did not change significantly after chemotherapy, 27.0 ± 3.9 ml at baseline and 28.1 ± 5.5 ml early after chemo (p=0.343).

Visceral and subcutaneous fat

One waist fat MRI scan was missing. Visceral fat volume increased significantly from 186 ± 125 ml to 227 ± 162 ml (p=0.039), whereas subcutaneous fat volume did not change. The visceral/subcutaneous fat ratio did significantly increase from 0.38 ± 0.11 to 0.42 ± 0.12 (p=0.025).

DISCUSSION

The main finding of this study is that LV diastolic function is decreased 3 months after start of cisplatin-based chemotherapy for TC. Decreased diastolic function was accompanied by an unfavorable change in metabolic profile as measured by increased serum LDL and total cholesterol and decreased insulin sensitivity. Additionally, visceral fat volume and visceral/subcutaneous fat ratio increased. Several studies reported increased cardiovascular risk factors, increased incidence of cardiovascular disease and diminished cardiac function as long-term complications years after treatment with cisplatin-based chemotherapy (5,6,13,22,23). Only few studies report on the (sub-)acute cardiovascular effects of cisplatin-based chemotherapy (3,8,24). To the best of our knowledge we are the first to investigate the acute effects of chemotherapy on cardiac function. Altena et al showed deterioration of diastolic heart function assessed with echocardiography approximately 10 months after chemotherapy (3). In contrast, we assessed cardiac function immediately after completion of chemotherapy.

In the present study the LV E/A ratio decreased, reflecting deterioration in diastolic LV function. Since the E/A ratio is load dependent and thus influenced by the filling status of the patient, an estimation of LV filling pressure was determined (E/Ea) (18), which did not change after chemotherapy. Therefore, the decreased E/A ratio after chemotherapy presumably reflects disturbed intrinsic relaxation of the LV, rather than change in LV filling pressure. A previous study showed progressive deterioration of diastolic heart function, 10 months and 6.9 years after cisplatin-based chemotherapy (13). Therefore, acute changes in diastolic function observed in the present study might be of prognostic clinical significance. Long-term follow-up data of our patient group would be interesting to have some information of the predictive value of these early cardiac changes. LV ejection fraction (LVEF), an important parameter of systolic function, did not change. Change in LV diastolic function with preserved LVEF after treatment with cisplatin-based chemotherapy is in line with previous studies (3,13,23). It is known that diastolic dysfunction precedes a decline in systolic function and can be regarded as an important prognostic marker of ongoing disease (25,26). For future studies it would be interesting to combine echocardiography with cardiac MRI, since previous studies suggest that early impairment of systolic function may also be detected using strain echocardiography and that it could be predictive of subsequent reduction in LVEF (27). Furthermore, in further studies biomarkers such as N-terminal pro-brain natriuretic peptide and troponin I could be determined, because determination of these biomarkers may be useful in evaluation of early cardiac toxicity (27).

Cisplatin can directly injure cardiomyocytes through oxidative stress and mitochondrial damage (28). Additionally, cisplatin and bleomycin cause decreased endothelial cell

survival and induce apoptosis of endothelial cells in vitro (8). These endothelial changes may promote inflammation and atherosclerosis, which can contribute to chemotherapy-induced vascular toxicity. In addition, endothelial cells at the endocardium play an obligatory role in maintaining cardiac function (29). Cisplatin-based chemotherapy may also indirectly lead to cardiovascular disease, via increased prevalence of cardiovascular risk factors (10,22). Increased prevalence of cardiovascular risk factors, such as dyslipidemia, central obesity and insulin resistance, can lead to accelerated atherosclerosis (12). In this study the follow-up time is presumably too short for these indirect effects of chemotherapy to contribute to impaired cardiac function. We could not establish a direct relationship between cardiac function and metabolic profile. However, already 3 months after start of chemotherapy, we identify a shift to an unfavorable metabolic profile: visceral fat volume, visceral/subcutaneous fat ratio, LDL-cholesterol and total cholesterol were increased and insulin sensitivity decreased. Visceral fat is more deleterious than subcutaneous fat and is associated with the metabolic syndrome and cardiovascular disease (10,30,31). The metabolic syndrome consists of a cluster of risk factors: dyslipidemia, hypertension, central obesity and insulin resistance. This syndrome is associated with a long-term increased risk for atherosclerotic disease (10,32), with cardiovascular disease as one of the major complications. Via insulin resistance and the concomitant increased release of adipokines such as resistin, the metabolic syndrome is associated with endothelial dysfunction (33). High C-reactive protein (CRP) levels are associated with the metabolic syndrome and endothelial dysfunction (34). In this study we did not measure CRP levels unfortunately, but in subsequent studies these levels should be measured. A recent study showed that the metabolic syndrome is more prevalent and develops at earlier age in TC survivors, treated with cisplatin-based chemotherapy (35). Visceral adipose tissue contributes to insulin resistance (30), which is associated with decreased cardiac function (25,36,37), even in absence of diabetes mellitus (38,39). In the metabolic syndrome, insulin resistance and (visceral) adiposity is correlated with myocardial TG accumulation, which might negatively influence cardiac function (40,41). In this study we did not find a difference between myocardial TG content before and after chemotherapy. The number of measurements of myocardial TG (n=8) content is probably too small to draw firm conclusions regarding myocardial TG changes early after chemotherapy. Another explanation could be that the follow-up period is too short, so the oxidative capacity of the myocardium is still sufficient, preventing storage of TG in the myocardium.

Diastolic cardiac function progressively deteriorates in TC survivors treated with cisplatin-based chemotherapy (13). Subclinical changes in cardiac diastolic function may therefore precede late clinical dysfunction. If these early changes are predictive for later abnormalities in cardiac function, such changes may be used to monitor patients

more specifically. Furthermore, patients treated with cisplatin-based chemotherapy are at increased risk of developing an unfavorable cardiovascular-risk profile, which can contribute to development of long-term cardiac failure. Accordingly, early detection of risk factors for cardiovascular disease is important, as treatment of the unfavorable metabolic changes with lifestyle intervention or medication can contribute to an improved long-term prognosis in patients treated with cisplatin-based chemotherapy.

In conclusion, treatment with cisplatin-based chemotherapy for TC induces acute alterations in diastolic cardiac function, paralleled by unfavorable metabolic changes. Although the predictive significance of the diastolic cardiac changes for long-term cardiovascular morbidity is not clear at present, it seems plausible that they may eventually lead to overt cardiovascular disease. As the detrimental metabolic changes can contribute to the development of cardiovascular disease, these risk factors should be monitored and treated if necessary.

REFERENCES

1. International Germ Cell Consensus Classification: a prognostic factor-based staging system for metastatic germ cell cancers. International Germ Cell Cancer Collaborative Group. *J Clin Oncol* 15:594-603, 1997
2. Einhorn EH: Testicular cancer: an oncological success story. *Clin Cancer Res* 3:2630-2632, 1997
3. Altena R, de Haas EC, Nuver J, Brouwer CA et al.: Evaluation of sub-acute changes in cardiac function after cisplatin-based combination chemotherapy for testicular cancer. *Br J Cancer* 100:1861-1866, 2009
4. Stefenelli T, Kuzmits R, Ulrich W, Glogar D: Acute vascular toxicity after combination chemotherapy with cisplatin, vinblastine, and bleomycin for testicular cancer. *Eur Heart J* 9:552-556, 1988
5. Huddart RA, Norman A, Shahidi M, Horwich A et al.: Cardiovascular disease as a long-term complication of treatment for testicular cancer. *J Clin Oncol* 21:1513-1523, 2003
6. Meinardi MT, Gietema JA, van der Graaf WT, van Veldhuisen DJ et al.: Cardiovascular morbidity in long-term survivors of metastatic testicular cancer. *J Clin Oncol* 18:1725-1732, 2000
7. Montiel M, Urso L, de la Blanca EP, Marsigliante S et al.: Cisplatin reduces endothelial cell migration via regulation of type 2-matrix metalloproteinase activity. *Cell Physiol Biochem* 23:441-448, 2009
8. Nuver J, de Haas EC, Van ZM, Gietema JA et al.: Vascular damage in testicular cancer patients: a study on endothelial activation by bleomycin and cisplatin in vitro. *Oncol Rep* 23:247-253, 2010
9. Raghavan D, Cox K, Childs A, Grygiel J et al.: Hypercholesterolemia after chemotherapy for testis cancer. *J Clin Oncol* 10:1386-1389, 1992
10. de Haas EC, Oosting SF, Lefrandt JD, Wolffenbuttel BH et al.: The metabolic syndrome in cancer survivors. *Lancet Oncol* 11:193-203, 2010
11. Strumberg D, Brugge S, Korn MW, Koeppen S et al.: Evaluation of long-term toxicity in patients after cisplatin-based chemotherapy for non-seminomatous testicular cancer. *Ann Oncol* 13:229-236, 2002
12. Nuver J, Smit AJ, Sleijfer DT, van Gessel AI et al.: Microalbuminuria, decreased fibrinolysis, and inflammation as early signs of atherosclerosis in long-term survivors of disseminated testicular cancer. *Eur J Cancer* 40:701-706, 2004
13. Altena R, Hummel YM, Nuver J, Smit AJ et al.: Longitudinal changes in cardiac function after cisplatin-based chemotherapy for testicular cancer. *Ann Oncol* 22:2286-2293, 2011
14. van der Meer RW, Doornbos J, Kozerke S, Schar M et al.: Metabolic imaging of myocardial triglyceride content: reproducibility of 1H MR spectroscopy with respiratory navigator gating in volunteers. *Radiology* 245:251-257, 2007
15. Rijzewijk LJ, van der Meer RW, Smit JW, Diamant M et al.: Myocardial steatosis is an independent predictor of diastolic dysfunction in type 2 diabetes mellitus. *J Am Coll Cardiol* 52:1793-1799, 2008
16. Katz A, Nambi SS, Mather K, Baron AD et al.: Quantitative insulin sensitivity check index: a simple, accurate method for assessing insulin sensitivity in humans. *J Clin Endocrinol Metab* 85:2402-2410, 2000
17. Lamb HJ, Doornbos J, van der Velde EA, Kruit MC et al.: Echo planar MRI of the heart on a standard system: validation of measurements of left ventricular function and mass. *J Comput Assist Tomogr* 20:942-949, 1996

18. Paelinck BP, de Roos A, Bax JJ, Bosmans JM et al.: Feasibility of tissue magnetic resonance imaging: a pilot study in comparison with tissue Doppler imaging and invasive measurement. *J Am Coll Cardiol* 45:1109-1116, 2005
19. Pattynama PM, Lamb HJ, van der Velde EA, van der Wall EE et al.: Left ventricular measurements with cine and spin-echo MR imaging: a study of reproducibility with variance component analysis. *Radiology* 187:261-268, 1993
20. Naressi A, Couturier C, Castang I, de BR et al.: Java-based graphical user interface for MRUI, a software package for quantitation of in vivo/medical magnetic resonance spectroscopy signals. *Comput Biol Med* 31:269-286, 2001
21. Jonker JT, Lamb HJ, van der Meer RW, Rijzewijk LJ et al.: Pioglitazone compared with metformin increases pericardial fat volume in patients with type 2 diabetes mellitus. *J Clin Endocrinol Metab* 95:456-460, 2010
22. Haugnes HS, Wethal T, Aass N, Dahl O et al.: Cardiovascular risk factors and morbidity in long-term survivors of testicular cancer: a 20-year follow-up study. *J Clin Oncol* 28:4649-4657, 2010
23. Nuver J, Smit AJ, Sleijfer DT, van Gessel AI et al.: Left ventricular and cardiac autonomic function in survivors of testicular cancer. *Eur J Clin Invest* 35:99-103, 2005
24. Nuver J, Smit AJ, van der Meer J, van den Berg MP et al.: Acute chemotherapy-induced cardiovascular changes in patients with testicular cancer. *J Clin Oncol* 23:9130-9137, 2005
25. Battiprolu PK, Gillette TG, Wang ZV, Lavandero S et al.: Diabetic Cardiomyopathy: Mechanisms and Therapeutic Targets. *Drug Discov Today Dis Mech* 7:e135-e143, 2010
26. Falcao-Pires I, Leite-Moreira AF: Diabetic cardiomyopathy: understanding the molecular and cellular basis to progress in diagnosis and treatment. *Heart Fail Rev* 17:325-344, 2012
27. Monsuez JJ: Detection and prevention of cardiac complications of cancer chemotherapy. *Arch Cardiovasc Dis* 105:593-604, 2012
28. El-Awady e, Moustafa YM, Abo-Elmatty DM, Radwan A: Cisplatin-induced cardiotoxicity: Mechanisms and cardioprotective strategies. *Eur J Pharmacol* 650:335-341, 2011
29. Brutsaert DL: Cardiac endothelial-myocardial signaling: its role in cardiac growth, contractile performance, and rhythmicity. P*hysiol Rev* 83:59-115, 2003
30. Mathieu P, Pibarot P, Larose E, Poirier P et al.: Visceral obesity and the heart. *Int J Biochem Cell Biol* 40:821-836, 2008
31. Despres JP, Lemieux I: Abdominal obesity and metabolic syndrome. *Nature* 444:881-887, 2006
32. Alberti KG, Zimmet P, Shaw J: Metabolic syndrome--a new world-wide definition. A Consensus Statement from the International Diabetes Federation. *Diabet Med* 23:469-480, 2006
33. Verma S, Li SH, Wang CH, Fedak PW et al.: Resistin promotes endothelial cell activation: further evidence of adipokine-endothelial interaction. *Circulation* 108:736-740, 2003
34. Devaraj S, Kumaresan PR, Jialal I: C-reactive protein induces release of both endothelial microparticles and circulating endothelial cells in vitro and in vivo: further evidence of endothelial dysfunction. *Clin Chem* 57:1757-1761, 2011
35. Haas de E.C., Altena R, Boezen HM, Zwart N et al.: Early development of the metabolic syndrome after chemotherapy for testicular cancer. *Ann Oncol* First published November 6, 2012. doi: 10.1093/annonc/mds527: 2012
36. Rijzewijk LJ, van der Meer RW, Lamb HJ, de Jong HW et al.: Altered myocardial substrate metabolism and decreased diastolic function in nonischemic human diabetic cardiomyopathy: studies

with cardiac positron emission tomography and magnetic resonance imaging. *J Am Coll Cardiol* 54:1524-1532, 2009

37. Voulgari C, Papadogiannis D, Tentolouris N: Diabetic cardiomyopathy: from the pathophysiology of the cardiac myocytes to current diagnosis and management strategies. *Vasc Health Risk Manag* 6:883-903, 2010
38. Bajraktari G, Koltai MS, Ademaj F, Rexhepaj N et al.: Relationship between insulin resistance and left ventricular diastolic dysfunction in patients with impaired glucose tolerance and type 2 diabetes. *Int J Cardiol* 110:206-211, 2006
39. Dinh W, Lankisch M, Nickl W, Scheyer D et al.: Insulin resistance and glycemic abnormalities are associated with deterioration of left ventricular diastolic function: a cross-sectional study. *Cardiovasc Diabetol* 9:63, 2010
40. Kankaanpaa M, Lehto HR, Parkka JP, Komu M et al.: Myocardial triglyceride content and epicardial fat mass in human obesity: relationship to left ventricular function and serum free fatty acid levels. *J Clin Endocrinol Metab* 91:4689-4695, 2006
41. Hammer S, Snel M, Lamb HJ, Jazet IM et al.: Prolonged caloric restriction in obese patients with type 2 diabetes mellitus decreases myocardial triglyceride content and improves myocardial function. *J Am Coll Cardiol* 52:1006-1012, 2008

Chapter 11

Ultrahigh field 7T MR carotid vessel wall imaging: initial experience in comparison with 3T

Eleanore S.J. Kröner, Linda D. van Schinkel, Maarten J. Versluis, Niels J. Brouwer, Pieter J. van den Boogaard, Ernst E. van der Wall, Albert de Roos, Andrew G. Webb, Hans-Marc J. Siebelink, Hildo J. Lamb

Investigative Radiology 2012; 47: 697-704

ABSTRACT

Background

Magnetic Resonance Imaging (MRI) of the vessel wall enables determination of luminal area, vessel wall thickness, and atherosclerotic plaque characteristics. For clinical application, high spatial resolution, deriving from optimal signal-to-noise-ratio (SNR) and contrast-to-noise-ratio (CNR) is paramount. Vessel wall MRI is expected to benefit from higher magnetic field strength. Therefore, the purposes of the present study were to develop an ultrahigh field 7T MRI hardware and protocols for vessel wall imaging of the carotid artery and to compare quantitative parameters of vessel wall morphology and image quality between 3T and 7T MRI.

Methods

18 volunteers (11 males, 7 females, mean age 29 ± 7 yrs) underwent MRI-examinations at 7T (using a custom built surface transmit/receive coil of 15 cm diameter) and at 3T (using a commercial phased-array coil with two flexible oval elements,14 x 17 cm each). MRI of the left common carotid artery vessel wall was performed at 7T with identical in-plane resolution as that of 3T MRI (0.46 x 0.46 mm^2) providing transverse T1- and T2-weighted images. Blinded analysis of morphologic measurements (luminal area and vessel wall area), SNR for vessel wall (SNR_{VW}), and the CNR between the lumen and the vessel wall (CNR) were compared between 7T and 3T.

Results

Morphologic carotid vessel wall measurements were comparable between 7T and 3T for both T1-weighted images (luminal area: intraclass correlation [ICC]: 0.81 and vessel wall area: ICC: 0.84) and T2-weighted images (luminal area: ICC: 0.97 and vessel wall area: ICC: 0.92). At 7T, SNR_{VW} and CNR were significantly higher as compared to 3T MRI for both T1- ($p<0.001$) and T2-weighted images ($p<0.05$), with gain factors ranging from 1.3 to 3.6.

Conclusions

Ultrahigh field 7T MR carotid vessel wall imaging is feasible. 7T MRI of the common carotid artery has comparable accuracy for determining luminal area and vessel wall area and has improved SNR_{VW} and CNR as compared to 3T MRI. Therefore, ultrahigh field 7T vessel wall MRI may enable more detailed assessment of plaque morphology.

INTRODUCTION

Atherosclerosis and its thrombotic complications are the major cause of morbidity and mortality in industrialized countries (1). Early detection of atherosclerosis by a non-invasive imaging tool may permit optimized risk stratification, prevention and early treatment initiation in patients with various degrees of atherosclerotic disease (2). Magnetic resonance imaging (MRI) has emerged as a promising imaging modality for studying atherosclerotic disease in humans in vivo (2).

For clinical application, high spatial resolution, deriving from optimal signal-to-noise-ratio (SNR) and contrast-to-noise-ratio (CNR) is paramount. A new generation of ultrahigh field MR scanners operating at 7T has recently become available for clinical research (3-6). In many applications ultrahigh field MRI provides higher SNR and CNR, which can be used to increase spatial resolution (3,7-9). Therefore, it is expected that MR imaging of the carotid vessel wall may potentially benefit from higher magnetic field strength.

At present only limited data are available on the feasibility of 7T carotid artery MRI (10). To our knowledge, no comparative studies between 3T and 7T imaging of the carotid artery that investigate vessel morphology measurements (luminal area and vessel wall area) and quantification of image quality (SNR and CNR) have been performed..

Therefore, the purposes of the present study were to develop an ultrahigh field 7T MRI protocol for vessel wall imaging of the carotid artery and to compare quantitative parameters of vessel wall morphology and image quality between 3T and 7T MRI.

METHODS

Patient population and study protocol

Subjects

18 volunteers (11 males, 7 females, mean age 29 ± 7 yrs) were included. None of these volunteers had a previous history of cardiovascular disease. Approval from the local Medical Ethical Committee was obtained and all volunteers gave written informed consent.

General MRI protocol

Subjects underwent MRI examinations of the left carotid artery consecutively on 3T and 7T MR systems. Scanning was performed using commercial 3T and 7T scanners (Achieva, Philips, Best, The Netherlands). The MR systems were equipped with a commercial vec-

tor ECG module. The electrodes of the vector were placed on the anterior chest wall, with two electrodes (lead 1 [L1], L2) in the sternum and one electrode (L3) vertical to L1 and L2, just below the sternum. In addition one electrode (L4) was placed horizontal to L2, on the left thorax in the mid axillary line (5). All subjects were positioned head first and in the supine position in the scanner.

Similar protocols were employed at both MR field strengths: After acquisition of a three-dimensional (3D) time-of-flight (TOF) sequence to localize the vessel bifurcation, sagittal and coronal 2D survey scans of the left carotid artery were acquired. The multi-contrast carotid vessel wall protocol was planned on these images and consisted of a T1 fast gradient echo (FGE) sequence, a T2 turbo spin echo (TSE) sequence and a 3D TOF sequence. The scan parameters for the multi-contrast protocol at 3T and 7T field strength are given in the next section and an overview is provided in Table 1. The main difference between the T1-weighted protocols at 7T and 3T is that 7T black blood (BB) preparation was performed using local saturation slabs saturating the inflowing venous and arterial blood. In contrast, at 3T BB preparation was performed by a global inversion followed by a slice-selective 10 mm thick re-inversion using the body coil. The difference in BB preparation between 7T and 3T is due to the absence of a body coil at 7T MR system and limited RF coverage of the transmit/receive (T/R) coil at 7T. For the T2-weighted TSE protocols no BB prepulse was used. For the TOF images a saturation slab superior to the imaging stack was placed at 3T, which was not the case at 7T.

Table 1. Scan parameters for carotid vessel wall imaging protocols at 3T and 7T

	Black-blood T1-weighted	**Black-blood T1-weighted**	**Black-blood T2-weighted**	**Black-blood T2-weighted**	**Time-of-Flight**	**Time-of-Flight**
	3T	**7T**	**3T**	**7T**	**3T**	**7T**
Acquisition sequence	FGE	FGE	TSE	TSE	FFE	FFE
Acquisition mode	2D	2D	2D	2D	3D	3D
Echo time (ms)	3.5	3.7	50	50	3.30	3.6
Repetition time (ms)	12.4	13	2 heartbeats	2 heartbeats	26.20	15
Excitation flip angle (degrees)	45	45	90	90	20	20
FOV (mm)	140 x 140	140 x 140	140 x 140	140 x 140	140 x 140	140 x 140
Resolution (mm^2)	0.46 x 0.46	0.46 x 0.46	0.46 x 0.46	0.46 x 0.46	0.46 x 0.46	0.46 x 0.46
Slice thickness/gap (mm)	2; 0.7	2; 0.7	2; 0.7	2; 0.7	2; 0.7	2; 0.7

3T: 3 Tesla magnetic field strengt, 7T: 7 Tesla magnetic field strength, FGE: fast gradient echo, TSE: turbo spin echo, FOV: field of view.

3T MRI acquisition

RF coil

A standard Philips SENSE-flex-M surface coil with two flexible elements of 14×17cm was positioned around the neck, as previously described (11). An example of coil positioning at 3T and 7T is provided in Figure 1.

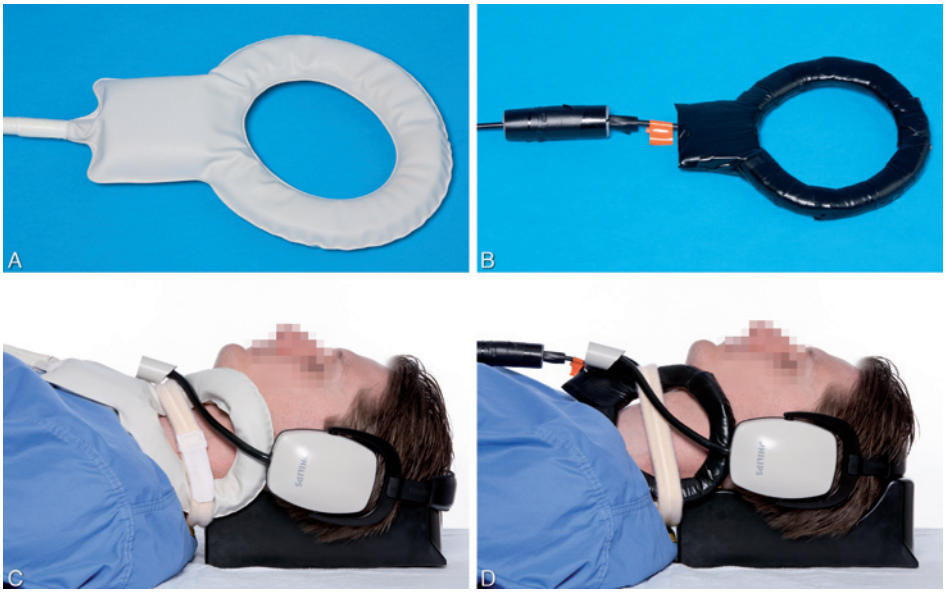

Figure 1. A: Standard Philips SENSE-flex-M surface coil (14 x 17 cm) used for the 3T MR acquisition is shown. **B:** Custom-built local surface transmit/receive coil of 15-cm diameter used for the 7T acquisition is shown. **C:** Coil positioning and scanning set-up at 3T MRI. **D:** Coil positioning and scanning set-up at 7T.

Survey

The 3T protocol has been previously described (11). In short, two survey scans in sagittal and coronal direction were planned on a 3D TOF sequence scout scan.

Multicontrast 3T protocol

Subsequently the multi-contrast 3T protocol, including three sequences were planned on the two surveys scans, perpendicular to the course of the common carotid artery in both views. Nine contiguous transverse slices of 2-mm thickness, with identical in-plane resolution (0.46×0.46mm^2), were positioned with the middle of the stack (slice number 5) at the level of the carotid bifurcation of the left carotid artery. The scan parameters were:

1: 2D BB T1-weighted fast gradient echo (FGE) sequence (scan parameters; field-of-view (FOV) 140 x 140 mm, 2.0 mm slice thickness, repetition time (TR): 12.41 ms / echo time (TE): 3.54 ms / flip angle (FA): 45º, acquired pixel size 0.46 x 0.46 x 2 mm^3 , scan duration per slice = 1.3 minutes at a typical heart rate of 65 beats per minutes, ECG triggering at end-diastole), with up to second order shimming.

2: 2D BB T2-weighted turbo spin echo (TSE) sequence (scan parameters; FOV 140 x 140 mm, 2.0 mm slice thickness, TR / TE / FA: 2 heartbeats/ 50 ms / 90º, acquired pixel size 0.46 x 0.46 x 2 mm^3, scan duration per slice = 1.5 minutes at a typical heart rate of 65 beats per minutes, ECG triggering at end-diastole), using linear shimming.

All BB images were obtained with spectral presaturation inversion recovery (SPIR) fat suppression.

3: 3D TOF sequence (scan parameters; FOV: 300 x 300 mm, 2.0 mm slice thickness, TR / TE / FA: 26.20 ms / 3.3 ms/ 20º, acquired pixel size 0.46 x 0.46 x 2 mm^3, scan duration per slice = 0.4 minutes, acquired without ECG triggering), using linear shimming.

7T MRI acquisition

RF Coil

A 15-cm diameter local surface T/R surface coil was locally developed. The coil was segmented into six sections by series connected non-magnetic capacitors (American Technical Ceramics). The coil was positioned at the left side of the neck. A cushion was used to fix the position of the neck (Figure 1).

Survey Scans

Three FGE sequence survey scans were performed to facilitate planning of the carotid vessel wall protocol. A 2D TOF sequence was acquired with the following parameters, voxel size = 1 x 1.2 x 5 mm^3 and a FOV= 300 x300 mm^2, 20 transverse slices, TR/ TE/ FA= 7.7 ms / 3.7 ms / 20°, during free breathing and without using ECG triggering. The scan covered 10 cm of the left carotid artery in 38 seconds scan duration. The second survey was planned by defining three points in the center of the common, internal and external carotid arteries, which resulted in an oblique sagittal view of the carotid bifurcation. The third survey was planned in an oblique sagittal plane. The survey scans were acquired using a single slice ECG triggered FGE following parameters: voxel size = 0.46 x 0.47 x 2.5 mm^3, FOV = 140 x 140 mm^2, TR /TE / FA = 12 ms / 3.6 ms / 20°, resulting in an average scan duration of 56 seconds each.

Multi Contrast 7T protocol

Subsequently the multi-contrast 7T protocol, including three sequences were planned on the two surveys scans, perpendicular to the course of the common carotid artery in both views. To ensure registration between 7T and 3T scans, the 7T images, consisting of five contiguous transverse slices of 2-mm thickness, with identical in-plane resolution as 3T (0.46×0.46mm^2), were positioned with the top-slice at the level of the carotid bifurcation of the left carotid artery. Acquisition of slices continued in the proximal (caudal) direction covering 1.0 cm of the left common carotid artery.

A localized tip angle calibration was performed as a preparation step before the actual sequences to calibrate the tip angle in the target region (12), and linear shimming was performed in the same region. The scan parameters were:

1: 2D BB T1-weighted FGE sequence (scan parameters: FOV = 140 x 140 mm^2, TR / TE / FA = 13 ms / 3.7 ms / 45°, scan duration per slice = 1.25 minutes at a typical heart rate of 65 beats per minutes). Three saturation slabs (35 mm thickness), consisting of pairs of manufacturer provided adiabatic RF pulses, were used (two were placed inferior, and one superior and performed interleaved) to suppress flowing blood after which 8 excitations were performed, with linear profile encoding. The slices were measured sequentially and the saturation slabs followed each slice to obtain optimal blood suppression. Acquisitions were triggered to end diastole.

2: 2D BB T2-weighted fat suppressed TSE sequence (scan parameters: FOV = 140 x140 mm^2, TR / TE / FA = 2 heartbeats / 50 ms / 90°, TSE factor = 8, scan duration per slice = 1.2 minutes at a typical heart rate of 65 beats per minutes). Cardiac triggering was performed at end diastole. Fat suppression was performed using a spectrally selective adiabatic inversion pulse to improve the homogeneity of the suppression.

3: 3D TOF sequence (scan parameters: FOV = 140 x 140 mm^2, TR / TE / FA = 15 ms / 3.6 ms / 20°, scan duration per slice = 0.3 minutes, acquired without ECG triggering).

MR analysis

The cross-sectional images of the three sequences for the 3T and 7T scans were matched using the bifurcation of the carotid artery as a marker. The 3T and 7T analysis of morphologic measurements and measurements of image quality was performed on one slice of the left common carotid artery (4 mm proximal (caudal) to the carotid bifurcation) using Vessel MASS software (Leiden University Medical Center, Leiden, the Netherlands) (13).

Morphological measurements were performed by one observer for each individual sequence (T1- and T2 sequence for luminal area and vessel wall area; TOF sequence for luminal area) for 3T and 7T images (Figure 2). To test intra-observer reproducibility, each scan was analyzed twice by one experienced observer (Observer 1, two years of experience in cardiac MRI). To test inter-observer reproducibility, the scans were analyzed

by a second observer (Observer 2, one year experience of cardiac MRI) and data were compared with the first observer.

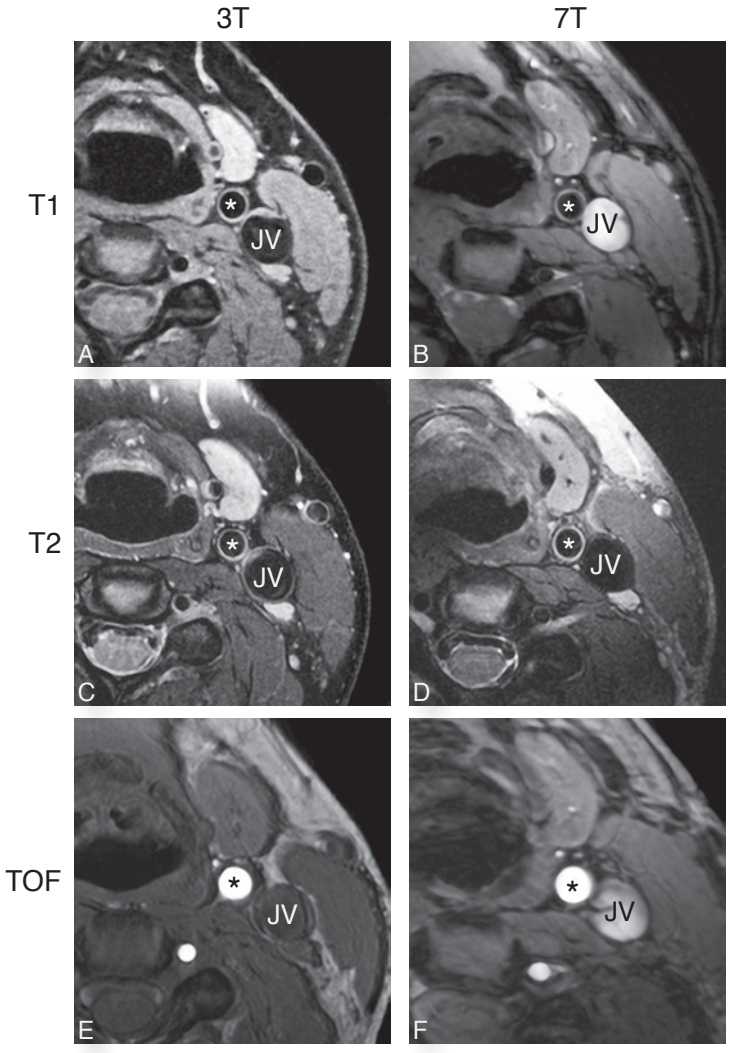

Figure 2. Example of multi-contrast black-blood images (T1- and T2-weighted) and time-of-flight image (TOF) of the left carotid artery obtained on 3T and 7T scanners with identical spatial resolution. A and B: T1-weighted, C and D: T2-weighted, E and F: TOF. Asterisks are provided on the transverse slices to indicate vessel lumen. 3T: 3-T magnetic field strength, 7T: 7-T magnetic field strength, JV: jugular vein, T1: T1-weighted images, T2: T2-weighted images.

Measurements of image quality (SNR vessel wall (SNR_{VW}) and CNR lumen/wall) were performed by one observer (Observer 1) for the T1- and T2 sequences. In addition, the SNR_{VW} and CNR were compared between 3T and 7T taking into account the non-gaussian distribution of the signal close to zero (4). SNR was calculated as SNR= S/σ (14). S is the true signal intensity corrected for the noise contribution and is obtained by the measured signal (S_m) and the measured background signal (S_n): $S = (S_m^2 - S_n^2)^{1/2}$. The true standard deviation of the noise (σ) depends on the number of receivers. For 7T, when a single single receiver is used the measured standard deviation needs to be divided by 0.655 (11) to obtain σ. Although at 3T two receiver coils were used, the elements are spaced sufficiently apart (left and right side of the neck) such that coupling between the two is negligible. An identical correction factor was therefore applied to the data acquired at 3T and 7T.

CNR was calculated as the difference between vessel wall and lumen SNR: CNR= SNR vessel - SNR lumen. Signal intensity from the background noise was sampled by a manually drawn region of interest in the corner of each image, devoid of signal and artifact. Mean signal intensity ± standard deviation of the vessel wall area and luminal area were provided by Vessel MASS software (Leiden University Medical Center, Leiden, the Netherlands).

Statistical analysis

The correlation between morphologic measurements obtained at 3T and 7T MRI was tested with intraclass correlation (ICC) for absolute agreement. ICCs close to 1.0 indicate good agreement between two measurements. The mean differences between repeated measurements against the mean value of repeated scans were described by Bland-Altman plots (15). For the morphological measurements, both intra-observer and inter-observer mean relative errors (MREs) were calculated. For this calculation, the absolute difference between two measurements was calculated per volunteer and divided by the first measurement, to yield the relative error. Consecutively, the MRE was then calculated.

SNR_{VW} and CNR values are expressed as median (interquartile range). Data from the different measurements were compared using the Wilcoxon signed ranks test for non-parametric paired observations. A p-value <0.05 was considered statistically significant.

All statistical analyses were performed using SPSS v. 18.0 (SPSS, Chicago, IL).

RESULTS

All 18 volunteers underwent successful MRI scanning at the 3T and 7T MR system.

Lumen and vessel wall

Figure 2 illustrates example carotid artery imaging of the left common carotid artery from a healthy volunteer at 3T and 7T.

The agreement between 3T and 7T images was calculated using the ICCs. An overview of the calculated ICCs and MRE (%) for the luminal area and vessel wall area is provided in Table 2. Morphologic carotid vessel wall measurements were comparable between 7T and 3T for both T1-weighted images (luminal area: ICC: 0.81, vessel wall area: ICC: 0.84), T2-weighted images (luminal area: ICC: 0.97, vessel wall area: ICC: 0.92) and TOF images (luminal area: ICC: 0.97).

Table 2. Results of comparison of morphological measurements at matched location between 3T and 7T

	3 T	7 T	3T vs 7T	
	Mean (sd) (mm^2)	**Mean (sd) (mm^2)**	**MRE (%)**	**ICC (CI)**
T1 luminal area	33.16 (6.5)	31.07 (5.88)	5.8	0.85 (0.65; 0.94)
T1 vessel wall area	17.83 (3.32)	17.17 (3.71)	3.8	0.85 (0.64; 0.94)
T2 luminal area	33.11 (10.15)	33.28 (8.98)	1.8	0.97 (0.91; 0.99)
T2 vessel wall area	16.36 (4.58)	16.62 (4.1)	2.8	0.91 (0.78; 0.97)
TOF luminal area	34.91 (8.39)	34.54 (9.42)	1.5	0.97 (0.91; 0.99)

3T: 3 Tesla magnetic field strength, 7T: 7 Tesla magnetic field strength, T1: T1-weighted images, T2: T2-weighted images, TOF: time-of-flight, MRE: mean relative error, ICC: intraclass correlation coefficient.

In differences, for lumen and vessel wall area between 3T and 7T measurements are presented (Bland Altman plots) in Figure 3 for both the T1- and T2-weighted images and TOF images. No dependence of the difference vs. the mean was observed.

Furthermore, both intra-observer and inter-observer reproducibility (including ICCs and MRE) for lumen- and vessel wall measurements for both the 3T and the 7T acquisitions was calculated (Table 3). No trend for differences was observed for the intra- and inter-observer reproducibility between the field strengths.

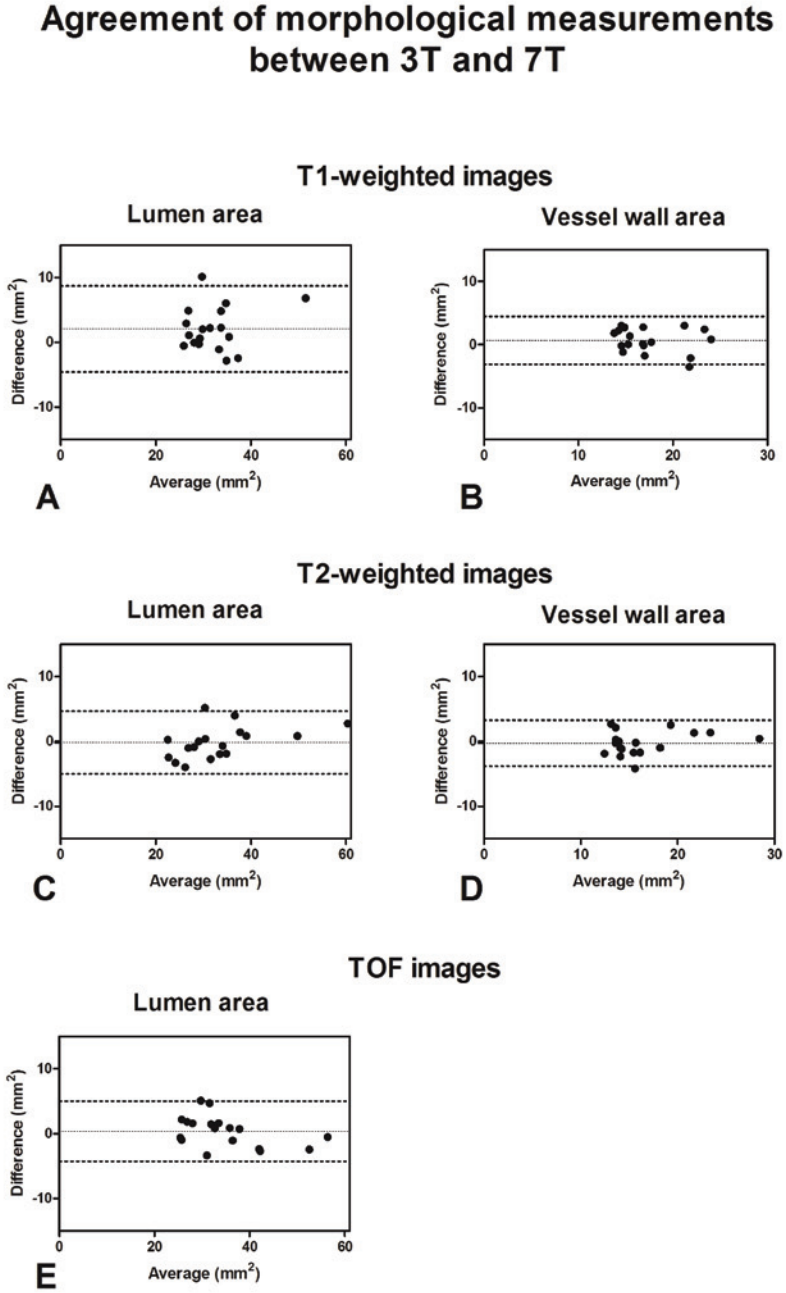

Figure 3. Agreement of morphological measurements between 3T and 7T. Bland-Altman plots for luminal area and vessel wall area, acquired at 3T and 7T, presented for T1-and T2-weighted images and TOF. A and B: T1-weighted, C and D :T2-weighted, E: TOF. 3T: 3 Tesla magnetic field strength, 7T: 7 Tesla magnetic field strength, T1: T1-weighted images, T2: T2-weighted images, TOF: time-of-flight.

Table 3. Intra-observer and Inter-observer Reproducibility of Morphologic Measurements

		Observer 1 Measurement 1	Observer 1 Measurement 2	Intra-observer		Observer 2	Inter-observer	
		Mean (sd) (mm^2)	Mean (sd) (mm^2)	MRE %	ICC	Mean (sd) (mm^2)	MRE %	ICC
3T	T1 luminal area	33.16 (6.5)	33.26 (6.8)	0.3	0.98 (0.95; 0.99)	33.76 (5.8)	2.6	0.89 (0.73; 0.96)
	T1 vessel wall area	17.83 (3.32)	16.68 (1.6)	6	0.76 (0.43; 0.91)	16.86 (2.85)	4.7	0.77 (0.47; 0.91)
	T2 luminal area	33.11(10.15)	33.27 (9.46)	1.1	0.99 (0.96; 0.99)	33.05 (8.11)	1.4	0.93 (0.83; 0.97)
	T2 vessel wall area	16.36 (4.58)	16.23 (4.37)	0.14	0.93 (0.82; 0.97)	15.75 (3.2)	1.4	0.76 (0.47; 0.90)
	TOF luminal area	34.91 (8.39)	34.22 (8.45)	1.8	0.96 (0.90; 0.99)	32.59 (8.65)	6.8	0.93 (0.55; 0.98)
7T	T1 luminal area	31.07 (5.88)	30.35 (5.7)	2.2	0.96 (0.89; 0.99)	30.47 (6.6)	2.1	0.92 (0.79; 0.97)
	T1 vessel wall area	17.17 (3.71)	17.4 (4.14)	1.5	0.90 (0.75; 0.96)	15.82 (3.09)	6.4	0.66 (0.28; 0.86)
	T2 luminal area	33.28 (8.98)	34 (9.7)	2.0	0.98 (0.96; 0.99)	34.37 (9.8)	3.3	0.95 (0.88; 0.98)
	T2 vessel wall area	16.62 (4.1)	16.4 (4.1)	1.1	0.96 (0.90; 0.99)	15.2 (3.33)	7.5	0.80 (0.42; 0.93)
	TOF luminal area	34.54 (9.42)	34.93 (9.88)	1.1	0.99 (0.96; 1.00)	32.19 (8.73)	6.4	0.92 (0.64; 0.98)

3T: 3 Tesla magnetic field strength, 7T: 7 Tesla magnetic field strength, T1: T1-weighted images, T2: T2-weighted images, TOF: time-of-flight, MRE: mean relative error, ICC: intraclass correlation coefficient.

SNR and CNR

Measurements of SNR_{VW} and CNR of the left carotid artery at 3T and 7T are presented in Figure 4. At 7T carotid vessel wall imaging provided a significant increase in SNR_{VW} and CNR for both the T1- ($p<0.001$) and T2-weighted images ($p<0.05$). The median gain factor for 7T T1-weighted images was 3.6 for SNR_{VW} and 2.8 for CNR. For T2-weighted images the median gain factor was 1.4 for SNR_{VW} and 1.3 for CNR. Examples (n=10) of T1-weighted images and T2-weighted images obtained at 7T are provided in Figure 5

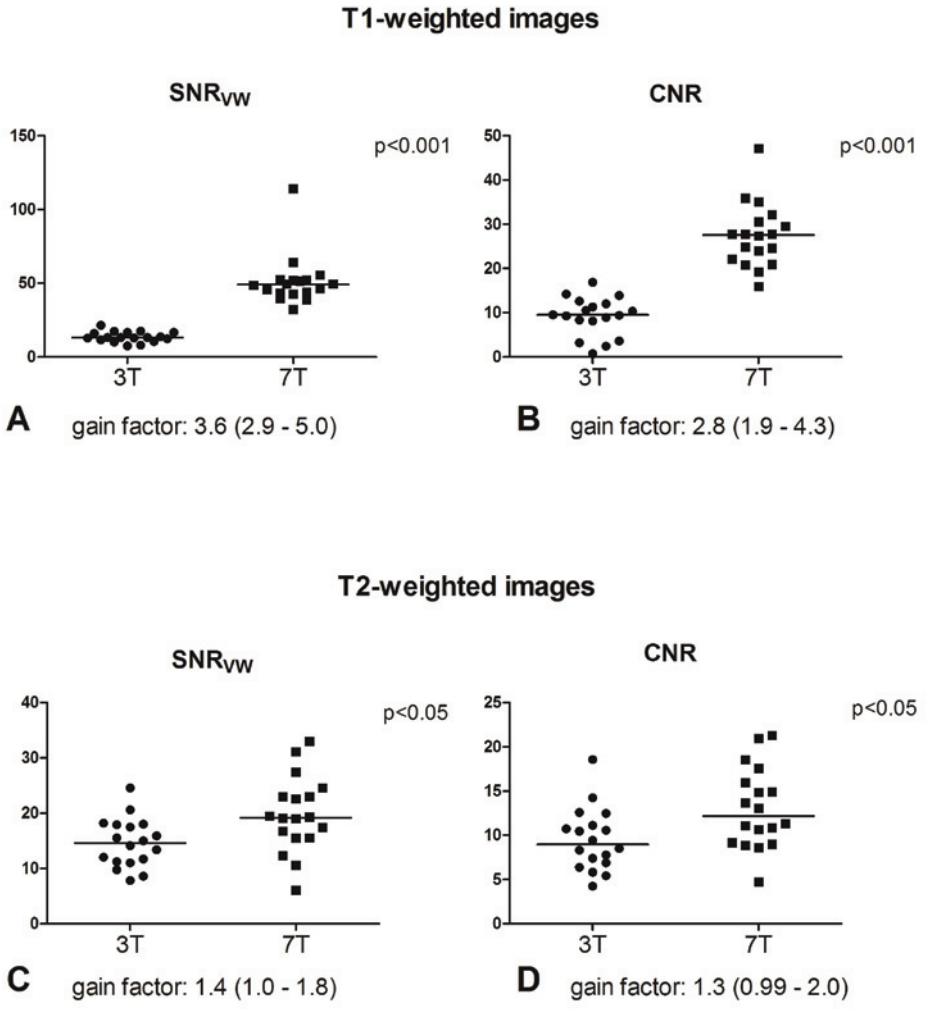

Figure 4. Comparison of image quality between 3T and 7T. Individual measurements of signal-to-noise ratio of the carotid vessel wall (SNR_{VW}) and contrast to noise ratio (CNR) for T1-weighted and T2-weighted images 3T and 7T are provided. A and B: T1-weighted, C and D: T2-weighted. Individual median gain factor (interquartile range) is provided. SNR_{VW} signal-to-noise-ratio for vessel wall, CNR: contrast-to-noise-ratio, 3T: 3 Tesla magnetic field strength, 7T: 7 Tesla magnetic field strength.

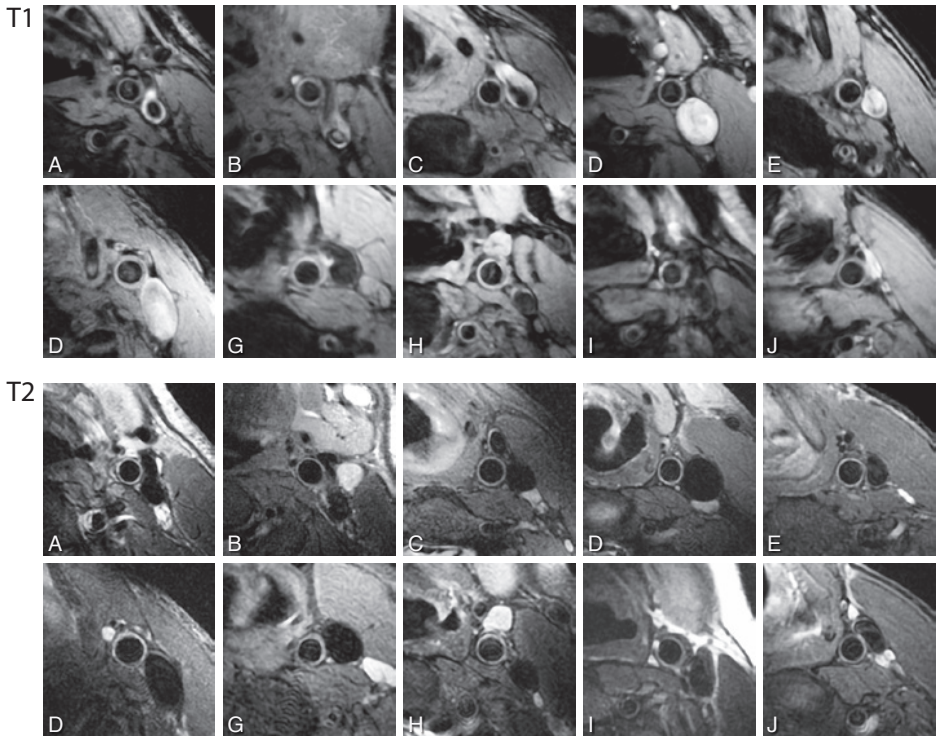

Figure 5. Examples of T1-weighted images and T2-weighted images obtained at 7T. A to J, ten examples of T1-weighted images and the corresponding T2-weighted images. T1, T1-weighted images; T2, T2-weighted images.

DISCUSSION

The present study, directly compares 3T and 7T carotid vessel wall imaging in healthy volunteers and demonstrates that in vivo carotid vessel wall imaging, with multi contrast protocol is technically feasible at ultrahigh field 7T MR equipped with a custom-built RF transmit and receive surface coil. Furthermore, this is the first study comparing morphological measurements and measurements of image quality in a quantitative setting. The main findings of the study are: i) 7T BB common carotid vessel wall imaging, at a predefined position in the common carotid artery relative to the flow divider, is feasible using local saturation slabs, ii) morphologic carotid vessel wall measurements (luminal area and vessel wall area) and intra- and inter-observer reproducibility are comparable between 3T and 7T, iii) ultrahigh field 7T MRI carotid vessel wall imaging improves SNR_{vw} and CNR compared to 3T.

Our study highlights the potential of 7T carotid MR imaging for assessment of carotid luminal area and vessel wall area, since accurate delineation of the carotid artery vessel

wall structure is crucial to detect carotid atherosclerosis and atherosclerotic changes of the vessel wall over time.

A recent study showed initial in vivo results of imaging of the carotid arteries at 7T in three volunteers (10). Estimation of luminal narrowing was performed with high-resolution magnetic resonance angiography images, with a non-contrast 3D FLASH sequence. In addition, proton density and T2-weighted TSE images were used for the analysis of the carotid vessel wall (10).

The feasibility of carotid vessel wall imaging at 7T is further confirmed by the present study in a larger population, and our data show that the feasibility of analysis of the vessel wall also extends to T1-weighted images obtained at 7T.

The present study also provided a comparison of the morphologic measurements at 3T versus 7T. In comparison with previous studies on vessel morphology, the agreement on interscan- and inter-observer reproducibility is in the same magnitude as that observed at 3T (11,16).

Carotid vessel wall MRI at 7T is of significant interest because it may provide higher SNR_{VW} and CNR (3). As a consequence spatial resolution can be improved (8). These advances hold potential for more detailed assessment of carotid atherosclerotic plaque morphology (17). The present study provides a direct quantitative comparison for SNR_{VW} and CNR at 3T and 7T. SNR_{VW} and CNR values at 3T were in the same magnitude as previously shown by Underhill et al, comparing carotid vessel wall imaging at 1.5T and 3T (18). At ultrahigh field strength (7T), improved SNR_{VW} and CNR were observed in our study, both for the T1-weighted gradient echo ($p<0.001$) and for the T2-weighted TSE images ($p<0.005$). T1-weighted images are the cornerstone for identification of carotid plaque composition and therefore, the significant gains in image quality with median gain factors of 3.6 and 2.8 for SNR_{VW} and CNR respectively, may increase applications to improved carotid vessel wall imaging at ultrahigh field strength (19,20).

The improved SNR_{VW} and CNR suggest that 7T MRI is a potential technique to assess carotid atherosclerosis in more detail. The vessel wall area is thought to be a surrogate marker for atherosclerotic disease and detailed assessment of carotid atherosclerosis and plaque morphology permits the assessment of disease burden (21-23) and identification of vulnerable patients who are at risk of future vascular events (22). A more detailed assessment of atherosclerosis may also permit an increased identification of changes in the carotid artery vessel wall structure over time and can be used to monitor progression of the disease or to monitor intervention (2).

The following limitations need to be acknowledged. Our study focused on the technical feasibility of 7T carotid vessel wall imaging of the common carotid artery in a population of healthy volunteers, without occlusive plaques or reduced flow. Whether carotid vessel wall imaging at 7T MR systems will lead to a better identification of atherosclerosis cannot be concluded from the present study and therefore further study is warranted. In addition, 7T imaging of the internal and external carotid artery distal to the carotid bifurcation was not performed. Therefore, the results of the present study (including the observed improvement in image quality at 7T) only relate to one slice of the common carotid artery. Further evaluation of the feasibility of carotid vessel wall imaging should involve more challenging populations, i.e. patients with extensive carotid plaques, a longer trajectory of the carotid artery, bilateral carotid artery imaging and the development of dedicated coils at 7T. Indeed, carotid imaging is expected to benefit (in terms of penetration depth and image quality) from using more sophisticated transmit array coils as is shown in other applications at high field as well (3,6,10). Kraff et al. showed that, when using a multi-element T/R coil at 7T it is possible to image both carotid arteries at the same time; however there are still image inhomogeneities present (10). In the current study, even though the coverage of the local T/R coil was limited, sufficient RF penetration was obtained for adequate visualization of one of the carotid arteries. The RF field was sufficiently homogeneous that, with the proper sequence and hardware modification, it was possible to achieve the most relevant image contrasts for carotid artery imaging (black blood T1-weighted and T2-weigthed images and TOF images). Furthermore, although the design of our 7T feasibility study involved a comparison of 3T and 7T acquisitions under identical conditions, in the future, the parameters of 7T imaging sequences need to be optimized for time efficiency.

In conclusion, this study shows our initial experience and feasibility of ultrahigh field 7T MR carotid vessel wall imaging. Morphologic carotid vessel wall measurements were comparable between 7T and 3T. The 7T MR of the common carotid artery showed improved SNR_{VW} and CNR compared with 3T MRI. Therefore, ultrahigh field 7T vessel wall MRI may permit a more detailed assessment of carotid atherosclerosis and plaque morphology.

REFERENCES

1. Lloyd-Jones D, Adams RJ, Brown TM, Carnethon M et al.: Heart disease and stroke statistics--2010 update: a report from the American Heart Association. *Circulation* 121:e46-e215, 2010
2. Corti R, Fuster V: Imaging of atherosclerosis: magnetic resonance imaging. *Eur Heart J* 32:1709-1719, 2011
3. Niendorf T, Sodickson DK, Krombach GA, Schulz-Menger J: Toward cardiovascular MRI at 7 T: clinical needs, technical solutions and research promises. *Eur Radiol* 20:2806-2816, 2010
4. Umutlu L, Kraff O, Orzada S, Fischer A et al.: Dynamic contrast-enhanced renal MRI at 7 Tesla: preliminary results. *Invest Radiol* 46:425-433, 2011
5. van Elderen SG, Versluis MJ, Webb AG, Westenberg JJ et al.: Initial results on in vivo human coronary MR angiography at 7 T. *Magn Reson Med* 62:1379-1384, 2009
6. Vaughan JT, Snyder CJ, DelaBarre LJ, Bolan PJ et al.: Whole-body imaging at 7T: preliminary results. *Magn Reson Med* 61:244-248, 2009
7. Korteweg MA, Veldhuis WB, Visser F, Luijten PR et al.: Feasibility of 7 Tesla breast magnetic resonance imaging determination of intrinsic sensitivity and high-resolution magnetic resonance imaging, diffusion-weighted imaging, and (1)H-magnetic resonance spectroscopy of breast cancer patients receiving neoadjuvant therapy. *Invest Radiol* 46:370-376, 2011
8. van Elderen SG, Versluis MJ, Westenberg JJ, Agarwal H et al.: Right coronary MR angiography at 7 T: a direct quantitative and qualitative comparison with 3 T in young healthy volunteers. *Radiology* 257:254-259, 2010
9. Vaughan JT, Garwood M, Collins CM, Liu W et al.: 7T vs. 4T: RF power, homogeneity, and signal-to-noise comparison in head images. *Magn Reson Med* 46:24-30, 2001
10. Kraff O, Bitz AK, Breyer T, Kruszona S et al.: A transmit/receive radiofrequency array for imaging the carotid arteries at 7 Tesla: coil design and first in vivo results. *Invest Radiol* 46:246-254, 2011
11. Alizadeh DR, Doornbos J, Tamsma JT, Stuber M et al.: Assessment of the carotid artery by MRI at 3T: a study on reproducibility. *J Magn Reson Imaging* 25:1035-1043, 2007
12. Versluis MJ, Kan HE, van Buchem MA, Webb AG: Improved signal to noise in proton spectroscopy of the human calf muscle at 7 T using localized B1 calibration. *Magn Reson Med* 63:207-211, 2010
13. Adame IM, van der Geest RJ, Wasserman BA, Mohamed MA et al.: Automatic segmentation and plaque characterization in atherosclerotic carotid artery MR images. *MAGMA* 16:227-234, 2004
14. Yarnykh VL, Terashima M, Hayes CE, Shimakawa A et al.: Multicontrast black-blood MRI of carotid arteries: comparison between 1.5 and 3 tesla magnetic field strengths. *J Magn Reson Imaging* 23:691-698, 2006
15. Bland JM, Altman DG: Statistical methods for assessing agreement between two methods of clinical measurement. *Lancet* 1:307-310, 1986
16. Li F, Yarnykh VL, Hatsukami TS, Chu B et al.: Scan-rescan reproducibility of carotid atherosclerotic plaque morphology and tissue composition measurements using multicontrast MRI at 3T. *J Magn Reson Imaging* 31:168-176, 2010
17. Cury RC, Houser SL, Furie KL, Stone JR et al.: Vulnerable plaque detection by 3.0 tesla magnetic resonance imaging. *Invest Radiol* 41:112-115, 2006
18. Underhill HR, Yarnykh VL, Hatsukami TS, Wang J et al.: Carotid plaque morphology and composition: initial comparison between 1.5- and 3.0-T magnetic field strengths. *Radiology* 248:550-560, 2008

19. Zhao X, Underhill HR, Yuan C, Oikawa M et al.: Minimization of MR contrast weightings for the comprehensive evaluation of carotid atherosclerotic disease. *Invest Radiol* 45:36-41, 2010
20. Kwee RM, van Engelshoven JM, Mess WH, Ter Berg JW et al.: Reproducibility of fibrous cap status assessment of carotid artery plaques by contrast-enhanced MRI. *Stroke* 40:3017-3021, 2009
21. Zhao XQ, Yuan C, Hatsukami TS, Frechette EH et al.: Effects of prolonged intensive lipid-lowering therapy on the characteristics of carotid atherosclerotic plaques in vivo by MRI: a case-control study. *Arterioscler Thromb Vasc Biol* 21:1623-1629, 2001
22. Corti R, Fuster V, Fayad ZA, Worthley SG et al.: Lipid lowering by simvastatin induces regression of human atherosclerotic lesions: two years' follow-up by high-resolution noninvasive magnetic resonance imaging. *Circulation* 106:2884-2887, 2002
23. Corti R, Fuster V, Fayad ZA, Worthley SG et al.: Effects of aggressive versus conventional lipid-lowering therapy by simvastatin on human atherosclerotic lesions: a prospective, randomized, double-blind trial with high-resolution magnetic resonance imaging. *J Am Coll Cardiol* 46:106-112, 2005

Chapter 12

7 Tesla cardiovascular MR imaging: initial clinical experience

Linda D. van Schinkel, Eleanore S.J. Kröner, Maurice B. Bizino, Jurgen E.M. Mourik, Maarten J. Versluis, Pieter J. van den Boogaard, Cosimo Bonetti, Eleonora I. Kastaneer, Johannes W.A. Smit, Albert de Roos, Andrew G. Webb, Hans-Marc J. Siebelink, Hildo J. Lamb

Submitted

ABSTRACT

Background

The purposes of this study were to test coronary stent safety at 7T cardiovascular magnetic resonance (CMR) by determining displacement and heating for cobalt alloy stents. Furthermore, to assess initial clinical feasibility of 7T CMR in healthy volunteers and patients with cardiovascular disease in the format of a multiple-case presentation.

Methods

Coronary stents (Cobalt Alloy) ranging from 5-85.8 mm in length were tested for safety by measuring magnetically induced displacement and radiofrequency induced heating according to standardized American Society for Testing and Material test methods. CMR was performed at 7T with various custom-built transmit/receive coils and imaging sequences for evaluation of coronary magnetic resonance angiography, vessel wall imaging, systolic and diastolic heart function and myocardial delayed enhancement.

Results

The 7T magnetic field did not induce a force greater than that of gravity on the stents and the maximum temperature rise was below 1°C. Preliminary results in the format of a multiple-case presentation demonstrated clinical feasibility of 7T CMR in healthy volunteers and patients with cardiovascular disease.

Conclusion

7T CMR is safe to perform in patients with cobalt alloy coronary stents (5-85.8 mm in length) and clinical CMR at 7T is feasible. Technical challenges have to be overcome before routine clinical application becomes possible.

INTRODUCTION

Cardiovascular magnetic resonance (CMR) is considered the gold standard modality for clinical assessment of cardiovascular anatomy, function and myocardial viability (1). CMR might benefit from a higher magnetic field strength, because the increased signal to noise ratio (SNR) allows higher spatial resolution imaging. This is especially important for coronary magnetic resonance angiography (MRA) and vessel wall imaging.

Promising CMR results have been reported in comparative studies using 3T versus 1.5T (2-5) and 7T versus 3T (6). However, the increased field strength produces a series of technical challenges for CMR (2,7). CMR requires robust compensation for heart motion, breathing motion and field inhomogeneity. Another challenge is acquisition of a reliable electrocardiogram (ECG) (8). Snyder et al. showed initial feasibility for CMR at 7T (9), with a subsequent study deriving quantitative assessment of functional parameters in healthy volunteers (10). To our knowledge, there is only limited data available on the feasibility of CMR in patients with cardiovascular disease at 7T. For example, despite recent progress in obtaining human coronary MR images (8) and carotid artery MR images (11) at 7T, specific work on vessel wall imaging at 7T is scarce.

Before clinical CMR at 7T can be performed, coronary stent safety has to be determined. The static magnetic field of the MR system exerts a force during patient positioning on ferromagnetic objects, possibly causing displacement of, for example, coronary artery stents. Furthermore, medical implants can potentially interact with the rapidly changing RF field, thereby inducing unwanted currents and heating of surrounding tissue.

Therefore, the first purpose of the present study was to test coronary stent safety at 7T MR by determining displacement and heating for cobalt alloy stents ranging in length from 5 to 85.8 mm in a worst case scenario. The second purpose was to assess initial clinical feasibility of 7T CMR in healthy volunteers and patients with cardiovascular disease in the format of a multiple-case presentation.

METHODS

All experiments and scans were performed on a 58 cm clear bore Philips 7 Tesla Achieva system (Philips Medical Systems, Best, The Netherlands).

Coronary artery stent safety

Coronary stents (Cobalt Alloy, Medtronic) ranging from 5 to 85.8 mm in length were used in this study. The longest stent (85.8 mm) consisted of four separate stents (1x30,

1x24 and 2x18 mm), which were combined with a small overlap between two adjacent stents. All stents were inflated to obtain an internal diameter of 3 mm.

The magnetically induced displacement force was assessed for each stent size using the deflection angle method, according to the procedure described by the American Society for Testing and Materials (ASTM) (12). The magnetically induced displacement was measured by the angular deflection using a protractor mounted on a stand with the zero degree mark at the 6 o'clock position. A stent was hung on the device by a 0.1 mm nylon thread. The angular deflection from the vertical was measured for all stent lengths with the protractor placed at the position where the magnetic field produces the greatest magnetically-induced deflection. During all these measurements the air circulation in the scanner bore was switched off.

Measurements of RF-induced heating were performed according to the ASTM Standard Test method for measurement of radiofrequency-induced heating on or near passive implants (13) with some necessary modifications. A tissue-mimicking phantom (149 mm x 59 mm x 47 mm) was formulated from 1.55 g/L sodium chloride (NaCl) and 31 g/L hydroxyethylcellulose (HEC) in sterile water. To obtain a gel free of air bubbles the phantom was ultrasonicated. The gel was positioned in the 7T scanner room for at least 24 hours prior to testing to obtain a transparent gel that was free of bubbles and temperature-stabilized. A stent was placed in the middle of the phantom, 2.5 cm from the bottom: this is comparable to the depth of a stent in a patient's body. Two fiber optic temperature probes (Opsens, Quebec, Canada) were used to measure the temperature during MRI-induced heating. The first temperature probe was positioned at the tip of the stent, the site of maximum heating (14), the second was used as a reference and was placed well away from the stent. The temperature was measured every 2.1 seconds and the measurements started 30 seconds before the MRI heating started and ended 30 seconds after the heating stopped.

Besides different lengths of stent, the effect of different relative positions of more than one stent was investigated. Two stents were used, one with a length of 42.4 mm and the other with a length of 19.5 mm. In the first situation, the two stents were placed in a straight line with each other. For the second situation, the two stents were placed at different angles relative to each other. In the last situation, one stent was placed on top of the other stent, forming a T-shape. Temperature measurements were performed in the gap between the two stents. The same custom-built quadrature cardiac coil as used for the clinical imaging experiments (see later) was used for the heating experiments. The phantom was placed with the stent directly below the overlap point of the two loops, which is the position of maximum electric field and therefore maximum heating. The phantom was tested with the stent both parallel and perpendicular to the main

axis of the coil. A multi-slice gradient echo sequence (similar to a cardiac cine-scan) was used. By over-riding in software the manufacturer's signal absorption rate (SAR) limits, a time-averaged SAR of 5W/kg was produced, well above the regulatory limit of 2 W/kg.

Clinical imaging protocols

All studies were conducted according to the principles of the Declaration of Helsinki (current version adopted by the 59th WMA General Assembly, Seoul, October 2008), in accordance with the Medical Research Involving Human Subjects Act (WMO) and according to local guidelines, as specified by the local medical ethical committee.

The MR system was equipped with a vector ECG module. Electrodes were placed at the anterior chest wall: Two electrodes (lead 1 [L1] and L2) at the level of the sternum, one electrode (L3) vertical to L1 and L2, just below the sternum, one electrode (L4) horizontal to L2, on the left thorax along the mid-axillary line (8). ECG triggering was effective in about 80% of patients. All subjects were placed in the bore head first and in a supine position.

Coronary artery MRA

Bright blood coronary MRA of the right coronary artery was performed in a twenty-three year old female healthy volunteer. A custom-built quadrature two element surface transceiver (T/R) coil with two overlapping loops of 18 cm diameter was used. Scout images in coronal, transverse and sagittal orientations were used to plan ECG triggered, breath-hold transverse cine scout imaging for both determination of the period of minimal coronary motion and the volume targeting of the 3D stack in parallel with the mid-diastolic right coronary artery (RCA). The RCA was imaged by using a navigator-gated, vector ECG triggered 3D segmented k-space gradient-echo combined with a spectrally selective adiabatic inversion recovery pulse for fat suppression. The in plane field-of-view (FOV) was 420 x 270 mm^2 with a coverage of 30 mm, TR was 4.06 ms, TE 1.32 ms, FA 15^o and voxel size 0.82 x 0.82 x 2.0 mm.

Vessel wall imaging left carotid artery

As described previously a flexible 15-cm diameter local surface T/R surface coil was constructed for vessel wall imaging (11). The coil was segmented into six sections by series connected non-magnetic capacitors (American Technical Ceramics) and was positioned at the left side of the neck. A cushion was used to fix the position of the neck.

After acquisition of a three-dimensional (3D) time-of-flight (TOF) sequence to localize the vessel bifurcation, sagittal and coronal 2D scout scans of the left carotid artery were acquired. The multi-contrast carotid vessel wall protocol was planned on these images and consisted of a T1 segmented fast gradient echo (FGE) sequence, a T2 turbo

spin echo (TSE) sequence and a 3D TOF sequence. At 7T BB preparation is performed using local saturation slabs that saturate the inflowing venous and arterial blood. For the T_2-weighted TSE protocols no BB prepulse was used.

Cardiac function

Scout images in coronal, transverse and sagittal orientations are used to plan ECG triggered, breath-hold transverse cine scout imaging, performed using TE 1.7 ms, TR 4 ms, FA 15°, and reconstructed pixel size 0.88x0.88 mm. To determine systolic left ventricular (LV) volumes, function and mass, the LV was imaged in a short-axis orientation, as previously described (15). Endocardial and epicardial LV contours were manually drawn in the end-systolic and end-diastolic phases of the short-axis data, using software package MASS® (Medis, Leiden, the Netherlands). LV and right ventricular (RV) ejection fraction (EF), stroke volume (SV), LV and RV end-diastolic volume (LVEDV/RVEDV), LV/RV end-systolic volume (LVESV/RVESV) and LV/RV end-diastolic mass (LVED/RVED mass) were assessed. Transmitral flow was measured for assessment of LV diastolic function, using a velocity sensitivity of 150 cm/s, TE 2.6 ms, TR 4.6 ms, FA 20°, reconstructed pixel size 1.5x1.5 mm. Flow velocities in early diastole (E) and at atrial contraction (A) were measured and their peak flow ratio was calculated (E/A ratio) using the FLOW® software (Medis, Leiden, the Netherlands) (16,17)

Delayed enhancement

Delayed enhancement acquisitions were performed approximately 15 minutes after intravenous administration of 0.1 mmol/kg Gadolinium using an inversion-recovery turbo-gradient echo sequence, TE 1.06 ms, TR 3.7 ms, FA 15°, reconstructed pixel size 1.5x1.5 mm. The inversion time was determined with a Look-Locker scan to null the normal myocardial signal.

RESULTS

Coronary artery stent safety

The deflection angle of stents in the length range from 5.0 mm to 85.8 mm varied between 10° and 17°. The average deflection angle was 13° (Figure 1). The results of the RF induced heating are shown in Figure 2. For a stent length between 5.0 and 31.2 mm and between 58.7 and 85.8 mm the change in temperature, and thus the heating, was very low (max 0.1°C). However, for stent lengths between 35.2 and 51.7 mm the heating was higher (max 1.0°C). Overall, an average temperature rise of 0.09 ± 0.28°C (parallel position) and 0.00 ± 0.06°C (perpendicular position) was found. No large temperature change was found for the different relative positions of two stents. The highest temperature change (0.2°C in 6 min) was found for two stents that were placed in a straight line with a small gap in-between.

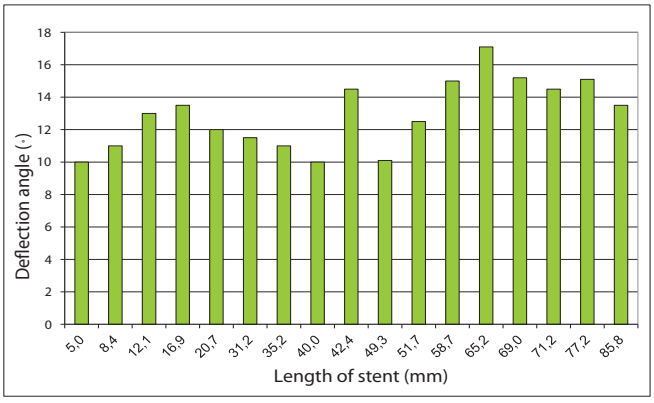

Figure 1. Deflection angle of cobalt allow coronary artery stents, measured for length range from 5.0 mm to 85.8 mm.

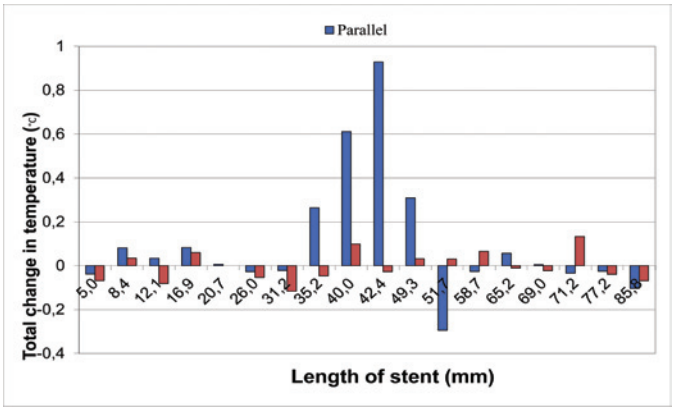

Figure 2. Total change in temperature for different lengths of stents. Blue bars represent total change in temperature at the tip of the stent in parallel orientation with respect to the magnetic field. Purple bars represent total change in temperature at the tip of the stent when placed perpendicular to the magnetic field.

Cardiovascular MRI – healthy volunteers

(i) Coronary artery MRA

Figure 3 shows a section imaged with a bright blood coronary MRA sequence. Good fat suppression and high vessel sharpness enable a clear delineation of the RCA. Furthermore, anatomic details of the coronary, such as the conus and side branches, are clearly visible
.

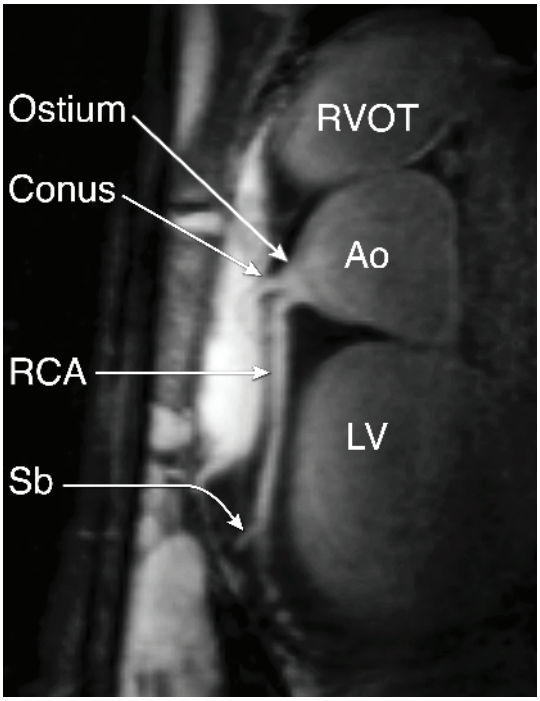

Figure 3. MRA of the right coronary artery (RCA) in a twenty-three-year old healthy female volunteer obtained with a bright blood coronary MRA sequence. Several structures can be identified in this image: the ostium, conus and a portion of the RCA. Notice the good fat suppression and high vessel sharpness. RVOT = right ventricular outflow tract, Ao = aortic root, LV = left ventricle, Sb = Side branch.

(ii) Vessel wall imaging of the carotid artery

In Figure 4 the left carotid artery of a 32 year old healthy male is depicted. The top row represents T1-weighted images and the bottom row T2-weighted images.

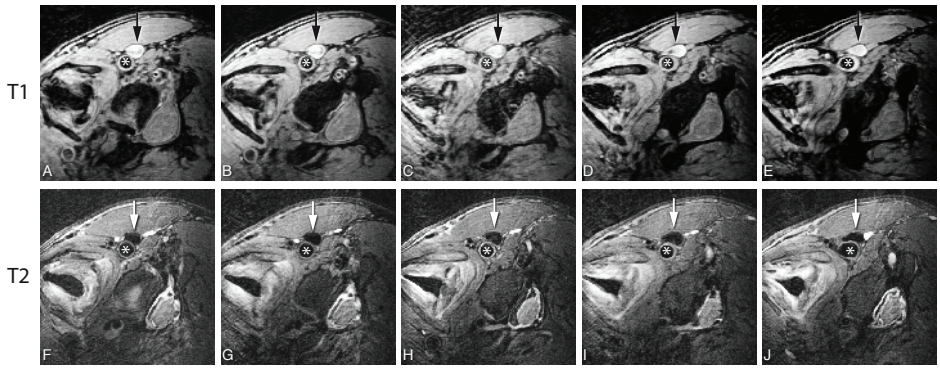

Figure 4. Left carotid artery of a thirty-two year old healthy male. The * is centered in the left carotid artery, the arrow points to the jugular vein. Top row represents T1-weighted images, bottom row T2-weighted images.

(iii) Systolic function

Figure 5 shows cardiac cine images of a healthy twenty-nine year old female. Left ventricular, two-chamber, four-chamber and short axis images are shown in end-diastolic and end-systolic phase. RF penetration depth is sufficient to assess left and right ventricular heart function.

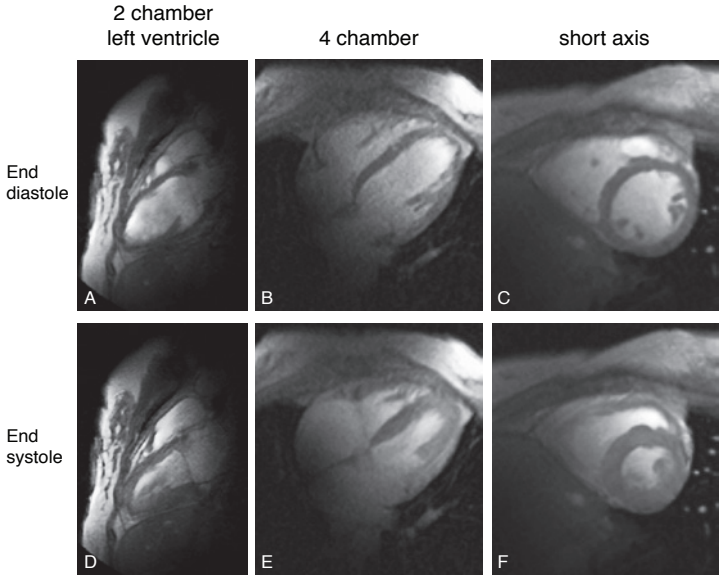

Figure 5. Cine imaging of a twenty-nine year old healthy volunteer. The upper panels are acquired in end-diastole, the lower panels in end-systole. Images A and B depict 2-chamber views, B and E depict 4-chamber views and images C and F represent the short axis view. RF penetration depth is sufficient to assess left ventricular and right ventricular heart function.

Figure 6 shows more recent results acquired in a healthy twenty-five year old female volunteer using a transmit array of eight segmented dipoles (18). Eight custom-built transmit/receive switches were interfaced with the dual transmit system via four Wilkinson lumped element 1:2 splitters. Note the improved homogeneity of RF penetration and increased coverage of the heart in comparison to Figure 5. Improved coverage is also reflected by visualization of anatomic structures outside the heart, such as the spine.

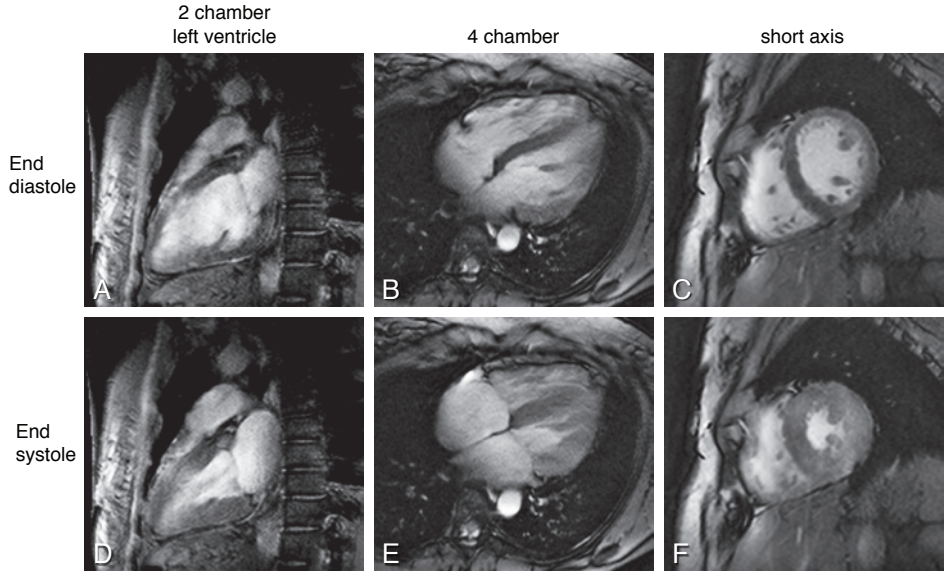

Figure 6. Recent results from our group in a twenty-five year old healthy female volunteer using a transmit array of eight segmented dipoles. The upper panels are scanned in end-diastole, the lower panels in end-systole. Images A and D are 2-chamber views, B and E depict 4-chamber views and images C and F represent the short axis view.

Cardiovascular MRI – clinical cases

(i) Global systolic dysfunction.

In Figures 7 (A) and (B) global systolic dysfunction in a 65 year old male is shown. This patient was admitted to the coronary care unit with chest pain and had no previous medical history. His ECG showed complete left bundle branch block, and cardiac enzymes were negative. In order to rule out coronary artery disease, coronary catheterization was performed and no significant coronary artery disease was found. Echocardiography showed a dilated left ventricle with severely diminished left ventricular function, with a left ventricular ejection fraction (LVEF) of 23% and no significant valvular disease. The patient had no clinical signs of infection and detailed history taking revealed no

infectious episode in the recent past. Therefore, recent and acute myocarditis was not suspected. MRI was performed to assess cardiac function and the etiology of the cardiomyopathy. Cardiac MRI showed a substantially dilated, globally hypokinetic left ventricle with an LVEF of 22%, in concordance with the echocardiographic findings. Panels A and B of Figure 7 distinctly show the reduced myocardial contractility. There were no signs of focal wall motion impairments. The most probable diagnosis was idiopathic dilated cardiomyopathy.

(ii) Systolic dysfunction after right coronary artery infarction

Figures 7 (C) and (D) show the short axis view at end diastole and end systole in a 52 year old man with a history of an occluded RCA with collateral filling via the left coronary artery. The patient was seen at the outpatient clinic for a second opinion concerning treatment of coronary artery disease. He complained of atypical chest pain despite appropriate cardiac medication. The echocardiographic window of this patient was very poor and therefore 7T MRI was performed to assess cardiac function. MRI showed basal, midventricular and apical hypokinesia of the inferior wall. The LV was not dilated and function was quantified as follows: end-diastolic volume (EDV) 176ml, end-systolic volume (ESV) 87ml, stroke volume (SV) 88ml and LVEF 50%. For further evaluation stress myocardial perfusion scintigraphy was performed, showing extensive ischemia in the inferior-, septal- and anterior myocardium. Coronary catheterization was performed and revealed significant coronary artery disease in all 3 coronary arteries for which the patient was treated with coronary artery bypass grafting.

(iii) Systolic dysfunction after left anterior descending artery infarction

Figures 7 (E) and (F) show regional systolic dysfunction in a patient after partial occlusion of the left anterior descending (LAD) coronary. The patient is a 60 year old male who was admitted with acute anterior myocardial infarction and no previous medical history. Two hours before admission he experienced chest pain with radiation of pain to his left arm. He was transported to the hospital for an emergency percutaneous coronary intervention (PCI). His coronary angiogram showed an occluded ramus descendens anterior (RDA) after the 2nd diagonal branch. He received balloon angioplasty of the occlusion and a drug eluting stent (Promus 3.5 x 20 mm) was placed in the RDA en coronary blood flow was restored. His circumflex- and right coronary artery showed luminal narrowing of 30-40%, for which no intervention was required. Patient was admitted to the coronary care unit, was put on medication and recovered quickly. He was discharged after 2 days and MRI was performed after 6 days to assess LV function and infarct burden. MRI showed a global moderate systolic function, with profound midventricular hypokinesia/akinesia, mainly in the anteroseptal- and anterior wall, expanding to the apex. The apical

segment showed dyskinesia compatible with aneurysm development. LV volumes were EDV 165ml, ESV 104ml, SV 61ml and LVEF was 37%.

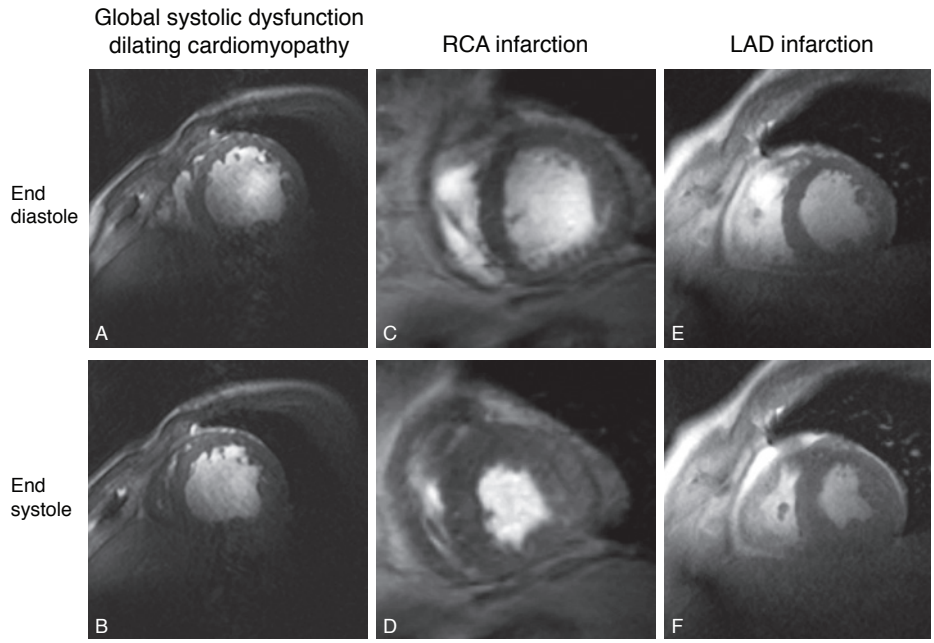

Figure 7. Three different kinds of systolic dysfunction. All images are in short axis orientation. Panel a and b reflect global systolic dysfunction, respectively, at end diastole and at end systole. Note impaired ventricular contraction comparing A and B, representing low ejection fraction. C and D reflect systolic dysfunction after RCA infarction, showing regional akinesia in inferior wall. Panels E and F show focal systolic dysfunction in the anteroseptal myocardial region, compatible with a significant coronary artery stenosis in the LAD.

(iv) Transmitral flow in diastolic dysfunction

Figure 8 depicts normal and abnormal diastolic heart function, assessed at 7T MRI. The flow curve across the mitral valve is shown. The upper panel illustrates normal diastolic function in a 33 year old healthy male. The lower panel demonstrates impaired diastolic function of a 62 year old male. This patient had diabetes mellitus and was seen at the cardiology outpatient clinic for evaluation of stable angina pectoris due to an occluded right coronary artery with collateral filling by the left coronary artery. An MRI was performed to assess cardiac function. MRI showed a non dilated left ventricle with basal- and midventricular mild septal hypertrophy. Mild hypokinesia was seen basal inferior. The E/A ratio was <1 and no regurgitation of the valves was observed.

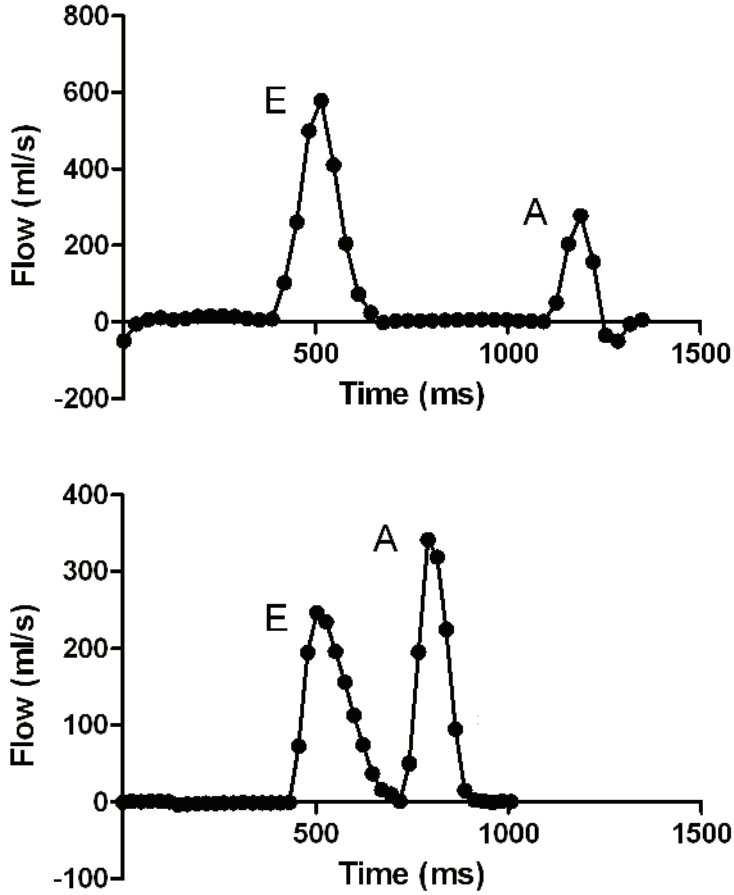

Figure 8. Diastolic function. Upper panel: an example of a normal flow (E>A) pattern across the mitral valve. Lower panel: diastolic dysfunction (E<A) in a patient with diabetes mellitus and coronary artery disease.

(v) Delayed enhancement

The same 60 year old male (Figures 7 E and F), with systolic dysfunction after LAD infarction, also had signs of transmural delayed enhancement (Figure 9). Delayed enhancement was located at the sites of wall motion abnormalities, in accordance with scar tissue related to the myocardial infarction. Note that the posterior wall is too dark to reliably assess delayed enhancement in that part of the myocardium, possibly related to inhomogeneous distribution of 180 degree inversion flip angles. This is clearly a case in which the improved image quality afforded by transmit arrays, as shown in Figure 6, will be critical in the future.

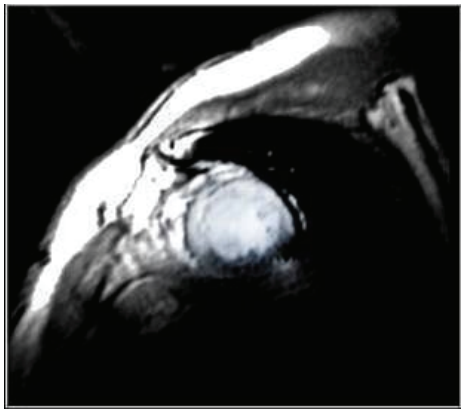

Figure 9. Transmural delayed enhancement in the anteroseptal myocardial wall. As can be appreciated from this figure, image quality is still insufficient to adequately assess scar tissue.

(vi) Prominent trabecularization.

The final case is a 33 year old man who was seen at the outpatient clinic for evaluation of palpitations. He experienced short episodes of fast palpitations of sudden onset without syncope. Echocardiography was performed and showed suspicion of non-compaction cardiomyopathy. An MRI was performed to assess cardiac anatomy and function. The MRI showed prominent trabecularization in the apical inferolateral wall, with normal myocardial wall thickness (Figure 10). No criteria for left ventricular non-compaction cardiomyopathy were met. LV function was normal, with an LVEF of 57%. Patient is currently in a good condition and the palpitations were later attributed to AV nodal re-entry tachycardia.

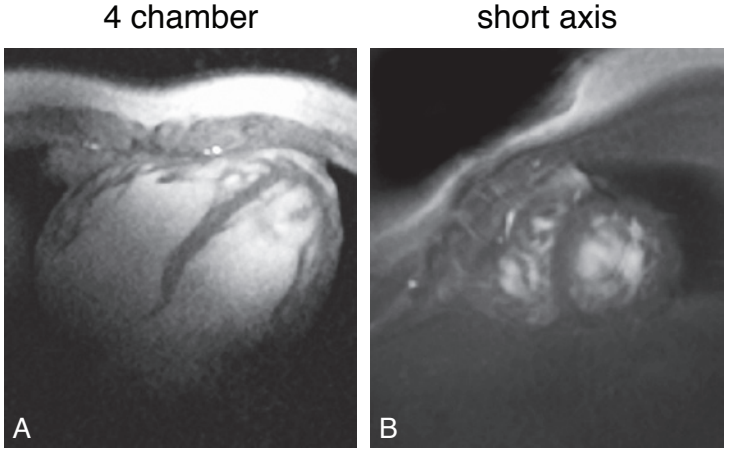

Figure 10. Prominent trabecularization in a 33 year old male. Panel A shows a 4 chamber view, panel B a short axis view at end diastole. The trabeculae are mainly seen in the apical area.

DISCUSSION

Coronary artery stent safety

According to the ASTM test method a deflection angle of less than 45 degrees is considered safe. The force exerted by the magnet is then equal or less than that of gravity. For all tested stent lengths the deflection angle was lower than 45 degrees (max. 13 degrees) and therefore it may be concluded that the 7T MR system did not exert an extra force on the stents. In general, the RF induced heating was higher for the parallel position (0.09 ± 0.28) compared to the perpendicular position (0.00 ± 0.06). This can be explained by the shape of the electric field, which couples more tightly to the test device in this orientation. The highest temperature change was found for a stent length of 42.4 mm (0.93°C in 6 min). Almost no heating was induced in stents longer or shorter than 42.4 mm, indicating that for this particular stent type the critical length lies around the 42.4 mm.

Patients may have multiple stents, depending on the passage or the weak places of the blood vessels. This leads to stents inserted close to each other or placed in a certain relative position. These stents can interact with each other and together they can undergo an interaction with the RF-field of the MR system. To simulate this, several relative positions were tested. Almost no heating was seen. The highest heating (0.20°C in 6 min) was seen for two stents placed in a straight line with a small gap in-between. The heating was probably induced by the largest stent (42.4 mm) because that was found to be the critical length.

A rise of 1°C is generally acceptable in a normal healthy body. The highest increase in temperature for stents was 0.93°C. This temperature rise was only found for one stent length (42.4 mm). For the other stent lengths the maximal temperature rise was far below 1°C (max: 0.35°C).

These results agree well with those of a recent study which also suggested that, if guidelines for local/global SAR are followed, extra RF heating induced by stents may be insignificant (19). In that study two non ferromagnetic coronary stent configurations with lengths of 40 mm and 27 mm were used to assess the safety of scanning of coronary stents at 7T MR. In this study we assessed more stent lengths, ranging from 5 to 85.8 mm. Our results therefore add to the existing data on safety of coronary stent scanning at 7T.

Healthy volunteers and clinical cases

Several previous studies showed that ultrahigh field 7T CMR is feasible (9,10,20), despite many technical challenges. Ultrahigh field CMR is very promising (7,21), since the higher SNR inherent to higher magnetic field strengths is advantageous for cine CMR. Additionally, the potential of enhanced spatial resolution may lead to advantages for CMR (7).

MRA has several advantages over coronary computed tomography (CTA) and coronary angiography (CAG): it is non-invasive, non-irradiating and the use of a contrast agent is not required. At 1.5T, a number of studies on the diagnostic accuracy of MRA have proven that proximal coronary artery disease (CAD) can be reliably identified or ruled out (22,23). Higher SNR has been reported in MRA of the RCA at 7T when compared to 3 T (6). The increased SNR can potentially be used to increase spatial resolution with the potential of more accurate detection of significant coronary artery stenosis.

Besides imaging of coronary arteries, we recently showed that ultrahigh field 7T MR imaging also offers potential for imaging of the carotid vessel wall (11). We demonstrated an improved vessel wall SNR and CNR as compared to 3T MR images for both the T1- and T2-weighted images. In the future, this may potentially allow a more detailed assessment of carotid atherosclerosis or plaque morphology in patients.

Previous studies showed that assessment of LV volumes, function and mass at 7T agree well with 1.5T, which is the accepted reference standard in CMR (10,24). A recent study by Suttie et al (25) reported that steady state free precession (SSFP) and fast low angle shot (FLASH) cine imaging at 7T is technically feasible and provides valid assessment of LV volumes and mass compared with CMR imaging at lower, i.e. 1.5T and 3T, field strengths (25).

Another challenge in the field of CMR is imaging of the right ventricle (RV). The non-invasive imaging of function, size and anatomy of the RV is difficult, due to several factors, such as the asymmetric and variable shape of the RV, the mainly longitudinal systolic contraction, thin myocardial wall and location behind the sternum (26). As for LV volumes, function and mass, 1.5T is the golden standard for assessment of the RV. However, the accuracy of quantifying for example RV mass and characterization of myocardial tissue remains uncertain. It is important to improve imaging techniques, since anatomy and function of the RV are known to be predictors of morbidity and mortality in a variety of cardiac diseases, such as arrythmogenic RV cardiomyopathy (27). The potential improvements in SNR and thereby spatial resolution at 7T MR could add to better imaging quality of RV morphology and function. Recently, the first study on RV imaging at 7T was published, showing that cine imaging of the RV is feasible at ultrahigh field MRI and achieves image quality comparable to the quality at 1.5T (26). There is little literature on assessment of LV diastolic function at ultrahigh field MRI. To our knowledge, only one previous study investigated LV diastolic filling on 7T (10). Trans-mitral flow was assessed with velocity-encoded (VE) MRI, and a strong agreement between trans-mitral stroke volume and E/A ratio at 1.5T and 7T was found. The early and atrial peak filling rates displayed a greater, though not significant, variation at 7T versus 1.5T. These results show that trans-mitral flow assessment with VE MRI is feasible at 7T.

In previous publications it has been shown that functional cardiac scans, coronary magnetic resonance angiography, and vessel wall imaging are all feasible in humans at 7T. In this paper we show that functional and anatomic imaging, even using a simple RF coil setup, are useful within a clinical setting, while also highlighting some of the current inadequacies, mainly associated with limited RF penetration. Many other groups have shown that the use of multi-element transmit arrays can mitigate many of these penetration effects. In parallel, Figure 4 shows improved coverage using a transmit array of eight segmented dipoles (18). Extensive B1 shimming was not performed, with equal phases applied to each segmented dipole, and so image quality may well be improved by optimizing the individual phases. Currently, these types of array require full characterization in terms of safety, SAR monitoring, before they can be used in "routine" clinical practice. The clear improvement in image quality over a single transmit system, combined with our demonstration of clinical potential even with the single transmit system, point to rapid advancements for clinical application.

In conclusion, 7T cardiovascular MRI is safe to perform in patients with cobalt alloy coronary stents ranging from 5 to 85.8 mm. Clinical cardiovascular MRI at 7T is feasible. Technical challenges have to be overcome before routine clinical application becomes possible. Clinical practice has to prove the benefit of ultrahigh field MRI as compared to lower field MRI at 1.5T and 3T.

REFERENCES

1. Pennell DJ, Sechtem UP, Higgins CB, Manning WJ et al.: Clinical indications for cardiovascular magnetic resonance (CMR): Consensus Panel report. *J Cardiovasc Magn Reson* 6:727-765, 2004
2. Gutberlet M, Schwinge K, Freyhardt P, Spors B et al.: Influence of high magnetic field strengths and parallel acquisition strategies on image quality in cardiac 2D CINE magnetic resonance imaging: comparison of 1.5 T vs. 3.0 T. *Eur Radiol* 15:1586-1597, 2005
3. Noeske R, Seifert F, Rhein KH, Rinneberg H: Human cardiac imaging at 3 T using phased array coils. *Magn Reson Med* 44:978-982, 2000
4. Sommer T, Hackenbroch M, Hofer U, Schmiedel A et al.: Coronary MR angiography at 3.0 T versus that at 1.5 T: initial results in patients suspected of having coronary artery disease. *Radiology* 234:718-725, 2005
5. Yarnykh VL, Terashima M, Hayes CE, Shimakawa A et al.: Multicontrast black-blood MRI of carotid arteries: comparison between 1.5 and 3 tesla magnetic field strengths. *J Magn Reson Imaging* 23:691-698, 2006
6. van Elderen SG, Versluis MJ, Westenberg JJ, Agarwal H et al.: Right coronary MR angiography at 7 T: a direct quantitative and qualitative comparison with 3 T in young healthy volunteers. *Radiology* 257:254-259, 2010
7. Niendorf T, Graessl A, Thalhammer C, Dieringer MA et al.: Progress and promises of human cardiac magnetic resonance at ultrahigh fields: A physics perspective. *J Magn Reson* 229:208-222, 2013
8. van Elderen SG, Versluis MJ, Webb AG, Westenberg JJ et al.: Initial results on in vivo human coronary MR angiography at 7 T. *Magn Reson Med* 62:1379-1384, 2009
9. Snyder CJ, DelaBarre L, Metzger GJ, van de Moortele PF et al.: Initial results of cardiac imaging at 7 Tesla. *Magn Reson Med* 61:517-524, 2009
10. Brandts A, Westenberg JJ, Versluis MJ, Kroft LJ et al.: Quantitative assessment of left ventricular function in humans at 7 T. *Magn Reson Med* 64:1471-1477, 2010
11. Kroner ES, van Schinkel LD, Versluis MJ, Brouwer NJ et al.: Ultrahigh-field 7-T magnetic resonance carotid vessel wall imaging: initial experience in comparison with 3-T field strength. *Invest Radiol* 47:697-704, 2012
12. American Society for Testing and Materials (ASTM.Designation: F 2052-02): Standard test method for measurement of magnetically induced displace- ment force on passive implants in the magnetic resonance environment. In *Annual Book of ASTM Standards: Section 13-Medical Devices and Services*. West Conshohocken, Pennsylvania, 2013, p. 1576-1580
13. American Society for Testing and Materials International (ASTM.DesignationF2182-02a): Standard test method for measurement of radio frequency in- duced heating near passive implants during magnetic resonance imaging. In *American Society for Testing and Materials International (ASTM. Designation: F 2182-02a)*. 2006,
14. Yeung CJ, Susil RC, Atalar E: RF heating due to conductive wires during MRI depends on the phase distribution of the transmit field. *Magn Reson Med* 48:1096-1098, 2002
15. Lamb HJ, Doornbos J, van der Velde EA, Kruit MC et al.: Echo planar MRI of the heart on a standard system: validation of measurements of left ventricular function and mass. *J Comput Assist Tomogr* 20:942-949, 1996
16. Paelinck BP, de Roos A, Bax JJ, Bosmans JM et al.: Feasibility of tissue magnetic resonance imaging: a pilot study in comparison with tissue Doppler imaging and invasive measurement. *J Am Coll Cardiol* 45:1109-1116, 2005

17. Pattynama PM, Lamb HJ, van der Velde EA, van der Wall EE et al.: Left ventricular measurements with cine and spin-echo MR imaging: a study of reproducibility with variance component analysis. *Radiology* 187:261-268, 1993
18. A.J.E.Raaijmakers and Voogt, D. W. J. Klomp P. R. Luijten C. A. T. van den Berg. Dipole antenna without ceramic substrate and still low SAR: the fractionated dipole antenna. 2013. Int. Soc.Magn. Reson.Med. Salt Lake City, Utah, 2013. 4382.
19. Santoro D, Winter L, Muller A, Vogt J et al.: Detailing radio frequency heating induced by coronary stents: a 7.0 Tesla magnetic resonance study. P*LoS One* 7:e49963, 2012
20. Vaughan JT, Snyder CJ, DelaBarre LJ, Bolan PJ et al.: Whole-body imaging at 7T: preliminary results. *Magn Reson Med* 61:244-248, 2009
21. Niendorf T, Sodickson DK, Krombach GA, Schulz-Menger J: Toward cardiovascular MRI at 7 T: clinical needs, technical solutions and research promises. *Eur Radiol* 20:2806-2816, 2010
22. Kato S, Kitagawa K, Ishida N, Ishida M et al.: Assessment of coronary artery disease using magnetic resonance coronary angiography: a national multicenter trial. *J Am Coll Cardiol* 56:983-991, 2010
23. Kim WY, Danias PG, Stuber M, Flamm SD et al.: Coronary magnetic resonance angiography for the detection of coronary stenoses. *N Engl J Med* 345:1863-1869, 2001
24. von Knobelsdorff-Brenkenhoff F, Frauenrath T, Prothmann M, Dieringer MA et al.: Cardiac chamber quantification using magnetic resonance imaging at 7 Tesla--a pilot study. *Eur Radiol* 20:2844-2852, 2010
25. Suttie JJ, DelaBarre L, Pitcher A, van de Moortele PF et al.: 7 Tesla (T) human cardiovascular magnetic resonance imaging using FLASH and SSFP to assess cardiac function: validation against 1.5 T and 3 T. *NMR Biomed* 25:27-34, 2012
26. von Knobelsdorff-Brenkenhoff F, Tkachenko V, Winter L, Rieger J et al.: Assessment of the right ventricle with cardiovascular magnetic resonance at 7 Tesla. *J Cardiovasc Magn Reson* 15:23, 2013
27. Marcus FI, McKenna WJ, Sherrill D, Basso C et al.: Diagnosis of arrhythmogenic right ventricular cardiomyopathy/dysplasia: proposed modification of the task force criteria. *Circulation* 121:1533-1541, 2010

Chapter 13

Summary and conclusions

The first part of this thesis focuses on assessing end-organ damage in individuals with metabolic syndrome and diabetes mellitus using magnetic resonance imaging (MRI) and spectroscopy (^{1}H-MRS). We performed cross sectional and intervention studies to investigate the contribution of obesity, dietary conditions, metabolic environment and exogenous disruptors (chemotherapy) to cardiovascular end-organ damage and the reversibility of this damage with a low caloric diet. The effects of interventions, dietary as well as non-dietary, were explored using imaging technology. As ethnicity is an important aspect of the pathophysiology in diabetes mellitus, we also examined the influence of ethnic factors on diabetes mellitus and its complications. The second part of this thesis focuses on safety, feasibility and implementation of innovative MR techniques at higher field strengths for assessment of cardiovascular disease.

Chapter 2 describes the relationship between left ventricular diastolic function and aortic stiffness in patients with type 1 diabetes mellitus (T1DM). T1DM is associated with aortic stiffening and with left ventricular (LV) diastolic dysfunction, but the relationship between a stiffer aorta and LV diastolic dysfunction is still largely unknown. Pulse wave velocity (PWV) is a marker for aortic stiffness and can readily be assessed with velocity-encoded MRI. Speckle tracking, a relatively new echocardiographic method, is suggested to provide a more sensitive evaluation of global LV diastolic function than traditional echocardiographic Doppler techniques of mitral inflow. Furthermore, speckle tracking strain analysis permits a concise evaluation of left atrial (LA) compliance. PWV, LV and LA longitudinal strain were assessed in 41 T1DM patients. It was found that aortic PWV, assessed with MRI, is inversely associated with LV diastolic function indices and reduced LA compliance, measured with speckle tracking strain analysis in patients with T1DM. The more conventional echocardiographic inflow parameters of diastolic dysfunction were not associated with PWV. The correlation between aortic stiffness and impaired LV diastolic function can be caused by two possible separate mechanisms. First, increased aortic stiffness is associated with higher end-diastolic pressure and increased afterload, which can directly affect LV diastolic function (1). Secondly, advanced glycation products that are generated in the course of DM and cause cross-linking of collagen molecules in the myocardium and in vessel walls can simultaneously affect both the myocardium and the aortic wall (2). The results of this study suggest that aortic PWV can be used as an integrated marker for LV diastolic function and LA compliance in this patient group. Further studies are required to assess the potential clinical and prognostic implication of these findings. In the future, PWV or the speckle tracking diastolic function parameters could potentially be used to assess cardiovascular risk in patients with T1DM, which could eventually lead to adjustments in treatment.

Aortic stiffening may affect multiple end organs by decreasing end-organ perfusion, including the brain.

Although T1DM is not primarily a brain disease, it is associated with brain damage, such as cerebral atrophy, white matter hyperintensities and decreased cognitive functioning (3-5). Aortic stiffening may play a central role in the development of brain injury (6) and previous studies have shown that aortic stiffness is associated with generalized white matter atrophy in T1DM and related systemic diseases (7). In **Chapter 3,** the association between PWV and white matter integrity of the brain is evaluated. Forty-two patients with T1DM were studied and PWV was measured using a 1.5 Tesla (T) MRI scanner. Diffusion Tensor Imaging (DTI) is a validated and sensitive technique for detecting brain disease with MRI, which, in contrast to conventional methods, enables alterations in white matter microstructure to be detected. DTI is a technique that allows early detection of white matter damage, even in regions that appear normal on conventional anatomical images. We concluded that aortic stiffness is associated with white matter integrity independently of other potential confounders, such as age, gender, mean arterial pressure, body mass index (BMI), smoking, duration of diabetes and HbA1c levels, in patients with T1DM. This suggests a vascular contribution to early subtle microstructural deficits. Future prospective studies are needed to improve knowledge of the prognostic and therapeutic consequences of these microstructural changes in the brain white matter. An earlier recognition of microstructural brain damage might lead to earlier or more intense treatment, for example of vascular risk factors such as hypertension or hypercholesterolemia.

In **Chapter 4,** the effects of T1DM on cortical gray matter volume are studied. Cortical gray matter and the thalamus and hippocampus, two subcortical structures, are affected in patients with T1DM. Previous studies on hippocampal and thalamic volumes showed reduced volumes in patients with T1DM (8-11). However, no studies have investigated in-depth volume loss in gray matter areas other than the hippocampus and thalamus in T1DM. Voxel-based morphometry (VBM) is a relatively novel and sophisticated analysis technique which can be used to identify subtle gray matter alterations (12). 62 patients with T1DM and 62 age- and gender-matched healthy controls underwent MR imaging of the brain. Basal ganglia, amygdala, hippocampus and thalamus volumes were assessed with VBM. In this chapter we show that in T1DM patients, volume loss occurs in all of these gray matter areas, except for the amygdala. In addition, our results show that after correcting for potential confounding factors, the thalamus, hippocampus and putamen were still significantly smaller in patients with T1DM. The finding that T1DM differentially affects specific gray matter areas is challenging, but difficult to explain. Potential differences in the susceptibility of the thalamus, hippocampus and putamen

and other graymatter structures to T1DM related factors might be involved. The clinical significance and underlying mechanisms remain to be elucidated.

In **Chapter 5,** the effects are described of a 16-week (very) low calory diet ((V)LCD) on cardiovascular function and ectopic fat depositions in overweight patients with type 2 diabetes mellitus (T2DM) and coronary artery disease (CAD).

Prolonged caloric restriction in obese patients with T2DM without established coronary atherosclerosis improves myocardial function and leads to a decrease in ectopic fat, including myocardial and pericardial fat (13,14). The aim of this study was to evaluate whether T2DM patients with CAD also benefit from prolonged caloric restriction. 27 overweight patients with T2DM and CAD were subjected to a 16-week (V)LCD.

After the diet, substantial beneficial changes in glucoregulation and cardiovascular function were found. These improvements were paralleled by reductions in all fat compartments, as well as in ectopic fat accumulation in the liver and heart.

Myocardial triglyceride (TG) accumulation is the net result of excessive free fatty acids (FFA) uptake in relation to FFA oxidation. Patients with T2DM have increased myocardial TG content (15), which is associated with impaired myocardial function (16). Reducing myocardial TG leads to improved cardiac function in uncomplicated T2DM patients (13) and our study indicated that this also applies to patients with T2DM and CAD. Moreover, we also noted a decrease in pericardial fat. Pericardial fat consists of two layers, i.e., epicardial fat and paracardial fat, both of which are associated with insulin resistance, T2DM and cardiovascular disease (CVD) (17-20). The effects on pericardial fat observed in our study are therefore considered to be beneficial.

A further benefit was the decrease seen in left ventricular (LV) mass and heart rate, since both are important predictors for CVD (21,22). The finding that LV ejection fraction (LVEF) increased after the (V)LCD is clinically relevant, as LVEF is one of the most important predictors of survival (23). Our study also revealed a decrease in PWV of 0.7 m/s, indicating a less stiff aorta. Given the fact that PWV increases with 0.7m/s per 10 years of aging (24), this is a significant improvement. These data show that cardiovascular function and ectopic fat accumulation are susceptible to dietary intervention in complicated T2DM, a finding which has important clinical implications. Since T2DM is associated with increased cardiovascular risk (25) and CVD is the main cause of death in patients T2DM (26,27), the results of this study are clinically relevant and prove that dietary interventions, superposed on optimal pharmacological therapy, are worthwhile strategies, even in advanced complicated T2DM.

The effects of bariatric surgery on ectopic fat depositions and cardiovascular function are described in **Chapter 6**. Cardiac ectopic fat depositions, i.e. myocardial TG and

pericardial fat, are thought to play a role in the pathogenesis of CVD, the main cause of death in T2DM patients. While diet-induced weight loss results in a decrease in cardiac ectopic fat stores, it is less clear whether this also holds for surgically induced weight loss. Myocardial TG, pericardial fat and cardiac function were assessed in 10 obese, insulin-dependent T2DM patients before and 16 weeks after Roux-en-Y gastric bypass (RYGB) surgery. After the surgery, these patients lost a considerable amount of weight and showed improvements in glycemic control. The loss of body weight led to a significant decrease in visceral and subcutaneous fat depots. Additionally, a substantial reduction in ectopic cardiac fat was found, with a differential response of the pericardial fat layers after RYGB surgery: although epicardial fat volume was found to have diminished, the relative decrease in paracardial fat volume was much higher. Increased epicardial fat volume has been associated with insulin resistance, T2DM and CVD (17-20). The role of paracardial fat is currently less clear. Some studies have shown that paracardial fat is a better predictor of cardiovascular risk than epicardial fat (28). Myocardial TG did not decrease and cardiovascular function did not improve after RYGB. These findings suggest that weight loss after RYGB in T2DM patients affects paracardial adipose tissue differently than epicardial adipose tissue. The clinical implications of these findings have yet to be determined. Studies with longer follow-up periods could help determine these implications.

Chapter 7 describes the effects of a 5-day high fat high caloric (HFHC) diet on cardiovascular function in young, healthy South Asians and Caucasians. Twelve Dutch South Asian and twelve Dutch Caucasian healthy males, matched for age (19-25 years) and BMI (<25 kg/m^2), with a positive family history for T2DM were subjected to a 5-day HFHC-diet, consisting of the subject's regular diet, supplemented with 375 ml of cream per day. Cardiovascular function was assessed with MRI. This study shows that young, healthy South Asians have smaller cardiac dimensions compared to matched Caucasians, even after adjusting for the smaller body surface area (BSA) in South Asians. Furthermore, diastolic cardiac function in South Asians is different. In addition, although the ejection fraction (EF), a gross parameter of systolic function, was similar between both groups, more subtle parameters of systolic function were different. A 5-day HFHC-diet did not increase these differences. The South Asians were also shown to have a higher PWV at baseline. PWV is a powerful independent predictor of cardiovascular events (29). Whether these differences contribute to the higher incidence of CVD in South Asians, however, remains to be determined. The 5-day HFHC-diet did not increase the observed functional cardiovascular differences between both groups, suggesting that these findings cannot be explained by a different metabolic response to dietary fat consumption between both ethnicities at young age.

In the study described above, the metabolic effects of the HFHC-diet were assessed, as well; the results are reported in **Chapter 8**. Previous studies showed that South Asians have high hepatic and intramyocellular lipid content compared to Caucasians (30,31). This suggests that South Asians have an impaired mitochondrial fatty acid beta-oxidation in either skeletal muscle and/or adipose tissue, resulting in ectopic fat deposition in peripheral tissues, eventually leading to insulin resistance and other metabolic dysfunctions (32). South Asians may therefore be less well able to handle a Western-type high fat diet than Caucasians.

Recent studies have identified the nutrient and energy-sensing mammalian target of rapamycin (mTOR)-pathway as a modulator of both insulin sensitivity and mitochondrial function (33,34). We hypothesized that differences in mTOR activity between the two ethnicities may underlie or contribute to the increased risk of T2DM in South Asians, assuming that alterations in the mTOR-pathway may lead to mitochondrial dysfunction and subsequent impaired fatty acid handling. In addition, hepatic and peripheral insulin sensitivity, substrate oxidation, abdominal fat distribution and skeletal muscle insulin signaling and mitochondrial respiratory-chain content were assessed. As mitochondrial dysfunction may be unveiled by high fat load, participants were subjected to a 5-day HFHC-diet. The participants underwent a 2-step hyperinsulinemic euglycemic clamp with skeletal muscle biopsies and indirect calorimetry both prior to starting and after completing a 5-day HFHC-diet.

This study revealed that a 5-day HFHC-diet is already sufficient to affect insulin-stimulated non-oxidative glucose disposal in healthy, young, lean South Asians males, whereas no diet effect was found in age- and BMI-matched Caucasians, suggesting that healthy young South Asians might have an innate impaired metabolic adaptation to dietary fat overload. The mTOR-pathway does not seem to be involved, at least not in skeletal muscle. These findings might provide new leads for further investigations aimed at elucidating the pathogenesis of insulin resistance and T2DM in South Asians. For example, it might be interesting to investigate the role of white adipose tissue in the impaired glucose handling in South Asians as compared to Caucasians.

Chapter 9 presents the results of a study into the effects of an 8-day VLCD on cardiovascular function, ectopic fat distribution and myocardial TG in twelve middle-aged, overweight South Asians and twelve age-, sex- and BMI-matched Caucasians. At baseline South Asians were more insulin resistant than Caucasians. Just as was the case in young healthy South Asians and Caucasians, the middle-aged participants exhibited smaller cardiac dimensions, despite adjusting for BSA. PWV was higher in the distal aorta in South Asian. No difference was seen in systolic and diastolic cardiac function, myocardial and pericardial fat between groups. After the VLCD body weight reduced

and myocardial TG increased in both ethnicities. Diastolic function had decreased to a similar extent in both groups. However, paracardial fat and PWV showed a differential effect in response to the VLCD, with a more favorable response observed in Caucasians.

The results of our study show a comparable flexibility of the heart to a VLCD in middle-aged overweight and insulin resistant South Asians as compared to age-, sex- and BMI-matched but less insulin resistant Caucasians. However, the response of South Asians to an 8-day VLCD appears to be less favorable with respect to paracardial fat volume and PWV.

Chapter 10 demonstrates that cisplatin-based chemotherapy for testicular cancer (TC) induces acute alterations in diastolic cardiac function, paralleled by unfavorable metabolic changes. Treatment with cisplatin-based chemotherapy is associated with an increased prevalence of cardiovascular risk factors, such as central obesity and metabolic disturbances, including dyslipidemia and insulin resistance. Treatment of TC with cisplatin, bleomycin and etoposide (BEP) combination chemotherapy is also associated with acute vascular toxicity and subacute changes in cardiac function (35,36), as well as with long-term cardiovascular disease. Little is known about the acute effects of cisplatin-based chemotherapy, defined as effects occurring 3 months after the start of chemotherapy, on cardiac function, body fat distribution and metabolic parameters. Cardiac function, fat distribution and metabolic parameters were assessed in 14 patients with TC prior to commencing chemotherapy and shortly after the last chemotherapy cycle, approximately three months after the start of the therapy. We showed that treatment with cisplatin-based chemotherapy for TC induces acute alterations in diastolic cardiac function, which was accompanied by unfavorable metabolic changes. Although the predictive significance of these diastolic cardiac changes for long-term cardiovascular morbidity is not clear at present, it seems plausible that they may eventually lead to overt cardiovascular disease. As the detrimental metabolic changes can contribute to the development of cardiovascular disease, these risk factors should be monitored and treated if necessary.

The study in **Chapter 11** compares 3T and 7T carotid vessel wall imaging in healthy volunteers. MRI of the vessel wall enables determination of luminal area, vessel wall thickness, and atherosclerotic plaque characteristics. For clinical application, high spatial resolution, deriving from optimal signal-to-noise-ratio (SNR) and contrast-to-noise-ratio (CNR) is paramount. In many applications, ultrahigh field MRI provides higher SNR and CNR, which can be used to increase spatial resolution (37-40). MR imaging of the carotid vessel wall may therefore benefit from higher magnetic field strength. 18 volunteers underwent MRI-examinations at 7T (using a custom-built surface transmit/receive coil

of 15 cm diameter) and at 3T (using a commercial phased-array coil with two flexible oval elements, each 14 x 17 cm). MRI of the left common carotid artery vessel-wall was performed at 7T with the identical in-plane resolution as that of 3T MRI (0.46 x 0.46 mm^2) providing transverse T1- and T2-weighted images. The results indicate that morphologic carotid vessel wall measurements (luminal area and vessel wall area) and intra- and inter-observer reproducibility are comparable between 3T and 7T. Furthermore, 7T MRI carotid vessel wall imaging improves SNR_{VW} and CNR compared to 3T.

This chapter highlights the potential of 7T carotid MR imaging for assessment of carotid luminal area and vessel wall area, since accurate delineation of the carotid artery vessel wall structure is crucial to detect carotid atherosclerosis and atherosclerotic changes of the vessel wall over time.

The increased field strength produces a series of technical challenges for cardiovascular MRI (41,42). Cardiovascular MRI requires robust compensation for heart motion, breathing motion and field inhomogeneity. Another challenge is obtaining a reliable electrocardiogram (43). **Chapter 12** describes the results of a study on coronary stent safety at 7T MR by determining displacement and heating for cobalt alloy stents ranging in length from 5 to 85.8 mm in a worst-case scenario. Furthermore, it describes the initial clinical feasibility of 7T cardiovascular MRI in healthy volunteers and patients with CVD in the format of a multiple-case presentation. The results of this study show that 7T cardiovascular MRI is safe to perform in patients with cobalt alloy coronary stents ranging in size from 5 to 85.8 mm and that clinical cardiovascular MRI at 7T is feasible in healthy volunteers and in patients with cardiovascular disease. Technical challenges have to be overcome before routine clinical application becomes possible. Clinical practice has to prove the benefit of ultrahigh field MRI as compared to lower field MRI at 1.5T and 3T.

In conclusion, patients with DM experience cardiovascular complications of their disease.

Obesity is a major risk factor for developing T2DM, and the increasing prevalence of obesity has led to a concomitant increase in the prevalence of T2DM. T2DM is one of the most common chronic diseases in the world. The pathogenesis of cardiovascular complications in T2DM is multifactorial, but a major role seems to be attributable to ectopic accumulation of TG in skeletal muscle, liver and in and around the heart. Weight loss is currently considered the most effective treatment for T2DM. A reduction in ectopic fat is thought to be one of the responsible mechanisms for improved insulin sensitivity after weight loss (44). However, sustained weight loss is difficult as permanent changes in lifestyle are required to prevent the lost weight from being regained. Bariatric surgery is

another possible treatment for T2DM since it results in massive weight loss and marked improvement in glycemic control, or even in remission of T2DM.

In patients with T1DM, the aorta is stiffer as compared to healthy volunteers and this is correlated with LV diastolic function and white matter brain integrity. T1DM also influences gray matter volume.

Patients with T2DM have an increased risk of mortality due to CVD. We showed that even in patients with T2DM and CAD a 16-week (V)LCD can improve cardiovascular function and ectopic fat distribution. This highlights the importance of dietary interventions in this patient group and indicates that the cornerstone of treatment remains weight loss. Since the prevalence of overweight/obesity and concomitant T2DM is reaching epidemic proportions, the main focus should be on the prevention of obesity. In addition to the results of the 16-week (V)LCD study, a study in T2DM patients before and 16 weeks after bariatric surgery showed a more pronounced reduction of paracardial fat, compared to epicardial fat. The implications of this finding need to be elucidated in future studies.

Furthermore, the studies in this thesis have shown that, already at a young age, there are differences in cardiac dimensions and function between South Asians and Caucasians. In addition, a HFHC-diet impairs insulin sensitivity in young, lean, healthy South Asians but not in Caucasians. The ectopic fat distribution is the same in South Asians and Caucasians, both in young and in middle-aged subjects. However, paracardial fat and PWV showed a differential response to a VLCD, with a more favorable response in Caucasians. Our findings contribute to a greater understanding of the increased risk of CVD and T2DM in South Asians. Nevertheless, more studies need to be performed to investigate and hopefully better understand the mechanisms behind this increased risk.

Finally, this thesis describes the results of the feasibility of carotid vessel wall imaging performed at 7T. Furthermore, data on coronary stent safety at 7T and initial clinical feasibility of cardiovascular MRI in patients with cardiovascular disease are presented.

REFERENCES

1. Leite-Moreira AF, Correia-Pinto J, Gillebert TC: Afterload induced changes in myocardial relaxation: a mechanism for diastolic dysfunction. *Cardiovasc Res* 43:344-353, 1999
2. Aronson D: Cross-linking of glycated collagen in the pathogenesis of arterial and myocardial stiffening of aging and diabetes. *J Hypertens* 21:3-12, 2003
3. Biessels GJ, Staekenborg S, Brunner E, Brayne C et al.: Risk of dementia in diabetes mellitus: a systematic review. *Lancet Neurol* 5:64-74, 2006
4. Gouw AA, van der Flier WM, Fazekas F, van Straaten EC et al.: Progression of white matter hyperintensities and incidence of new lacunes over a 3-year period: the Leukoaraiosis and Disability study. *Stroke* 39:1414-1420, 2008
5. Knopman DS, Mosley TH, Catellier DJ, Sharrett AR: Cardiovascular risk factors and cerebral atrophy in a middle-aged cohort. *Neurology* 65:876-881, 2005
6. van Elderen SG, Brandts A, Westenberg JJ, van der Grond J et al.: Aortic stiffness is associated with cardiac function and cerebral small vessel disease in patients with type 1 diabetes mellitus: assessment by magnetic resonance imaging. *Eur Radiol* 20:1132-1138, 2010
7. van Elderen SG, Brandts A, van der Grond J, Westenberg JJ et al.: Cerebral perfusion and aortic stiffness are independent predictors of white matter brain atrophy in type 1 diabetic patients assessed with magnetic resonance imaging. *Diabetes Care* 34:459-463, 2011
8. Lobnig BM, Kromeke O, Optenhostert-Porst C, Wolf OT: Hippocampal volume and cognitive performance in long-standing Type 1 diabetic patients without macrovascular complications. *Diabet Med* 23:32-39, 2006
9. Hershey T, Perantie DC, Wu J, Weaver PM et al.: Hippocampal volumes in youth with type 1 diabetes. *Diabetes* 59:236-241, 2010
10. Musen G, Lyoo IK, Sparks CR, Weinger K et al.: Effects of type 1 diabetes on gray matter density as measured by voxel-based morphometry. *Diabetes* 55:326-333, 2006
11. Northam EA, Rankins D, Lin A, Wellard RM et al.: Central nervous system function in youth with type 1 diabetes 12 years after disease onset. *Diabetes Care* 32:445-450, 2009
12. Ashburner J, Friston KJ: Voxel-based morphometry--the methods. *Neuroimage* 11:805-821, 2000
13. Hammer S, Snel M, Lamb HJ, Jazet IM et al.: Prolonged caloric restriction in obese patients with type 2 diabetes mellitus decreases myocardial triglyceride content and improves myocardial function. *J Am Coll Cardiol* 52:1006-1012, 2008
14. Snel M, Jonker JT, Hammer S, Kerpershoek G et al.: Long-term beneficial effect of a 16-week very low calorie diet on pericardial fat in obese type 2 diabetes mellitus patients. *Obesity (Silver Spring)* 20:1572-1576, 2012
15. McGavock JM, Lingvay I, Zib I, Tillery T et al.: Cardiac steatosis in diabetes mellitus: a 1H-magnetic resonance spectroscopy study. *Circulation* 116:1170-1175, 2007
16. Rijzewijk LJ, van der Meer RW, Smit JW, Diamant M et al.: Myocardial steatosis is an independent predictor of diastolic dysfunction in type 2 diabetes mellitus. *J Am Coll Cardiol* 52:1793-1799, 2008
17. Greif M, Becker A, von ZF, Lebherz C et al.: Pericardial adipose tissue determined by dual source CT is a risk factor for coronary atherosclerosis. *Arterioscler Thromb Vasc Biol* 29:781-786, 2009
18. Iacobellis G, Leonetti F: Epicardial adipose tissue and insulin resistance in obese subjects. *J Clin Endocrinol Metab* 90:6300-6302, 2005

19. Rosito GA, Massaro JM, Hoffmann U, Ruberg FL et al.: Pericardial fat, visceral abdominal fat, cardiovascular disease risk factors, and vascular calcification in a community-based sample: the Framingham Heart Study. *Circulation* 117:605-613, 2008
20. Wang CP, Hsu HL, Hung WC, Yu TH et al.: Increased epicardial adipose tissue (EAT) volume in type 2 diabetes mellitus and association with metabolic syndrome and severity of coronary atherosclerosis. *Clin Endocrinol (Oxf)* 70:876-882, 2009
21. Kannel WB, Kannel C, Paffenbarger RS, Jr., Cupples LA: Heart rate and cardiovascular mortality: the Framingham Study. *Am Heart J* 113:1489-1494, 1987
22. Levy D, Garrison RJ, Savage DD, Kannel WB et al.: Prognostic implications of echocardiographically determined left ventricular mass in the Framingham Heart Study. *N Engl J Med* 322:1561-1566, 1990
23. Chareonthaitawee P, Sorajja P, Rajagopalan N, Miller TD et al.: Prevalence and prognosis of left ventricular systolic dysfunction in asymptomatic diabetic patients without known coronary artery disease referred for stress single-photon emission computed tomography and assessment of left ventricular function. *Am Heart J* 154:567-574, 2007
24. Westenberg JJ, Scholte AJ, Vaskova Z, van der Geest RJ et al.: Age-related and regional changes of aortic stiffness in the marfan syndrome: Assessment with velocity-encoded MRI. *J Magn Reson Imaging* 2011
25. Wang CC, Reusch JE: Diabetes and cardiovascular disease: changing the focus from glycemic control to improving long-term survival. *Am J Cardiol* 110:58B-68B, 2012
26. Centers for Disease Control and Prevention: 2011 National Diabetes Fact Sheet. *www cdc gov/diabetes/pubs/factsheet11 htm* 2011
27. Stamler J, Vaccaro O, Neaton JD, Wentworth D: Diabetes, other risk factors, and 12-yr cardiovascular mortality for men screened in the Multiple Risk Factor Intervention Trial. *Diabetes Care* 16:434-444, 1993
28. Sicari R, Sironi AM, Petz R, Frassi F et al.: Pericardial rather than epicardial fat is a cardiometabolic risk marker: an MRI vs echo study. *J Am Soc Echocardiogr* 24:1156-1162, 2011
29. Mitchell GF, Hwang SJ, Vasan RS, Larson MG et al.: Arterial stiffness and cardiovascular events: the Framingham Heart Study. *Circulation* 121:505-511, 2010
30. Anand SS, Tarnopolsky MA, Rashid S, Schulze KM et al.: Adipocyte hypertrophy, fatty liver and metabolic risk factors in South Asians: the Molecular Study of Health and Risk in Ethnic Groups (mol-SHARE). P*LoS One* 6:e22112, 2011
31. Petersen KF, Dufour S, Feng J, Befroy D et al.: Increased prevalence of insulin resistance and nonalcoholic fatty liver disease in Asian-Indian men. P*roc Natl Acad Sci U S A* 103:18273-18277, 2006
32. Snel M, Jonker JT, Schoones J, Lamb H et al.: Ectopic fat and insulin resistance: pathophysiology and effect of diet and lifestyle interventions. *Int J Endocrinol* 2012:983814, 2012
33. Um SH, Frigerio F, Watanabe M, Picard F et al.: Absence of S6K1 protects against age- and diet-induced obesity while enhancing insulin sensitivity. *Nature* 431:200-205, 2004
34. Khamzina L, Veilleux A, Bergeron S, Marette A: Increased activation of the mammalian target of rapamycin pathway in liver and skeletal muscle of obese rats: possible involvement in obesity-linked insulin resistance. *Endocrinology* 146:1473-1481, 2005
35. Altena R, de Haas EC, Nuver J, Brouwer CA et al.: Evaluation of sub-acute changes in cardiac function after cisplatin-based combination chemotherapy for testicular cancer. *Br J Cancer* 100:1861-1866, 2009

36. Stefenelli T, Kuzmits R, Ulrich W, Glogar D: Acute vascular toxicity after combination chemotherapy with cisplatin, vinblastine, and bleomycin for testicular cancer. *Eur Heart J* 9:552-556, 1988
37. Niendorf T, Sodickson DK, Krombach GA, Schulz-Menger J: Toward cardiovascular MRI at 7 T: clinical needs, technical solutions and research promises. *Eur Radiol* 20:2806-2816, 2010
38. van Elderen SG, Versluis MJ, Westenberg JJ, Agarwal H et al.: Right coronary MR angiography at 7 T: a direct quantitative and qualitative comparison with 3 T in young healthy volunteers. *Radiology* 257:254-259, 2010
39. Vaughan JT, Garwood M, Collins CM, Liu W et al.: 7T vs. 4T: RF power, homogeneity, and signal-to-noise comparison in head images. *Magn Reson Med* 46:24-30, 2001
40. Yarnykh VL, Terashima M, Hayes CE, Shimakawa A et al.: Multicontrast black-blood MRI of carotid arteries: comparison between 1.5 and 3 tesla magnetic field strengths. *J Magn Reson Imaging* 23:691-698, 2006
41. Gutberlet M, Schwinge K, Freyhardt P, Spors B et al.: Influence of high magnetic field strengths and parallel acquisition strategies on image quality in cardiac 2D CINE magnetic resonance imaging: comparison of 1.5 T vs. 3.0 T. *Eur Radiol* 15:1586-1597, 2005
42. Niendorf T, Graessl A, Thalhammer C, Dieringer MA et al.: Progress and promises of human cardiac magnetic resonance at ultrahigh fields: A physics perspective. *J Magn Reson* 229:208-222, 2013
43. van Elderen SG, Versluis MJ, Webb AG, Westenberg JJ et al.: Initial results on in vivo human coronary MR angiography at 7 T. *Magn Reson Med* 62:1379-1384, 2009
44. Snel M, Jonker JT, Schoones J, Lamb H et al.: Ectopic fat and insulin resistance: pathophysiology and effect of diet and lifestyle interventions. *Int J Endocrinol* 2012:983814, 2012

Chapter 14

Nederlandse samenvatting

NEDERLANDSE SAMENVATTING

Wereldwijd neemt de prevalentie van overgewicht en obesitas snel toe. Het aantal mensen met overgewicht is verdubbeld sinds 1980. In 2008 waren er wereldwijd meer dan 1.4 miljard mensen met overgewicht (BMI ≥ 25 kg/m^2), waarvan er 500 miljoen mensen zelfs ernstig overgewicht (obesitas, BMI ≥ 30 kg/m^2) hadden. Geschat wordt dat deze aantallen in 2030 verder toegenomen zijn tot 2.2 miljard mensen met overgewicht, waarvan 1.1 miljard met obesitas.

Diabetes mellitus (DM) is een ziekte waarbij de glucoseregulatie in het lichaam verstoord is. Insuline is een hormoon dat gemaakt wordt in de alvleesklier en het is van belang voor het reguleren van de glucoseconcentratie in het bloed. Bij gezonde mensen zorgt insuline ervoor dat te hoge glucosespiegels weer omlaag gaan, doordat insuline onder andere de opname van glucose in de perifere weefsels stimuleert. Diabetes is een van de meest voorkomende chronische ziektes ter wereld. Er zijn meerdere types DM, de onderzoeken beschreven in dit proefschrift betreffen type 1 en 2. Type 1 diabetes mellitus (T1DM) is de variant die al op jonge leeftijd ontstaat en niet geassocieerd is met overgewicht. Daarentegen is overgewicht wel een belangrijke risicofactor voor type 2 diabetes mellitus (T2DM), en het is dus niet verwonderlijk dat tegelijk met de prevalentie van overgewicht ook de prevalentie van T2DM toeneemt. De geschatte prevalentie T2DM in 2030 is tussen de 4.4% en 6.4%, wat aangeeft hoe groot het probleem is voor de volksgezondheid. DM heeft negatieve effecten op bijna alle weefsels en organen in het lichaam. Bekende complicaties van zowel T1DM als T2DM worden gezien in hart en bloedvaten, het (centrale) zenuwstelsel, de nieren en de ogen ('eindorgaanschade').

De pathogenese van T2DM is nog niet geheel opgehelderd, maar is in ieder geval multifactorieel. Bij T2DM is er sprake van een verminderde functie van de cellen in de alvleesklier die insuline produceren, de bètacellen. Tevens is er een verminderde gevoeligheid van de weefsels voor insuline, wat ook wel insulineresistentie wordt genoemd en leidt tot verhoogde glucosespiegels. Dit wordt deels genetisch bepaald. Zo hebben bepaalde etniciteiten, zoals Hindostanen, een verhoogd risico op T2DM. Bij overgewicht neemt de hoeveelheid vetweefsel toe. Teveel vetweefsel veroorzaakt een chronische staat van laaggradige ontsteking, wat weer kan leiden tot T2DM. Ook ectopische vetstapeling speelt een belangrijke rol in de pathogenese van T2DM. Ectopische vetstapeling is vetstapeling (triglyceriden (TG) stapeling) in organen die niet primair bedoeld zijn voor de opslag van vet, zoals het hart, de lever en de skeletspieren. Door de opslag van vet in deze weefsels, zijn ze minder gevoelig voor insuline. Ook exogene factoren kunnen de glucosehuishouding verstoren door de gevoeligheid voor insuline te verminderen. Hierbij kan gedacht worden aan exogene toxiciteit door bijvoorbeeld chemotherapie.

Patiënten met DM hebben een verhoogd risico op hart- en vaatziekten. Ongeveer 50% van de patiënten met T2DM sterft aan hart- en vaatziekten. De pathogenese van de cardiovasculaire complicaties is ingewikkeld, maar ook hier lijkt een belangrijke rol toe te schrijven aan ectopische vetstapeling.

Meer dan 80% van de T2DM patiënten heeft overgewicht en daarom blijft gewichtsvermindering de hoeksteen van hun behandeling. Gewichtsverlies kan bewerkstelligd worden door middel van diëten, met lichamelijke activiteit of met behulp van bariatrische chirurgie. Daarnaast bestaat de behandeling van T2DM uit glucose-, lipiden- en bloeddruk verlagende medicatie. Behandeling is gericht op het verlichten van de klachten en het voorkomen van complicaties.

Magnetic Resonance Imaging (MRI) technieken zijn uiterst geschikt om de anatomie van hart en bloedvaten en de hersenen goed in beeld te brengen. Tevens kunnen ectopische vetdeposities met behulp van MRI technieken goed in beeld worden gebracht.

De toenemende incidentie van T2DM wordt, ook in Westerse landen, met name gezien bij mensen van Zuid Aziatische afkomst. De wereldbevolking bestaat voor een vijfde uit Zuid Aziaten. In Nederland noemen we deze bevolkingsgroep, die oorspronkelijk afkomstig is van het Indiase subcontinent (India, Pakistan, Bangladesh, Nepal en Sri Lanka) Hindostanen. Niet alleen is de prevalentie van T2DM hoger bij Hindostanen, maar T2DM ontstaat bij hen op jongere leeftijd en bij een lager lichaamsgewicht in vergelijking tot blanke Kaukasiërs. Bovendien verloopt de ziekte vaak ernstiger bij Hindostanen. Daarnaast hebben Hindostanen een verhoogd risico op hart- en vaatziekten in vergelijking tot blanke Kaukasiërs. De gemiddelde leeftijd van een eerste hartinfarct is bij Hindostanen lager en de mortaliteit van hart- en vaatziekten is hoger. Een goede verklaring hiervoor is nog niet gevonden en is een onderwerp van veel wetenschappelijk onderzoek.

Het doel van dit proefschrift is het in beeld brengen en onderzoeken van eindorgaanschade bij mensen met het metabool syndroom en DM door middel van MRI. Bovendien worden de veiligheid, uitvoerbaarheid en implementatie van innovatieve MRI technieken met hogere veldsterktes voor het onderzoeken van cardiovasculaire ziekten geëvalueerd. We hebben cross-sectionele en interventie studies uitgevoerd om te onderzoeken wat de invloed is van overgewicht, dieet en exogene invloeden (chemotherapie) op cardiovasculaire eindorgaan schade. Tevens onderzochten we de omkeerbaarheid van deze cardiovasculaire schade met dieetinterventies. De invloed van etniciteit op DM (gericht op Hindostanen) en de complicaties daarvan werden ook onderzocht in dit proefschrift.

Hoofdstuk 2 beschrijft de relatie tussen de diastolische functie van de linker ventrikel (LV) en de stijfheid van de aorta in patiënten met T1DM. T1DM is geassocieerd met een

stijvere (minder elastische) aorta en met diastolische disfunctie van de LV. Of er een relatie is tussen een stijvere aorta en LV diastolische disfunctie is echter niet bekend. Pulse wave velocity (PWV) is een indicator voor aorta stijfheid en is een goede onafhankelijke voorspeller voor hart- en vaatziekten. PWV kan goed gemeten worden met behulp van MRI technieken. 'Speckle tracking' is een relatief nieuwe echocardiografische methode die globale LV diastolische functie beter kan vaststellen dan traditionele Doppler echocardiografie van de mitralisklep. Bovendien kan met speckle tracking de compliantie van het linker atrium (LA) goed worden geëvalueerd. Met speckle tracking kan de strain van het LV en het LA worden bepaald. Strain is een maat voor snelheid van deformatie van het myocardweefsel. De PWV, LV en LA longitudinale strain werden bepaald bij 41 patiënten met T1DM. Deze studie toont aan dat een hogere PWV in de aorta, gemeten met MRI, geassocieerd is met verminderde LV diastolische functie en LA compliantie, gemeten met speckle tracking in patiënten met T1DM. De meer conventionele echocardiografische instroom parameters van diastolische disfunctie waren niet geassocieerd met PWV. De correlatie tussen een stijvere aorta en een verminderde diastolische functie kan door twee mogelijke mechanismen verklaard worden. Ten eerste kan de verhoogde aorta stijfheid direct de LV diastolische functie beïnvloeden door hogere eind-diastolische druk en verhoogde afterload. Ten tweede kunnen de 'advanced glycation products' (AGEs) die worden gevormd bij diabetes, cross linking van collageen moleculen in het myocard en in vaatwanden veroorzaken. AGEs zijn eiwitten of lipiden die beschadigd zijn na blootstelling aan hoge glucoseconcentraties, zoals bij patiënten met DM Deze AGEs kunnen de stijfheid van zowel het myocard als van de aortawand beïnvloeden. De resultaten van deze studie suggereren dat de PWV van de aorta gebruikt kan worden als een geïntegreerde marker voor LV diastolische functie en LA compliantie in deze patiëntengroep. Vervolgstudies zijn nodig om de klinische en prognostische implicaties van deze bevindingen te onderzoeken. In de toekomst kunnen PWV of de diastolische functie parameters verkregen met speckle tracking mogelijk gebruikt worden om een inschatting van het cardiovasculaire risico te maken bij patiënten met T1DM. Dat zou mogelijk kunnen leiden tot veranderingen in de behandeling van deze patiënten.

Toegenomen stijfheid van de aorta kan invloed hebben op de perfusie van verschillende eindorganen, waaronder de hersenen. Alhoewel T1DM niet een primaire hersenaandoening is, is T1DM wel geassocieerd met hersenschade, zoals cerebrale atrofie, witte stof afwijkingen en verminderd cognitief functioneren. Mogelijk speelt toegenomen stijfheid van de aorta een rol in het ontstaan van hersenschade. Eerdere studies hebben aangetoond dat stijfheid van de aorta geassocieerd is met gegeneraliseerde witte stof atrofie in patiënten met T1DM. In **hoofdstuk 3** wordt de associatie tussen PWV van de aorta en witte stof integriteit van de hersenen geëvalueerd. Bij 42 patiënten met

T1DM werd de PWV van de aorta gemeten met een 1.5 Tesla (T) MRI. Diffusion Tensor Imaging (DTI) is een gevalideerde en sensitieve techniek om hersenschade op te sporen met MRI. In tegenstelling tot conventionele methoden, kunnen met DTI veranderingen in de microstructuur van de witte stof opgespoord worden. DTI maakt het mogelijk om witte stof schade vroeg op te sporen, zelfs in gebieden die er normaal uitzien op conventionele anatomische opnames. We stelden vast dat aorta stijfheid geassocieerd is met witte stof integriteit, onafhankelijk van leeftijd, geslacht, gemiddelde arteriële polsdruk, BMI, roken, ziekteduur en HbA1c waarden bij patiënten met T1DM. Dit wijst op een vasculaire component van vroege subtiele microstructurele beschadigingen. Prospectieve studies zijn nodig om de prognostische en therapeutische consequenties van deze microstructurele veranderingen in de witte stof van de hersenen vast te stellen. Het eerder ontdekken van microstructurele hersenschade, kan leiden tot een vroegere of intensievere behandeling, bijvoorbeeld van vasculaire risicofactoren zoals hypertensie of hypercholesterolemie.

In **hoofdstuk 4** hebben we de gevolgen van T1DM op het volume van de corticale grijze stof bestudeerd. Corticale grijze stof en de thalamus en hippocampus, twee subcorticale structuren, kunnen aangedaan zijn bij patiënten met T1DM. Eerdere studies toonden verminderde volumes van hippocampus en de thalamus bij patiënten met T1DM. Er is echter beperkt onderzoek gedaan bij patiënten met T1DM naar volume verlies in grijze stof gebieden, anders dan de hippocampus en de thalamus. Voxel-based morphometry (VBM) is een relatief nieuwe en geavanceerde analyse techniek, waarmee subtiele grijze stof veranderingen vastgesteld kunnen worden. Bij 62 patiënten met T1DM en 62 op leeftijd en geslacht gematchte gezonde controles werd een MRI van de hersenen gemaakt. Volumes van de basale ganglia, amygdala, hippocampus en thalamus werden onderzocht met VBM. In dit hoofdstuk tonen we aan dat patiënten met T1DM volume verlies hebben van al deze grijze stof gebieden, met uitzondering van de amygdala. Bovendien laten onze resultaten zien dat na correctie voor andere factoren (waaronder leeftijd, geslacht, roken, BMI en hypertensie), de thalamus, hippocampus en putamen nog steeds significant kleiner zijn bij patiënten met T1DM. Een verklaring voor het feit dat T1DM geen uniforme invloed heeft op de verschillende grijze stof gebieden is niet direct voor handen. De klinische relevantie en onderliggende mechanismen moeten nog worden opgehelderd.

In **hoofdstuk 5** worden de effecten besproken van een 16 weken durend (zeer) laag calorisch dieet ((Z)LCD) (~450-1000kcal/dag) op de cardiovasculaire functie en ectopische vetdeposities bij patiënten met overgewicht, T2DM en coronairlijden. Eerdere studies hebben uitgewezen dat langdurige calorische restrictie in patiënten met overgewicht

en T2DM *zonder* coronairlijden leidt tot verbetering van de myocardiale functie en vermindering van ectopisch vet, waaronder myocardiaal en pericardiaal vet. Het doel van onze studie was om te onderzoeken of patiënten met overgewicht en T2DM *met* coronairlijden ook baat hebben bij een 16 weken durend (Z)LCD. 27 patiënten met overgewicht, T2DM en coronairlijden volgden 16 weken een (Z)LCD. Na het dieet werd een substantiële verbetering van de glucoregulatie en van de cardiovasculaire functie, gemeten met MRI, gevonden. Deze verbeteringen gingen gepaard met reductie van de volumes van alle vetcompartimenten en van ectopische vet accumulatie in de lever en het hart. Myocardiale TG accumulatie is het netto resultaat van overmatige opname van vrije vetzuren in relatie tot de oxidatie van vrije vetzuren. Patiënten met T2DM hebben een toegenomen stapeling van TG in het myocard. Dit is geassocieerd met een verminderde myocardiale functie. Vermindering van TG in het myocard resulteert in een verbetering van de hartfunctie in patiënten met ongecompliceerde T2DM en volgens de huidige studie ook bij patiënten met T2DM en coronairlijden. Bovendien vonden we een afname van pericardiaal vet. Pericardiaal vet bestaat uit twee lagen, epicardiaal en paracardiaal vet. Toegenomen epicardiaal vet volume is geassocieerd met insulineresistentie, T2DM en hart- en vaatziekten. De rol van paracardiaal vet is momenteel minder duidelijk. Sommige studies hebben aangetoond dat paracardiaal vet een betere predictor is voor cardiovasculair risico dan epicardiaal vet. Om deze redenen beschouwen we de reductie van pericardiaal vet in deze studie als gunstig. LV massa en de hartfrequentie verminderden, wat een positief effect is, aangezien beide belangrijke voorspellers zijn van hart- en vaatziekten. Daarnaast nam de LV ejectiefractie (LVEF) toe na het (Z)LCD, wat klinisch relevant is, omdat de LVEF een van de belangrijkste voorspellers van overleving is. Ook werd een verlaging van de PWV van de aorta van 0.7m/s gevonden, wat wijst op een minder stijve aorta. Aangezien PWV met elke 10 jaar ouder worden 0.7m/s toeneemt, is de afname van PWV in deze studie een significante verbetering. Deze data tonen aan dat cardiovasculaire functie en ectopische vet accumulatie gevoelig zijn voor dieetinterventies in gecompliceerde T2DM en dat heeft belangrijke klinische implicaties. Aangezien T2DM geassocieerd is met een verhoogd cardiovasculair risico en hart- en vaatziekten de belangrijkste doodsoorzaak zijn in patiënten met T2DM, zijn de resultaten van deze studie klinisch relevant. Tevens bewijzen de resultaten dat dieetinterventies, naast optimale farmacologische therapie, nuttig zijn, ook in patiënten met T2DM met coronairlijden.

De effecten van bariatrische chirurgie op ectopische vetdeposities en cardiovasculaire functie worden beschreven in **hoofdstuk 6**. Cardiale ectopische vetdeposities, te weten myocardiaal en pericardiaal vet, spelen een rol in de pathogenese van hart- en vaatziekten. Gewichtsverlies door dieetinterventies resulteert in een afname van het cardiale

ectopische vet, maar het is onduidelijk of dit ook geldt voor gewichtsverlies na bariatrische chirurgie. Myocardiale TG accumulatie, pericardiaal vet en hartfunctie werden onderzocht bij 10 patiënten met overgewicht en insuline-afhankelijke T2DM voor en 16 weken na een Roux-en-Y gastric bypass (RYGB) operatie. Na de operatie vielen de patienten veel af en er was sprake van een verbeterde glucoregulatie. Het gewichtsverlies ging gepaard met een afname van visceraal en subcutaan vet. Daarnaast werd na RYGB een substantiële afname in het ectopische cardiale vet gevonden. In deze studie nam het epicardiale vet volume af, maar de relatieve afname in het paracardiale vet volume was veel hoger.

De myocardiale TG accumulatie nam niet af en de cardiovasculaire functie verbeterde niet na RYGB. Deze bevindingen suggereren dat gewichtsverlies na RYGB in patiënten met T2DM andere effecten heeft op paracardiaal vet weefsel dan op epicardiaal vet weefsel. De klinische implicaties van deze bevindingen moet nog vastgesteld worden. Hiervoor dienen studies met langere follow-up duur te worden uitgevoerd.

Zoals eerder genoemd, hebben Hindostanen een hoger risico op hart- en vaatziekten dan blanke Kaukasiërs. Het is niet bekend of er reeds op jonge leeftijd verschillen in cardiale dimensies en/of cardiovasculaire functie zijn tussen de etniciteiten. Het verhoogde risico op hart- en vaatziekten zou kunnen samenhangen met een ander metabolisme of andere verdeling van ectopische vetdeposities. In **Hoofdstuk 7** staan de effecten van een 5 dagen durend hoog vet hoog calorisch (HVHC) (~3775kcal/dag) dieet op cardiovasculaire functie beschreven bij jonge, gezonde Hindostanen en blanke Kaukasiërs. Met deze studie wilden wij onderzoeken of er een verschil is in cardiale dimensies en cardiovasculaire functie tussen jonge Hindostanen en blanke Kaukasiërs en of er een andere respons is op een hoog vet dieet. Twaalf Nederlandse Hindostanen en 12 Nederlandse Kaukasische gezonde mannen, gematcht voor leeftijd (19-25 jaar) en BMI (<25 kg/m^2), met een positieve familie geschiedenis voor T2DM, ondergingen een 5 dagen durend HVHC dieet, bestaande uit het normale dieet aangevuld met 375 ml slagroom per dag. De cardiovasculaire functie werd gemeten met behulp van MRI. Deze studie toont aan dat jonge, gezonde Hindostanen kleinere cardiale dimensies (afmetingen) hebben, vergeleken met gematchte blanke Kaukasiërs, zelfs na correctie voor hun kleinere lichaamsoppervlakte. Ook is de diastolische hartfunctie van Hindostanen anders, de cardiale relaxatie is verlengd in Hindostanen. Hoewel de ejectie fractie (EF), een grove parameter voor systolische functie, gelijk was binnen de twee groepen, waren meer subtiele parameters van systolische functie verschillend tussen beide groepen, wijzend op een verlengde cardiale contractie in Hindostanen. Een 5 dagen HVHC dieet vergrootte deze verschillen niet. Hindostanen hadden een hogere PWV voor start van het dieet. Na het dieet was er geen significant verschil meer tussen de

PWV in beide etniciteiten. PWV van de aorta is een krachtige onafhankelijke voorspeller van cardiovasculaire events. Of deze verschillen bijdragen aan de hogere incidentie van hart- en vaatziekten in Hindostanen moet nog worden vastgesteld. Het 5 dagen HVHC dieet vergrootte de gevonden verschillen in cardiovasculaire functie niet. Dit suggereert dat onze bevindingen niet verklaard kunnen worden door een verschillende metabole respons op vet in de voeding tussen de twee etnische groepen op jonge leeftijd.

In de hierboven beschreven studie werden tevens de metabole effecten van het HVHC dieet geëvalueerd; deze resultaten worden beschreven in **hoofdstuk 8**. Eerdere studies tonen aan dat Hindostanen hogere vet waarden hebben in de lever en spieren dan blanke Kaukasiërs. Dit kan erop wijzen dat Hindostanen een slechtere mitochondriële vrije vetzuur bèta-oxidatie hebben in skeletspier en/of vetweefsel, waardoor er ectopische vetdepositie plaatsvindt in perifere weefsels, uiteindelijk leidend tot insulineresistentie en andere metabole disfuncties. Hindostanen zouden daardoor mogelijk minder goed in staat zijn om het Westerse hoog vet dieet te verwerken dan blanke Kaukasiërs.

Recente studies hebben de 'nutrient and energy-sensing mammalian target of rapamycine (mTOR)-pathway' aangemerkt als modulator van zowel insuline gevoeligheid als mitochondriële functie. Onze hypothese was dat verschillen in mTOR activiteit tussen de twee etniciteiten mogelijk ten grondslag liggen of bijdragen aan het verhoogde risico op T2DM in Hindostanen. Hierbij gingen wij ervan uit dat veranderingen in de mTOR-pathway kunnen leiden tot mitochondriële disfunctie en de daarop volgende slechtere verwerking van vrije vetzuren. Daarnaast werden gevoeligheid van de lever voor insuline en perifere insuline gevoeligheid, substraat oxidatie, abdominale vetverdeling, insuline verwerking in de skeletspier en mitochondriële functie onderzocht. Omdat mitochondriële disfunctie mogelijk aan het licht gebracht kan worden door hoge vet belasting, ondergingen de deelnemers een 5 dagen durend HVHC dieet. Ze ondergingen een 2-staps hyperinsulinemische euglycaemische clamp met biopten van de skeletspier en indirecte calorimetrie voor en na het dieet. De hyperinsulinemische euglycaemische clamp wordt gezien als de gouden standaard voor het vaststellen van insulinegevoeligheid.

Deze studie toont aan dat een 5 dagen HVHC dieet al voldoende is om insuline gestimuleerde non-oxidatieve glucose verwerking te beïnvloeden in jonge, slanke Hindostanen, terwijl geen effect van het dieet werd waargenomen in leeftijd en BMI gematchte blanke Kaukasiërs. Dit suggereert dat jonge gezonde Hindostanen mogelijk een aangeboren verminderde metabole adaptatie voor hoge vetbelasting in het dieet hebben.

De mTOR-pathway in de skeletspier lijkt, in deze studie, geen verklaring voor de gevonden verschillen in insuline gevoeligheid. Deze bevindingen kunnen nieuwe

aanknopingspunten geven voor verder onderzoek gericht op het ophelderen van de pathogenese van insulineresistentie en T2DM in Hindostanen. Zo zou het interessant zijn om de rol van vetweefsel te onderzoeken in de verminderde glucose verwerking in Hindostanen in vergelijking met blanke Kaukasiërs.

In **hoofdstuk 9** worden de effecten beschreven van een 8 dagen durend zeer laag calorisch dieet (ZLCD) in 12 Hindostanen van middelbare leeftijd met overgewicht en 12 voor leeftijd en BMI gematchte blanke Kaukasiërs op de cardiovasculaire functie, ectopische vetverdeling en myocardiale TG. Het doel van deze studie was te onderzoeken of er een verschil is in metabole en functionele cardiovasculaire flexibiliteit op een kortdurend ZLCD tussen Hindostanen en blanke Kaukasiërs. Voor het dieet waren de Hindostanen reeds meer ongevoelig voor insuline dan blanke Kaukasiërs. Net als bij de jonge gezonde Hindostanen en blanke Kaukasiërs, waren de cardiale dimensies kleiner bij Hindostanen van middelbare leeftijd dan in blanke Kaukasiërs, ook na correctie voor lichaamsoppervlakte. De PWV was hoger in het distale deel van de aorta in Hindostanen. Systolische en diastolische cardiale functie, myocardiaal en pericardiaal vet waren niet verschillend tussen beide groepen. Na het ZLCD daalde het lichaamsgewicht en steeg de myocardiale TG accumulatie in beide etnische groepen. Bovendien verminderde de diastolische functie in dezelfde mate in beide groepen. Echter, het paracardiale vet en de PWV lieten een verschillende respons zien op het ZLCD, met een gunstiger respons in de Kaukasische groep.

De resultaten van onze studie tonen een vergelijkbare respons van het hart ten aanzien van TG accumulatie in reactie op een ZLCD in Hindostanen van middelbare leeftijd, met overgewicht en insulineresistentie in vergelijking met op leeftijd en BMI gematchte, maar minder insuline resistente, blanke Kaukasiërs. Er lijkt echter een minder gunstige respons te zijn op het 8 dagen durend ZLCD in Hindostanen ten aanzien van het paracardiale vet volume en de PWV.

Behandeling met op cisplatinum gebaseerde chemotherapie is geassocieerd met een verhoogde prevalentie van cardiovasculaire risicofactoren, zoals centrale adipositas en metabole verstoringen, zoals dyslipidemie en insulineresistentie. Behandeling van testiskanker (teelbalkanker) met cisplatinum, bleomycine en etoposide (BEP) chemotherapie is ook geassocieerd met acute vasculaire toxiciteit en subacute veranderingen in hartfunctie en met, op de lange termijn, cardiovasculaire ziekte. Er is echter weinig bekend over de acute effecten van op cisplatinum gebaseerde chemotherapie op cardiale functie, lichaamsvetverdeling en metabole parameters. Acute effecten worden gedefinieerd als de effecten die ontstaan binnen 3 maanden na start van de chemotherapie.

Hoofdstuk 10 toont aan dat op cisplatinum gebaseerde chemotherapie voor testiskanker acute veranderingen in diastolische cardiale functie induceert, wat gepaard gaat met ongunstige metabole veranderingen. Cardiale functie, vetverdeling en metabole parameters werden onderzocht in 14 patiënten met testiskanker voor start van chemotherapie en kort na de laatste chemotherapie, dit was ongeveer 3 maanden na start van de therapie. Wij toonden aan dat behandeling met op cisplatinum gebaseerde chemotherapie voor testiskanker, acute veranderingen in diastolische hartfunctie induceert, die gepaard gaan met ongunstige metabole veranderingen. Alhoewel de voorspellende betekenis van deze diastolische cardiale veranderingen voor cardiovasculaire morbiditeit op de lange termijn op dit moment nog niet duidelijk is, lijkt het aannemelijk dat ze uiteindelijk daadwerkelijk kunnen leiden tot hart- en vaatziekten. Aangezien de nadelige metabole veranderingen bij kunnen dragen aan het ontwikkelen van hart- en vaatziekten, moeten deze risicofactoren worden gemonitord en zo nodig worden behandeld.

Met behulp van MRI van de vaatwand kan onderscheid gemaakt worden tussen het lumen, de dikte van de vaatwand en de karakteristieken van atherosclerotische plaques. Voor klinische toepasbaarheid is hoge spatiële resolutie, verkregen door optimale signaal-ruis ratio en contrast-ruis ratio, noodzakelijk. In vele toepassingen geeft ultra-sterk veld MRI een betere signaal-ruis ratio en contrast-ruis ratio, welke gebruikt kunnen worden om de spatiële resolutie te verhogen. Naar verwachting kan MRI beeldvorming van de vaatwand van de carotiden dus profiteren van een hogere magneet veldsterkte. Het onderzoek beschreven in **hoofdstuk 11** vergelijkt de beeldvorming van de vaatwand van de carotiden van gezonde vrijwilligers op 3T en 7T, dus op een lagere respectievelijk hogere magneet veldsterkte. Achttien vrijwilligers ondergingen MRI onderzoeken op 7T (waarbij gebruik werd gemaakt van een zelfgebouwde zend/ontvang coil van 15 cm diameter) en op 3T (waarbij gebruik gemaakt werd van een commerciële coil met twee flexibele ovale elementen, elk van 14 x 17 cm). MRI van de vaatwand van de linker carotis werd uitgevoerd op 7T met identieke in-plane resolutie als op 3T MRI (0.46 x 0.46 mm^2). Hiermee werden transversale T1 en T2 gewogen afbeeldingen verkregen. De resultaten laten zien dat zowel de morfologische metingen van de carotis vaatwand (zowel de luminale als de vaatwand regio) als de intra- en inter-observer reproduceerbaarheid vergelijkbaar zijn tussen 3T en 7T. Bovendien verbetert beeldvorming van de carotis vaatwand op 7T MRI ten opzichte van op 3T de signaal-ruis ratio van de vaatwand en de contrast-ruis ratio.

Dit hoofdstuk illustreert de mogelijke waarde van 7T MRI voor de beoordeling van het lumen en de vaatwand van de arteria carotis, aangezien accurate afgrenzing van de

vaatwand van de arteria carotis van belang is om atherosclerose en atherosclerotische veranderingen van de vaatwand op te sporen.

De hogere veldsterkte brengt een reeks technische uitdagingen voor cardiovasculaire MRI met zich mee. Cardiovasculaire MRI vereist goede compensatie voor de beweging van het hart en de ademhaling en voor veldinhomogeniteit. Een andere uitdaging is het verkrijgen van een betrouwbaar elektrocardiogram. **Hoofdstuk 12** beschrijft de resultaten van een studie naar veiligheid van stents in de coronairvaten (kransslagaders) op 7T MRI, door het bepalen van verplaatsing en opwarming van cobalt alloy stents, een type coronairstent, met een lengte van 5-85.8 mm in een 'worst-case' scenario. Daarbij worden ook de initiële resultaten beschreven van de klinische uitvoerbaarheid van 7T cardiovasculaire MRI in gezonde vrijwilligers en patiënten met hart- en vaatziekten. De resultaten van deze studie tonen aan dat cardiovasculaire MRI op 7T veilig is in patiënten met cobalt alloy coronair stents met een lengte tussen 5 en 85.8mm. Verder laten de resultaten zien dat klinische cardiovasculaire MRI op 7T uitvoerbaar is bij gezonde vrijwilligers en bij patiënten met hart- en vaatziekten. Technische uitdagingen moeten nog overwonnen worden voordat 7T routinematig klinisch gebruikt kan worden. In de klinische praktijk zal het voordeel van een ultra-hoge veldsterkte MRI boven een lagere veldsterkte MRI, zoals 1.5 of 3.0T, moeten blijken.

Concluderend: DM leidt tot cardiovasculaire complicaties. Overgewicht en obesitas zijn een belangrijke risicofactor voor het ontwikkelen van T2DM en de toenemende prevalentie van overgewicht en obesitas heeft geleid tot een daarmee samengaande toename in de prevalentie van T2DM. T2DM is een van de meest voorkomende chronische ziekten in de wereld. De pathogenese van de cardiovasculaire complicaties in T2DM is multifactorieel, maar een belangrijke rol lijkt toe te schrijven aan de ectopische accumulatie van TG in skeletspier, de lever en in en rondom het hart. Gewichtsverlies wordt momenteel gezien als de meest effectieve behandeling van T2DM. Een afname in ectopisch vet wordt beschouwd als een van de mechanismen voor toegenomen insuline gevoeligheid na gewichtsverlies. Echter, blijvend gewichtsverlies is moeilijk, aangezien permanente leefstijlveranderingen nodig zijn om te voorkomen dat er weer gewichtstoename plaatsvindt. Bariatrische chirurgie is een andere mogelijke behandeling voor T2DM, aangezien dit resulteert in fors gewichtsverlies, duidelijke verbetering in de glycemische controle en zelfs tot remissie van T2DM.

Patiënten met T1DM hebben een stijvere aorta dan gezonde vrijwilligers en dit is gecorreleerd met LV diastolische functie en witte stof integriteit in het brein. T1DM heeft ook gevolgen voor het volume van de grijze stof.

Wij hebben aangetoond dat bij patiënten met T2DM en coronairlijden een 16 weken durend (Z)LCD de cardiovasculaire functie en ectopische vet distributie kan verbeteren. Dit benadrukt het belang van dieetinterventies in deze patiëntengroep en onderstreept dat gewichtsverlies de hoeksteen van de behandeling blijft.

Aangezien de prevalentie van overgewicht/obesitas en van T2DM een epidemische omvang bereikt, dient de nadruk te liggen op preventie van overgewicht. Naast de resultaten van het 16 weken (Z)LCD, toonde een studie in T2DM patiënten voor en 16 weken na bariatrische chirurgie een sterkere afname in paracardiaal vet, in vergelijking tot epicardiaal vet. De implicaties van deze bevindingen moeten worden onderzocht in toekomstige studies.

Verder tonen de studies in dit proefschrift aan dat al op jonge leeftijd verschillen bestaan in cardiale dimensies en functie tussen Hindostanen en blanke Kaukasiërs. Daarnaast verslechtert een HVHC dieet de insuline gevoeligheid in jonge, slanke, gezonde Hindostanen, maar niet in blanke Kaukasiërs. De ectopische vetverdeling is vergelijkbaar tussen Hindostanen en blanke Kaukasiërs, zowel in de jonge groep als in de groep van middelbare leeftijd. Echter, paracardiaal vet en PWV lieten een verschillende respons zien op een ZLCD, met een gunstiger respons bij blanke Kaukasiërs.

Onze bevindingen dragen bij aan een beter begrip van het verhoogde risico op hart- en vaatziekten en T2DM in Hindostanen. Desalniettemin zijn er meer studies nodig om de mechanismen, die leiden tot een verhoogd risico, te onderzoeken en hopelijk nog beter te begrijpen. Tot slot beschrijft dit proefschrift de resultaten van de toepasbaarheid van de beeldvorming van de carotis vaatwand op 7T MRI. Bovendien worden data over veiligheid van coronairstents op 7T en de initiële toepasbaarheid van cardiovasculaire MRI in patiënten met hart- en vaatziekten getoond.

LIST OF PUBLICATIONS

Kröner ESJ, **van Schinkel LD**, Versluis MJ, Brouwer NJ, van den Boogaard PJ, van der Wall EE, de Roos A, Webb AG, Siebelink HM, Lamb HJ. Ultrahigh-field 7-T magnetic resonance carotid vessel wall imaging: initial experience in comparison with 3-T field strength. *Invest Radiol*. 2012; 47: 697-704

van Schinkel LD, Auger D, van Elderen SGC, Ajmone Marsan N, Delgado V, Lamb HJ, Ng ACT, Smit JWA, Bax JJ, Westenberg JJM, de Roos A. Aortic stiffness is related to left ventricular diastolic function in patients with diabetes mellitus type 1: assessment with MRI and speckle tracking strain analysis. *Int J Cardiovasc Imaging*. 2013; 29: 633-641

Jonker JT, de Mol P, de Vries ST, Widya RL, Hammer S, **van Schinkel LD**, van der Meer RW, Gans RO, Webb AG, Kan HE, de Koning EJ, Bilo HJ, Lamb HJ. Exercise and type 2 diabetes mellitus: changes in tissue-specific fat distribution and cardiac function. *Radiology*. 2013; 269: 434-42

van Schinkel LD, Willemse PM, van der Meer RW, Burggraaf J, van Elderen SGC, Smit JWA, de Roos A, Osanto S, Lamb HJ. Chemotherapy for testicular cancer induces acute alterations in diastolic heart function. *Br J Cancer*. 2013; 109: 891-6

van Schinkel LD, Bakker LEH, Jonker JT, de Roos A, Pijl H, Meinders AE, Jazet IM, Smit JWA, Lamb HJ. Functional and metabolic imaging of the cardiovascular system in young healthy South Asians and Caucasians unveils early differences. *Diabetes* Care. 2013; 36: 178-179

van Schinkel LD, Willemse PM, van der Meer RW, Burggraaf J, van Elderen SGC, Smit JWA, de Roos A, Osanto S, Lamb HJ. Reply: Comment on 'Chemotherapy for testicular cancer induces acute alterations in diastolic heart function'. *Br J Cancer*. 2014; 110: 265

Jonker JT, Djaberi R, **van Schinkel LD**, Hammer S, Bus MT, Kerpershoek G, Kharagjitsingh AV, Romijn JA, Bax JJ, Jukema JW, de Roos A, Smit JWA, Lamb HJ. Very-low-calorie diet increases myocardial triglyceride content and decreases diastolic left ventricular function in type 2 diabetes with cardiac complications. *Diabetes Care*. 2014; 37: e1-2

Bakker LEH, **van Schinkel LD**, Guigas B, Streefland TC, Jonker JT, van Klinken JB, van der Zon GC, Lamb HJ, Smit JWA, Pijl H, Meinders AE, Jazet IM. A 5-day high-fat, high-calorie

diet impairs insulin sensitivity in healthy, young South Asian men but not in Caucasian men. *Diabetes*. 2014; 63: 248-58

van Schinkel LD, Sleddering MA, Lips MA, Jonker JT, de Roos A, Lamb HJ, Jazet IM, Pijl H, Smit JWA. Effects of bariatric surgery on pericardial ectopic fat depositions and cardiovascular function. *Clin Endocrinol*. 2014; in press

Tjeerdema N, **Van Schinkel LD**, Westenberg JJ, Van Elderen SG, Van Buchem MA, Smit JWA, Van der Grond J, De Roos A. Aortic stiffness is associated with white matter integrity in patients with type 1 diabetes. *Eur Radiol*. 2014; in press

van Schinkel LD, Tjeerdema N, van Elderen SGC, van der Grond J, Smit JWA, de Roos A. Impact of type 1 diabetes mellitus on regional gray matter volume. Submitted

van Schinkel LD, Lamb HJ, Westenberg JJM, Dronkers CEA, Jukema JW, de Roos A, Smit JWA. Caloric restriction improves cardiovascular function in advanced type 2 diabetes mellitus. Submitted

van Schinkel LD, Bakker LEH, Jonker JT, de Roos A, Pijl H, Meinders AE, Jazet IM, Lamb HJ, Smit JWA. Cardiovascular function in middle-aged overweight South Asians compared with Caucasians: response to short-term caloric restriction. Submitted

van Schinkel LD, Kröner ESJ, Bizino MB, Mourik JEM, Versluis MJ, van den Boogaard PJ, Bonetti C, Kastaneer EI, Smit JWA, de Roos A, Webb AG, Siebelink HJ, Lamb HJ. Submitted

Boon MR, Bakker LEH, Haks MC, Quinten E, Schaart G, van Beek L, Wang Y, **van Schinkel LD**, van Harmelen V, Meinders AE, Hesselink M, Ottenhoff THM, Willems van Dijk K, Guigas B, Jazet IM, Rensen PCN. Short-term high-fat diet increases macrophage markers in skeletal muscle accompanied by impaired insulin signaling in healthy male subjects. Submitted

CURRICULUM VITAE

Linda Danielle van Schinkel werd op 29 mei 1984 geboren te 's-Gravenhage. Zij behaalde haar gymnasiumdiploma cum laude aan het Maerlant Lyceum te 's-Gravenhage in 2002. Hierna startte zij met de opleiding Geneeskunde aan de Universiteit van Leiden. In de periode van 2006 tot en met 2008 liep zij co-assistentschappen, waaronder een keuze co-assistenschap gynaecologie in het 's Lands Hospitaal in Paramaribo, Suriname. Zij behaalde het doctoraal examen en het artsexamen, beiden in 2008. Hierna werkte zij een jaar als arts-assistent niet in opleiding op de afdeling interne geneeskunde van het HagaZiekenhuis te 's-Gravenhage. In januari 2010 startte zij met haar promotieonderzoek in het Leids Universitair Medisch Centrum op de afdelingen Endocrinologie en Radiologie, onder begeleiding van Prof. dr. J.W.A. Smit, Prof. dr. A. de Roos en Prof. dr. H.J. Lamb. De onderzoeksresultaten staan in dit proefschrift beschreven. In mei 2013 is zij begonnen aan de opleiding interne geneeskunde in het HagaZiekenhuis te 's-Gravenhage (opleiders dr. M.O. van Aken en Prof. dr. J.W. de Fijter).